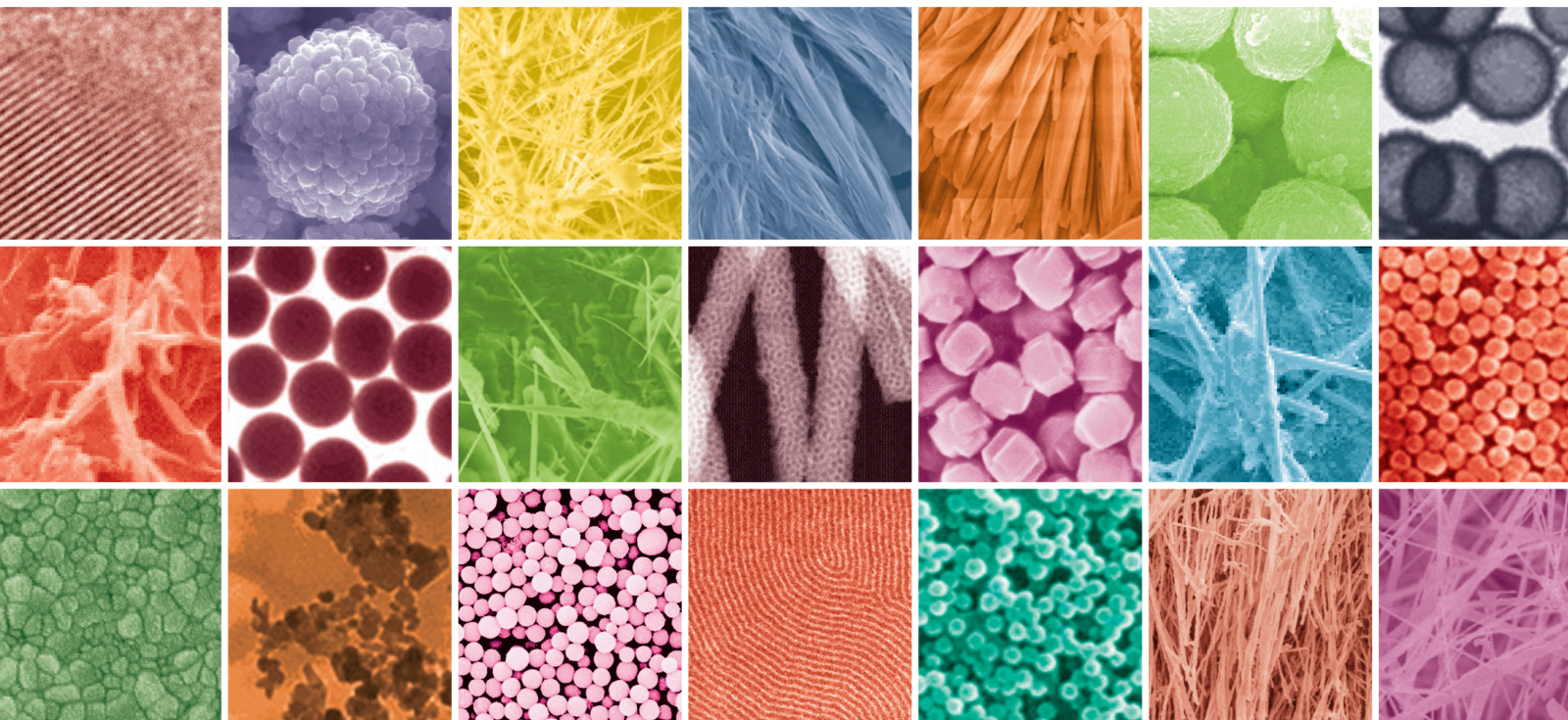


Advanced Nano/Micro Materials for Drug Delivery Applications

Lead Guest Editor: Anuj Kumar

Guest Editors: Garima Agrawal and Vijay K. Thakur





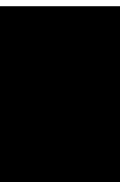
Advanced Nano/Micro Materials for Drug Delivery Applications

Journal of Nanomaterials

**Advanced Nano/Micro Materials for
Drug Delivery Applications**

Lead Guest Editor: Anuj Kumar

Guest Editors: Garima Agrawal and Vijay K.
Thakur





Copyright © 2020 Hindawi Limited. All rights reserved.

This is a special issue published in "Journal of Nanomaterials." All articles are open access articles distributed under the Creative Commons Attribution License, which permits unrestricted use, distribution, and reproduction in any medium, provided the original work is properly cited.



Chief Editor

Stefano Bellucci , Italy













Associate Editors

Ilaria Armentano, Italy
Stefano Bellucci , Italy
Paulo Cesar Morais , Brazil
William Yu , USA

Academic Editors

Buzuayehu Abebe, Ethiopia
Domenico Acierno , Italy
Sergio-Miguel Acuña-Nelson , Chile
Katerina Aifantis, USA
Omer Alawi , Malaysia
Nageh K. Allam , USA
Muhammad Wahab Amjad , USA
Martin Andersson, Sweden
Hassan Azzazy , Egypt
Ümit Ağbulut , Turkey
Vincenzo Baglio , Italy
Lavinia Balan , France
Nasser Barakat , Egypt
Thierry Baron , France
Carlos Gregorio Barreras-Urbina, Mexico
Andrew R. Barron , USA
Enrico Bergamaschi , Italy
Sergio Bietti , Italy
Raghvendra A. Bohara, India
Mohamed Bououdina , Saudi Arabia
Victor M. Castaño , Mexico
Albano Cavaleiro , Portugal
Kondareddy Cherukula , USA
Shafiul Chowdhury, USA
Yu-Lun Chueh , Taiwan
Elisabetta Comini , Italy
David Cornu, France
Miguel A. Correa-Duarte , Spain
P. Davide Cozzoli , Italy
Anuja Datta , India
Loretta L. Del Mercato, Italy
Yong Ding , USA
Kaliannan Durairaj , Republic of Korea
Ana Espinosa , France
Claude Estournès , France
Giuliana Faggio , Italy
Andrea Falqui , Saudi Arabia





Matteo Ferroni , Italy
Chong Leong Gan , Taiwan
Siddhartha Ghosh, Singapore
Filippo Giubileo , Italy
Iaroslav Gnilitzkiy, Ukraine
Hassanien Gomaa , Egypt
Fabien Grasset , Japan
Jean M. Greneche, France
Kimberly Hamad-Schifferli, USA
Simo-Pekka Hannula, Finland
Michael Harris , USA
Hadi Hashemi Gahruei , Iran
Yasuhiko Hayashi , Japan
Michael Z. Hu , USA
Zhengwei Huang , China
Zafar Iqbal, USA
Balachandran Jeyadevan , Japan
Xin Ju , China
Antonios Kellarakis , United Kingdom
Mohan Kumar Kesarla Kesarla , Mexico
Ali Khorsand Zak , Iran
Avvaru Praveen Kumar , Ethiopia
Prashant Kumar , United Kingdom
Jui-Yang Lai , Taiwan
Saravanan Lakshmanan, India
Meiyong Liao , Japan
Shijun Liao , China
Silvia Licoccia , Italy
Zainovia Lockman, Malaysia
Jim Low , Australia
Rajesh Kumar Manavalan , Russia
Yingji Mao , China
Ivan Marri , Italy
Laura Martinez Maestro , United Kingdom
Sanjay R. Mathur, Germany
Tony McNally, United Kingdom
Pier Gianni Medaglia , Italy
Paul Munroe, Australia
Jae-Min Myoung, Republic of Korea
Rajesh R. Naik, USA
Albert Nasibulin , Russia
Ngoc Thinh Nguyen , Vietnam
Hai Nguyen Tran , Vietnam
Hiromasa Nishikiori , Japan

Sherine Obare , USA
Abdelwahab Omri , Canada
Dillip K. Panda, USA
Sakthivel Pandurengan , India
Dr. Asisa Kumar Panigrahy, India
Mazeyar Parvinzadeh Gashti , Canada
Edward A. Payzant , USA
Alessandro Pegoretti , Italy
Oscar Perales-Pérez, Puerto Rico
Anand Babu Perumal , China
Suresh Perumal , India
Thathan Premkumar , Republic of Korea
Helena Prima-García, Spain
Alexander Pyatenko, Japan
Xiaoliang Qi , China
Haisheng Qian , China
Baskaran Rangasamy , Zambia
Soumyendu Roy , India
Fedlu Kedir Sabir , Ethiopia
Lucien Saviot , France
Shu Seki , Japan
Senthil Kumaran Selvaraj , India
Donglu Shi , USA
Muhammad Hussnain Siddique , Pakistan
Bhanu P. Singh , India
Jagpreet Singh , India
Jagpreet Singh, India
Surinder Singh, USA
Thangjam Ibomcha Singh , Republic of Korea
Korea
Vidya Nand Singh, India
Vladimir Sivakov, Germany
Tushar Sonar, Russia
Pingan Song , Australia
Adolfo Speghini , Italy
Kishore Sridharan , India
Marinella Striccoli , Italy
Andreas Stylianou , Cyprus
Fengqiang Sun , China
Ashok K. Sundramoorthy , India
Bo Tan, Canada
Leander Tapfer , Italy
Dr. T. Sathish Thanikodi , India
Arun Thirumurugan , Chile
Roshan Thotagamuge , Sri Lanka

Valeri P. Tolstoy , Russia
Muhammet S. Toprak , Sweden
Achim Trampert, Germany
Tamer Uyar , USA
Cristian Vacacela Gomez , Ecuador
Luca Valentini, Italy
Viet Van Pham , Vietnam
Antonio Vassallo , Italy
Ester Vazquez , Spain
Ajayan Vinu, Australia
Ruibing Wang , Macau
Magnus Willander , Sweden
Guosong Wu, China
Ping Xiao, United Kingdom
Zhi Li Xiao , USA
Yingchao Yang , USA
Hui Yao , China
Dong Kee Yi , Republic of Korea
Jianbo Yin , China
Hesham MH Zakaly , Russia
Michele Zappalorto , Italy
Mauro Zarrelli , Italy
Osman Ahmed Zeleke, Ethiopia
Wenhui Zeng , USA
Renyun Zhang , Sweden









Contents

Development and Characterization of Soy Lecithin Liposome as Potential Drug Carrier Systems for Codelivery of Letrozole and Paclitaxel

Minh Thanh Vu , Ngoc Thuy Trang Le , Truc Le-Buu Pham, Ngoc Hoi Nguyen , and Dai Hai Nguyen 








Research Article (9 pages), Article ID 8896455, Volume 2020 (2020)

Evaluation of the Cytotoxic Effect of Rutin Prenanoemulsion in Lung and Colon Cancer Cell Lines

Tran Thanh Hoai , Phan Thi Yen , Tran Thi Bich Dao , Luu Hai Long , Duong Xuan Anh , Luu Hai Minh , Bui Quoc Anh , and Nghiem Thi Thuong 






Research Article (11 pages), Article ID 8867669, Volume 2020 (2020)

Therapeutic Nanomaterials for Neurological Diseases and Cancer Therapy

Kankai Wang , Xiaohong Zhu , Enxing Yu , Priyanka Desai, Hao Wang, Chun-li Zhang , Qichuan Zhuge , Jianjing Yang , and Jiangnan Hu 




Review Article (18 pages), Article ID 2047379, Volume 2020 (2020)

Gelatin Encapsulated Curcumin Nanoparticles Moderate Behavior of Human Primary Gingival Fibroblasts In Vitro

Mai Thi-Hoang Nguyen , Khanh Loan Ly , Thoai Quoc Kieu , Hiep Thi Nguyen , and Nam Cong-Nhat Huynh 




Research Article (11 pages), Article ID 2985721, Volume 2020 (2020)

Recent Trends in Nanocarrier-Based Targeted Chemotherapy: Selective Delivery of Anticancer Drugs for Effective Lung, Colon, Cervical, and Breast Cancer Treatment

Ke-Tao Jin , Ze-Bei Lu, Jin-Yang Chen, Yu-Yao Liu, Huan-Rong Lan, Hai-Ying Dong, Fan Yang , Yuan-Yuan Zhao, and Xiao-Yi Chen 



Review Article (14 pages), Article ID 9184284, Volume 2020 (2020)

A Combination Therapy of pHRE-Egr1-HSV-TK/Anti-CD133McAb-¹³¹I/MFH Mediated by FePt Nanoparticles for Liver Cancer Stem Cells

Mei Lin , Yanhong Xiao , Xingmao Jiang, Jun Zhang, Ting Guo , and Yujuan Shi

Research Article (15 pages), Article ID 7180613, Volume 2020 (2020)

Galactosamine-Conjugating Zwitterionic Block Copolymer for Reduction-Responsive Release and Active Targeted Delivery of Doxorubicin to Hepatic Carcinoma Cells

Jingming Zhai, Biyu Zhou, Yanhui An, Binzhong Lu, Yonggang Fan , and Junbo Li 

Research Article (11 pages), Article ID 7863709, Volume 2020 (2020)

Research Article

Development and Characterization of Soy Lecithin Liposome as Potential Drug Carrier Systems for Codelivery of Letrozole and Paclitaxel

Minh Thanh Vu ^{1,2}, Ngoc Thuy Trang Le ^{2,3}, Truc Le-Buu Pham,⁴ Ngoc Hoi Nguyen ^{2,3}
and Dai Hai Nguyen ^{2,3}

¹Institute of Chemistry and Materials, 17 Hoang Sam, Cau Giay, Hanoi City 100000, Vietnam

²Graduate University of Science and Technology, Vietnam Academy of Science and Technology, Hanoi City 100000, Vietnam

³Institute of Applied Materials Science, Vietnam Academy of Science and Technology, Ho Chi Minh City 700000, Vietnam

⁴Biotechnology Center of Ho Chi Minh City, 2374, Highway 1, Trung My Tay Ward, District 12, Ho Chi Minh City 700000, Vietnam

Correspondence should be addressed to Dai Hai Nguyen; nguyendaihai@iams.vast.vn

Received 19 August 2020; Revised 5 November 2020; Accepted 15 December 2020; Published 30 December 2020

Academic Editor: Garima Agrawal

Copyright © 2020 Minh Thanh Vu et al. This is an open access article distributed under the Creative Commons Attribution License, which permits unrestricted use, distribution, and reproduction in any medium, provided the original work is properly cited.

In the present work, a dual-drug-loaded soy lecithin liposomal system was developed by coencapsulation of Letrozole (LET) with Paclitaxel (PTX) to improve the efficacy in breast cancer therapy. Liposomes were synthesized by the thin film layer hydration. To sufficiently evaluate the characteristics of these liposomes, the particle size, zeta potential, morphology, drug encapsulation, *in vitro* drug release, and cytotoxicity were ascertained. Results showed promisingly anticancer potentials, as the following parameters indicated: nanosize diameter (around 193 nm) and negative surface charge. Data collected from the coloaded drug liposomes showed suitable encapsulation efficiency (50.56% for PTX and 31.13% for LET). Controlled and sustained releases were achieved up to 72 h for both the loaded drugs following the diffusion mechanism. In addition, the *in vitro* cytotoxicity study on the human breast cancer cell line (MCF-7) given the dual-drug-loaded liposome showed greater inhibition of cell growth than the single drug. Consequently, LET and PTX coloaded liposomes made from soy lecithin are expected to be an ingenious drug-delivery system for combination chemotherapy.

1. Introduction

Breast cancer therapy using oestrogen-targeted drugs is one of the most successful anticancer strategies to date. Accordingly, Letrozole (LET), a third-generation aromatase inhibitor, is the antioestrogen drug that is commonly used in the treatment of breast cancer [1, 2]. By successfully preventing aromatase which produces oestrogen, LET slows down the growth of hormone-responsive breast tumours *in vivo*. However, research has shown that LET has some negative effects on patients, including diarrhoea, constipation, fever, fatigue, and chest pains [3]. Regarding its overall effects on human health, LET was reported to possess potential efficacy that could be enhanced by advancing in combination with other chemotherapeutic agents [4–7]. Therefore, researchers have currently focused on LET combination therapies, particularly

with chemotherapy, to take advantage of therapies using multiple drugs including coordinately distributed drugs to specific sites, reduce toxicity, and increase efficacy of drugs, as well as slow the rate of developing drug resistance, in order to advance in the full potentials of chemodrug treatments [8]. In the process of theoretical searching for the chemotherapeutic agent in the LET combination therapy, Paclitaxel (PTX) seems to be a great candidate [9]. By preventing the cells from dividing and replicating and causing the death of the cells in various proposed mechanisms, PTX in combination with LET is expected to destroy any of the remaining cancer cells, which are left uninhibited during the developing of LET [9–11]. Chen et al. have published their study in *Anti-Cancer Drugs*, reporting that exemestane, one of the aromatase inhibitors (AIs), could combine with Paclitaxel for the treatment of aromatase-positive gynecological cancer [9].

This combination allowed reducing the Paclitaxel dosage and therefore the toxicity of the treatment. Besides, clinical trials for ALs, a class of drugs used in the treatment of breast cancer in postmenopausal women and gynecomastia in men, are underway. As a result of this, it is valuable and has a contributing meaning to the scientific community to develop a codelivery system utilizing LET and PTX as loaded drugs and to evaluate its efficacy in the current status of breast cancer treatment.

In the combination therapy of agents with different solubility and pharmacokinetic properties such as LET plus PTX, it is considered that finding the ideal carrier systems/materials is the biggest challenge. Accompanied by these difficulties, nanoparticles with the abilities to sufficiently encapsulate and deliver dissimilar anticancer agents have been developed. Notably, liposome-based nanoparticles have been rising as a part of the technologies that health organizations already adopted for treatment purposes because of numerous benefits [12–15]. Liposomes (Lips) are microscopic lamellar structures that can be formed in the admixture of the soy lecithin and cholesterol and completed by the subsequent hydration in aqueous media [16–18]. Regarding this, liposomes have been widely evaluated and utilized in the controlled as well as the targeted drug delivery as novel systems in cancer treatment. For instance, these systems enhance the delivery of drugs to specific body organs and cells; in some cases, they can even reduce drug toxicity and facilitate the administration of different kinds of diagnoses [19]. He and Ma found that these nanoparticles reduced drug dosage in the case of medication errors [1]. Moreover, liposomes were reported to successfully codeliver drugs in the combination of LET in therapy as well as PTX combination therapy with other agents [5, 20–22]. Therefore, liposomes are predicted to exert their promising properties in improving the therapeutic efficacy of LET by co-loading and codelivery with PTX for the treatment of breast cancer cells with faster absorption of the medication into the body, reducing side effects, and enhanced maximal dose tolerance.

In this regard, the aim of this study was to develop soy lecithin liposomal systems for the coencapsulated LET and PTX. It should be noted that the proposed liposomes were made from soy lecithin and cholesterol, which were prepared by hydrating a thin lipid film then reducing the particle size distribution by sonication followed by extrusion. This study also assessed the properties of the named nanoparticles, including particle size, polydispersity index, zeta potential, and morphology. In addition, *in vitro* tests that entailed the drug loading and releasing efficiency were conducted. The cytotoxic effect of single and combined drugs in human breast cancer cell lines (MCF-7) was evaluated by WST assay. In summary, this study is aimed at the drug delivery system's preparation, investigation, and understanding of the application of LET in combination with PTX.

2. Materials and Methods

2.1. Materials. Letrozole (LET) was synthesized in the previous study [23]. Paclitaxel (PTX) was purchased from Samyang Corporation (Seoul, Korea). Soy lecithin and

Tween 80 (polyoxyethylene sorbitan monooleate) were obtained from Tokyo Chemical Industry Co., Ltd. (Tokyo, Japan). Cholesterol was supplied by Sigma-Aldrich (St Louis, MO, USA). Cetyltrimethylammonium bromide (CTAB) and all solvents were of analytical grade and obtained from Merck (Darmstadt, Germany). A dialysis bag (Spectra/Por, regenerated cellulose) was purchased from Spectrum Laboratories Inc. (Canada). The Dulbecco's Modified Eagle's Medium: Nutrient Mixture F-12 (DMEM/F-12) and fetal bovine serum (FBS) were purchased from Thermo Fisher Scientific (Ho Chi Minh City, Vietnam). Human breast cancer cell lines (MCF-7) were obtained from the University of Tsukuba (Tsukuba, Ibaraki, Japan) [24].

2.2. Preparation of Soy Lecithin Liposomes. Liposomes were aseptically prepared by the thin-film hydration method. The lipid phase components (soy lecithin, cholesterol, CTAB, LET, and PTX) were accurately weighed and dissolved in chloroform:methanol mixture (2:1, *v/v*), in the ratio of 9:1 soy lecithin:cholesterol, 1% CTAB, 5% LET, and 5% PTX. The solution was transferred to a round-bottom flask and connected to a BUCHI rotavapor R-114 and BUCHI water bath B-480 with applied vacuum and temperature maintained at 45°C until the complete evaporation of solvents. The obtained dry, thin lipid film was hydrated with 0.5% Tween 80 by stirring at room temperature. The suspension was sonicated by the probe sonicator for 30 min and was further homogenized by a miniextruder (EmulsiFlex-05 homogenizer, Avestin Inc., Ottawa, Canada) for 10 cycles. The obtained liposomal suspension was centrifuged at 16000 rpm for 30 min to separate the unencapsulated drugs. The resulting formulation was lyophilized and stored at 2–8°C for further analysis.

2.3. Characterizations. The size distribution and zeta potential of the liposomal formulations were characterized by dynamic light scattering (DLS) using a Zetasizer Nano SZ (SZ-100, Horiba). The measurement was determined through a helium-neon (He-Ne) laser beam with the detection angle and the temperatures as 90° and 25°C, respectively. Samples were diluted with deionized water prior to measurement to reach the phospholipid concentration of 1000 ppm. The morphology of LET-PTX-Lips was examined by a transmission electron microscope (TEM) using JEM-1400, JEOL (Tokyo, Japan). The sample was diluted with deionized water (1 mg/mL). One drop of the liposomal formulation was deposited onto a carbon-copper grid (300-mesh, Ted Pella, Inc., USA) and air-dried at room temperature.

2.4. Stability Study. Lips, LET-Lips, and LET-PTX-Lips were preserved in a fridge at 2–8°C for one week and measured by their size and zeta value.

2.5. Determination of Encapsulation Efficiency and In Vitro Release Study. High Performance Liquid Chromatography (HPLC) was applied for the identification and quantitation of LET and PTX in the liposomal formulations using Flexar PDA Plus LC Detector (PerkinElmer, USA). The mobile phase consisted of acetonitrile/water with the volume ratio of (40:60). The mobile phase was degassed prior to use and

delivered isocratic ally at a flow rate of 1 mL/min through the reverse-phase Fortis C18 column (150 mm, 4.6 mm, pore size 5 μm ; Fortis Technologies Ltd., Cheshire, UK), and a UV detector at 227 nm was used to monitor the column eluent. For determining the LET and PTX concentration in the liposomal formulations, a slight modification of the ultracentrifuge method of Yang et al. was applied [25]. An aliquot of 1 mL of the formulation was mixed with 10 mL of PBS (pH 7.4) and centrifuged at 1000 rpm for 10 min at 25°C. Then, centrifugation at 16000 rpm for 30 min was performed to precipitate 11 mL of liposome supernatant, which was then decanted and washed twice with PBS (pH 7.4). The liposome pellets were then dissolved with 6 mL solvent and sonicated for 10 min for subsequent characterization. Collected samples were filtered through the 0.22 μm PTFE syringe filters prior to analysis.

The encapsulation efficiency (EE%) of the liposomal formulation for each drug was calculated using the following equation [26]:

$$\text{EE (\%)} = \frac{W_p}{W_s} \times 100, \quad (1)$$

where W_p is the amount of drugs in the liposome pellet and W_s is the amount of drugs in the liposome suspension.

The release profile of liposomal formulation was studied *in vitro* in PBS buffer (pH 7.4) at the presence of 2% Tween 80. About 1 mL of the liposomal formulation was tightly sealed in a dialysis bag (MW cutoff 3.5 kDa) and immersed in 10 mL dialysis medium. The release study was performed at 37°C in a shaker bath (100 rpm). At defined time intervals (1, 2, 3, 6, 12, 24, 36, 48, 60, and 72 h), an aliquot of 1 mL sample was taken from the release medium followed by the immediate supplementation of the equal volume of the fresh medium. Controls containing free drug were prepared in the amount equal to the amount of the drug contained in the liposome and tested along with the liposomal dispersions. Samples were filtered (pore size = 0.22 μm) before being analysed by the above-mentioned HPLC method to determine the LET and PTX content.

2.6. Release Kinetics Study. To analyse the *in vitro* release patterns of both LET and PTX in coloaded form LET-PTX-Lips, four drug release kinetic models, including zero-order kinetic model, first-order kinetic order, Higuchi model, and Korsmeyer-Peppas model, were used. The zero-order kinetic model was the relationship between time and cumulative % drug release, which could define the process of the constant drug released from a drug delivery system, and the drug level in the blood remained constant throughout the delivery. Meanwhile, the first-order kinetic model was the relationship of time and log cumulative % of drug remaining. This model was applied to evaluate the concentration-dependent manner of the drug release. The Higuchi model was the relationship between the square root of time and cumulative % drug release, which was used to identify whether the prime mechanism of the drug release was a diffusion controlled release mechanism or not. Finally, the Korsmeyer-Peppas model was the relationship of time and log cumulative

% drug release which helped to understand the dissolution mechanisms of the drugs from the matrix. Graphs of the zero-order, first-order, Higuchi, and Korsmeyer-Peppas models were drawn based on equations (2), (3), (4), and (5), respectively, and Microsoft Excel, then the rate constant and correlation values were obtained by applying a linear regression fit [27, 28].

$$C = k_0 t, \quad (2)$$

$$\log(100 - C) = -\frac{k_f t}{2.303}, \quad (3)$$

$$C = k_H \sqrt{t}, \quad (4)$$

$$C = k_K t^n, \quad (5)$$

where C is the cumulative % drug released at time t , k_0 is the zero-order rate constant, k_f is the first-order rate constant, k_H is the Higuchi dissolution constant, k_K is the Korsmeyer-Peppas constant, and n is the exponent that describes a particular diffusion mechanism.

2.7. Cell Culture and Viability Test. The cells were grown in DMEM/F-12 containing 10% FBS and 2% penicillin/streptomycin (10,000 U/mL penicillin and 10 mg/mL streptomycin) in humidified air with 5% CO_2 at 37°C. Cells were inoculated in a 96-well plate with a density of 3×10^4 cells/well. After 24 h, cells were treated with reagents at a concentration of 10–100 $\mu\text{g}/\text{mL}$ of Lips and 1 $\mu\text{g}/\text{mL}$ of free LET, free LET-PTX, LET-Lips, and LET-PTX-Lips for 24 h, then 20 μL of WST was added to each well and incubated for 4 h at 37°C. Each plate was set to a microplate reader (IN Cell Analyzer 2500HS), and the absorbance values were measured at 450 nm. Results were expressed as cell viability (%) by using equation (6). The cells, treated with medium, were considered as the control (100% viable).

$$\text{Cell viability (\%)} = \frac{\text{absorbance at 450 nm for sample}}{\text{absorbance at 450 nm for control}} \times 100\%. \quad (6)$$

2.8. Statistical Analysis. Quantitative data were expressed as mean \pm standard deviation for $n = 3$. The statistical analysis was performed using ANOVA followed by Student's t -test with $p < 0.05$ considered as statistically significant.

3. Results and Discussion

3.1. Characterizations of LET-PTX-Lips. The size and zeta potential of a nanocarrier play important roles to properly deliver drugs in the human body. Indeed, the best circulation time in the bloodstream can be obtained with particle size in between 100 and 200 nm, which are small enough to go through the filtration of the spleen and selective uptake of the liver [29, 30]. This size range allows nanoparticles to focus more efficiently on tumours. Meanwhile, the zeta potential is a good indicator to quantify the stability of nanoparticles in physiological conditions. It was reported that negative charges resulted in preventing fusion and

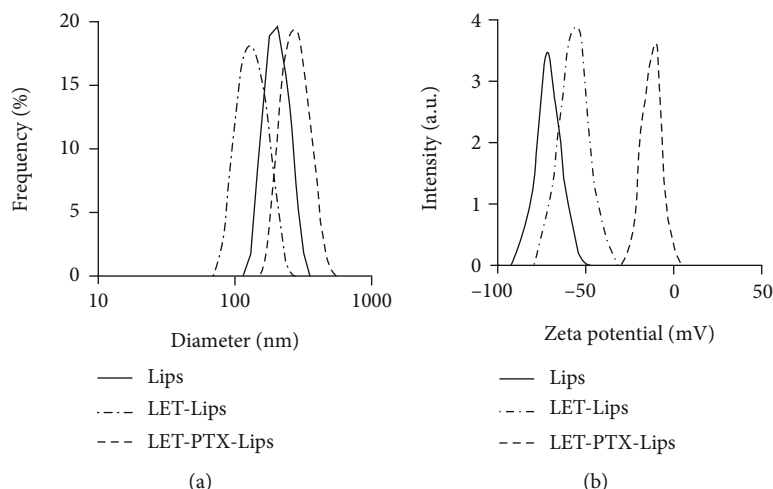


FIGURE 1: (a) Size distribution and (b) zeta potential of Lips, LET-Lips, and LET-PTX-Lips.

aggregation and also reduced the phagocytosis [31, 32]. As exposed in Figure 1(a), the DLS particle sizes of Lips, LET-Lips, and the complex LET-PTX-Lips were 169.70 ± 0.32 nm, 216.20 ± 2.47 nm, and 193.10 ± 8.70 nm, respectively. The particle size of the obtained liposomes increased due to the increase of the hydrophobic drugs mainly residing in the lipid phase, and this phenomenon has also been observed in several previous studies. For instance, Sarfraz et al. showed an increase in liposome size from 127 ± 11.14 nm with oleonic acid loaded into lipid bilayer to 225.33 ± 28.02 nm coencapsulated with doxorubicin [33]. Remarkably, the polydispersity index of all prepared samples was less than 0.5, indicating that the size repartition is quite homogeneously distributed. Otherwise, as shown in Figure 1(b), the zeta potentials of Lips, LET-Lips, and LET-PTX-Lips were -69.20 ± 0.55 mV, -54.50 ± 0.89 mV, and -13.75 ± 4.41 mV, respectively. The drastic decrease in zeta potential of LET-PTX-Lips (-13.75 ± 4.41 mV) was significantly lower than that of Lips (-69.20 ± 0.55 mV), which suggested that the stability of Lips has been reduced after codelivery of LET and PTX.

The TEM image showed that Lips and LET-PTX-Lips were spherical in terms of morphology, and the liposomal system possessed the size range which fell into the therapeutic-potential range (Figure 2). Moreover, no aggregation or fusion of Lips and LET-PTX-Lips was found, all of which were coherent with the DLS results. In light of these results, LET and PTX taken together might be encapsulated efficiently enough into Lips as spherical nanocarriers with an operational circulation in the human bloodstream.

3.2. Stability of the Synthesized Soy Lecithin Liposomes. The stability of Lips, LET-Lips, and LET-PTX-Lips was determined after a period of a week under 2–8°C conditions (Figure 3). During the studied period, all of Lips, LET-Lips, and LET-PTX-Lips presented similar effects with no significant change occurring in their size and zeta potential. The size of Lips increased to 172.70 nm, while those values of LET-Lips and LET-PTX-Lips bounded to 225.10 nm and 201.50 nm, respectively, on the last day of storage (Figure 3(a)). Similar

trends happened on the zeta potential (Figure 3(b)) that the absolute value was decreased slowly and yet still remained negative after one week for all the samples (-67.43 mV, -50.21 mV, and -12.22 mV for Lips, LET-Lips and LET-PTX-Lips, respectively). The stability of these liposomal formulations was due to the constraint of the lipid hydrolysis rate existing in the lipid bilayer at cold temperatures (2–8°C). Moreover, at temperatures below 35°C, the lipid was in the gel phase which maintained their molecular conformation as well as the geometry of the lipid bilayer [14]. Therefore, Lips, LET-Lips, and LET-PTX-Lips were proven to be stable under the storing temperatures.

3.3. Drug Loading Efficiency and In Vitro Release Profiles. It should be noted that when using lipid nanoparticles as drug carriers, it is vital to determine and understand the drug that can be loaded to the nanoparticles. In this study, EE of LET-PTX-Lips was determined to be $31.13 \pm 0.60\%$ and $50.56 \pm 1.91\%$ for LET and PTX, respectively. The difference between EE values of LET and PTX in Lips might be caused by their molecular size and weight. PTX with the significantly higher size and molecular weight could compete against LET and occupy more space inside the lipid bilayer during synthesis of LET-PTX-Lips. Besides, the lipophilic nature of the two drugs lead to competition between them for the hydrophobic space in the lipid bilayers during entrapment, as a similar case described in Shavi et al. and Deniz et al., where higher cholesterol concentrations lead to a decrease in the encapsulation efficiency of ANA and celecoxib [34, 35]. Through these results, EE of LET and PTX demonstrated the possibility of entrapping two drugs in the synthesized Lips with an important percentage of encapsulated drugs.

As shown in Figure 4, the *in vitro* drug release was conducted to analyse the behavior of LET, PTX, and LET-PTX and the capacity of Lips to control drug release. From the evaluation of results demonstrated in Figure 4, it can be established that LET and PTX exhibited similar release profiles. The fast release of free LET and free PTX was observed in 72 h (LET, $90.05\% \pm 4.6\%$; PTX, $94.79\% \pm 4.5\%$) while the late slow release is ascribed to the sustained release of the two

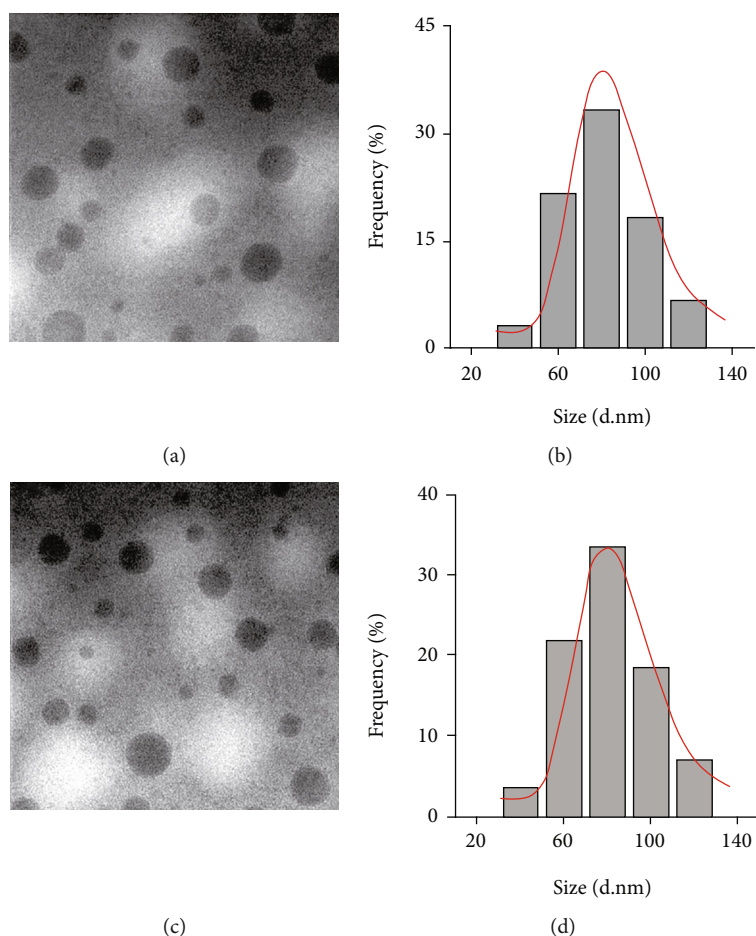


FIGURE 2: (a, c) TEM images at scale bar 200 nm and (b, d) particle size distribution of Lips and LET-PTX-Lips.

drugs from Lips. The cumulative release reached $31.70\% \pm 3.2\%$ for LET and $53.29\% \pm 3.9\%$ for PTX from Lips at 72 h. In other words, the release behavior of drugs from loaded Lips was significantly slower than that of free drugs. This was similar to the previous studies, which indicated that the prepared Lips was shown to have a sustained release profile which was consistent with most liposomal drug delivery systems [36–38].

3.4. Kinetic Models of Drug Release. The release patterns of LET and PTX from LET-PTX-Lips in Figure 4 were fitted to the zero-order model, first-order model, Higuchi model, and Korsmeyer-Peppas model to determine the highest correlation with experimental results. The *in vitro* release study was conducted in 72 h and showed about 31% and 53% of the initial LET and PTX, respectively, were released. It was reported that the first 60% of drug release was typically sufficient for determining the best fit model of the drug release [39]. Therefore, the release data of the system in 72 h was used to fit to the four models. Table 1 lists the kinetic release parameters and regression coefficients calculated from the four kinetic models.

As seen in Table 1 and Figure 5, it was found that the Higuchi and Korsmeyer-Peppas models showed a higher degree of correlation coefficients (R^2) than the two other

models. Therefore, the discussion of LET-PTX-Lips release kinetics was focused on the Higuchi and Korsmeyer-Peppas models. LET was released followed the equation $y = 3.2513x + 7.287$ ($R^2 = 0.8355$); meanwhile, PTX was released following the equation $y = 5.8797x + 6.7726$ ($R^2 = 0.9532$). These results suggested that LET and PTX released from LET-PTX-Lips followed diffusion mechanism [40]. This is reasonable because the Higuchi model describes the release of active agents that are less solubly dispersed in homogeneous matrices and submitted to a diffusing medium with the consideration of the dissolution of a lipophilic, homogeneous, and planar matrix [41]. Moreover, the Korsmeyer-Peppas model, which was developed based on the Higuchi model, is important to classify the possible release profile of active agents in dosage forms [42]. The model Korsmeyer-Peppas power law equation stated the type of diffusion based on the slope values. Both the slope values of LET and PTX in Korsmeyer-Peppas equations (n) were lower than 0.5 which implies that the two drugs released from LET-PTX-Lips may be modelled similar to a polymeric system undergoing degradation [43, 44].

3.5. Cytotoxicity Assay. The cytotoxicity of the samples was tested on MCF-7 cells via WST assay (Figure 6). For the WST test of Lips, the cells were noticed to have entirely

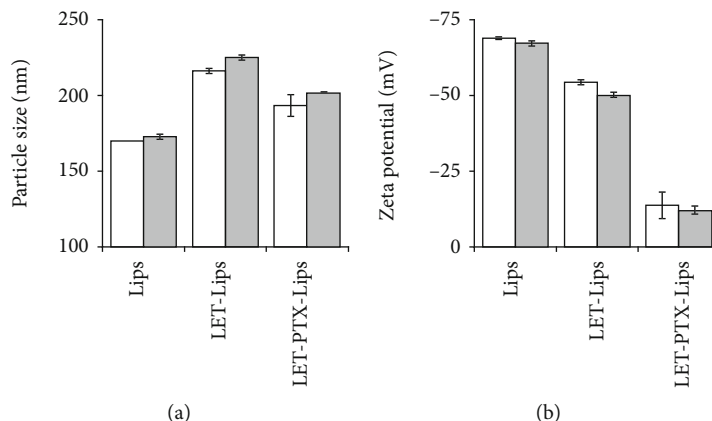


FIGURE 3: (a) Particle size distribution and (b) zeta potential of Lips, LET-Lips, and LET-PTX-Lips after preparation (blank column) and one week of storage at 2-8°C (gray column).

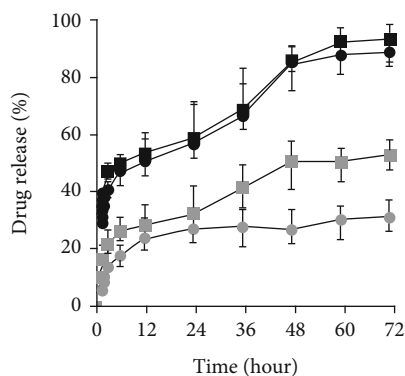


FIGURE 4: *In vitro* release profiles of free LET (black circle), free PTX (black square), and LET (grey circle) and PTX (grey square) from LET-PTX-Lips at 37°C in PBS (pH = 7.4; $n = 3$, mean \pm standard deviation).

TABLE 1: Rate constants and correlation coefficients of LET-PTX-Lips obtained through the zero-order kinetic model, first-order kinetic model, Higuchi model, and Korsmeyer-Peppas model.

Models		LET	PTX
Zero-order	k_0	0.3247	0.6248
	R^2	0.6524	0.8431
First-order	k_f	0.0018	0.0041
	R^2	0.6941	0.9047
Higuchi	k_H	3.2513	5.8797
	R^2	0.8355	0.9532
Korsmeyer-Peppas	n	0.3116	0.3502
	R^2	0.8103	0.9495

normal morphology until the highest concentration of Lips (100 $\mu\text{g}/\text{mL}$). Lips showed over 80% cell viability with concentrations ranging from 10 $\mu\text{g}/\text{mL}$ to 100 $\mu\text{g}/\text{mL}$, which indicated a potential nanocarrier with great biocompatibility in cancer treatment (Figure 6(b)). Also, the result of the WST

assay of Lips demonstrated that the cytotoxic effect seen with drug-loading Lips was solely due to the drugs which were released from the system. On the other hand, LET and LET-PTX in free forms as well as LET and LET-PTX loaded in Lips at the concentration of 1 $\mu\text{g}/\text{mL}$ of LET were treated on MCF-7 cells to evaluate the contribution of PTX to the anticancer efficacy of LET. Most cells were not damaged when exposed to free LET; meanwhile, at the same concentration of LET, free LET-PTX did not show the intact shape of cells (Figure 6(a)). Investigated under a light microscope with 20x objective lens, cells were either in the pyknosis state, in which the nucleus shrunk and the cells' content was condensed at the center or periphery, or in the karyorrhexis state, in which the nucleus was disintegrated (data not shown), indicating the progress of the intrinsic pathway of apoptosis. A similar trend occurred when comparing the cell viability between LET-Lips and LET-PTX-Lips samples: LET-Lips gave about 85% of surviving cells versus LET-PTX-Lips which gave about 78% of surviving cells (Figure 6(b)). These results showed that PTX could contribute to the increased efficacy of LET in both free forms and liposome-loaded forms. It can be explained that the free drug was uptaken by the cell via passive diffusion of a higher concentration gradient, causing the immediate toxicity in cells [45], whilst the drug loaded into the liposome was taken up via receptor-mediated endocytosis, by which the liposome vesicle fuses with the lysosome and ends up being digested. Additionally, it could be observed that the Lips coencapsulation of LET and PTX showed an obviously higher cell viability than the drugs in free forms, which was explained by the slow release that had been shown in an *in vitro* drug release study, indicating that Lips potentiated the capability of controlling drug release.

4. Conclusions

The formulation of drug delivery systems composed of Lips encapsulating LET and PTX has been working fine using the thin film hydration method. The resulting sample shows in TEM images the spherical particle with a diameter around 193 nm, staying in the required range of 100-200 nm. The

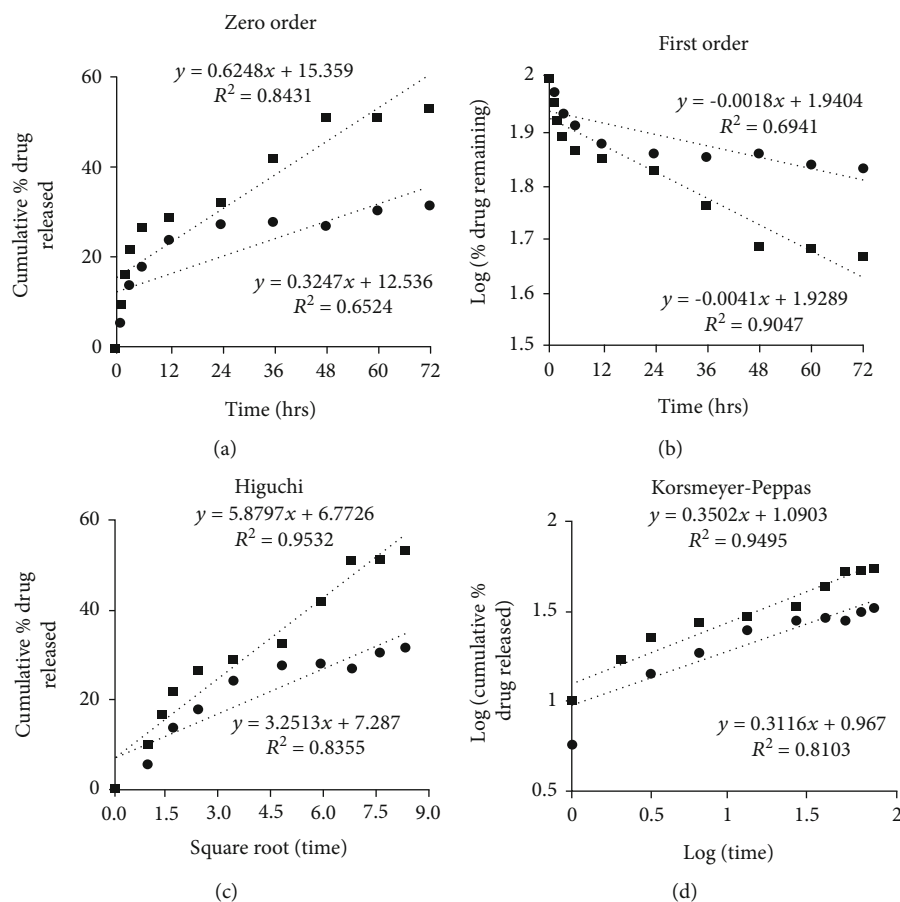


FIGURE 5: Release kinetics of Letrozole (solid circle) and Paclitaxel (solid square) from LET-PTX-Lips fitted to four kinetic models: (a) zero-order kinetic model, (b) first-order kinetic model, (c) Higuchi model, and (d) Korsmeier-Peppas model.

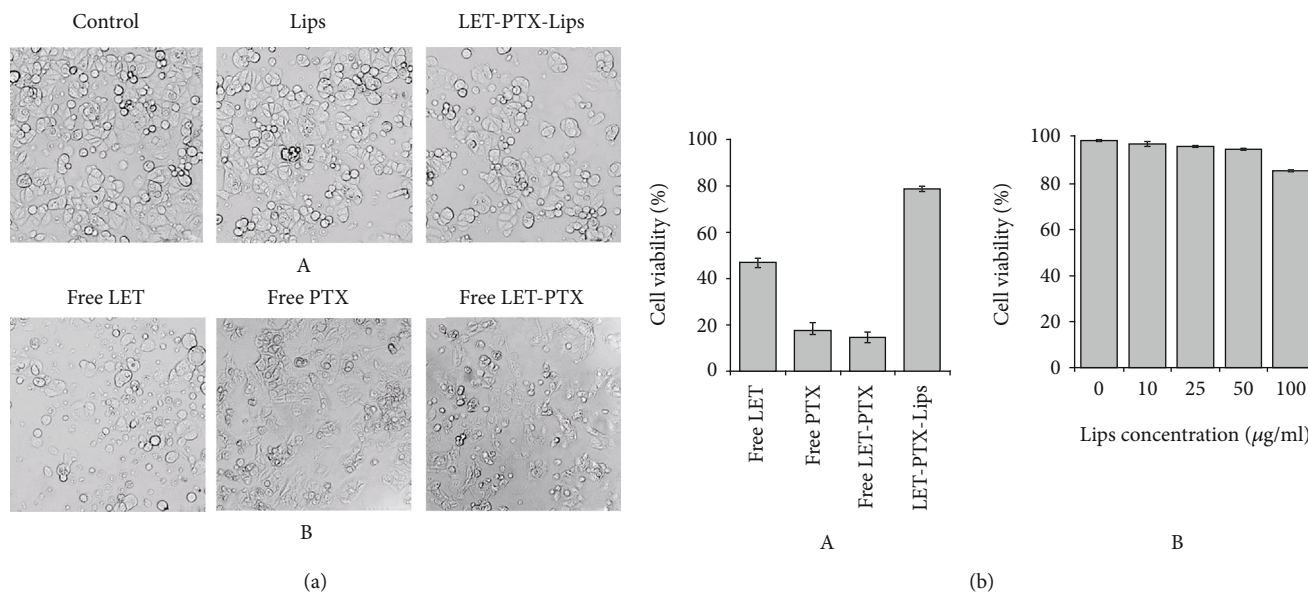


FIGURE 6: (a) Images of MCF-7 cells incubated with (A) control, free LET, and free LET-PTX at a concentration of 1 µg/mL of LET and (B) Lips (100 µg/mL), LET-Lips, and LET-PTX-Lips at a concentration of 1 µg/mL of LET (scale bar = 100 nm) for 24 h. (b) Viability of MCF-7 cells incubated with (A) free LET, free LET-PTX, LET-Lips, and LET-PTX-Lips at a concentration of 1 µg/mL of LET and (B) Lips at different concentrations for 24 h. The data represent the mean values ± the standard deviation (SD) (n = 4).

zeta potential results show particles negatively charged making the LET-PTX-Lips complex a potential candidate for *in vivo* drug release. HPLC results reveal EE of $31.13 \pm 0.60\%$ and $50.56 \pm 1.91\%$ for LET and PTX, respectively. Moreover, the release profiles which followed the Higuchi model prove the prolonged release of LET and PTX. The WST assay indicated an obvious increase of the toxicity of the complex compared to the single drug. After all these measurements and results, it seems that the prepared LET-PTX-Lips could be a potential drug delivery system with the goal of treating cancer.

Data Availability

The data used to support the findings of this study are included within the article.

Conflicts of Interest

The authors declare that there is no conflict of interest regarding the publication of this paper.

Acknowledgments

This work was supported by the Vietnam National Foundation for Science and Technology Development (NAFOSTED) under grant number 104.06-2018.320.

References

- [1] D. X. He and X. Ma, "Clinical utility of letrozole in the treatment of breast cancer: a Chinese perspective," *Oncotargets and Therapy*, vol. 9, pp. 1077–1084, 2016.
- [2] A. Yassemi, S. Kashanian, and H. Zhaleh, "Folic acid receptor-targeted solid lipid nanoparticles to enhance cytotoxicity of letrozole through induction of caspase-3 dependent-apoptosis for breast cancer treatment," *Pharmaceutical Development and Technology*, vol. 25, no. 4, pp. 397–407, 2020.
- [3] B. Alemrayat, A. Elhissi, and H. M. Younes, "Preparation and characterization of letrozole-loaded poly (d, l-lactide) nanoparticles for drug delivery in breast cancer therapy," *Pharmaceutical Development and Technology*, vol. 24, no. 2, pp. 235–242, 2019.
- [4] S. Johnston, M. Pegram, M. Press et al., *Lapatinib combined with letrozole vs. letrozole alone for front line postmenopausal hormone receptor positive (HR+) metastatic breast cancer (MBC): first results from the EGF30008 Trial*, AACR, 2009.
- [5] L. S. Schwartzberg, S. X. Franco, A. Florance, L. O'Rourke, J. Maltzman, and S. Johnston, "Lapatinib plus Letrozole as First-Line Therapy for HER-2+Hormone Receptor-Positive Metastatic Breast Cancer," *The oncologist*, vol. 15, no. 2, pp. 122–129, 2010.
- [6] A. C. Wolff, A. A. Lazar, I. Bondarenko et al., "Randomized phase III placebo-controlled trial of letrozole plus oral temsirolimus as first-line endocrine therapy in postmenopausal women with locally advanced or metastatic breast cancer," *Journal of clinical oncology*, vol. 31, no. 2, pp. 195–202, 2013.
- [7] R. S. Finn, J. P. Crown, I. Lang et al., "The cyclin-dependent kinase 4/6 inhibitor palbociclib in combination with letrozole versus letrozole alone as first-line treatment of oestrogen receptor-positive, HER2-negative, advanced breast cancer (PALOMA-1/TRIO-18): a randomised phase 2 study," *The Lancet Oncology*, vol. 16, no. 1, pp. 25–35, 2015.
- [8] F. A. Fisusi and E. O. Akala, "Drug combinations in breast cancer therapy," *Pharmaceutical nanotechnology*, vol. 7, no. 1, pp. 3–23, 2019.
- [9] D. Chen, W. Hackl, O. Ortmann, and O. Treeck, "Effects of a combination of exemestane and paclitaxel on human tumor cells *in vitro*," *Anti-Cancer Drugs*, vol. 15, no. 1, pp. 55–61, 2004.
- [10] O. C. Olson, H. Kim, D. F. Quail, E. A. Foley, and J. A. Joyce, "Tumor-associated macrophages suppress the cytotoxic activity of antimetabolic agents," *Cell Reports*, vol. 19, no. 1, pp. 101–113, 2017.
- [11] S. R. Hall, *The Anticancer Activity and Mechanisms of Action of Jadomycins in Multidrug Resistant Human Breast Cancer Cells*, Dalhousie University, 2018.
- [12] K. Samanta, S. Setua, S. Kumari, M. Jaggi, M. M. Yallapu, and S. C. Chauhan, "Gemcitabine combination nano therapies for pancreatic cancer," *Pharmaceutics*, vol. 11, no. 11, p. 574, 2019.
- [13] P. Schöffski, S. Cresta, I. A. Mayer et al., "A phase Ib study of pictilisib (GDC-0941) in combination with paclitaxel, with and without bevacizumab or trastuzumab, and with letrozole in advanced breast cancer," *Breast Cancer Research*, vol. 20, no. 1, p. 109, 2018.
- [14] N. T. T. Le, V. D. Cao, T. N. Q. Nguyen, T. T. H. Le, T. T. Tran, and T. T. Hoang Thi, "Soy lecithin-derived liposomal delivery systems: surface modification and current applications," *International Journal of Molecular Sciences*, vol. 20, no. 19, pp. 1–27, 2019.
- [15] U. Bulbake, S. Doppalapudi, N. Kommineni, and W. Khan, "Liposomal formulations in clinical use: an updated review," *Pharmaceutics*, vol. 9, no. 4, p. 12, 2017.
- [16] H. He, Y. Lu, J. Qi, Q. Zhu, Z. Chen, and W. Wu, "Adapting liposomes for oral drug delivery," *Acta Pharmaceutica Sinica B*, vol. 9, no. 1, pp. 36–48, 2019.
- [17] M. Li, C. Du, N. Guo et al., "Composition design and medical application of liposomes," *European Journal of Medicinal Chemistry*, vol. 164, pp. 640–653, 2019.
- [18] N. T. T. Le, D. T. D. Nguyen, N. H. Nguyen, C. K. Nguyen, and D. H. Nguyen, "Methoxy polyethylene glycol-cholesterol modified soy lecithin liposomes for poorly water-soluble anti-cancer drug delivery," *Journal of Applied Polymer Science*, vol. 138, p. 49858, 2020.
- [19] H. Daraee, A. Etemadi, M. Kouhi, S. Alimirzalu, and A. Akbarzadeh, "Application of liposomes in medicine and drug delivery," *Artificial cells, nanomedicine, and biotechnology*, vol. 44, no. 1, pp. 381–391, 2014.
- [20] M. Maniyar, A. Chakraborty, and C. Kokare, "Formulation and evaluation of letrozole-loaded spray dried liposomes with PEs for topical application," *Journal of Liposome Research*, vol. 30, no. 3, pp. 274–284, 2019.
- [21] A. Zajdel, A. Wilczok, K. Jelonek et al., "Cytotoxic effect of paclitaxel and lapatinib co-delivered in poly(lactide-co-poly (ethylene glycol) micelles on HER-2-negative breast cancer cells," *Pharmaceutics*, vol. 11, no. 4, p. 169, 2019.
- [22] M. S. Franco, M. C. Roque, and M. C. Oliveira, "Short and long-term effects of the exposure of breast cancer cell lines to different ratios of free or co-encapsulated liposomal paclitaxel and doxorubicin," *Pharmaceutics*, vol. 11, no. 4, p. 178, 2019.
- [23] T. L. Nguyen, T. H. Nguyen, C. K. Nguyen, and D. H. Nguyen, "Redox and pH responsive poly (amidoamine) dendrimer-

- heparin conjugates via disulfide linkages for letrozole delivery," *BioMed Research International*, vol. 2017, 7 pages, 2017.
- [24] B. Shashni and Y. Nagasaki, "Nitroxide radical-containing nanoparticles attenuate tumorigenic potential of triple negative breast cancer," *Biomaterials*, vol. 178, pp. 48–62, 2018.
- [25] T. Yang, F.-D. Cui, M.-K. Choi et al., "Liposome formulation of paclitaxel with enhanced solubility and stability," *Drug Delivery*, vol. 14, no. 5, pp. 301–308, 2008.
- [26] T. L. Nguyen, T. H. Nguyen, and D. H. Nguyen, "Development and in vitro evaluation of liposomes using soy lecithin to encapsulate paclitaxel," *International Journal of Biomaterials*, vol. 2017, 7 pages, 2017.
- [27] M. Barzegar-Jalali, K. Adibkia, H. Valizadeh et al., "Kinetic analysis of drug release from nanoparticles," *Journal of Pharmacy & Pharmaceutical Sciences*, vol. 11, no. 1, pp. 167–177, 2008.
- [28] C. G. England, M. C. Miller, A. Kuttan, J. O. Trent, and H. B. Frieboes, "Release kinetics of paclitaxel and cisplatin from two and three layered gold nanoparticles," *European Journal of Pharmaceutics and Biopharmaceutics*, vol. 92, pp. 120–129, 2015.
- [29] E. Nance and M. McKenna, "Challenges and barriers," in *Nanoparticles for Biomedical Applications*, pp. 89–107, Elsevier, 2020.
- [30] N. T. T. Le, L. P. T. Pham, D. H. T. Nguyen et al., "Liposome-based nanocarrier system for phytoconstituents," *Novel Drug Delivery Systems for Phytoconstituents*, p. 45, 2019.
- [31] N. A. Charoo, Z. Rahman, and M. A. Khan, "Nanoparticles for improvement in oral bioavailability," in *Nanoarchitectonics in Biomedicine*, pp. 371–410, Elsevier, 2019.
- [32] D. H. Surve, P. Dandekar, P. V. Devarajan, and A. B. Jindal, "Intracellular delivery: an overview," in *Targeted Intracellular Drug Delivery by Receptor Mediated Endocytosis*, pp. 3–41, Springer, 2019.
- [33] M. Sarfraz, A. Afzal, T. Yang et al., "Development of dual drug loaded nanosized liposomal formulation by a reengineered ethanolic injection method and its pre-clinical pharmacokinetic studies," *Pharmaceutics*, vol. 10, no. 3, p. 151, 2018.
- [34] G. V. Shavi, M. S. Reddy, R. Raghavendra et al., "PEGylated liposomes of anastrozole for long-term treatment of breast cancer: in vitro and in vivo evaluation," *Journal of Liposome Research*, vol. 26, no. 1, pp. 28–46, 2015.
- [35] A. Deniz, A. Sade, F. Severcan, D. Keskin, A. Tezcaner, and S. Banerjee, "Celecoxib-loaded liposomes: effect of cholesterol on encapsulation and in vitro release characteristics," *Bioscience Reports*, vol. 30, no. 5, pp. 365–373, 2010.
- [36] K. Jiang, M. Shen, and W. Xu, "Arginine, glycine, aspartic acid peptide-modified paclitaxel and curcumin co-loaded liposome for the treatment of lung cancer: in vitro/vivo evaluation," *International Journal of Nanomedicine*, vol. 13, pp. 2561–2569, 2018.
- [37] J. Meng, F. Guo, H. Xu, W. Liang, C. Wang, and X.-D. Yang, "Combination Therapy using Co-encapsulated Resveratrol and Paclitaxel in Liposomes for Drug Resistance Reversal in Breast Cancer Cells _in vivo_," *Scientific Reports*, vol. 6, no. 1, p. 22390, 2016.
- [38] L. R. Tefas, B. Sylvester, I. Tomuta et al., "Development of anti-proliferative long-circulating liposomes co-encapsulating doxorubicin and curcumin, through the use of a quality-by-design approach," *Drug design, development and therapy*, vol. 11, pp. 1605–1621, 2017.
- [39] R. Bettini, P. L. Catellani, P. Santi, G. Massimo, N. A. Peppas, and P. Colombo, "Translocation of drug particles in HPMC matrix gel layer: effect of drug solubility and influence on release rate," *Journal of Controlled Release*, vol. 70, no. 3, pp. 383–391, 2001.
- [40] C. Subal, *Modelling of Drug Release: The Higuchi Equation and its Application*, 2006, Pharmabiz. com.
- [41] M. L. Bruschi, "Mathematical models of drug release," *Strategies to modify the drug release from pharmaceutical systems*, 2015.
- [42] N. A. Peppas and B. Narasimhan, "Mathematical models in drug delivery: how modeling has shaped the way we design new drug delivery systems," *Journal of Controlled Release*, vol. 190, pp. 75–81, 2014.
- [43] J. Siepmann and N. A. Peppas, "Modeling of drug release from delivery systems based on hydroxypropyl methylcellulose (HPMC)," *Advanced drug delivery reviews*, vol. 64, pp. 163–174, 2012.
- [44] G. Singhvi and M. Singh, "In-vitro drug release characterization models," *International Journal of Pharmaceutical Studies and Research*, vol. 2, no. 1, pp. 77–84, 2011.
- [45] J. Sun, L. Jiang, Y. Lin et al., "Enhanced anticancer efficacy of paclitaxel through multistage tumor-targeting liposomes modified with RGD and KLA peptides," *International Journal of Nanomedicine*, vol. 12, pp. 1517–1537, 2017.

Research Article

Evaluation of the Cytotoxic Effect of Rutin Prenanoemulsion in Lung and Colon Cancer Cell Lines

Tran Thanh Hoai ¹, Phan Thi Yen ², Tran Thi Bich Dao ², Luu Hai Long ³,
Duong Xuan Anh ³, Luu Hai Minh ², Bui Quoc Anh ² and Nghiem Thi Thuong ¹

¹School of Chemical Engineering, Hanoi University of Science and Technology, Hanoi, Vietnam 10000

²Nhathai New Technology JSC, Hoang Mai, Hanoi, Vietnam

³Faculty of Biotechnology-Agricultural Academy, Hanoi, Vietnam

Correspondence should be addressed to Nghiem Thi Thuong; thuong.nghiemthi@hust.edu.vn

Received 27 August 2020; Revised 20 October 2020; Accepted 24 October 2020; Published 18 November 2020

Academic Editor: Anuj Kumar

Copyright © 2020 Tran Thanh Hoai et al. This is an open access article distributed under the Creative Commons Attribution License, which permits unrestricted use, distribution, and reproduction in any medium, provided the original work is properly cited.

In this work, prenanoemulsion of rutin was prepared using PEG and Tween as emulsifiers via homogenization and evaporation techniques. The particle size of rutin was investigated with high-resolution transmission electron microscopy (HR-TEM); particle size distribution and its chemical structure were analysed by nuclear magnetic resonance (NMR) and Fourier transformed infrared (FT-IR) spectroscopy. It was found that rutin in the prenanoemulsion has excellent solubility in water with the size approximately 15 nm. The chemical structure of nanorutin in prenanoemulsion was identical to that of the pure rutin. It suggested that there is no chemical modification of rutin in the prenanoemulsion. From high-performance liquid chromatography (HPLC), the amount of rutin in the prenanoemulsion was determined to be 9.27%. The cytotoxic effect of rutin in the preemulsion was investigated via *in vitro* tests to determine rutin's efficacy in A549 lung cancer cell and colon cancer cell treatment. The results demonstrated that rutin in the prenanoemulsion could inhibit A549 lung cancer cells and colon cancer cells efficiently.

1. Introduction

Rutin (3,3',4',5,7-pentahydroxyflavone-3-rhamnoglucoside) whose chemical structure is shown in Figure 1 is a flavonol, which is plentifully found in many typical plants such as passion flowers, buckwheats, black teas, and apples. It has diverse biological activities and pharmacological applications, i.e., antioxidation, antitumor, anti-inflammatory, antiviral, and low toxicity with potential clinical applications [1]. Amongst all the applications, the anticancer effect of rutin has been extensively investigated. Lin et al. reported that rutin with the dose of 120 mg/kg caused a significant reduction in the tumor size of the murine model implanted human leukemia HL-60 cells [2]. From the study on the LAN-5 neuroblastoma cell line, rutin showed the capability of decreasing levels of MYCN mRNA, the secretion of

TNF- α , and reducing BCL2 expression as well as BCL2/BAX ratio [3]. Besides, rutin also showed its effect on many other cancer cell lines such as CRC colorectal cancer cells, B16F10 lung cancer cells, and HTC liver cancer cells. It was demonstrated that rutin affected the cell capture and apoptosis processes, reducing the number of metastatic nodules and cytotoxicity [4–6]. However, rutin was slightly absorbed in the gastrointestinal tract due to the poor water solubility (0.8 mg/mL) [7]. Hence, the oral bioavailability of rutin is rather low (around 20%) [8].

Numerous approaches have been investigated to improve the bioavailability of rutin. These approaches include the preparation of nanoparticulate systems [9–13], nanophytosome [14], and cyclodextrin complexes [15, 16]. Recently, nanoparticle-based drug delivery systems have been further utilized in cancer treatment. The advantages of the nanoparticle-based drug

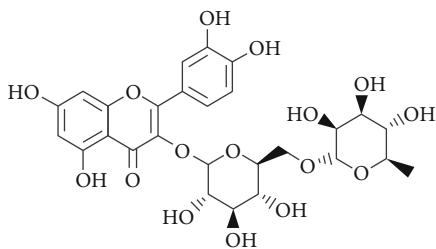


FIGURE 1: The chemical structure of rutin [26].

delivery systems are that nanoparticle drugs could be designed to achieve longer circulation time, better stability, more improved internal medicine accumulations and concentrations, and better ability of reducing the toxicity to normal tissues [17]. Nanoparticle-based drug delivery systems (such as nanoemulsion, liposomes, prenanoemulsion, niosomes, and nanoparticles) are commonly stabilized with surfactants or polymers [18]. Recently, the prenanoemulsion drug delivery system has been emerging as one of the most interesting approaches to improve the poor solubility of drugs. Prenanoemulsion is a mixture composed of surfactants, cosurfactants, and drug substances, which can form a nanoemulsion under conditions of gastrointestinal fluids and gastrointestinal motilities after the oral administration. It was noted that prenanoemulsion does not contain water and thus its physical and chemical stability lasts longer than those in nanoemulsion [19]. The formation of rutin in nanoemulsion with a particle size less than 100 nm could enhance the solubility and the absorption of drugs in the gastrointestinal tract [20]. The solubility and stability of the prenanoemulsion system closely depend on screening surfactants such as Tween-80, Labrasol, Cremophor RH 40, and Kolliphor-HS15 together with other cosurfactants, i.e., Carbitol, Transcutol-P, and polyethylene glycol- (PEG-) 200, 400, and 600 [21]. The selection of the excipients for the preparation of the prenanoemulsion as anticancer drug delivery systems must ensure that the system should have long-standing stability, a long circulation time, and the ability to increase the drug accumulation in cancer cells. Another requirement is that the system should not be toxic to normal cells.

Rutin is widely acknowledged for good solubility in Tween-80 and PEG-600 [21]. Tween-80 is a nonionic surfactant which is well known for its hydrophilicity and biodegradability. It exhibits no toxicity for cell at low concentration [22]. Previous works showed that Tween-80 has the ability to inhibit the mononuclear phagocyte systems and prolong the circulation time of the nanoparticles which then extend drug release times [23, 24]. PEG, on the other hand, is a polymer possessing hydrophilicity, biocompatibility, and nonallergenicity. It plays a role as a good stabilizer for the colloidal system [24, 25]. Therefore, in this study, Tween-80 and PEG-600 were selected as the excipients for the preparation of prenanoemulsion of rutin. To the best of our knowledge, there is few research on the formulation of rutin in the preemulsion system and its cytotoxicity on lung and colon cancers [21]. The aim of our study is to assess the cytotoxic effect of the prenanoemulsion system of rutin in lung cancer (A549) cells, colon cancer (Caco-2)

cells, and HDF human fibroblast cells. The rutin in the prenanoemulsion system containing Tween-80 and PEG-600 was prepared with the optimal formulation of substances. The efficacy in anticancer treatments and the safety of fabricated rutin prenanoemulsion were evaluated through the MTS assay. In the *in vitro* test, the lung cancer (A549) cells, colon cancer (Caco-2) cells, and HDF human fibroblast cells were treated with the rutin prenanoemulsion, pure rutin, and the excipients (mixture of Tween-80 and PEG-600), respectively.

2. Materials and Methods

2.1. Materials. Rutin was provided by Tokyo Chemical Industry Co., Ltd. (APAC). Ethanol (99.8%) and polyethylene glycol with a molecular weight of 600 g/mol (PEG-600) were supplied by the NOF Corporation of Shibuya-Ku, Tokyo. Tween-80 was provided by INEOS Oxide (Lavéra France). DMEM (Gibco), CellTiter 96® Aqueous One Solution Cell Proliferation Assay (MTS) (Promega), and fetal bovine serum (FBS) and penicillin-streptomycin (PS) were supplied by Sigma-Aldrich. All reagents were analytical grade and used as being received without further purification.

The cell lines used in the *in vitro* tests were included lung cancer (A549) cell lines, colon cancer (Caco-2) cell lines, and HDF human fibroblast cell lines provided by ATCC.

2.2. Methods

2.2.1. Preparation of the Rutin Prenanoemulsion Drug Delivery System. A solution of rutin was prepared by dissolving rutin in ethanol at the concentration of 0.02 g/mL and stirring at 400 rpm for 10 minutes at room temperature. PEG-600 and Tween-80 were then added to the solution at a ratio 10% *w/w* and 30% *w/w*, respectively. The rutin prenanoemulsion system was maintained at 60°C, mixed at 400 rpm by using a magnetic stirrer for 30 minutes, and continuously dispersed using the ultrasonicator. The prenanoemulsion system was left overnight at room temperature then homogenized for 60 minutes at a normal condition. After that, the prenanoemulsion system was evaporated for 60 minutes at 50°C to remove residual ethanol. Finally, it was stored at room temperature for further analysis.

2.3. Characterizations. The water solubility of the rutin prenanoemulsion was tested by the Tyndall effect. Rutin preemulsion dispersion and rutin dispersion were prepared by adding the same amount of the prenanoemulsion of rutin and pure rutin into two beakers containing water. The red-wavelength laser was beamed through each dispersion, and the photographs were taken.

The morphology of the rutin in the water dispersion was observed using the transmission electron microscopy (TEM) (JEOL Co., JEM-2100, Tokyo, Japan) at an acceleration voltage of 200 kV. The prenanoemulsion of rutin was dispersed in water and then dropped into a specimen. The specimen was dried in a vacuum oven before observation. The average size of the rutin nanoparticles in the suspension was also estimated.

The particle size distribution of rutin prenanoemulsion was determined by a dynamic laser scattering technique (DLS) using Horiba SZ-100. The sample was diluted with water to a suitable concentration, and the measurement was carried out at a scattering angle of 90° at room temperature three times.

The FTIR of rutin prenanoemulsion, pure rutin, PEG, and Tween-80 were recorded on the JASCO 4600 spectrometer in the range of 4000–400 cm⁻¹ with a resolution of 4 cm⁻¹. The number of scans is 64. All FTIR measurements were performed at room temperature.

The NMR measurements of samples were performed with the JEOL FT-NMR 400 MHz (Japan). The samples were dissolved in methanol-d₄ and subjected to the measurement with 128 scans. The chemical shift is referenced with the proton signal of methanol-d₄.

The amount of the rutin in the rutin prenanoemulsion was determined by the HPLC equipped with UV detected. Chromatographic conditions used the Agilent Zorbax Eclipse XDB C18 column (150 × 4.6 mm; 5 μm), ultraviolet spectrophotometer at 257 nm, and mobile phase: methanol–1% acetic acid solution (40:60, v/v). The method has a linear range of 4.97–298.47 μg/mL, limit of quantity 0.205 μg/mL, and recovery from 99.87%–102.3%.

2.4. Cell Viability Assay Test. The cell viability was determined to compare the cytotoxic of pure rutin and rutin prenanoemulsion in A549 lung cancer cells, Caco-2 colon cancer cells, and HDF human fibroblasts after the MTS assay. The cells were seeded in 96-well microtiter plates at a density of 5000 cells/well in Dulbecco's modified Eagle's medium (DMEM). The mediums were supplied with 10% fetal bovine serum (FBS) and 1% penicillin-streptomycin (PS) and were maintained in a humidified incubator containing 5% CO₂ at 37°C for 24 hours. After being seeded, the cells were treated with various pure rutin concentrations, prenanoemulsion rutin, excipients, control vehicle solution (DMSO 0.1% in phosphate buffer saline), or control solutions (culture medium without test sample and DMSO). Seventy-two hours after the treatment, 20 μL MTS was added to a culture medium, and incubation was continued at 37°C for 4 hours. The color intensity was measured at 490 nm with an ELISA microplate reader (BioTek Synergy® HT microplate reader (USA)). The experiments were performed in triplicate.

A549 lung cancer cells were incubated with multiple concentrations of samples of 30, 50, 100, 150, 200, and 300 μM.

Caco-2 colon cancer cells were incubated at various concentrations of samples of 20, 30, 50, 100, 150, 200, and 300 μM.

HDF human fibroblast cells were incubated at a range of concentrations of samples from 50 to 300 μM.

The MTS assay is based on the conversion of MTS substrate [3-(4,5-dimethylthiazol-2-yl)-5-(3-carboxymethoxyphenyl)-2-(4-sulfophenyl)-2H-tetrazolium] into MTS-formazan by the dehydrogenase respiratory enzyme in the mitochondria of living cells. The MTS-formazan solution that dissolves in the culture medium has a blue-violet color and maximizes the absorption at 490 nm. The number of living cells is directly

proportional to the formazan concentration, expressed in the solution's optical density value at 490 nm.

The percentage of living cells determined from OD490 values was obtained using the following equation:

$$\text{The percentage of living cells (\%)} = \frac{\text{OD490 (sample)} - \text{OD490 (blank)}}{\text{OD490 (control)} - \text{OD490 (blank)}} \times 100\% \quad (1)$$

2.5. Statistical Analysis. All the results were presented as ±standard error of the mean value. Statistical analysis was performed using ANOVA. A value of $p < 0.05$ was considered statistically significant.

3. Results and Discussion

3.1. Characterizations. The screening formulation of the prenanoemulsion system was usually considered involving the following factors. First, the formulation composition should be simple, safe, and compatible. Second, the formulation should have good solubility and effective droplet size after forming a microemulsion [27, 28]. The selection of the surfactant/cosurfactant mixtures was primarily considered for the homogeneity of the system. This is much related to the Hydrophilic-Lipophilic Balance (HLB) of the surfactant. The surfactants with HLB of 12–15 are good choices for the best efficiency. Tween-80 with HLB of 15 combined with PEG-600 as cosurfactant can adjust the HLB of surfactant and increase the stability of microemulsion and enhance the solubility of hydrophobic drug [29]. Therefore, the excipients, Tween-80 and PEG-600, were chosen to load rutin in the preemulsion system. Several formulations were performed to evaluate the formation of prenanoemulsion of rutin. The best results were obtained with PEG-600 and Tween-80 at a concentration of 10% w/w and 30% w/w, respectively. We used this formulation of rutin preemulsion for further studies.

The solubility of prenanoemulsion of rutin in water is assessed indirectly through dispersing of preemulsion into the water and observed the light scattered through the dispersion, that is, the Tyndall effect.

The Tyndall effect is a phenomenon which is based on the light scattering caused by particles in colloidal or suspension. This effect is employed to verify scattering ray caused by particles in the colloidal or suspension and assess the homogeneity of the solution from the scattering [30]. When the beam of light with a wavelength in the range of 630–680 nm went through liquid-containing particles with the size from 40 to 900 nm, these particles scatter the ray; thus, they become brighter spots which can be observed [30]. The image of the Tyndall effect of the two dispersions containing pure rutin and rutin in the prenanoemulsion is presented in Figure 2. The observed results indicated that rutin in the preemulsion with PEG/Tween was well dispersed in water.

The morphology of rutin particle in the prenanoemulsion is investigated and shown in Figure 3. The rutin nanoparticles had a spherical shape with a smooth surface. The rutin particles were uniform in size and shape and distributed evenly in the water emulsion. The average size of the rutin

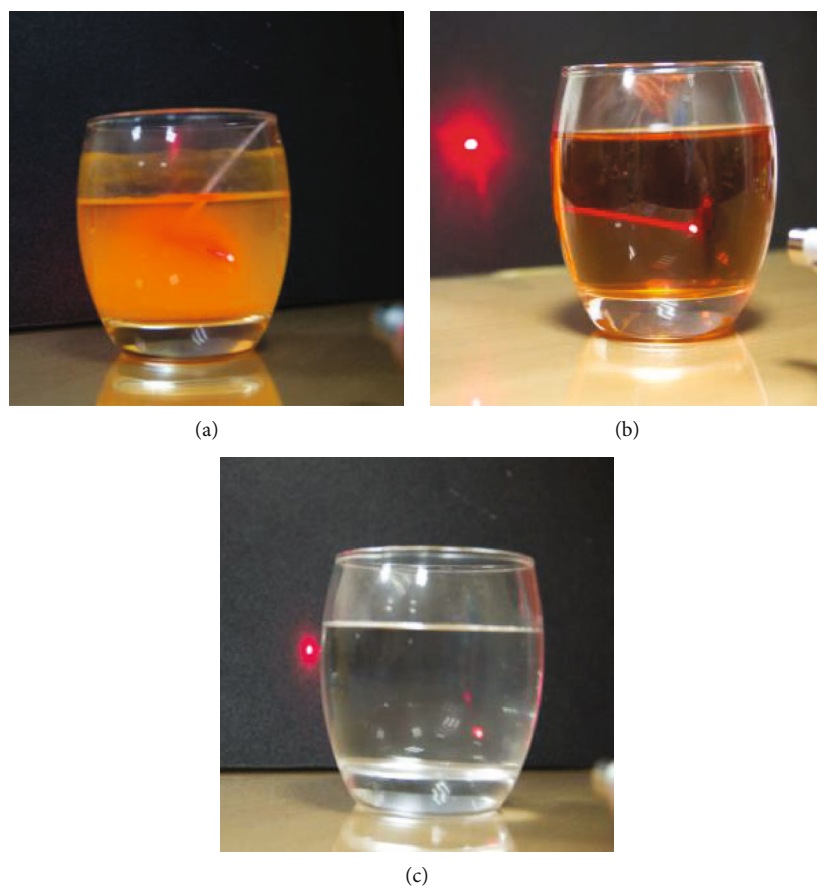


FIGURE 2: The Tyndall effect of (a) rutin in water, (b) prenanoemulsion of rutin in water, and (c) pure water.

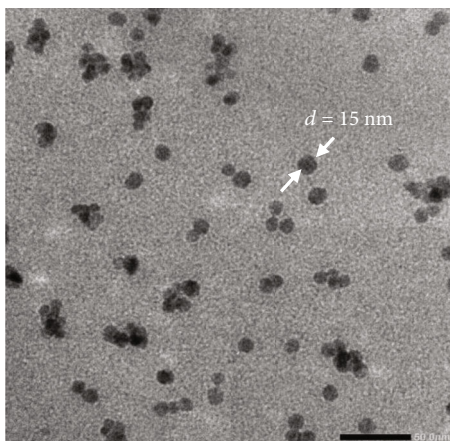


FIGURE 3: The HR-TEM image of nanorutin after dissolving the preemulsion in water.

nanoparticles was about 15 nm. Previous studies [31–33] have shown that nanoparticles with size ranging from 10 to 100 nm are suitable for drug delivery in the body. Nanoparticles with a size larger than 10 nm will not be leaked into capillaries and will then be removed by single-pass renal clearance. Nanoparticles with size less than 100 nm can escape from being captured by the macrophage in the mono-

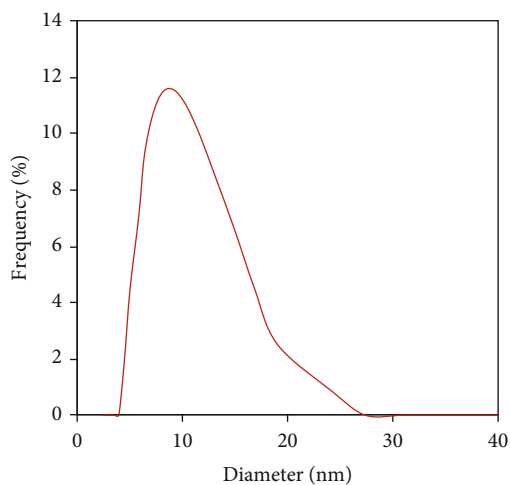


FIGURE 4: Particle size distribution profile of rutin emulsion in water.

nuclear phagocyte system and easily penetrate into the human organs, especially tumors. This is because the size of blood vessels of tumors ranges from 100 to 600 nm. Therefore, the size of nanoparticles less than 100 nm is optimal for the accumulation of the toxic compounds in the cancer cells [31–33]. Another reason is that the spherical-shaped

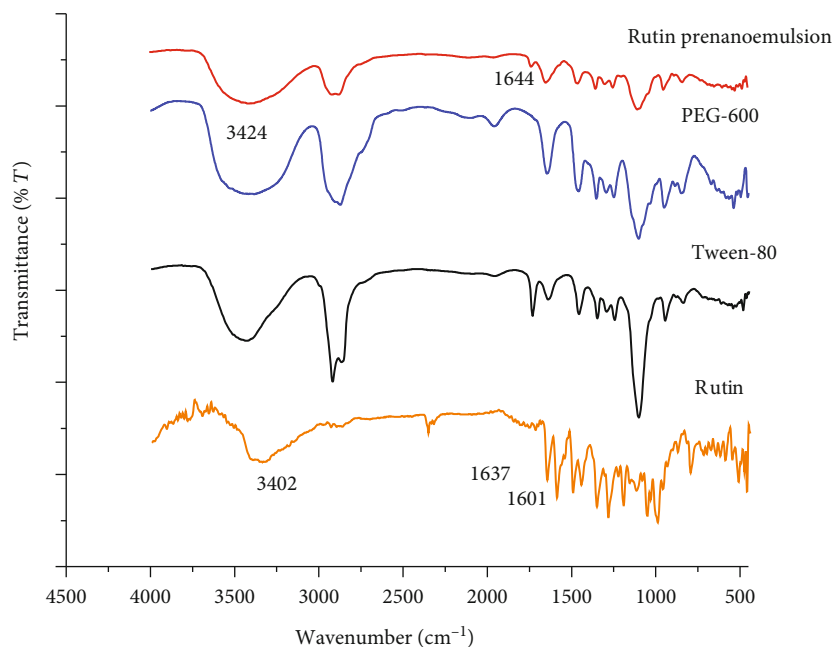


FIGURE 5: FTIR spectrum of rutin, PEG, Tween, and prenanoemulsion rutin.

nanoparticles have better mobility in the blood vessel than nanoparticles with other shapes. Thus, the prenanoemulsion of rutin as a drug delivery system was proved to be successfully fabricated. The dispersion of the prenanoemulsion system in water has generated rutin nanoparticles with the desired shapes and sizes targeted for enhancing its bioactivity.

The size distribution profile of rutin nanoemulsion is illustrated in Figure 4. It was seen that the distribution of rutin particle is unimodal with narrow distribution having a polydisperse index of 1.5. This suggested that the rutin particles are quite uniform with an average size of 8-15 nm. The size of rutin nanoparticles measured from DLS analysis was similar to that estimated from TEM.

The chemical structure of rutin and its interactions with a mixture of PEG/Tween in the prenanoemulsion with PEG/Tween was investigated by FTIR spectroscopy. Figure 5 shows the FTIR of pure rutin, rutin prenanoemulsion, PEG, and Tween. In the IR spectra of pure rutin, the absorption band at 3402 cm^{-1} was assigned to OH groups and =C-H bonds in the benzene ring. The absorption band at 1637 cm^{-1} was assigned to the vibration of the C=O bond. Additionally, the absorption band due to the C=C bond at 1601 cm^{-1} verified the presence of the aromatic alkene group. In the IR spectrum of rutin prenanoemulsion, the absorption band at 3424 cm^{-1} was ascribed for OH groups and aromatic C-H linkages. The absorption band appeared at 2980 cm^{-1} belonged to the aliphatic C-H bond in Tween and PEG. The characteristic absorption band of rutin prenanoemulsion was similar to those of PEG, and Tween and most of the characteristic bands corresponding to rutin did not appear. However, the carbonyl absorption band was shifted from 1637 cm^{-1} in the FTIR spectrum of rutin to 1644 cm^{-1} in the FTIR spectrum of rutin prenanoemulsion. The shift in the absorption band may be due to the interactions involving hydrogen bonding between rutin and PEG/Tween mixture.

The interactions probably favour the hydrophilic characteristics of rutin in the prenanoemulsion.

Figure 6 shows the $^1\text{H-NMR}$ spectrum of rutin prenanoemulsion. In the spectrum, the signal at 4.4 ppm is assigned to the proton of methanol- d_4 . The group of signals at 3.6-3.7 ppm is the characteristic peaks of PEG. The signals marked with asterisk were assigned to Tween-80. To assign thoroughly the signals of rutin, the rutin prenanoemulsion was acidified with HCl 1 M to remove substantial amount of PEG and Tween. The sedimental was collected and subjected to NMR measurement.

Figure 7 presents the $^1\text{H-NMR}$ spectra of pure rutin and rutin prenanoemulsion after the acidification. It could be seen that after the acidification, most of Tween and PEG were removed, corresponding to the significant decrease in the signal intensity of Tween and PEG. Consequently, the small signals of rutin were observed. The assignment for the signals is given in Figure 7. From the assignments, it confirmed that the chemical structure of rutin was almost preserved in the prenanoemulsion system. Therefore, we could conclude that the formation of prenanoemulsion with the PEG/Tween system did not change the chemical characteristics of rutin.

3.2. In Vitro Cytotoxicity of the Rutin Prenanoemulsion System. From the TEM result, the rutin nanoparticle was liberated into the water phase with the size of 15 nm. The efficacy of this drug delivery system could be enhanced due to the small size of active compounds of rutin. The anticancer effects and the safety of rutin prenanoemulsion were investigated through *in vitro* assay tests. In the *in vitro* assay, lung cancer cells, colon cancer cells, and human fibroblast cells were treated with various concentrations of pure rutin, rutin prenanoemulsion, and the excipients for 72 hours. The rutin concentration in the prenanoemulsion rutin sample was determined by HPLC with the UV detector. The analysis

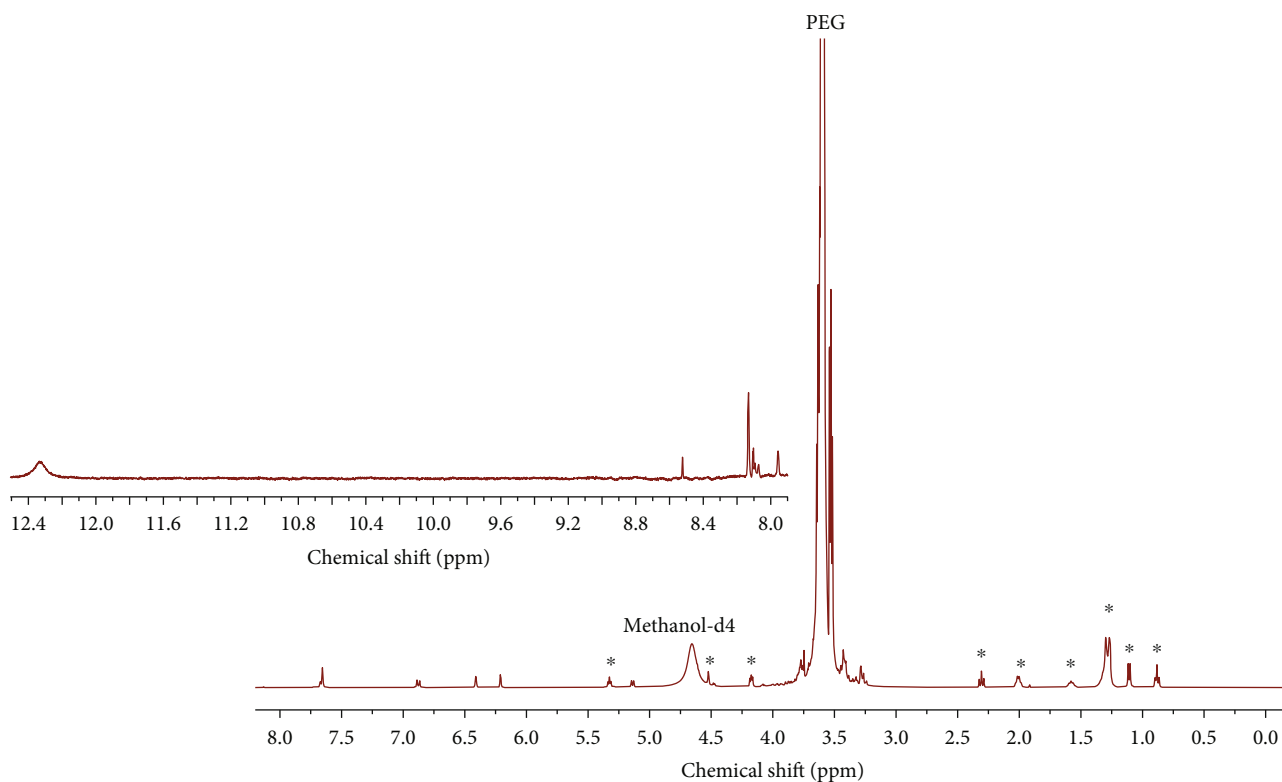


FIGURE 6: $^1\text{H-NMR}$ spectrum of rutin prenanoemulsion (400 MHz, in methanol- d_4).

showed that the amount of rutin in the prenanoemulsion is about 9.27%. From this concentration, the rutin prenanoemulsion sample was diluted to various rutin nanoemulsions with the concentration ranges from 30 to 300 μM for the MTS assay.

Figure 8 shows the MTS assay test results when lung cancer cells A549 were incubated with pure rutin, rutin nanoemulsion, and the excipients at the concentrations ranging from 30 to 300 μM for 72 hours. The reduction in the MTS test indicates the viability and the proliferation of the cells. The results in Figure 8 showed that the living rate of A549 lung cancer cell was remarkably different between the groups of wells supplemented with different reagents (control, pure rutin, rutin nanoemulsion, and excipients) and at different concentrations ($*p < 0.05$ and $^{\#}p < 0.05$). The viability of A549 lung cancer cells decreased as concentrations of nanoemulsion rutin increased in the range of 100–300 μM . At the same concentration of 150 μM , rutin nanoemulsion, pure rutin, and the excipients caused 44.04%, 4.65%, and 5.35% of cell death, respectively. At the concentration of 300 μM , the rutin nanoemulsion, pure rutin, and excipients, the rate of cell death in the wells was 99.74%, 4.4%, and 16.48%, respectively. These results revealed that at the concentration range of 150–300 μM , the rutin prenanoemulsion caused higher viability in inhibition and proliferation of the A549 lung cancer cells than pure rutin and the excipients.

The IC_{50} values of pure rutin, rutin nanoemulsion, and the excipients were determined by the rate of survival of A549 lung cancer cells after they were all treated with the studied concentrations. From the MTS assay results, the

typical equation describing the correlation between the rate of survival of A549 cells and the corresponding concentration of nanorutin was established as follows:

$$y = -83.56 \ln(x) + 471.32 (R^2 = 0.9654), \quad (2)$$

in which, x represents the concentration of nanorutin (μM) and y represents the percentage of viable cells of sample wells compared to control wells without samples.

From Equation (2), when y value was taken as 50, the IC_{50} values of nanoemulsion rutin in A549 lung cancer cell line were determined to be 154.8 μM . On the other hand, Figure 8 shows that the IC_{50} values of pure rutin and the excipients were higher than 300 μM . These results indicated that rutin prenanoemulsion can inhibit A549 lung cancer cells from concentrations higher than 150 μM ; pure rutin and the excipients are nontoxic to those cells at concentrations lower than 300 μM . In the study reported by Goitia et al., the cytotoxicity of the complex $(\text{Na}_2[\text{VO}(\text{rutin})(\text{OH})_2] \cdot 5\text{H}_2\text{O})$ in A549 lung cancer cells has the IC_{50} value of 93 μM [34]. The IC_{50} value of the complex was lower than the IC_{50} value of the rutin prenanoemulsion in this study (150 μM). These results indicate that the encapsulation of rutin in PEG/Tween plays an important role in the enhancement of cytotoxic activity. It may be explained that rutin nanoemulsion is well soluble in water. The increased hydrophilic moiety of rutin molecules in the nanoemulsion decreases the energy barrier and subsequently increases the intermembrane transfer rate by over 25-fold [35]. Therefore, the absorption of rutin in PEG into cells is higher than this of pure rutin.

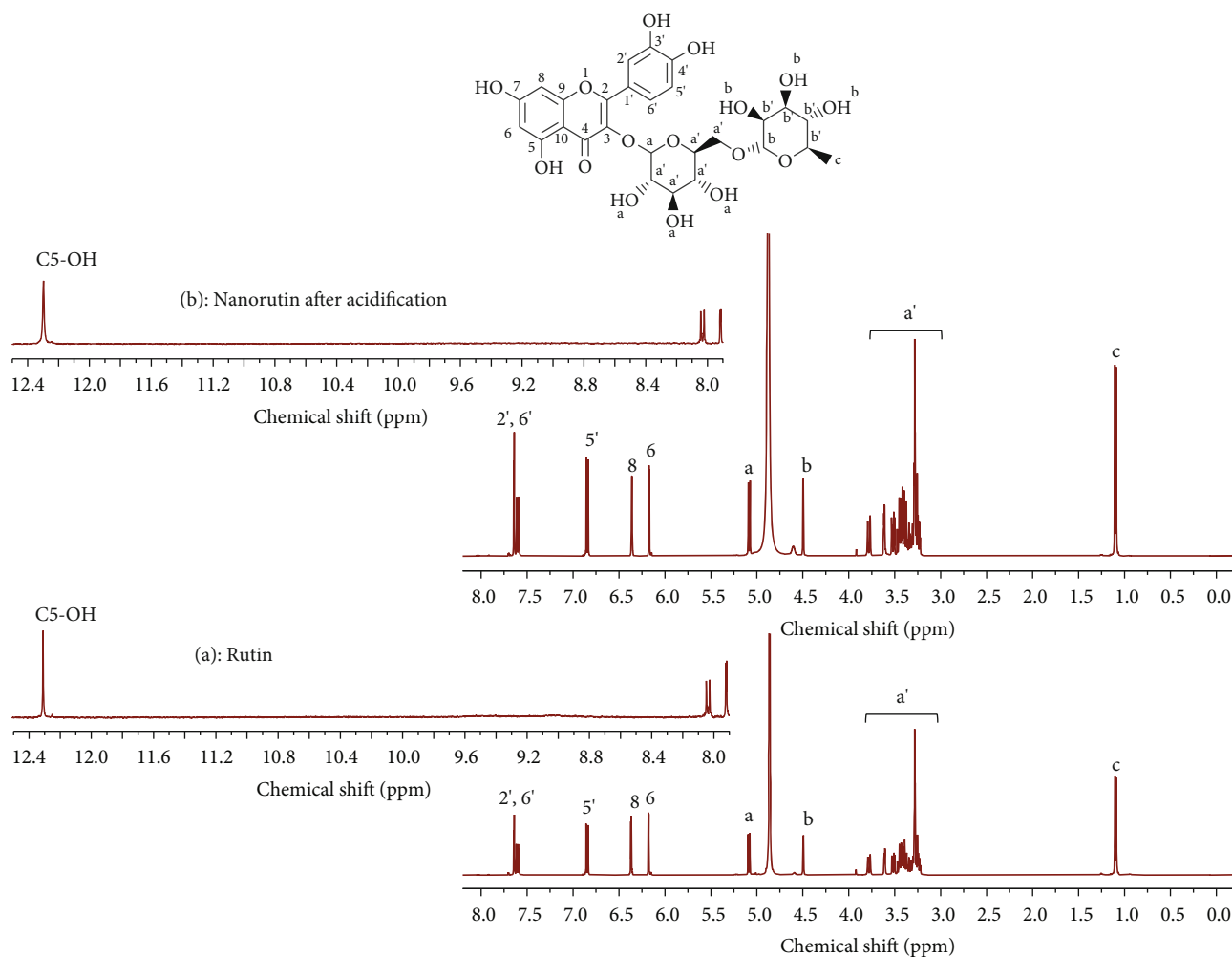


FIGURE 7: $^1\text{H-NMR}$ of (a) rutin and (b) rutin prenanoemulsion after acidification (400 MHz, in methanol- d_4).

To evaluate the cytotoxicity of the rutin prenanoemulsion in the Caco2 colon cancer cells, the assay was prepared in the same way as for the lung cancer cells. These results are shown in Figure 9.

Figure 9 shows the results of the MTS test when Caco2 colon cancer cells were incubated with pure rutin, rutin prenanoemulsion, and the excipients at concentrations in the range of 30-300 μM for 72 hours. As similar as the results observed for A549 lung cancer cell, the living rate of Caco2 colon cancer cell was drastically different between the groups of wells supplemented with different reagents (control, pure rutin, rutin prenanoemulsion, and the excipients) and at different concentrations ($*p < 0.05$ and $^{\#}p < 0.05$). The rutin prenanoemulsion had a cytotoxic effect on the viability and proliferation of Caco2 colon cancer cells within the concentration range of 150-500 μM . However, pure rutin and the excipients exhibited no cytotoxic effect in Caco2 cells at the concentration of less than 500 μM . At the concentrations of 500 μM , the rate of cell death in those wells containing rutin prenanoemulsion, pure rutin, or the excipients compared to the control wells was 82.17%, 25.45%, and 36.75%, respectively. From the results of the MTS assay, the general equation describing the correlation between the rate of

survival of Caco2 cells and the corresponding concentration of nanorutin was shown as follows:

$$y = -44.93 \ln(x) + 298.33 \quad (R^2 = 0.9949). \quad (3)$$

From Equation (3), the IC50 value of rutin prenanoemulsion in the Caco2 cell line was 251.5 μM . The IC50 value of pure rutin and the excipients was higher than 500 μM . The result demonstrated that the cytotoxic effect of pure rutin and rutin prenanoemulsion depends on the different cell lines (shown in Figure 10). ben Sghaier et al. also reported the similar results of IC50, in which the IC50 values of pure rutin in A549 lung and Caco2 cancer cells were 559.83 and 710.59 μM , respectively [36]. These results indicated that pure rutin and rutin prenanoemulsion had higher cytotoxicity to A549 cells than Caco2 cells. Rutin prenanoemulsion is more effective in treating anticancer than pure rutin. It is probably because that rutin prenanoemulsion dissolves in culture medium better than pure rutin. Moreover, with nanosize of rutin particles, i.e., 15 nm, rutin in the prenanoemulsion was easily penetrated through cell membranes. Previous studies have demonstrated that nanoparticles with

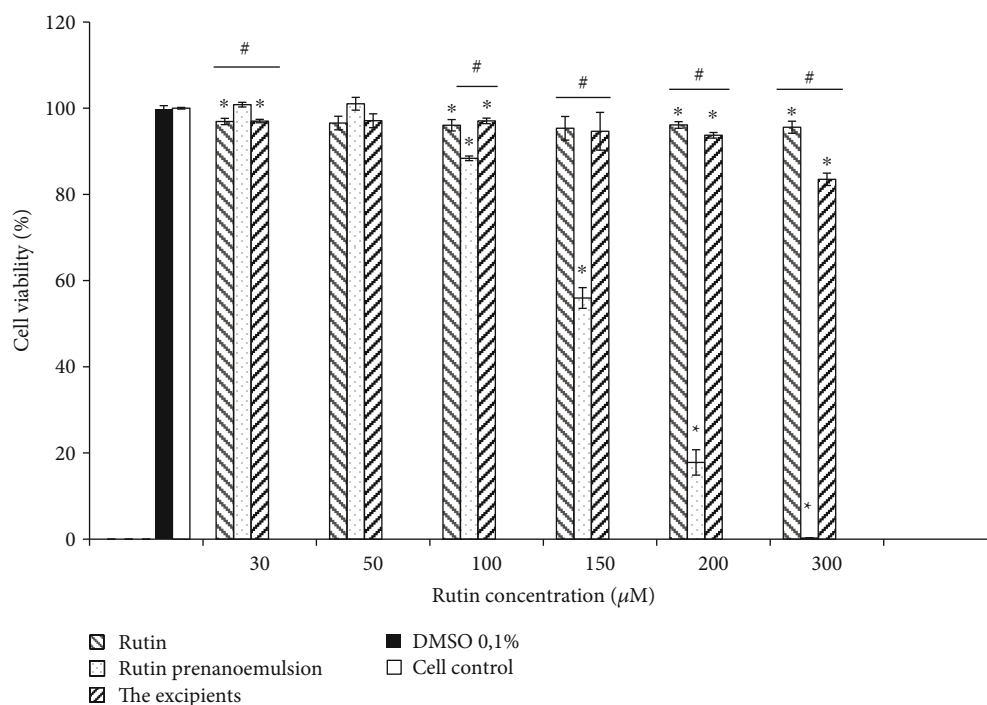


FIGURE 8: Cytotoxicity effects of pure rutin, prenanoemulsion of rutin, and excipients (PEG and Tween 80) to A549 lung cancer cells.

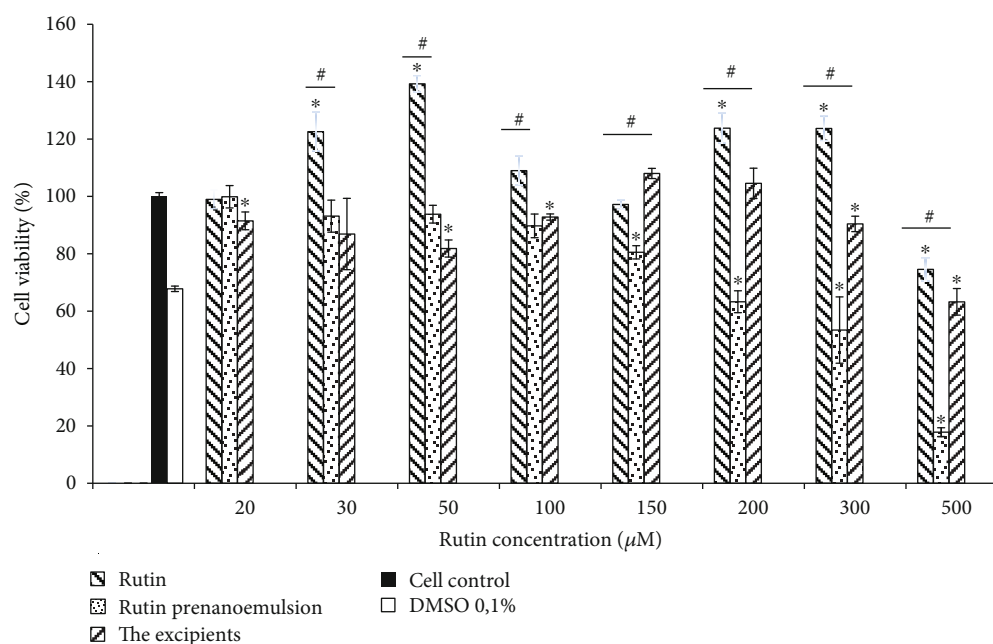


FIGURE 9: Cytotoxicity effects of pure rutin, rutin prenanoemulsion, and the excipients (PEG and Tween-80) to Caco2 colon cancer cells.

size ranging from 10 to 100 nm are ideal for the drug delivery system to intracellular internalization [37–39]. The bioavailability of rutin in preemulsion with the PEG/Tween mixture has been significantly enhanced. This is because the short-chain length of PEG causes a higher probability of nonspecific protein absorption resulting in a higher uptake of cancer

cells [40] and Tween-80 could help to increase the permeability through the cell membrane [41].

The MTS assay of rutin prenanoemulsion and the PEG/Tween mixture in healthy human fibroblast cell line was conducted to assess the safety of the rutin prenanoemulsion. Healthy human fibroblast cells were incubated with

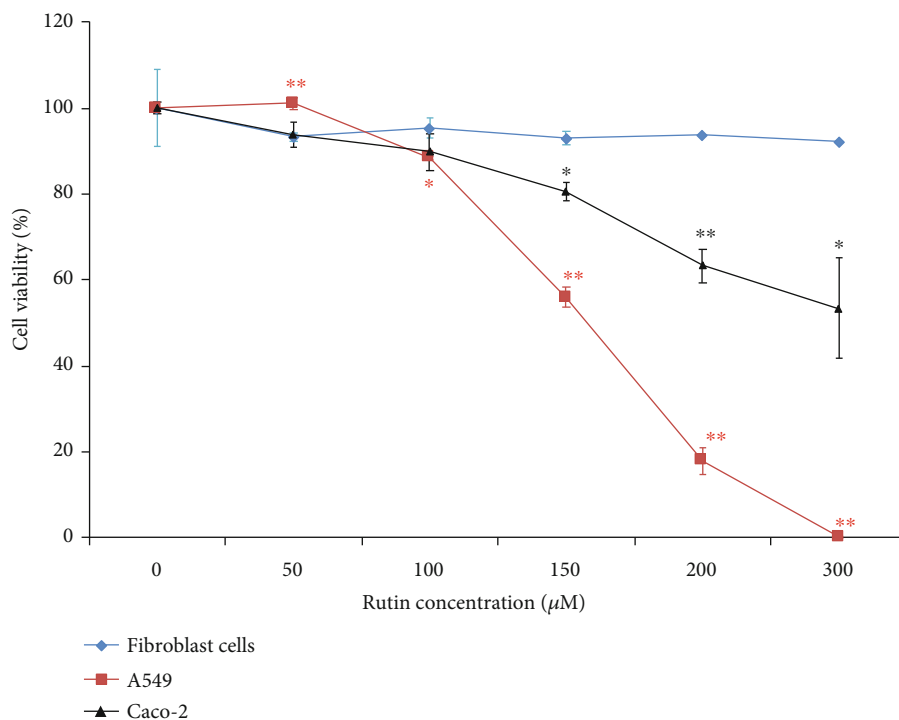


FIGURE 10: Comparing the inhibitory effect of rutin prenanoemulsion in cancer cell lines and healthy cell lines.

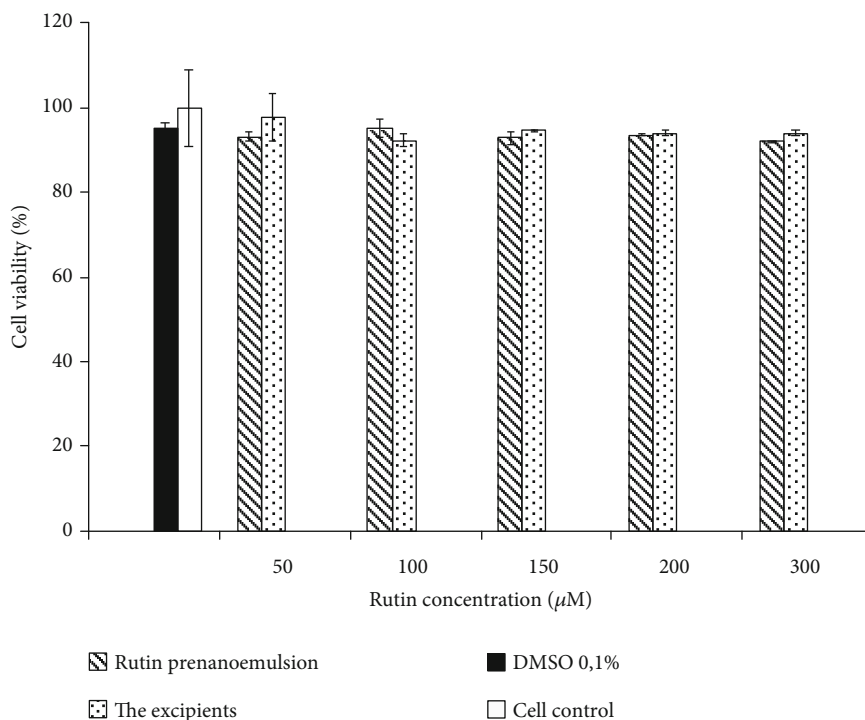


FIGURE 11: Cytotoxicity effects of rutin prenanoemulsion and the excipients (PEG-600 and Tween-80) to healthy human fibroblast cells.

prenanoemulsion rutin, the mixture PEG/Tween, control vehicle solution, or control solution at a concentration in the range 30-300 µM for 72 hours. Figure 11 shows the cytotoxicity effects of rutin prenanoemulsion and the excipi-

ents to healthy human fibroblast cells. It showed that rutin prenanoemulsion and the PEG/Tween mixture had no cytotoxic effects on fiber cells at the concentrations less than 300 µM. The results revealed that in the concentration range

of 100–300 μM , the rutin prenanoemulsion inhibited viability and proliferation of the cancer cells but showed the safety for normal cells.

4. Conclusions

The preparation of rutin prenanoemulsion was successfully made in this work. Rutin in the prenanoemulsion had a spherical shape with a size of 15 nm. The rutin prenanoemulsion showed good solubility in water. The chemical structure of rutin was unmodified in the prenanoemulsion system with PEG/Tween and subsequently preserved its bioactivities. When rutin was formed in the prenanoemulsion system with a small size, the rutin's bioactivity was enhanced double. The IC₅₀ of rutin in prenanoemulsion was determined to be 154.8 μM for A549 cancer cell treatment and 251.5 μM for Caco-2 cancer cell treatment. It reveals that the formation of the rutin prenanoemulsion has potential to become a new formulation which stabilizes the rutin and increases its bioactivity towards cancer diseases.

Data Availability

The data used to support the findings of this study are available from the corresponding author upon request.

Conflicts of Interest

The authors declare that there is no conflict of interest regarding the publication of this paper.

Acknowledgments

This research is funded by Hanoi University of Science and Technology (HUST) under Grant number T2018-PC-098. The authors would like to acknowledge Ms. Dao Thu Thao (Institute of Biotechnology, Vietnam Academy of Science and Technology) for her kind support with in vitro analysis.

References

- [1] J. B. Harborne, "Nature, distribution, and function of plant flavonoids," *Progress in Clinical and Biological Research*, vol. 213, pp. 15–24, 1986.
- [2] J. P. Lin, J. S. Yang, J. J. Lin et al., "Rutin inhibits human leukemia tumor growth in a murine xenograft model in vivo," *Environmental Toxicology*, vol. 27, no. 8, pp. 480–484, 2012.
- [3] H. Chen, Q. Miao, M. Geng et al., "Anti-tumor effect of rutin on human neuroblastoma cell lines through inducing G2/M cell cycle arrest and promoting apoptosis," *The Scientific World Journal*, vol. 2013, 8 pages, 2013.
- [4] C. Martínez Conesa, V. Vicente Ortega, M. J. Yáñez Gascón et al., "Treatment of metastatic melanoma B16F10 by the flavonoids tangeretin, rutin, and diosmin," *Journal of Agricultural and Food Chemistry*, vol. 53, no. 17, pp. 6791–6797, 2005.
- [5] J. Cristina Marcarini, M. S. Ferreira Tsuboy, R. Cabral Luiz, L. Regina Ribeiro, C. Beatriz Hoffmann-Campo, and M. Sérgio Mantovani, "Investigation of cytotoxic, apoptosis-inducing, genotoxic and protective effects of the flavonoid rutin in HTC hepatic cells," *Experimental and Toxicologic Pathology*, vol. 63, no. 5, pp. 459–465, 2011.
- [6] J. R. Araújo, P. Gonçalves, and F. Martel, "Chemopreventive effect of dietary polyphenols in colorectal cancer cell lines," *Nutrition Research*, vol. 31, no. 2, pp. 77–87, 2011.
- [7] M. R. Lauro, M. L. Torre, L. Maggi, F. de Simone, U. Conte, and R. P. Aquino, "Fast- and slow-release tablets for oral administration of flavonoids: rutin and quercetin," *Drug Development and Industrial Pharmacy*, vol. 28, no. 4, pp. 371–379, 2002.
- [8] X. Liu, D. Tang, X. Yin, Y. Gao, Y. Wei, and Y. Chen, "Pharmacokinetic study of rutin in normal and diabetic nephropathy rats," *Acta Academiae Medicinae Xuzhou*, vol. 29, pp. 708–712, 2009.
- [9] R. Mauludin, R. H. Müller, and C. M. Keck, "Development of an oral rutin nanocrystal formulation," *International Journal of Pharmaceutics*, vol. 370, no. 1–2, pp. 202–209, 2009.
- [10] J. S. Almeida, F. Lima, S. D. Ros, L. O. S. Bulhões, L. M. Carvalho, and R. C. R. Beck, "Nanostructured systems containing rutin: in vitro antioxidant activity and photostability studies," *Nanoscale Research Letters*, vol. 5, no. 10, pp. 1603–1610, 2010.
- [11] P. Kumar and A. K. P. Bhopal, "Formulation design and evaluation of rutin loaded self-emulsifying drug delivery system (SEDDs) using edible oil," *Asian Journal of Pharmaceutical and Clinical Research*, vol. 5, no. 1, pp. 76–78, 2012.
- [12] L. Banjare and N. Ghillare, "Development of biocompatible nanoparticles for sustained topical delivery of Rutin," *International journal of pharmaceutical and biological archives*, vol. 3, no. 2, pp. 326–332, 2012.
- [13] R. Kamel, M. Basha, and S. H. Abd El-Alim, "Development of a novel vesicular system using a binary mixture of sorbitan monostearate and polyethylene glycol fatty acid esters for rectal delivery of rutin," *Journal of Liposome Research*, vol. 23, no. 1, pp. 28–36, 2013.
- [14] Z. Hooresfand, S. Ghanbarzadeh, and H. Hamishehkar, "Preparation and characterization of rutin-loaded nanophytosomes," *Pharmaceutical Sciences*, vol. 21, no. 3, pp. 145–151, 2015.
- [15] K. V. Sri, A. Kondaiyah, J. V. Ratna, and A. Annapurna, "Preparation and characterization of quercetin and rutin cyclodextrin inclusion complexes," *Drug Development and Industrial Pharmacy*, vol. 33, no. 3, pp. 245–253, 2008.
- [16] T. A. Nguyen, B. Liu, J. Zhao, D. S. Thomas, and J. M. Hook, "An investigation into the supramolecular structure, solubility, stability and antioxidant activity of rutin/cyclodextrin inclusion complex," *Food Chemistry*, vol. 136, no. 1, pp. 186–192, 2013.
- [17] G. K. In and J. Nieva, "Emerging chemotherapy agents in lung cancer: nanoparticles therapeutics for non-small cell lung cancer," *Translational Cancer Research*, vol. 4, no. 4, pp. 340–355, 2015.
- [18] G. Wang and H. Uludag, "Recent developments in nanoparticle-based drug delivery and targeting systems with emphasis on protein-based nanoparticles," *Expert Opinion on Drug Delivery*, vol. 5, no. 5, pp. 499–515, 2008.
- [19] E. A. Mahmoud, E. R. Bendas, and M. I. Mohamed, "Preparation and evaluation of self-nanoemulsifying tablets of carvedilol," *AAPS PharmSciTech*, vol. 10, no. 1, pp. 183–192, 2009.
- [20] C. W. Pouton, "Formulation of poorly water-soluble drugs for oral administration: physicochemical and physiological issues and the lipid formulation classification system," *European Journal of Pharmaceutical Sciences*, vol. 29, no. 3–4, pp. 278–287, 2006.

- [21] M. Ahmad, Sahabjada, J. Akhtar et al., "Development of a new rutin nanoemulsion and its application on prostate carcinoma PC3 cell line," *EXCLI Journal*, vol. 16, pp. 810–823, 2017.
- [22] G. Kaur and S. K. Mehta, "Developments of polysorbate (Tween) based microemulsions: preclinical drug delivery, toxicity and antimicrobial applications," *International Journal of Pharmaceutics*, vol. 529, no. 1-2, pp. 134–160, 2017.
- [23] N. Watrous-Peltier, J. Uhl, V. Steel, L. Brophy, and E. Merisko-Liversidge, "Direct suppression of phagocytosis by amphiphatic polymeric surfactants," *Pharmaceutical Research*, vol. 9, no. 9, pp. 1177–1183, 1992.
- [24] X. Tao, Y. Li, Q. Hu et al., "Preparation and drug release study of novel nanopharmaceuticals with polysorbate 80 surface adsorption," *Journal of Nanomaterials*, vol. 2018, Article ID 4718045, 2018.
- [25] M. F. Tai, C. W. Lai, and S. B. Abdul Hamid, "Facile synthesis polyethylene glycol coated magnetite nanoparticles for high colloidal stability," *Journal of Nanomaterials*, vol. 2016, Article ID 8612505, 7 pages, 2016.
- [26] S. Georgeta, P. Pana, H. Tunde, and B. Sanda, "The isolation and identification of rutin from pharmaceutical products. An. Univ. Oradea Fasc," in *Ecotoxicol. Zooteh. Tehnol. Ind*, pp. 109–113, Aliment, 2016.
- [27] V. B. Borhade, H. A. Nair, and D. D. Hegde, "Development and characterization of self-microemulsifying drug delivery system of tacrolimus for intravenous administration," *Drug Development and Industrial Pharmacy*, vol. 35, no. 5, pp. 619–630, 2009.
- [28] S.-x. Cui, S.-f. Nie, L. Li, C.-g. Wang, W.-s. Pan, and J.-p. Sun, "Preparation and evaluation of self-microemulsifying drug delivery system containing vinpocetine," *Drug development and industrial pharmacy*, vol. 35, no. 5, pp. 603–611, 2009.
- [29] G. Eccleston, J. Swarbrick, and J. Boylan, *Encyclopedia of Pharmaceutical Technology*, Swarbric I, 1994.
- [30] C. Pang, J. Y. Jung, J. W. Lee, and Y. T. Kang, "Thermal conductivity measurement of methanol-based nanofluids with Al₂O₃ and SiO₂ nanoparticles," *International Journal of Heat and Mass Transfer*, vol. 55, no. 21-22, pp. 5597–5602, 2012.
- [31] H. Maeda and Y. Matsumura, "Tumorotropic and lymphotropic principles of macromolecular drugs," *Critical Reviews in Therapeutic Drug Carrier Systems*, vol. 6, no. 3, pp. 193–210, 1989.
- [32] F. Yuan, M. Dellian, D. Fukumura et al., "Vascular permeability in a human tumor xenograft: molecular size dependence and cutoff size," *Cancer Research*, vol. 55, no. 17, pp. 3752–3756, 1995.
- [33] H. Maeda, "Macromolecular therapeutics in cancer treatment: the EPR effect and beyond," *Journal of Controlled Release*, vol. 164, no. 2, pp. 138–144, 2012.
- [34] H. Goitia, P. Quispe, L. G. Naso et al., "Interactions of rutin with the oxidovanadium (iv) cation. Anticancer improvement effects of glycosylated flavonoids," *New Journal of Chemistry*, vol. 43, no. 45, pp. 17636–17646, 2019.
- [35] J. R. Silvius and M. J. Zuckermann, "Interbilayer transfer of phospholipid-anchored macromolecules via monomer diffusion," *Biochemistry*, vol. 32, no. 12, pp. 3153–3161, 2002.
- [36] M. b. Sghaier, A. Pagano, M. Mousslim, Y. Ammari, H. Kovacic, and J. Luis, "Rutin inhibits proliferation, attenuates superoxide production and decreases adhesion and migration of human cancerous cells," *Biomedicine & Pharmacotherapy*, vol. 84, pp. 1972–1978, 2016.
- [37] H. S. Choi, W. Liu, P. Misra et al., "Renal clearance of quantum dots," *Nature Biotechnology*, vol. 25, no. 10, pp. 1165–1170, 2007.
- [38] G. Gaucher, M. H. Dufresne, V. P. Sant, N. Kang, D. Maysinger, and J. C. Leroux, "Block copolymer micelles: preparation, characterization and application in drug delivery," *Journal of Controlled Release*, vol. 109, no. 1-3, pp. 169–188, 2005.
- [39] A. Aderem and D. M. Underhill, "Mechanisms of phagocytosis in macrophages," *Annual Review of Immunology*, vol. 17, no. 1, pp. 593–623, 1999.
- [40] C. Cruje and D. Chithrani, "Polyethylene glycol density and length affects nanoparticle uptake by cancer cells," *Journal of Nanomedicine Research*, vol. 1, no. 1, 2014.
- [41] H. Riehm and J. L. Biedler, "Potentiation of drug effect by Tween 80 in Chinese hamster cells resistant to actinomycin D and daunomycin," *Cancer Research*, vol. 32, no. 6, pp. 1195–1200, 1972.

Review Article

Therapeutic Nanomaterials for Neurological Diseases and Cancer Therapy

Kankai Wang ¹, **Xiaohong Zhu** ¹, **Enxing Yu** ¹, **Priyanka Desai**,² **Hao Wang**,¹
Chun-li Zhang ^{1,3}, **Qichuan Zhuge** ¹, **Jianjing Yang** ¹ and **Jiangnan Hu** ^{1,4}

¹Zhejiang Provincial Key Laboratory of Aging and Neurological Disorder Research, Department of Neurosurgery, The First Affiliated Hospital of Wenzhou Medical University, Wenzhou, China

²Department of Microbiology, Immunology and Genetics, University of North Texas Health Science Center, Fort Worth, Texas 76107, USA

³Department of Molecular Biology, University of Texas Southwestern Medical Center, 6000 Harry Hines Blvd, Dallas, TX 75390-9148, USA

⁴Department of Pharmaceutical Sciences, University of North Texas Health Science Center, Fort Worth, Texas 76107, USA

Correspondence should be addressed to Qichuan Zhuge; zhugeqichuan@vip.163.com, Jianjing Yang; yangjianjing2@163.com, and Jiangnan Hu; hu.jiangnan@hotmail.com

Received 11 April 2020; Accepted 3 August 2020; Published 25 September 2020

Guest Editor: Garima Agrawal

Copyright © 2020 Kankai Wang et al. This is an open access article distributed under the Creative Commons Attribution License, which permits unrestricted use, distribution, and reproduction in any medium, provided the original work is properly cited.

In the recent decade, nanomedicine and nanotechnology have been broadly developed leading to a significant advancement in biomedical research as well as clinical practices. The application of several functionalized nanomaterials on the molecular and cellular levels has yielded a lot of promising progresses in various fields of regenerative medicine including disease diagnosis, combinational cell therapy, tissue engineering, and drug and gene delivery. In this review, we will summarize the recent approaches of nanoscale materials utilized in neurological diseases and cancer therapy, with highlights on the most current findings and future prospects of diverse biomedical nanomaterials for tissue regeneration, drug innovations, and the synthesis of delivery system.

1. Introduction

Nanomedicine is a promising field that uses nanosized (10–100 nm) materials to facilitate the diagnosis and treatment of diseases. These nanomaterials with being used as a drug are also used as a carrier, a scaffold, or an imaging agent [1–3]. In common, all these applications could benefit from the extraordinary properties of nanomaterials, such as high specific surface area, transformable shape and size, and tunable chemical reactivity. A high surface area gives nanomaterials a huge adsorption capacity to load various molecules of a certain density like drugs, proteins, genes, and metal ion for the drug delivery, targeting ability, or disease interventions. In addition, shape (sphere, rod, wire, fiber, tube, etc.) and size can also influence the characteristics of nanomaterials [4, 5]. All these clues indicate that nanomaterials

possess an ever-changing capacity, enabling them to adapt to different application environments.

Neurological diseases and cancer are affecting approximately billions of people worldwide irrespective of age, sex, education, or income. Neurological diseases, including Alzheimer's (AD), Parkinson's (PD), and stroke, have caused tremendous pressure on human health. Not only is the pathogenic mechanism still unclear, the special anatomical location of the brain and its criticality also make few drugs safe to achieve therapeutic effects. The blood-brain barrier (BBB) is obviously one of the key barriers. It prevents most drugs from freely entering and leaving the brain, but its integrity is vital to the safety of the central nervous system. Therefore, we can only try to bypass or cross this barrier in certain ways without destroying the BBB. Drugs based on nanomaterials are one of the promising ways to realize this idea. In

addition, specially designed nanomaterials can also improve the thrombolytic process of ischemic stroke and the effect of stem cell transplantation. Similarly, in cancer treatment, nanomaterials rely on their unique advantages to accurately target some biotoxic drugs to cancer tissues without causing damage to normal tissues [6].

Currently, a wide variety of nanomaterials have been tested in neurological diseases and tumors, including liposomes, micelles, polymeric nanomaterials, carbon nanotubes, quantum dots, and metallic nanomaterials. Each of them shows great promise in clinical applications, although there are still many shortcomings to be resolved. Several nanomaterials, including liposomal vincristine, liposomal irinotecan, PEGylated IFN beta-1a, and PEGylated factor VIII, have been approved by the US FDA, or in the FDA clinical trial processes [7] which signify the development of nanomaterials and their journey from lab to bedside. In this review, we will focus on the application of nanomedicine in neurological diseases and cancer.

2. Therapeutic Nanomaterials for Neurological Diseases

2.1. Nanomaterial for Neurodegeneration. Neurodegenerative diseases such as Alzheimer's (AD), Parkinson's (PD), and amyotrophic lateral sclerosis (ALS) generally have a long pathological damage process, which causes inestimable harm to the patients and their families [8]. Since the 1990s, with the continuous maturity of nanotechnology, the technical barriers to nanomaterial research have disappeared [9]. In the studies of neurodegenerative diseases, nanomaterials have gradually entered the field of vision for researchers. Various nanomaterials including lipid-based nanomaterials (liposomes, solid lipid nanoparticle (SLN)), polymeric nanomaterials (micelle, dendrimer, nanocapsule, and nanosphere), and inorganic nanomaterials have been used for research.

At present, the research direction of nanomaterials in neurodegenerative diseases is mainly focused on drug delivery, maintaining drug concentration, and early accurate diagnosis and treatment of diseases based on the characteristics of nanomaterials. For example, lipid-based nanomaterials and polymeric nanomaterials showed great biocompatibility and membrane penetrating power [10, 11]. They have significant advantages over traditional drugs in their ability to cross the blood-brain barrier (BBB), along with the slow and controlled release of the drug. In the research of PD, the use of poly lactide-co-glycolide (PLGA) as a controlled release shell for levodopa or neurotrophic factors has been studied by researchers for more than 20 years [12–14]. Gold nanomaterials, carbon nanotubes, and other inorganic nanomaterials are easy to shape and transform and can be stably identified by imaging and laboratory methods. An interesting study published in 2017 pointed out that the BBB permeability of gold nanomaterials is closely related to their shape; the size with 20 nm circular particles could achieve the strongest penetration [15]. Nowadays, with the development of imaging science, various studies on the enhancement of imaging performance of gold nanomaterials have emerged endlessly. Some research groups demonstrated that dopamine could

enhance Raman spectroscopic scattering on the surface of self-assembled gold nanomaterials, making it possible to monitor dopamine levels in the brain [16]. The applications of various nanomaterials in the treatment of neurodegenerative diseases were exhibited in Table 1 [17].

2.2. Nanomaterials for Neuroprotection. Stroke is the leading cause of death and disability around the world [49–51]. 87% of cases are ischemic stroke, caused by cerebral vascular embolism. However, there are no more effective treatments in clinical practice, except for tissue plasminogen activator-(tPA-) mediated thrombolytic or mechanical thrombectomy within the prescribed time [52, 53]. Currently, nanomaterials are considered to have great potential in the field of stroke treatment [54, 55]. Three research directions attract the most attention: (i) construction of safer and more efficient tPA-coated nanomaterials, (ii) antioxidants delivered through nanomaterials to reduce reperfusion injury, and (iii) generation of neuroprotective nanoscale exosomes.

Novel tPA-coated nanomaterials have been reported multiple times in the thrombolysis studies. Various kinds of structures and materials were applied in such researches. Shear- [56, 57], sound- [58–61], light- [62], and magnetic- [63, 64] sensitive nanomaterials were designed to improve the thrombolytic efficiency of tPA and reduce its side effect by changing the external physical environment. A previous study in our lab demonstrated that nickel-nanorod-composed nanomotors could be used as an independent input to strengthen the efficacy of tPA in a mouse embolism model [63]. Later on, we synthesized tPA-coated Fe₃O₄ nanorods, which could be accurately targeted at the thrombus site under the guidance of a magnetic field. Fascinatingly, a mechanically rotated force could be created in an external rotational magnetic field, which not only provides physical strength to break down the clot but also allows more tPA to be delivered at the blood clot and create better penetration; as such, the plasminogen can be bound to a new site to enhance the effect of chemical thrombolysis; significant enhancement was both achieved in vitro [64] and in vivo [65] ischemic stroke mouse model studies. Similarly, nanomaterial functionalized methods have also been used to improve the targeting of tPA therapy. A recent study, conducted by Chauvierre et al., demonstrated that tPA-fucoidan-coated nanomaterials were able to bind the P-selectin of activated platelets in thrombus due to the nanomolar affinity between fucoidan and P-selectin. As a result, the therapeutic dose and hemorrhagic complications of tPA were dramatically reduced, and the time window of tPA treatment could be much wider. However, the cytotoxicity and systemic side effects of these nanomaterials are still a big challenge [66].

Reperfusion injury is caused by the free radicals like reactive oxygen species (ROS), reactive nitrogen species (RNS), and nitric oxide (NO) from injured cells, inflammatory cells, and endothelial cells that are stimulated when blood is restored in ischemic brain tissue [67, 68]. However, the direct use of free radical scavengers has not been reported to be able to achieve pleasant clinical results. To overcome these limitations, scientists shifted the gear to synthesize all kinds of

TABLE 1: List of the application of nanomaterials for the neurodegenerative diseases.

Type	Nanomaterials	Drugs delivered	Disease	Findings	Disadvantages	References
Lipid-based nanomaterials	Prp CsiRNA-RVG-9r-liposomes	Prp CsiRNA RVG-9rPrp Cs	Neurodegenerative protein misfolding diseases (NPMD)	Increase delivery efficiency, prolong half-life of drug in peripheral circulation, and increase BBB passage rate.	In animal experiments, mice treated with nanomaterials have a certain probability of causing type III acute allergic reaction.	[18]
	Fus-liposomes-rhFGF20	rhFGF20	Parkinson's disease (PD)	Extend drug half-life, high encapsulation rate, increase BBB penetration ability, slow-release drugs, targeting, high biocompatibility.	Not mentioned.	[19]
	RVG29-liposomes	N-3,4-Bis(pivaloyloxy)-dopamine	PD	High BBB penetrability, high biocompatibility, striatum nigra targeting, drug sustained release.	Not mentioned.	[20]
	PEG-liposomes-MBs	GDNF+Nurr1	PD	Ultrasound-guided ability, ultrasound-guided BBB penetration ability, sustained release, and extended drug half-life.	Poor BBB penetration.	[21]
	RMP7-If-PEG-liposomes	Quercetin	Alzheimer's disease (AD)	High BBB penetration ability, SK-N-MC cell targeting, drug sustained release.	May be able to induce inflammation.	[22]
	NGF-SM-ApoE-liposomes	Nerve growth factor, surface serotonin modulator, ApoE	AD	Maintain NGF activity, high biocompatibility, high BBB permeability, A β 1-42 and SK-N-MC cell targeting, sustained release of contents.	Not mentioned.	[23]
	Nanomicellar system (SANS)	L-DOPA	PD	Autonomous formation, easy to manufacture, epidermal permeability, drug sustained release.	Lack of targeting.	[24]
	LD crystalsomes (micellar)	L-DOPA	PD	Autonomous formation, easy to manufacture, drug sustained release, good biocompatibility, higher drug delivery efficiency.	The biological toxicity is not clear.	[25]
	Pluronic P85/F68 micelles	Baicalein	PD	Self-forming, stable character suitable for oral administration, sustained release, enhance content of crossing BBB capacity, enhance content of cell accumulation.	Weak BBB permeability, may cause damage to the structure and function of mitochondria.	[26]
	Polymeric nanomaterials	Mixed-shell polymeric micelle (MSPM)	None	A β deposits are targeted, A β deposits have strong affinity, reduce the production of proinflammatory factors, have good BBB permeability and strong biocompatibility.	Longer metabolic time.	[27]
	C(NCAM-C3)I(TPP)-N(nano)M(micelle)	Resveratrol	Automated assembly, good BBB permeability, high encapsulation efficiency, mitochondrial targeting, cumulative, drug sustained release, reduce expression of proinflammatory factors.	Longer metabolic time.	[28]	
	Micelle	Curcumin	Automatic formation, good drug encapsulation rate, drug sustained release, BBB permeability.	Not targeted itself.	[29]	
	PAMAM dendrimers	Carbamazepine	Improve the solubility of the package, increase the stability of the package, good drug packaging ability,		[30]	

TABLE 1: Continued.

Type	Nanomaterials	Drugs delivered	Disease	Findings	Disadvantages	References
				reduce the package of peripheral and cellular toxicity, good biocompatibility.	Not resistant to acid and alkali, high concentration, easy to kill, drug sustained release ability is poor.	
	G4HisMal-dendrimers	Boc-L-histidine	AD	High BBB permeability, good biocompatibility, $A\beta$ (1–40) targeting.	Not mentioned.	[31]
	Lactoferrin coupled PAMAM dendrimers (PAMAM-If)	Memantine	AD	Drug sustained release, controlled release, extended drug half-life, good encapsulation ability, high drug delivery efficiency, good BBB penetration, and brain targeting.	Have some blood toxicity.	[32]
	Phosphorus dendrimers	Phosphorus	PD	Some anti-HIV ability, inhibition of -SYN fibrosis.	Hematotoxicity.	[33]
	Carbosilane dendrimers	None	PD	Inhibits ASN fibrillation, reduces ROS, and protects nerve cells.	Not mentioned.	[34]
	Dopamine-loaded PLGA nanomaterials	Dopamine	PD	Prolonged half-life, slow-release, controlled-release, decreased peripheral circulation toxicity, good biocompatibility, decreased Ros, striatum targeting, BBB permeability.	Cause inflammation in the targeted area.	[35]
	Collagen-coated PLGA	None	PD	Good cell adhesion, good biocompatibility, and certain ability to promote cell growth.	Not mentioned.	[36]
	PLK2-PLGA-NP	PLK2	PD	Inhibition of drug degradation, improvement of enzyme stability and long-term drug release, good biocompatibility and strong encapsulation ability.	Not mentioned.	[37]
	Fe_3O_4 -PEG/PLGA-OX26	Magnetic Fe_3O_4 nanoparticles, OX26	AD	Strong drug loading, magnetic targeting, biocompatibility, sustained release, controlled release.	Larger particles.	[38]
	Hollow gold nanoparticles	Xanthoceraside	ND	Large drug loading, increased drug solubility, can be traced.	No targeted ability	[39]
	Hollow au/Ag nanostars	None	ND	Large surface area, high Raman spectrum activity, and high near-infrared light sensitivity.	Unknown biological toxicity.	[40]
	Concave cubic Qu-P80-AuPd	Quercetin	AD	Good biocompatibility, good BBB penetration, high loading capacity, low cytotoxicity, good biocompatibility, lysosomal targeting.	Not mentioned.	[41]
Inorganic nanomaterials	GNRs-APH-scFv, GAS	Thermophilic acylpeptide hydrolase	AD	Good biocompatibility, strong photothermal effect, near infrared light sensitivity, low toxicity, stable physical and chemical properties.	Self-BBB penetration is slightly worse.	[42]
	Single-wall carbon nanotubes and gold nanoparticles modified screen-printed electrodes	None	PD (dopamine monitoring)	High sensitivity, good stability, small damage, real-time monitoring.	Not mentioned.	[43]
		None	PD (early diagnosis)	High sensitivity, high detection accuracy, high degree of integration of DOPA.	Not mentioned.	[44]

TABLE 1: Continued.

Type	Nanomaterials	Drugs delivered	Disease	Findings	Disadvantages	References
	Functionalized random networks of carbon nanotube RN-CNT					
	Carbon nanotubes (CNTs)	None	PD	Reduce glial cell proliferation, increase stem cell proliferation, good biocompatibility.	Not mentioned.	[45]
	SWCNT-PEGs-If	L-16-hydroxydopamine	PD	Striatal targeting, high biocompatibility, good BBB permeability, strong drug loading capacity, low toxicity, sustained release.	Cause a certain inflammatory response.	[46]
	EMT nanomaterials	None	AD	Inhibition of fibrinogen interactions in abnormal clots.	Not mentioned.	[47]
	SBA-15 (silica holed nanorod)	L-DOPA	PD	Has good BBB permeability, good drug loading, and good biocompatibility.	No targeted ability.	[48]

novel nanomaterials with free radical scavengers like tocopherol [69], ascorbic acid [70], and melanin [71]. As a study reported by Liu's group, they conjugated melanin with nanomaterials to form a novel material, which could not only effectively scavenge the free radicals in a rat stroke model but also sufficiently inhibit the expression of inflammatory mediators. What is more important is that this biomaterial obtained fairly good biocompatibility, resulting in very minor adverse reactions to the degree that the human body could totally ignore [71]. In addition, antioxidant enzymes have also received widespread attention since they are more effective at removing free radicals than free radical scavengers. For instance, Yun and his colleagues combined superoxide dismutase (SOD) enzyme with multiple nanomaterials (liposomes, polybutylcyanoacrylate (PBCA), or poly lactide-co-glycolide (PLGA)) and added targeting antibodies. In vivo experiments show that this modified nanomaterial significantly reduced the infarct area in the hippocampus region after stroke by more than 50% [72]. Interestingly, nanoscale exosomes secreted by a variety of cells have been shown to improve the prognosis of stroke significantly [73–76]. Due to the complexity of exosome components, the underlying mechanism regarding the neuroprotective effect is really hard to explain. However, exosomes' certain properties, such as no cytotoxicity and ability to carry a variety of lipids, proteins, and nucleic acids through the BBB, may contribute to the therapeutic effect after stroke [77]. Put together, by leveraging the novel nanotechnology and nanomaterials in the neuroprotective medicine, the faster delivery, more biocompatible and efficient neuroprotective drugs that could be synthesized, and the better therapeutic strategies and approaches could be provided to eventually overcome the challenges we are facing right now.

2.3. Nanomaterials for Drug Delivery across the Blood-Brain Barrier. BBB is a multicell-composed membrane between the peripheral blood and the brain [78]. It not only blocks most pathogens from invading the brain but also prevents the entry of most drugs for targeting neurological diseases [79], except for those small lipophilic molecules with a molecular weight less than 400–500 Da and confined amount of hydrogen bonds less than 9–10, which can pass through the BBB [80]. In addition, even if the drug enters the brain smoothly, a large proportion of the active ingredients will be degraded or eliminated from the brain [81]. Such unique anatomical structure and physiological characteristics determine that lots of medicines that act in the brain seem very challenging. Therefore, many researchers around the world are trying to find novel solutions to address these situations by providing a better drug delivery system to penetrate the BBB, while maintaining sufficient drug activities.

Based on current researches, four major strategies were widely considered: (i) Bypassing the BBB, including methods like intracerebroventricular, intracerebral, intrathecal, intratympanic, and intranasal [82]. However, the limitations of invasiveness, cytotoxicity, and low efficiency make it an unsuitable method. (ii) BBB manipulation, focusing on increasing the permeability of the blood-brain barrier, but the consequence is that peripheral pathogens can also enter

the brain, causing diseases such as Parkinson's disease (PD), Alzheimer's disease (AD), amyotrophic lateral sclerosis (ALS), multiple sclerosis (MS), and intracranial infection [83, 84]. (iii) Drug modification, including improving drug liposolubility and modifying the drugs to increase the binding affinity with the specific receptors or carriers on BBB [85]. (iv) Nanomaterial-based drug delivery system (Figure 1), nanomaterials with multiple modifications could penetrate the BBB and localize to the brain tissues quickly and accurately, reducing enzymatic degradation, improving drug stability, and therefore maintaining a stable drug concentration to achieve the best therapeutic effect [86, 87]. Undoubtedly, due to the fact that the method involves easy modification of nanomaterials, this drug delivery system will be the focus of future scientists' research.

At present, various nanomaterials are used in biopharmaceutical research, including lipid-based nanomaterials, polymeric nanomaterials, and inorganic nanomaterials. One of the most promising biomaterials is the lipid-based nanomaterials, because of their stability and nontoxicity. Among which, the most well-reported lipid-based nanomaterials are liposomes as discussed below.

Liposomes are composed of phospholipid bilayers surrounding a hydrophilic core [88]. This structure gives liposomes the ability to support both hydrophilic and hydrophobic molecules, and these nanomaterials can be easily modified to make them stable and effectively localized in the specific cells after passing through BBB [89]. For example, a novel Y-shaped multifunctional targeting material c(RGDyK)-pHA-PEG-DSPE was designed to be incorporated with liposomes (c(RGDyK)-pHA-LS). In which, c(RGDyK) and pHA could circumvent the blood-brain tumor barrier (BBTB) and BBB, respectively. And the PEG-DSPE was added to escape the liposomal removal function of the reticuloendothelial system (RES). A multiple-ligand structure gives it an ability to circulate stably in the blood and target brain tumor cells specifically. In vitro and in vivo studies demonstrated that doxorubicin- (DOX-) loaded c(RGDyK)-pHA-LS display a better therapeutic effect than the DOX-loaded liposome only group [90]. This result indicated that more functional ligands should be applied to nanomaterial synthesis. For instance, monoclonal antibodies and receptor substrates were used as liposome ligands to allow more precise binding of nanomaterials to the BBB [91–93]. However, these receptors are distributed throughout the body, reducing the specificity of these nanomaterials. Corresponding side effects are also caused by the activation of receptors at various positions. Lipid-based nanomaterials also include solid lipid nanomaterials (SLN), which possess benefits like biocompatibility, improved drug stability, and massive load capacity and provided a controlled drug release within a few weeks. Although these nanomaterials have low hydrophilic molecular loading capacity and some special preparations in application, they are considered to have great potential in drug delivery [94, 95].

The other two nanomaterials, including polymeric nanomaterials and inorganic nanomaterials, are also hotspots of research. But same as lipid-based nanomaterials, there are still many restrictions waiting to be overcome. Ideally, safe

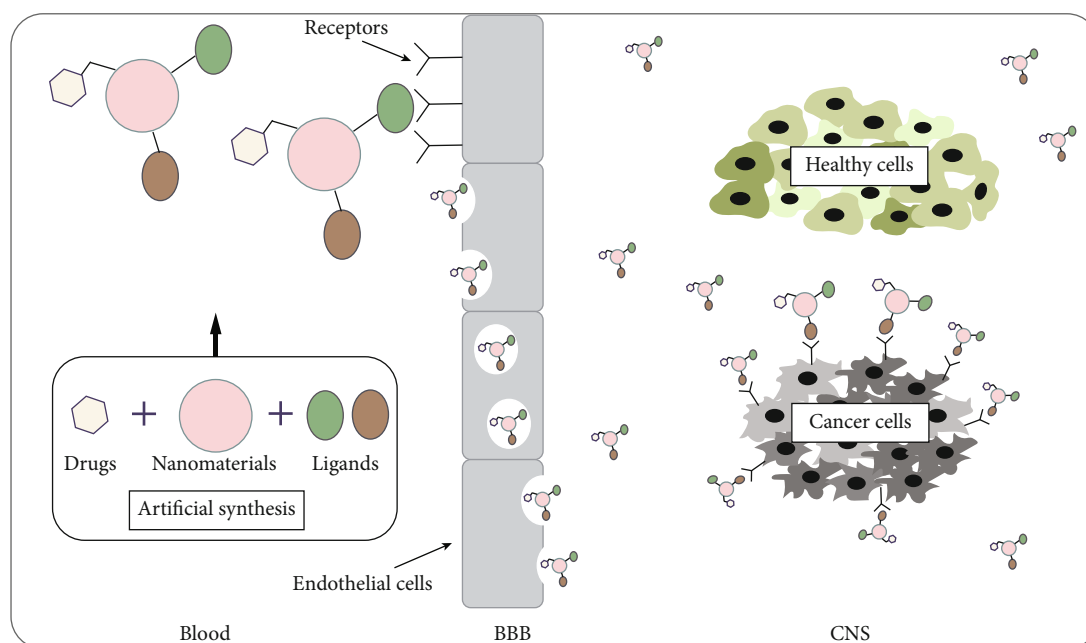


FIGURE 1: CNS drug delivery system. Nanomaterials composed of nanoscale carrier, drugs, and multiple functionalized ligands can penetrate the BBB and localize to the cancer cells through receptor-mediated endocytosis. This strategy allows the drug to exert a powerful killing effect on cancer cells and effectively reduces the off-target effect on healthy cells. CNS: central nervous system; BBB: blood-brain barrier.

nanomaterials that could be loaded with various drugs and be able to target the specific cells in the brain remotely are highly expected.

2.4. Nanomaterial Stem Cell Hybrids for Neuroscience. Stem cell transplant therapy using neural stem cells (NSCs), embryonic stem cells, mesenchymal stem cells (ESCs), or induced pluripotent stem cells (iPSCs) has been considered as a potential therapeutic strategy for neurological diseases, including stroke, brain trauma, PD, AD, and brain tumor [96]. The low survival rate of transplanted stem cells is the major reason why the majority of clinical trials fail. 30% of embryonic stem cells died within 3 days after transplantation into a rat stroke model, caused by reasons like immune rejection, lack of trophic factors, and extracellular matrix [97, 98]. Although there are a lot of studies reporting that the preconditioning of stem cells [99] or lesion microenvironment [100] may help to increase the cell survival ratio and acquire better prognosis, the limitations and challenges still remain [101, 102]. Recently, nanomaterial-composed scaffolds were used to facilitate stem cell transplantation therapy [103, 104]. Carbon nanotubes (CNTs) are considered promising nanomaterials due to their excellent electrical conductivity, which is beneficial for stem cell differentiation and intercellular communication [105]. Kam and his colleagues have synthesized laminin-SWNT (single-walled carbon nanotube) thin films in order to mimic the structure of living tissues in the human body, in which laminin is a significant part of the extracellular matrix. An *in vitro* study demonstrated that this material could support proliferation and differentiation of NSCs, indicated by the presence of synaptic connections [106]. Similarly, scaffolds like collagen/MMA/acrylic acid (PMMAA) [107], poly-L-lactic acid-co-poly-(3-caprolactone)/collagen

[108], terpolymer/collagen [109], poly-L-lactic acid (PLLA) [110], and poly(lactic-co-glycolic acid)/praphene oxide-l-theanine (PLGA/GO-TH) [111] are synthesized to enhance stem cell survival and promote the differentiation.

Interestingly, some nanomaterials even could be absorbed by stem cells and quickly spread throughout the cells. A nanomaterial with superparamagnetic iron oxide (SPIO) as the core and ZnO as the shell could be absorbed by human adipose tissue-derived stem cells (hATSC), and then, the transcription factors could be activated to modulate the neurogenesis [112]. In another study, retinoic acid- (RA-) loaded nanomaterials were taken up by NSC and the RA could be further released in the cells, leading to the activation of the SAPK/JNK signaling pathway and ultimately influencing the proneurogenic genes to benefit the differentiation of neural stem cells *in vitro* and *in vivo* [113]. This study suggested that some cell growth regulators could possibly be loaded to the nanomaterials as well and eventually acquire better effects. For instance, fibroblast growth factor receptor-1 (FGFR1) and its FGF-2 ligand were delivered into the brain subventricular zone, and the release of these growth factors could stimulate the neurogenesis in the adult brain [114].

Of course, transplantation therapy also faces the problem of a lack of monitoring system. Scientists in many fields are trying to build a nanomaterial-based imaging agent, which requires merits like long half-life, high selectivity, contrast-to-noise enhancement, and nontoxic. An amphiphilic fluorophore-derived nanomaterial with aggregate-induced emission (AIE) effect and self-assembly ability was used to label human embryonic stem cells (hESC) and monitor their differentiation. Experiments show that this monitoring could last for 40 days and has better fluorescence intensity and

biocompatibility [115]. These nanomaterials could also be radioactive, magnetic, paramagnetic, superparamagnetic, and electron-dense [116–121], which can be monitored by commercially available equipment (magnetic resonance imaging (MRI), computed tomography (CT), or fluorescence tomography (FT)) easily. However, the toxicity of nanomaterials to stem cells remains an open question.

3. Therapeutic Nanomaterials for Cancer

3.1. Nanomaterials as Immune-Modulating Agents. The biological immunity of cancer cells is divided into three steps: (i) cancer cells recognized by the immune system, (ii) targeting of the cancer cells for specific elimination, and (iii) immune system destroying cancer cells effectively [122]. Significant progress has been made in the field of cancer immunotherapy by regulating the human immune system to eliminate cancer cells. However, the problems of immune changes and delivery efficiency at nontumor sites caused by the systemic delivery of immunomodulatory compounds have not been well addressed, resulting in the limited application of immunotherapy. Nanotechnology offers a lot of innate advantages in these aspects. Combining immunomodulatory compounds by covalence conjugation [123], chelation [124], encapsulation [125], etc., can increase the functional efficacy of the immunomodulatory compounds and reduce their depletion in the peripheral circulation to avoid unnecessary immune responses.

Lipid-based nanomaterials and polymeric nanomaterials have good encapsulation capabilities. The modification of such nanomaterials makes it easier to obtain a single stable targeting than other materials or immunomodulatory compound only approach, therefore making it more reliable and controllable [126]. For inorganic nanomaterials, under certain conditions, they can become immunomodulators themselves. This is undoubtedly a huge distinctive advantage compared to other immune presenters that require targeted controlled release. For example, gold nanomaterials could produce a photothermal effect after receiving near-infrared light to stimulate the immune system to work, and gold nanomaterials are easily engulfed by monocytes [127].

At present, the application of nanomaterials in immunomodulatory therapy is mainly focused on the targeted delivery of immunomodulators and enhanced immune recognition of tumor cells [128, 129]. It is worth mentioning that a special nanomaterial used in immunomodulatory therapy is the virus-like particle (VLP). VLPs can be efficiently absorbed, processed, and presented by MHC class II molecules of DCs, thereby activating T cells. In addition, unlike many soluble antigens, VLPs efficiently cross-present through APCs via the class I MHC pathway, thereby activating CD8⁺ T cells [125].

3.2. Nanomaterials as Anticancer Drug Delivery System. Cancer is now responsible for the majority of global deaths and is expected to be the single most important obstacle to increase life expectancy in the 21st century [130]. Nanocarrier-targeted drug delivery systems have the potential to circumvent several shortcomings of conventional therapeutic for-

mulations. Nanomaterials with special ligand functionality can efficiently target cancer cells [131]. Moreover, nanomaterials can be designed for improving the solubility and stability of anticancer drugs, increased drug loading, improved half-life in the body, controlled release, and selective distribution by modifying their composition, size, morphology, and surface chemistry [132].

As an anticancer drug delivery system, it can be divided into three parts. The first part is the carrier, which refers to a variety of nanomaterials, such as metal nanomaterials, carbon-based materials, liposomes, and dendritic and macromolecule polymer nanomaterials [133]. Metal and metal oxide nanomaterials are ideal anticancer drug carriers due to their controllable size and shape, easily modified surface functionalization, and good biocompatibility. A recent study showed that docetaxel coupled with gold-doped apatite has anticancer effects in vitro. The material showed higher cytotoxicity to human liver cancer cell line HepG2 and showed improved bioavailability [134]. Carbon-based nanomaterials have many advantages, such as large specific surface area, high drug loading, and easy surface modification. They have also been widely studied in imaging, drug delivery, and diagnosis of tumors [135]. Recently, the study of drug delivery by multiwalled carbon nanotubes (MWCNTs) has shown that the release of drugs in the tumor site and the absorption of cells have shown the potential for the treatment of multidrug-resistant tumors [136]. Liposomes are the first nanomaterials to be used; it can prolong the circulation time of the drugs and reduce toxicity to healthy tissues around. Correspondingly, these vehicles offer several other advantages including biocompatibility, self-assembly, and high drug cargo loading [137]. Another polymer nanomaterial platform that has received much attention as a drug delivery system is polymer micelle nanomaterial. Recently, Peng et al. prepared a polymer micelle by combining temozolomide (TMZ) and anti-bcl-2 siRNA with a folic acid triblock copolymer to overcome the limitations of acquired drug resistance of glioma cells and BBB on drug delivery [138].

The second part is the combination and release of drugs with nanomaterials, such as the encapsulation of drugs by liposomes, or the modification of metals and metal oxide nanomaterials by drugs, and then the release of drugs through REDOX, pH-mediated release systems, or other stimulation methods, such as magnetic field, ultrasonic induction, and electrochemical triggering.

The third part is the targeted drug delivery system. Targeting can be divided into active and passive targeting. Passive targeting refers to the accumulation of nanomaterials in tumor sites due to the vascular barrier destruction and poor lymph node clearance in tumor sites. Active targeting is ligand-mediated targeting, including recognition and uptake of substrate [139, 140]. The system includes ligands like antibodies, proteins, nucleic acids, peptides, vitamins, and other organic molecules. Substrates can be molecules on the surface of cancer cells, substances in the internal environment of cancer cells, or proteins secreted by cancer cells [141, 142]. For example, Au nanomaterials coated with nuclear localizing signal (NLS) were able to escape the endosome and penetrate the nucleus of cancer cells to induce

TABLE 2: List of nanomaterials in cancer therapy.

Type	Nanomaterials	Drugs delivered	Disease	Findings	Disadvantages	References
	Liposomal annamycin	Annamycin	Acute lymphocytic leukemia, acute myeloid leukemia	Bypass multidrug resistance mechanisms of cellular drug resistance	Diarrhea, typhlitis, and nausea	[148]
	Liposomal doxorubicin	Doxorubicin	Non-Hodgkin's lymphoma	Prolong systemic circulation, a ligand for cell-specific targeting, and an imaging agent for diagnosis	Induce infusion reactions about activating the complement cascade	[149]
Lipid-based nanomaterials	Liposomal vincristine	Vincristine	Non-Hodgkin's lymphoma	Reduce neurotoxicity and increase dose intensity delivery	The risk of peripheral neuropathy	[150]
	Liposomal cisplatin	Cisplatin	Progressive osteogenic sarcoma metastatic to the lung	High reactivity, affinity to biomolecules, and low release rate at the tumor site	Possible immune-related reactions or the blood clearance in the case of PEGylated liposomes	[151]
	Docetaxel-loaded solid lipid nanomaterials	Docetaxel	Breast cancer Lung metastasis	High stability for at least 120 days	Short lifespan, poor durability, poor encapsulation	[152]
	Cisplatin-loaded solid lipid nanomaterials	Cisplatin	Breast cancer	Overcome dose-related toxicity, enhance targeting	Require additional microwave-assisted equipment	[153]
	HPMA copolymer—DACH platinate	ProLindac	Ovarian cancer	Increase platinum accumulation in tumors via the enhanced permeability and retention effect	Nausea and vomiting	[154]
	Polymer-lipid hybrid nanomaterials	Doxorubicin	Solid tumors	Prolong drug release, enhance systemic half-life, decrease toxicity, and targeted drug delivery	Potential biotoxicity of nanomaterials	[155]
	Poly(ethylene glycol)-block-poly(L-lactic-co-glycolic acid)	Docetaxel	Prostate cancers	Have good biocompatibility and effective cancer cell inhibition ability	Have potential biotoxicity due to slow drug clearance	[156]
Polymetric nanomaterials	Folic acid-PAMAM dendrimers	Methotrexate	Epithelial cancer	Increase its antitumor activity and markedly decreased its toxicity	The optimal dose of targeted drug has not been definitively established	[157]
	Poly(glycerol-succinic acid) dendrimers	Camptothecin	Various cancers	Enhance anticancer activity	Limit water solubility and resulting suboptimal pharmacokinetics	[158]
	Superparamagnetic iron oxide nanomaterials	Doxorubicin	Liver cancer	Enhance the biological effects of doxorubicin	Certain hepatorenal toxicity	[159]
	AOT-alginate nanomaterials	Doxorubicin	Breast cancer	Enhancement of therapeutic effect	Some cardiotoxicity	[160]
	Glycol chitosan nanomaterials	Doxorubicin	Solid tumors	Exhibit excellent tumor-homing efficacy, an effective strategy to overcome multidrug resistance	Low solubility	[161]
Inorganic nanomaterials	Anti-HER2 antibody-targeted gold nanomaterials	Nanoshell-assisted infrared photothermal therapy	Metastatic breast cancer	Retain high antimitotic potency, which could contribute to a higher therapeutic index in high EPR tumors	Potential biotoxicity	[162]
			Breast cancer	Reduce hepatic and renal toxicity	Some hepatic and renal toxicity	[163]

TABLE 2: Continued.

Type	Nanomaterials	Drugs delivered	Disease	Findings	Disadvantages	References
	Silica-based nanomaterials	Organotin metallodrug				
	Aminosilane-coated iron oxide nanomaterials	Thermotherapy	Brain tumors	Low toxicity, the possibility of radical cure	Complex operation, need further exploration	[164]
	Nanocrystalline 2-methoxyestradiol	Panzem NCD	Various cancers	Delivery of poorly water-soluble drug	Fatigue, nausea, mild transaminitis, and dysgeusia	[165, 166]
	ND-biopolymer nanocomposites	Doxorubicin	Liver cancer	Prolong and continue release of antitumor drugs	Complicated technology	[167]
Special category	Paclitaxel nanomaterials in porous	Paclitaxel	Solid tumors	Favorable preclinical safety and antitumor activity profiles	Fatigue, alopecia, nausea, vomiting, neuropathy, anorexia, and myalgia	[168]
	Albumin-bound nanomaterials	Doxorubicin, methotrexate	Various cancers	Decrease the glycolysis and metabolic tumor volume	Decrease antibody presence in the general circulation, which might lead to undesirable effects	[169]

DNA damage [143]. And nanomaterials coated with polyethylene glycol (PEG) achieve passive targeting of tumor tissue through EPR effect. The invisible coating of PEG and other polymers prevents the adsorption of serum proteins, increases cycle time, and increases the probability of particle penetration of tumor tissue [144]. When multiple ligands are combined with nanomaterials, their targeting also can be improved [145].

At present, multiple nanomaterials (Table 2) were demonstrated to benefit from cancer treatment, but due to their particularity, the biological toxicity of nanomaterials is still the major focus that we cannot ignore [146, 147].

3.3. Nanomaterials as a Combination Therapy for Cancers. Traditional single-drug or multidrug combination chemotherapy tends to produce serious adverse consequences due to the accumulation of drugs and their metabolism in vital organs. Moreover, tumor cells are prone to multidrug resistance, and the efficacy of chemotherapy drugs is often not up to the expected effect [170, 171]. In medical applications, liposomes and polymeric nanomaterial conjugates are the two major categories, accounting for more than 80% of all nanomaterial drugs.

Liposome is a kind of spherical lipid vesicles with a double-membrane structure. It is widely used as a drug carrier by reasons that it can effectively encapsulate hydrophilic and hydrophobic drugs to avoid adverse external stimuli and carry specific ligands to identify specific cell tissues and organs. For example, Doxil was the first liposome drug approved by the FDA for the treatment of Kaposi's sarcoma. It wraps doxorubicin (a widely used anticancer chemotherapy drug) in a liposome carrier to significantly extend the half-life of doxorubicin and increase the accumulation of the drug in tumor tissue [172, 173].

Another research hotspot is polymer-drug coupling of polymeric nanomaterials. The combination of small molecule drugs with polymeric nanomaterials can improve adverse reactions. It also enhances the passive delivery of drugs to leaky tumor tissue [174, 175]. In addition, metal nanomaterials and ceramic nanomaterials have demonstrated some specific therapeutic potential such as amino-silane-coated iron oxide nanomaterials, which have recently been used in brain tumors treated with thermotherapy; the survival time was prolonged by 4.5 times by means of magnetic field-induced excitation of iron oxide superparamagnetic nanomaterials and hyperthermia in a rat model [176].

In addition to the anticancer drugs that can inhibit or kill tumor cells, the interaction between nanomaterials and intracellular organelles also plays an important role in cancer treatment [177]. For example, lysosomes and endolysosomes of endogenous foreign bodies are used to monitor cell apoptosis cascade, calcium cycle, and ATP synthesis. The nucleus consists of DNA mutation, gene expression, cell proliferation, endoplasmic reticulum [178], and other Golgi complexes, which promote protein synthesis and transport to other organisms [179]. Despite recent breakthroughs in the research of nanomaterials in the field of tumors, more in-depth exploration is needed, such as the optimal properties of various nanomaterials, the numerous biological

barriers faced by nanomaterials, and the related cytotoxicity of nanomaterials.

4. Conclusion and Future Directions

As discussed above, nanomaterials have proved their importance in the medical field and provided new directions for the treatment of neurological diseases and cancers, although the disadvantages are remaining, such as lack of specialized equipment for efficient and high-quality nanomaterial synthesis, difficulty of assessing its safety and effectiveness, and some shortcomings of specific materials mentioned above. Future directions of nanomaterials should be in line with the following principles: (1) diameter within 100 nm, possess high scalability, and easy to be degraded; (2) low cost and high productivity; (3) biocompatibility, nontoxic, and without initiating the pathological processes like inflammation and thrombosis; (4) highly sufficient targeting and ability to penetrate multiple biological barriers, like BBB; (5) stable in the blood and resistant to be cleared by RES; and (6) loaded molecules could be released smoothly and achieve significant therapeutic effect for the diseases. In conclusion, the treatment of neurological diseases or cancers, in this regard, is an uphill battle that might be easily overcome with nanotechnology if solutions such as multimodal agents are actively practiced. Nevertheless, the future still holds promises for the field of nanomedicine to be exploited to its fullest extent for the potential advanced therapeutic approaches.

Abbreviations

AD:	Alzheimer's disease
AIE:	Aggregate-induced emission
ALS:	Amyotrophic lateral sclerosis
BBB:	Blood-brain barrier
BBTB:	Blood-brain tumor barrier
CNS:	Central nervous system
CNTs:	Carbon nanotubes
CT:	Computed tomography
DOX:	Doxorubicin
ESCs:	Mesenchymal stem cells
FGFR1:	Fibroblast growth factor receptor-1
FT:	Fluorescence tomography
hATSC:	Human adipose tissue-derived stem cells
iPSCs:	Induced pluripotent stem cells
MRI:	Magnetic resonance imaging
MS:	Multiple sclerosis
MWCNTs:	Multiwalled carbon nanotubes
NLS:	Nuclear localizing signal
NO:	Nitric oxide
NSCs:	Neural stem cells
PBCA:	Polybutylcyanoacrylate
PD:	Parkinson's disease
PEG:	Polyethylene glycol
PLGA:	Poly lactide-co-glycolide
PLLA:	Poly-L-lactic acid
PMMAAA:	Collagen/MMA/acrylic
RA:	Retinoic acid
RES:	Reticuloendothelial system

RNS:	Reactive nitrogen species
ROS:	Reactive oxygen species
SLN:	Solid lipid nanoparticle
SOD:	Superoxide dismutase
SPIO:	Superparamagnetic iron oxide
SWNT:	Single-walled carbon nanotubes
tPA:	Tissue plasminogen activator
TMZ:	Temozolomide
VLP:	Virus-like particle.

Conflicts of Interest

The author(s) declare(s) that they have no conflicts of interest.

Authors' Contributions

KW, XZ, and EY wrote the first draft. PD, HW, CZ, JY, and JH revised and edited the final manuscript. QZ, JY, and JH supervised the manuscript and provided critical input. All authors gave feedback and agreed on the final version of the manuscript.

Acknowledgments

This work was supported by the National Natural Science Foundation of China (No. 81771262), Zhejiang Health Science and Technology Project (2016RCA022), Zhejiang Key Research and Development Project (2017C03027), and American Heart Association Predoctoral Fellowship for JH (19PRE34380114).

References

- [1] V. T. Nguyen, T. H. Nguyen, L. H. Dang, H. Vu-Quang, and N. Q. Tran, "Folate-conjugated chitosan-pluronic P123 nanogels: synthesis and characterizations towards dual drug delivery," *Journal of Nanomaterials*, vol. 2019, Article ID 1067821, 14 pages, 2019.
- [2] J. Preechawong, K. Noulta, S. T. Dubas, M. Nithitanakul, and P. Sapsrithong, "Nanolayer film on poly(styrene/ethylene glycol dimethacrylate) high internal phase emulsion porous polymer surface as a scaffold for tissue engineering application," *Journal of Nanomaterials*, vol. 2019, Article ID 7268192, 10 pages, 2019.
- [3] C. Lin, S. Cai, and J. Feng, "Positive contrast imaging of SPIO nanoparticles," *Journal of Nanomaterials*, vol. 2012, Article ID 734842, 9 pages, 2012.
- [4] S. E. A. Gratton, P. A. Ropp, P. D. Pohlhaus et al., "The effect of particle design on cellular internalization pathways," *Proceedings of the National Academy of Sciences of the United States of America*, vol. 105, no. 33, pp. 11613–11618, 2008.
- [5] Y. Qiu, Y. Liu, L. Wang et al., "Surface chemistry and aspect ratio mediated cellular uptake of Au nanorods," *Biomaterials*, vol. 31, no. 30, pp. 7606–7619, 2010.
- [6] K.-T. Jin, Z. B. Lu, J. Y. Chen et al., "Recent trends in nanocarrier-based targeted chemotherapy: selective delivery of anticancer drugs for effective lung, colon, cervical, and breast cancer treatment," *Journal of Nanomaterials*, vol. 2020, Article ID 9184284, 14 pages, 2020.
- [7] D. Bobo, K. J. Robinson, J. Islam, K. J. Thurecht, and S. R. Corrie, "Nanoparticle-based medicines: a review of FDA-approved materials and clinical trials to date," *Pharmaceutical Research*, vol. 33, no. 10, pp. 2373–2387, 2016.
- [8] D. E. Bredesen, R. V. Rao, and P. Mehlen, "Cell death in the nervous system," *Nature*, vol. 443, no. 7113, pp. 796–802, 2006.
- [9] A. W. Hübler and O. Osuagwu, "Digital quantum batteries: energy and information storage in nanovacuum tube arrays," *Complexity*, vol. 15, no. 5, pp. 48–55, 2010.
- [10] A. Di Stefano, M. Carafa, P. Sozio et al., "Evaluation of rat striatal L-dopa and DA concentration after intraperitoneal administration of L-dopa prodrugs in liposomal formulations," *Journal of Controlled Release*, vol. 99, no. 2, pp. 293–300, 2004.
- [11] C. Y. Lin, Y. C. Lin, C. Y. Huang, S. R. Wu, C. M. Chen, and H. L. Liu, "Ultrasound-responsive neurotrophic factor-loaded microbubble-liposome complex: preclinical investigation for Parkinson's disease treatment," *Journal of Controlled Release*, vol. 321, pp. 519–528, 2020.
- [12] A. McRae and A. Dahlström, "Transmitter-loaded polymeric microspheres induce regrowth of dopaminergic nerve terminals in striata of rats with 6-OH-DA induced parkinsonism," *Neurochemistry International*, vol. 25, no. 1, pp. 27–33, 1994.
- [13] A. Aubert-Pouëssel, M. C. Venier-Julienne, A. Clavreul et al., "In vitro study of GDNF release from biodegradable PLGA microspheres," *Journal of Controlled Release*, vol. 95, no. 3, pp. 463–475, 2004.
- [14] E. D'Aurizio, P. Sozio, L. S. Cerasa et al., "Biodegradable microspheres loaded with an anti-Parkinson prodrug: an in vivo pharmacokinetic study," *Molecular Pharmaceutics*, vol. 8, no. 6, pp. 2408–2415, 2011.
- [15] O. Betzer, M. Shilo, R. OPOCHINSKY et al., "The effect of nanoparticle size on the ability to cross the blood-brain barrier: an in vivo study," *Nanomedicine*, vol. 12, no. 13, pp. 1533–1546, 2017.
- [16] J. H. An, W. A. el-Said, C. H. Yea, T. H. Kim, and J. W. Choi, "Surface-enhanced Raman scattering of dopamine on self-assembled gold nanoparticles," *Journal of Nanoscience and Nanotechnology*, vol. 11, no. 5, pp. 4424–4429, 2011.
- [17] K. S. Siddiqi, A. Husen, S. S. Sohrab, and M. O. Yassin, "Recent status of nanomaterial fabrication and their potential applications in neurological disease management," *Nanoscale Research Letters*, vol. 13, no. 1, article 231, 2018.
- [18] R. Titze-de-Almeida, S. S. Titze-de-Almeida, N. R. Ferreira, C. Fontanari, L. H. Faccioli, and E. del Bel, "Suppressing nNOS enzyme by small-interfering RNAs protects SH-SY5Y cells and nigral dopaminergic neurons from 6-OHDA injury," *Neurotoxicity Research*, vol. 36, no. 1, pp. 117–131, 2019.
- [19] J. Niu, J. Xie, K. Guo et al., "Efficient treatment of Parkinson's disease using ultrasonography-guided rhFGF20 proteoliposomes," *Drug Delivery*, vol. 25, no. 1, pp. 1560–1569, 2018.
- [20] M. Qu, Q. Lin, S. He et al., "A brain targeting functionalized liposomes of the dopamine derivative N-3,4-bis(pivaloyloxy)-dopamine for treatment of Parkinson's disease," *Journal of Controlled Release*, vol. 277, pp. 173–182, 2018.
- [21] P. Yue, L. Gao, X. Wang, X. Ding, and J. Teng, "Ultrasound-triggered effects of the microbubbles coupled to GDNF- and Nurr1-loaded PEGylated liposomes in a rat model of

- Parkinson's disease," *Journal of Cellular Biochemistry*, vol. 119, no. 6, pp. 4581–4591, 2018.
- [22] Y. C. Kuo and C. W. Tsao, "Neuroprotection against apoptosis of SK-N-MC cells using RMP-7- and lactoferrin-grafted liposomes carrying quercetin," *International Journal of Nanomedicine*, vol. Volume 12, pp. 2857–2869, 2017.
- [23] Y. C. Kuo and Y. J. Lee, "Rescuing cholinergic neurons from apoptotic degeneration by targeting of serotonin modulator- and apolipoprotein E-conjugated liposomes to the hippocampus," *International Journal of Nanomedicine*, vol. Volume 11, pp. 6809–6824, 2016.
- [24] A. C. Sintov, H. V. Levy, and I. Greenberg, "Continuous transdermal delivery of L-DOPA based on a self-assembling nanomicellar system," *Pharmaceutical Research*, vol. 34, no. 7, pp. 1459–1468, 2017.
- [25] X. Li, Q. Liu, D. Zhu, Y. Che, and X. Feng, "Preparation of levodopa-loaded crystallosomes through thermally induced crystallization reverses functional deficits in Parkinsonian mice," *Biomaterials Science*, vol. 7, no. 4, pp. 1623–1631, 2019.
- [26] T. Chen, Y. Li, C. Li et al., "Pluronic P85/F68 micelles of baicalin could interfere with mitochondria to overcome MRP2-mediated efflux and offer improved anti-Parkinsonian activity," *Molecular Pharmaceutics*, vol. 14, no. 10, pp. 3331–3342, 2017.
- [27] H. Yang, X. Li, L. Zhu et al., "Heat shock protein inspired nanochaperones restore Amyloid- β homeostasis for preventative therapy of Alzheimer's disease," *Advanced Science*, vol. 6, no. 22, article 1901844, 2019.
- [28] P. Yang, D. Sheng, Q. Guo et al., "Neuronal mitochondria-targeted micelles relieving oxidative stress for delayed progression of Alzheimer's disease," *Biomaterials*, vol. 238, article 119844, 2020.
- [29] Z. Mirzaie, M. Ansari, S. S. Kordestani, M. H. Rezaei, and M. Mozafari, "Preparation and characterization of curcumin-loaded polymeric nanomicelles to interference with amyloidogenesis through glycation method," *Biotechnology and Applied Biochemistry*, vol. 66, no. 4, pp. 537–544, 2017.
- [30] D. E. Igartúa, C. S. Martinez, C. F. Temprana, S. D. Alonso, and M. J. Prieto, "PAMAM dendrimers as a carbamazepine delivery system for neurodegenerative diseases: a biophysical and nanotoxicological characterization," *International Journal of Pharmaceutics*, vol. 544, no. 1, pp. 191–202, 2018.
- [31] E. Aso, I. Martinsson, D. Appelhans et al., "Poly(propylene imine) dendrimers with histidine-maltose shell as novel type of nanoparticles for synapse and memory protection," *Nanomedicine*, vol. 17, pp. 198–209, 2019.
- [32] A. Gothwal, H. Kumar, K. T. Nakhate et al., "Lactoferrin coupled lower generation PAMAM dendrimers for brain targeted delivery of memantine in aluminum-chloride-induced Alzheimer's disease in mice," *Bioconjugate Chemistry*, vol. 30, no. 10, pp. 2573–2583, 2019.
- [33] K. Milowska, J. Grochowina, N. Katir et al., "Viologen-phosphorus dendrimers inhibit α -Synuclein fibrillation," *Molecular Pharmaceutics*, vol. 10, no. 3, pp. 1131–1137, 2013.
- [34] K. Milowska, A. Szwed, M. Mutrynowska et al., "Carbosilane dendrimers inhibit α -synuclein fibrillation and prevent cells from rotenone-induced damage," *International Journal of Pharmaceutics*, vol. 484, no. 1-2, pp. 268–275, 2015.
- [35] R. Pahuja, K. Seth, A. Shukla et al., "Correction to trans-blood brain barrier delivery of dopamine-loaded nanoparticles reverses functional deficits in Parkinsonian Rats," *ACS Nano*, vol. 13, no. 7, pp. 8490–8490, 2019.
- [36] H. Moradian, H. Keshvari, H. Fasehee, R. Dinarvand, and S. Faghihi, "Combining NT3-overexpressing MSCs and PLGA microcarriers for brain tissue engineering: a potential tool for treatment of Parkinson's disease," *Materials Science & Engineering. C, Materials for Biological Applications*, vol. 76, pp. 934–943, 2017.
- [37] C. Rodríguez-Nogales, E. Garbayo, I. Martínez-Valbuena, V. Sebastián, M. R. Luquin, and M. J. Blanco-Prieto, "Development and characterization of polo-like kinase 2 loaded nanoparticles—a novel strategy for (serine-129) phosphorylation of alpha-synuclein," *International Journal of Pharmaceutics*, vol. 514, no. 1, pp. 142–149, 2016.
- [38] N. Cui, H. Lu, and M. Li, "Magnetic nanoparticles associated PEG/PLGA block copolymer targeted with anti-transferrin receptor antibodies for Alzheimer's disease," *Journal of Biomedical Nanotechnology*, vol. 14, no. 5, pp. 1017–1024, 2018.
- [39] D. L. Meng, L. Shang, X. H. Feng, X. F. Huang, and X. Che, "Xanthoceraside hollow gold nanoparticles, green pharmaceuticals preparation for poorly water-soluble natural anti-AD medicine," *International Journal of Pharmaceutics*, vol. 506, no. 1-2, pp. 184–190, 2016.
- [40] A. Garcia-Leis, A. Torreggiani, J. V. Garcia-Ramos, and S. Sanchez-Cortes, "Hollow Au/Ag nanostars displaying broad plasmonic resonance and high surface-enhanced Raman sensitivity," *Nanoscale*, vol. 7, no. 32, pp. 13629–13637, 2015.
- [41] Y. Liu, H. Zhou, T. Yin et al., "Quercetin-modified gold-palladium nanoparticles as a potential autophagy inducer for the treatment of Alzheimer's disease," *Journal of Colloid and Interface Science*, vol. 552, pp. 388–400, 2019.
- [42] D. Liu, W. Li, X. Jiang et al., "Using near-infrared enhanced thermozyme and dsFv dual-conjugated Au nanorods for detection and targeted photothermal treatment of Alzheimer's disease," *Theranostics*, vol. 9, no. 8, pp. 2268–2281, 2019.
- [43] D. Ji, N. Xu, Z. Liu et al., "Smartphone-based differential pulse amperometry system for real-time monitoring of levodopa with carbon nanotubes and gold nanoparticles modified screen-printing electrodes," *Biosensors & Bioelectronics*, vol. 129, pp. 216–223, 2019.
- [44] U. Tisch, Y. Aluf, R. Ionescu et al., "Detection of asymptomatic nigrostriatal dopaminergic lesion in rats by exhaled air analysis using carbon nanotube sensors," *ACS Chemical Neuroscience*, vol. 3, no. 3, pp. 161–166, 2012.
- [45] H. E. Marei, A. A. Elnegiry, A. Zaghoul et al., "Nanotubes impregnated human olfactory bulb neural stem cells promote neuronal differentiation in trimethyltin-induced neurodegeneration rat model," *Journal of Cellular Physiology*, vol. 232, no. 12, pp. 3586–3597, 2017.
- [46] Q. Guo, H. You, X. Yang et al., "Functional single-walled carbon nanotubes 'CAR' for targeting dopamine delivery into the brain of parkinsonian mice," *Nanoscale*, vol. 9, no. 30, pp. 10832–10845, 2017.
- [47] H. Derakhshankhah, M. J. Hajipour, E. Barzegari et al., "Zeolite nanoparticles inhibit $A\beta$ -Fibrinogen interaction and formation of a consequent abnormal structural clot," *ACS Applied Materials & Interfaces*, vol. 8, no. 45, pp. 30768–30779, 2016.
- [48] S. Swar, V. Makova, and I. Stibor, "Effectiveness of diverse mesoporous silica nanoparticles as potent vehicles for the drug L-DOPA," *Materials*, vol. 12, no. 19, 2019.

- [49] V. L. Feigin, B. Norrving, and G. A. Mensah, "Global burden of stroke," *Circulation Research*, vol. 120, no. 3, pp. 439–448, 2017.
- [50] X. Xu, B. Wang, C. Ren et al., "Age-related impairment of vascular structure and functions," *Aging and Disease*, vol. 8, no. 5, pp. 590–610, 2017.
- [51] X. Xu, B. Wang, C. Ren et al., "Recent progress in vascular aging: mechanisms and its role in age-related diseases," *Aging and Disease*, vol. 8, no. 4, pp. 486–505, 2017.
- [52] G. J. Hankey, "Stroke," *Lancet*, vol. 389, no. 10069, pp. 641–654, 2017.
- [53] C. Ren, Y. Yao, R. Han et al., "Cerebral ischemia induces angiogenesis in the peri-infarct regions via Notch1 signaling activation," *Experimental Neurology*, vol. 304, pp. 30–40, 2018.
- [54] S. Kyle and S. Saha, "Nanotechnology for the detection and therapy of stroke," *Advanced Healthcare Materials*, vol. 3, no. 11, pp. 1703–1720, 2014.
- [55] D. Huang, K. Wu, Y. Zhang et al., "Recent advances in tissue plasminogen activator-based nan thrombolysis for ischemic stroke," *Reviews on Advanced Materials Science*, vol. 58, no. 1, pp. 159–170, 2019.
- [56] N. Korin, M. Kanapathipillai, B. D. Matthews et al., "Shear-activated nanotherapeutics for drug targeting to obstructed blood Vessels," *Science*, vol. 337, no. 6095, pp. 738–742, 2012.
- [57] M. N. Holme, I. A. Fedotenko, D. Abegg et al., "Shear-stress sensitive lenticular vesicles for targeted drug delivery," *Nature Nanotechnology*, vol. 7, no. 8, pp. 536–543, 2012.
- [58] C. Correa-Paz, M. F. Navarro Poupard, E. Polo et al., "In vivo ultrasound-activated delivery of recombinant tissue plasminogen activator from the cavity of sub-micrometric capsules," *Journal of controlled release*, vol. 308, pp. 162–171, 2019.
- [59] H. Kawata, Y. Uesugi, T. Soeda et al., "A new drug delivery system for intravenous coronary thrombolysis with thrombus targeting and stealth activity recoverable by ultrasound," *Journal of the American College of Cardiology*, vol. 60, no. 24, pp. 2550–2557, 2012.
- [60] Y. Uesugi, H. Kawata, J. I. Jo, Y. Saito, and Y. Tabata, "An ultrasound-responsive nano delivery system of tissue-type plasminogen activator for thrombolytic therapy," *Journal of controlled release*, vol. 147, no. 2, pp. 269–277, 2010.
- [61] H. Jin, H. Tan, L. Zhao et al., "Ultrasound-triggered thrombolysis using urokinase-loaded nanogels," *International Journal of Pharmaceutics*, vol. 434, no. 1-2, pp. 384–390, 2012.
- [62] T. Hirano, M. Komatsu, H. Uenohara, A. Takahashi, K. Takayama, and T. Yoshimoto, "A novel method of drug delivery for fibrinolysis with Ho:YAG laser-induced liquid jet," *Lasers in Medical Science*, vol. 17, no. 3, pp. 165–172, 2002.
- [63] R. Cheng, W. Huang, L. Huang et al., "Acceleration of tissue plasminogen activator-mediated thrombolysis by magnetically powered nanomotors," *ACS Nano*, vol. 8, no. 8, pp. 7746–7754, 2014.
- [64] J. Hu, W. Huang, S. Huang, Q. ZhuGe, K. Jin, and Y. Zhao, "Magnetically active Fe₃O₄ nanorods loaded with tissue plasminogen activator for enhanced thrombolysis," *Nano Research*, vol. 9, no. 9, pp. 2652–2661, 2016.
- [65] J. Hu, S. Huang, L. Zhu et al., "Tissue plasminogen activator-porous magnetic microrods for targeted thrombolytic therapy after ischemic stroke," *ACS Applied Materials & Interfaces*, vol. 10, no. 39, pp. 32988–32997, 2018.
- [66] M. Juenet, R. Aid-Launais, B. Li et al., "Thrombolytic therapy based on fucoidan-functionalized polymer nanoparticles targeting P-selectin," *Biomaterials*, vol. 156, pp. 204–216, 2018.
- [67] M.-S. Sun, H. Jin, X. Sun et al., "Free radical damage in ischemia-reperfusion injury: an obstacle in acute ischemic stroke after revascularization therapy," *Oxidative medicine and cellular longevity*, vol. 2018, Article ID 3804979, 17 pages, 2018.
- [68] C. Ren, N. Li, S. Li et al., "Limb ischemic conditioning improved cognitive deficits via eNOS-dependent augmentation of angiogenesis after chronic cerebral hypoperfusion in rats," *Aging and Disease*, vol. 9, no. 5, pp. 869–879, 2018.
- [69] I. G. Zigoneanu, C. E. Astete, and C. M. Sabliov, "Nanoparticles with entrapped α -tocopherol: synthesis, characterization, and controlled release," *Nanotechnology*, vol. 19, no. 10, pp. 105606–105606, 2008.
- [70] C. E. Astete, D. Dolliver, M. Whaley, L. Khachatryan, and C. M. Sabliov, "Antioxidant poly(lactic-co-glycolic) acid nanoparticles made with α -tocopherol-ascorbic acid surfactant," *ACS Nano*, vol. 5, no. 12, pp. 9313–9325, 2011.
- [71] Y. Liu, K. Ai, X. Ji et al., "Comprehensive insights into the multi-antioxidative mechanisms of melanin nanoparticles and their application to protect brain from injury in ischemic stroke," *Journal of the American Chemical Society*, vol. 139, no. 2, pp. 856–862, 2017.
- [72] X. Yun, V. D. Maximov, J. Yu, Zhu, A. A. Vertegel, and M. S. Kindy, "Nanoparticles for targeted delivery of antioxidant enzymes to the brain after cerebral ischemia and reperfusion injury," *Journal of cerebral blood flow and metabolism*, vol. 33, no. 4, pp. 583–592, 2013.
- [73] K. Hira, Y. Ueno, R. Tanaka et al., "Astrocyte-derived exosomes treated with a semaphorin 3A inhibitor enhance stroke recovery via prostaglandin D₂Synthase," *Stroke*, vol. 49, no. 10, pp. 2483–2494, 2018.
- [74] H. Xin, M. Katakowski, F. Wang et al., "MicroRNA cluster miR-17-92 cluster in exosomes enhance neuroplasticity and functional recovery after stroke in rats," *Stroke*, vol. 48, no. 3, pp. 747–753, 2017.
- [75] T. Tian, H. X. Zhang, C. P. He et al., "Surface functionalized exosomes as targeted drug delivery vehicles for cerebral ischemia therapy," *Biomaterials*, vol. 150, pp. 137–149, 2018.
- [76] H. Xin, Y. Li, Y. Cui, J. J. Yang, Z. G. Zhang, and M. Chopp, "Systemic administration of exosomes released from mesenchymal stromal cells promote functional recovery and neurovascular plasticity after stroke in rats," *Journal of cerebral blood flow and metabolism*, vol. 33, no. 11, pp. 1711–1715, 2013.
- [77] L. Qing, H. Chen, J. Tang, and X. Jia, "Exosomes and their microRNA cargo: new players in peripheral nerve regeneration," *Neurorehabilitation and Neural Repair*, vol. 32, no. 9, pp. 765–776, 2018.
- [78] N. J. Abbott, L. Rönnbäck, and E. Hansson, "Astrocyte-endothelial interactions at the blood-brain barrier," *Nature Reviews. Neuroscience*, vol. 7, no. 1, pp. 41–53, 2006.
- [79] N. J. Abbott, A. A. K. Patabendige, D. E. M. Dolman, S. R. Yusof, and D. J. Begley, "Structure and function of the blood-brain barrier," *Neurobiology of Disease*, vol. 37, no. 1, pp. 13–25, 2010.
- [80] W. M. Pardridge, "The blood-brain barrier: bottleneck in brain drug development," *NeuroRx*, vol. 2, no. 1, pp. 3–14, 2005.

- [81] S. Krol, R. Macrez, F. Docagne et al., "Therapeutic benefits from nanoparticles: the potential significance of nanoscience in diseases with compromise to the blood brain barrier," *Chemical Reviews*, vol. 113, no. 3, pp. 1877–1903, 2013.
- [82] M. F. Bennewitz and W. M. Saltzman, "Nanotechnology for delivery of drugs to the brain for epilepsy," *Neurotherapeutics*, vol. 6, no. 2, pp. 323–336, 2009.
- [83] A. Ben-Zvi, B. Lacoste, E. Kur et al., "Mfsd2a is critical for the formation and function of the blood-brain barrier," *Nature*, vol. 509, no. 7501, pp. 507–511, 2014.
- [84] B. V. Zlokovic, "The blood-brain barrier in health and chronic neurodegenerative disorders," *Neuron*, vol. 57, no. 2, pp. 178–201, 2008.
- [85] K. A. Witt, T. J. Gillespie, J. D. Huber, R. D. Egleton, and T. P. Davis, "Peptide drug modifications to enhance bioavailability and blood-brain barrier permeability," *Peptides*, vol. 22, no. 12, pp. 2329–2343, 2001.
- [86] M. Saeedi, M. Eslamifard, K. Khezri, and S. M. Dizaj, "Applications of nanotechnology in drug delivery to the central nervous system," *Biomedicine & pharmacotherapy*, vol. 111, pp. 666–675, 2019.
- [87] D. Furtado, M. Björnalm, S. Ayton, A. I. Bush, K. Kempe, and F. Caruso, "Overcoming the blood-brain barrier: the role of nanomaterials in treating neurological diseases," *Advanced materials*, vol. 30, no. 46, article e1801362, 2018.
- [88] T. M. Allen and P. R. Cullis, "Liposomal drug delivery systems: from concept to clinical applications," *Advanced Drug Delivery Reviews*, vol. 65, no. 1, pp. 36–48, 2013.
- [89] Y. Zhou, Z. Peng, E. S. Seven, and R. M. Leblanc, "Crossing the blood-brain barrier with nanoparticles," *Journal of controlled release*, vol. 270, pp. 290–303, 2018.
- [90] Z. Belhadj, M. Ying, X. Cao et al., "Design of Y-shaped targeting material for liposome-based multifunctional glioblastoma-targeted drug delivery," *Journal of controlled release*, vol. 255, pp. 132–141, 2017.
- [91] J. W. Paul, S. Hua, M. Ilicic et al., "Drug delivery to the human and mouse uterus using immunoliposomes targeted to the oxytocin receptor," *American Journal of Obstetrics and Gynecology*, vol. 216, no. 3, pp. 283.e1–283.e14, 2017.
- [92] J. A. Loureiro, B. Gomes, G. Fricker et al., "Dual ligand immunoliposomes for drug delivery to the brain," *Colloids and Surfaces. B, Biointerfaces*, vol. 134, pp. 213–219, 2015.
- [93] Y.-S. Kang, H. J. Jung, J. S. Oh, and D. Y. Song, "Use of PEGylated immunoliposomes to deliver dopamine across the blood-brain barrier in a rat model of Parkinson's disease," *CNS Neuroscience & Therapeutics*, vol. 22, no. 10, pp. 817–823, 2016.
- [94] H. He, J. Yao, Y. Zhang et al., "Solid lipid nanoparticles as a drug delivery system to cross the blood-brain barrier," *Biochemical and Biophysical Research Communications*, vol. 519, no. 2, pp. 385–390, 2019.
- [95] G. Graverini, V. Piazzini, E. Landucci et al., "Solid lipid nanoparticles for delivery of andrographolide across the blood-brain barrier: in vitro and in vivo evaluation," *Colloids and Surfaces. B, Biointerfaces*, vol. 161, pp. 302–313, 2018.
- [96] R. Gonzalez, M. H. Hamblin, and J.-P. Lee, "Neural stem cell transplantation and CNS diseases," *CNS & Neurological Disorders Drug Targets*, vol. 15, no. 8, pp. 881–886, 2016.
- [97] L. Wei, L. Cui, B. J. Snider et al., "Transplantation of embryonic stem cells overexpressing Bcl-2 promotes functional recovery after transient cerebral ischemia," *Neurobiology of Disease*, vol. 19, no. 1-2, pp. 183–193, 2005.
- [98] A. Trounson and C. McDonald, "Stem cell therapies in clinical trials: progress and challenges," *Cell Stem Cell*, vol. 17, no. 1, pp. 11–22, 2015.
- [99] K. Wu, D. Huang, C. Zhu et al., "NT3P75-2 gene-modified bone mesenchymal stem cells improve neurological function recovery in mouse TBI model," *Stem Cell Research & Therapy*, vol. 10, no. 1, article 311, 2019.
- [100] J. Hu, L. Chen, X. Huang et al., "Calpain inhibitor MDL28170 improves the transplantation-mediated therapeutic effect of bone marrow-derived mesenchymal stem cells following traumatic brain injury," *Stem Cell Research & Therapy*, vol. 10, no. 1, article 96, 2019.
- [101] H. Ni, S. Yang, F. Siaw-Debrah et al., "Exosomes derived from bone mesenchymal stem cells ameliorate early inflammatory responses following traumatic brain injury," *Frontiers in Neuroscience*, vol. 13, p. 14, 2019.
- [102] C. Hu and L. Li, "Preconditioning influences mesenchymal stem cell properties in vitro and in vivo," *Journal of Cellular and Molecular Medicine*, vol. 22, no. 3, pp. 1428–1442, 2018.
- [103] L. Yang, S. T. D. Chueng, Y. Li et al., "A biodegradable hybrid inorganic nanoscaffold for advanced stem cell therapy," *Nature Communications*, vol. 9, no. 1, pp. 3147–3147, 2018.
- [104] Y. Zhang, S. Wang, and P. Yang, "Effects of graphene-based materials on the behavior of neural stem cells," *Journal of Nanomaterials*, vol. 2020, Article ID 2519105, 16 pages, 2020.
- [105] N. Saito, H. Haniu, Y. Usui et al., "Safe clinical use of carbon nanotubes as innovative biomaterials," *Chemical Reviews*, vol. 114, no. 11, pp. 6040–6079, 2014.
- [106] N. W. S. Kam, E. Jan, and N. A. Kotov, "Electrical stimulation of neural stem cells mediated by humanized carbon nanotube composite made with extracellular matrix protein," *Nano Letters*, vol. 9, no. 1, pp. 273–278, 2009.
- [107] W. Li, Y. Guo, H. Wang et al., "Electrospun nanofibers immobilized with collagen for neural stem cells culture," *Journal of Materials Science. Materials in Medicine*, vol. 19, no. 2, pp. 847–854, 2008.
- [108] M. P. Prabhakaran, J. R. Venugopal, and S. Ramakrishna, "Mesenchymal stem cell differentiation to neuronal cells on electrospun nanofibrous substrates for nerve tissue engineering," *Biomaterials*, vol. 30, no. 28, pp. 4996–5003, 2009.
- [109] A. Dhaliwal, M. Brenner, P. Wolujewicz et al., "Profiling stem cell states in three-dimensional biomaterial niches using high content image informatics," *Acta Biomaterialia*, vol. 45, pp. 98–109, 2016.
- [110] L. Wang and W. S. Kisaalita, "Characterization of micropatterned nanofibrous scaffolds for neural network activity readout for high-throughput screening," *Journal of biomedical materials research Part B, Applied biomaterials*, vol. 94, no. 1, pp. 238–249, 2010.
- [111] Z. Qi, X. Chen, W. Guo, C. Fu, and S. Pan, "Theanine-modified graphene oxide composite films for neural stem cells proliferation and differentiation," *Journal of Nanomaterials*, vol. 2020, Article ID 3068173, 10 pages, 2020.
- [112] J. I. Choi, H. T. Cho, M. K. Jee, and S. K. Kang, "Core-shell nanoparticle controlled hATSCs neurogenesis for neuropathic pain therapy," *Biomaterials*, vol. 34, no. 21, pp. 4956–4970, 2013.
- [113] T. Santos, R. Ferreira, J. Maia et al., "Polymeric nanoparticles to control the differentiation of neural stem cells in the






- subventricular zone of the brain,” *ACS Nano*, vol. 6, no. 12, pp. 10463–10474, 2012.
- [114] E. K. Stachowiak, I. Roy, Y. W. Lee et al., “Targeting novel integrative nuclear FGFR1 signaling by nanoparticle-mediated gene transfer stimulates neurogenesis in the adult brain,” *Integrative biology*, vol. 1, no. 5–6, pp. 394–403, 2009.
- [115] S. Zhou, H. Zhao, R. Feng et al., “Application of amphiphilic fluorophore-derived nanoparticles to provide contrast to human embryonic stem cells without affecting their pluripotency and to monitor their differentiation into neuron-like cells,” *Acta Biomaterialia*, vol. 78, pp. 274–284, 2018.
- [116] X. Michalet, F. F. Pinaud, L. A. Bentolila et al., “Quantum dots for live cells, in vivo imaging, and diagnostics,” *Science*, vol. 307, no. 5709, pp. 538–544, 2005.
- [117] N. K. Devaraj, E. J. Keliher, G. M. Thurber, M. Nahrendorf, and R. Weissleder, “18F labeled nanoparticles for in vivo PET-CT imaging,” *Bioconjugate Chemistry*, vol. 20, no. 2, pp. 397–401, 2009.
- [118] X. Meng, H. C. Seton, L. T. Lu, I. A. Prior, N. T. K. Thanh, and B. Song, “Magnetic CoPt nanoparticles as MRI contrast agent for transplanted neural stem cells detection,” *Nanoscale*, vol. 3, no. 3, pp. 977–984, 2011.
- [119] C. Corot, P. Robert, J. M. Idée, and M. Port, “Recent advances in iron oxide nanocrystal technology for medical imaging,” *Advanced Drug Delivery Reviews*, vol. 58, no. 14, pp. 1471–1504, 2006.
- [120] F. Hyafil, J. C. Cornily, J. E. Feig et al., “Noninvasive detection of macrophages using a nanoparticulate contrast agent for computed tomography,” *Nature Medicine*, vol. 13, no. 5, pp. 636–641, 2007.
- [121] J. C. Frias, K. J. Williams, E. A. Fisher, and Z. A. Fayad, “Recombinant HDL-like nanoparticles: a specific contrast agent for MRI of atherosclerotic plaques,” *Journal of the American Chemical Society*, vol. 126, no. 50, pp. 16316–16317, 2004.
- [122] C. Wang, Y. Ye, Q. Hu, A. Bellotti, and Z. Gu, “Tailoring biomaterials for cancer immunotherapy: emerging trends and future outlook,” *Advanced Materials*, vol. 29, no. 29, 2017.
- [123] S. Zhou, S. Kawakami, F. Yamashita, and M. Hashida, “Intranasal administration of CpG DNA lipoplex prevents pulmonary metastasis in mice,” *Cancer Letters*, vol. 287, no. 1, pp. 75–81, 2010.
- [124] T. Mocan, C. Matea, F. Tabaran, C. Iancu, R. Orasan, and L. Mocan, “In vitro administration of gold nanoparticles functionalized with MUC-1 protein fragment generates anti-cancer vaccine response via macrophage activation and polarization mechanism,” *Journal of Cancer*, vol. 6, no. 6, pp. 583–592, 2015.
- [125] B. W. Simons, F. Cannella, D. T. Rowley, and R. P. Viscidi, “Bovine papillomavirus prostate cancer antigen virus-like particle vaccines are efficacious in advanced cancers in the TRAMP mouse spontaneous prostate cancer model,” *Cancer Immunology, Immunotherapy*, vol. 69, no. 4, pp. 641–651, 2020.
- [126] T. Nakamura, H. Miyabe, M. Hyodo, Y. Sato, Y. Hayakawa, and H. Harashima, “Liposomes loaded with a STING pathway ligand, cyclic di-GMP, enhance cancer immunotherapy against metastatic melanoma,” *Journal of Controlled Release*, vol. 216, pp. 149–157, 2015.
- [127] Y. Ma, Y. Zhang, X. Li et al., “Near-infrared II phototherapy induces deep tissue immunogenic cell death and potentiates cancer immunotherapy,” *ACS Nano*, vol. 13, no. 10, pp. 11967–11980, 2019.
- [128] Q. Chen, M. Chen, and Z. Liu, “Local biomaterials-assisted cancer immunotherapy to trigger systemic antitumor responses,” *Chemical Society Reviews*, vol. 48, no. 22, pp. 5506–5526, 2019.
- [129] M. B. Heo and Y. T. Lim, “Programmed nanoparticles for combined immunomodulation, antigen presentation and tracking of immunotherapeutic cells,” *Biomaterials*, vol. 35, no. 1, pp. 590–600, 2014.
- [130] F. Bray, J. Ferlay, I. Soerjomataram, R. L. Siegel, L. A. Torre, and A. Jemal, “Global cancer statistics 2018: GLOBOCAN estimates of incidence and mortality worldwide for 36 cancers in 185 countries,” *CA: a Cancer Journal for Clinicians*, vol. 68, no. 6, pp. 394–424, 2018.
- [131] M. J. Akhtar, M. Ahamed, H. A. Alhadlaq, S. A. Alrokayan, and S. Kumar, “Targeted anticancer therapy: overexpressed receptors and nanotechnology,” *Clinica Chimica Acta*, vol. 436, pp. 78–92, 2014.
- [132] P. N. Navya and H. K. Daima, “Rational engineering of physicochemical properties of nanomaterials for biomedical applications with nanotoxicological perspectives,” *Nano Convergence*, vol. 3, no. 1, article 1, 2016.
- [133] P. N. Navya, A. Kaphle, S. P. Srinivas, S. K. Bhargava, V. M. Rotello, and H. K. Daima, “Current trends and challenges in cancer management and therapy using designer nanomaterials,” *Nano Convergence*, vol. 6, no. 1, article 23, 2019.
- [134] J. Wan, X. Ma, D. Xu, B. Yang, S. Yang, and S. Han, “Docetaxel-decorated anticancer drug and gold nanoparticles encapsulated apatite carrier for the treatment of liver cancer,” *Journal of Photochemistry and Photobiology. B*, vol. 185, pp. 73–79, 2018.
- [135] P. Navya, A. Kaphle, and H. Daima, “Nanomedicine in sensing, delivery, imaging and tissue engineering: advances, opportunities and challenges,” *Nanoscience*, pp. 30–56, 2018.
- [136] M. Kumar, G. Sharma, C. Misra et al., “Desmethyl tamoxifen and quercetin-loaded multiwalled CNTs: a synergistic approach to overcome MDR in cancer cells,” *Materials Science and Engineering: C*, vol. 89, pp. 274–282, 2018.
- [137] L. Sercombe, T. Veerati, F. Moheimani, S. Y. Wu, A. K. Sood, and S. Hua, “Advances and challenges of liposome assisted drug delivery,” *Frontiers in Pharmacology*, vol. 6, p. 286, 2015.
- [138] Y. Peng, J. Huang, H. Xiao, T. Wu, and X. Shuai, “Codelivery of temozolomide and siRNA with polymeric nanocarrier for effective glioma treatment,” *International Journal of Nanomedicine*, vol. Volume 13, pp. 3467–3480, 2018.
- [139] N. Bertrand, J. Wu, X. Xu, N. Kamaly, and O. C. Farokhzad, “Cancer nanotechnology: the impact of passive and active targeting in the era of modern cancer biology,” *Advanced Drug Delivery Reviews*, vol. 66, pp. 2–25, 2014.
- [140] D. Rosenblum, N. Joshi, W. Tao, J. M. Karp, and D. Peer, “Progress and challenges towards targeted delivery of cancer therapeutics,” *Nature Communications*, vol. 9, no. 1, p. 1410, 2018.
- [141] A. Verma and F. Stellacci, “Effect of surface properties on nanoparticle-cell interactions,” *Small*, vol. 6, no. 1, pp. 12–21, 2010.
- [142] R. Mout, D. F. Moyano, S. Rana, and V. M. Rotello, “Surface functionalization of nanoparticles for nanomedicine,” *Chemical Society Reviews*, vol. 41, no. 7, pp. 2539–2544, 2012.

- [143] M. S. Devadas, T. Devkota, S. Guha, S. K. Shaw, B. D. Smith, and G. V. Hartland, "Spatial modulation spectroscopy for imaging and quantitative analysis of single dye-doped organic nanoparticles inside cells," *Nanoscale*, vol. 7, no. 21, pp. 9779–9785, 2015.
- [144] Y. Zhang, P. Lundberg, M. Diether et al., "Histamine-functionalized copolymer micelles as a drug delivery system in 2D and 3D models of breast cancer," *Journal of Materials Chemistry B*, vol. 3, no. 12, pp. 2472–2486, 2015.
- [145] R. Weissleder, K. Kelly, E. Y. Sun, T. Shtatland, and L. Josephson, "Cell-specific targeting of nanoparticles by multivalent attachment of small molecules," *Nature Biotechnology*, vol. 23, no. 11, pp. 1418–1423, 2005.
- [146] R. Coradeghini, S. Gioria, C. P. García et al., "Size-dependent toxicity and cell interaction mechanisms of gold nanoparticles on mouse fibroblasts," *Toxicology Letters*, vol. 217, no. 3, pp. 205–216, 2013.
- [147] Z. Ji, X. Wang, H. Zhang et al., "Designed synthesis of CeO₂ nanorods and nanowires for studying toxicological effects of high aspect ratio nanomaterials," *ACS Nano*, vol. 6, no. 6, pp. 5366–5380, 2012.
- [148] M. Wetzler, D. A. Thomas, E. S. Wang et al., "Phase I/II trial of nanomolecular liposomal anamycin in adult patients with relapsed/refractory acute lymphoblastic leukemia," *Clinical Lymphoma, Myeloma & Leukemia*, vol. 13, no. 4, pp. 430–434, 2013.
- [149] E. Chen, B. M. Chen, Y. C. Su et al., "Premature drug release from polyethylene glycol (PEG)-coated liposomal Doxorubicin via formation of the membrane attack complex," *ACS Nano*, vol. 14, no. 7, pp. 7808–7822, 2020.
- [150] K. Sasaki, H. Kantarjian, W. Wierda et al., "Phase 2 study of hyper-CMAD with liposomal vincristine for patients with newly diagnosed acute lymphoblastic leukemia," *American Journal of Hematology*, vol. 95, no. 7, pp. 734–739, 2020.
- [151] F. Zahednezhad, P. Zakeri-Milani, J. Shahbazi Mojarrad, and H. Valizadeh, "The latest advances of cisplatin liposomal formulations: essentials for preparation and analysis," *Expert Opinion on Drug Delivery*, vol. 17, no. 4, pp. 523–541, 2020.
- [152] M. C. O. da Rocha, P. B. da Silva, M. A. Radicchi et al., "Docetaxel-loaded solid lipid nanoparticles prevent tumor growth and lung metastasis of 4T1 murine mammary carcinoma cells," *Journal of Nanobiotechnology*, vol. 18, no. 1, p. 43, 2020.
- [153] H. M. Aldawsari and S. Singh, "Rapid microwave-assisted cisplatin-loaded solid lipid nanoparticles: synthesis, characterization and anticancer study," *Nanomaterials*, vol. 10, no. 3, p. 510, 2020.
- [154] J. M. Rademaker-Lakhai, "A phase I and pharmacological study of the platinum polymer AP5280 given as an intravenous infusion once every 3 weeks in patients with solid tumors," *Clinical Cancer Research*, vol. 10, no. 10, pp. 3386–3395, 2004.
- [155] M. Rizwanullah, M. Alam, Harshita, S. R. Mir, M. M. A. Rizvi, and S. Amin, "Polymer-lipid hybrid nanoparticles: a next-generation nanocarrier for targeted treatment of solid tumors," *Current Pharmaceutical Design*, vol. 26, no. 11, pp. 1206–1215, 2020.
- [156] Q. Liu, H. Zhu, J. Qin, H. Dong, and J. du, "Theranostic vesicles based on bovine serum albumin and poly(ethylene glycol)-block-poly(L-lactic-co-glycolic acid) for magnetic resonance imaging and anticancer drug delivery," *Biomacromolecules*, vol. 15, no. 5, pp. 1586–1592, 2014.
- [157] J. F. Kukowska-Latallo, K. A. Candido, Z. Cao et al., "Nanoparticle targeting of anticancer drug improves therapeutic response in animal model of human epithelial cancer," *Cancer Research*, vol. 65, no. 12, pp. 5317–5324, 2005.
- [158] M. T. Morgan, Y. Nakanishi, D. J. Kroll et al., "Dendrimer-encapsulated camptothecins: increased solubility, cellular uptake, and cellular retention affords enhanced anticancer activity in vitro," *Cancer Research*, vol. 66, no. 24, pp. 11913–11921, 2006.
- [159] J. H. Maeng, D. H. Lee, K. H. Jung et al., "Multifunctional doxorubicin loaded superparamagnetic iron oxide nanoparticles for chemotherapy and magnetic resonance imaging in liver cancer," *Biomaterials*, vol. 31, no. 18, pp. 4995–5006, 2010.
- [160] C. Kim, H. Kim, H. Park, and K. Y. Lee, "Controlling the porous structure of alginate ferrogel for anticancer drug delivery under magnetic stimulation," *Carbohydrate Polymers*, vol. 223, article 115045, 2019.
- [161] S. J. Lee, H. S. Min, S. H. Ku et al., "Tumor-targeting glycol chitosan nanoparticles as a platform delivery carrier in cancer diagnosis and therapy," *Nanomedicine*, vol. 9, no. 11, pp. 1697–1713, 2014.
- [162] E. Cruz and V. Kayser, "Synthesis and enhanced cellular uptake in vitro of anti-HER2 multifunctional gold nanoparticles," *Cancers*, vol. 11, no. 6, p. 870, 2019.
- [163] K. Ovejero Paredes, D. Díaz-García, V. García-Almodóvar et al., "Multifunctional silica-based nanoparticles with controlled release of organotin metaldrug for targeted theranosis of breast cancer," *Cancers*, vol. 12, no. 1, p. 187, 2020.
- [164] G. Rego, M. Nucci, J. Mamani et al., "Therapeutic efficiency of multiple applications of magnetic hyperthermia technique in glioblastoma using aminosilane coated iron oxide nanoparticles: in vitro and in vivo study," *International Journal of Molecular Sciences*, vol. 21, no. 3, p. 958, 2020.
- [165] A. J. Tevaarwerk, K. D. Holen, D. B. Alberti et al., "Phase I trial of 2-methoxyestradiol nanocrystal dispersion in advanced solid malignancies," *Clinical Cancer Research*, vol. 15, no. 4, pp. 1460–1465, 2009.
- [166] D. Matej, J. Schilder, G. Sutton et al., "Activity of 2 methoxyestradiol (Panzem NCD) in advanced, platinum-resistant ovarian cancer and primary peritoneal carcinomatosis: a Hoosier oncology group trial," *Gynecologic Oncology*, vol. 115, no. 1, pp. 90–96, 2009.
- [167] A. Rehman, S. Houshyar, and X. Wang, "Nanodiamond in composite: biomedical application," *Journal of Biomedical Materials Research. Part A*, vol. 108, no. 4, pp. 906–922, 2020.
- [168] A. C. Mita, A. J. Olszanski, R. C. Walovitch et al., "Phase I and pharmacokinetic study of AI-850, a novel microparticle hydrophobic drug delivery system for paclitaxel," *Clinical Cancer Research*, vol. 13, no. 11, pp. 3293–3301, 2007.
- [169] K. Wosikowski, E. Biedermann, B. Rattel et al., "In vitro and in vivo antitumor activity of methotrexate conjugated to human serum albumin in human cancer cells," *Clinical Cancer Research*, vol. 9, no. 5, pp. 1917–1926, 2003.
- [170] S.-S. Feng and S. J. C. E. S. Chien, "Chemotherapeutic engineering: application and further development of chemical engineering principles for chemotherapy of cancer and other diseases," vol. 58, no. 18, pp. 4087–4114, 2003.
- [171] B. R. Ferrell, J. S. Temel, S. Temin et al., "Integration of palliative care into standard oncology care: American Society of Clinical Oncology clinical practice guideline update," *Journal of Clinical Oncology*, vol. 35, no. 1, pp. 96–112, 2017.

- [172] D. W. Northfelt, B. J. Dezube, J. A. Thommes et al., "Pegylated-liposomal doxorubicin versus doxorubicin, bleomycin, and vincristine in the treatment of AIDS-related Kaposi's sarcoma: results of a randomized phase III clinical trial," *Journal of Clinical Oncology*, vol. 16, no. 7, pp. 2445–2451, 1998.
- [173] R. Duncan, "Polymer conjugates as anticancer nanomedicines," *Nature Reviews. Cancer*, vol. 6, no. 9, pp. 688–701, 2006.
- [174] T. Tanaka, S. Shiramoto, M. Miyashita, Y. Fujishima, and Y. Kaneo, "Tumor targeting based on the effect of enhanced permeability and retention (EPR) and the mechanism of receptor-mediated endocytosis (RME)," *International Journal of Pharmaceutics*, vol. 277, no. 1-2, pp. 39–61, 2004.
- [175] J.-o. Deguchi, M. Aikawa, C.-H. Tung et al., "Inflammation in atherosclerosis: visualizing matrix metalloproteinase action in macrophages in vivo," *Circulation*, vol. 114, no. 1, pp. 55–62, 2006.
- [176] A. Jordan, R. Scholz, K. Maier-Hauff et al., "The effect of thermotherapy using magnetic nanoparticles on rat malignant glioma," *Journal of Neuro-Oncology*, vol. 78, no. 1, pp. 7–14, 2006.
- [177] S. D. Steichen, M. Caldorera-Moore, and N. A. Peppas, "A review of current nanoparticle and targeting moieties for the delivery of cancer therapeutics," *European Journal of Pharmaceutical Sciences*, vol. 48, no. 3, pp. 416–427, 2013.
- [178] E. Polo, M. Collado, B. Pelaz, and P. del Pino, "Advances toward more efficient targeted delivery of nanoparticles in vivo: understanding interactions between nanoparticles and cells," *ACS Nano*, vol. 11, no. 3, pp. 2397–2402, 2017.
- [179] K. Unfried, C. Albrecht, L.-O. Klotz, A. Von Mikecz, S. Grether-Beck, and R. P. F. Schins, "Cellular responses to nanoparticles: target structures and mechanisms," *Nanotoxicology*, vol. 1, no. 1, pp. 52–71, 2009.

Research Article

Gelatin Encapsulated Curcumin Nanoparticles Moderate Behavior of Human Primary Gingival Fibroblasts In Vitro

Mai Thi-Hoang Nguyen ¹, Khanh Loan Ly ^{2,3}, Thoai Quoc Kieu ¹, Hiep Thi Nguyen ^{2,3}
and Nam Cong-Nhat Huynh ¹

¹Department of Dental Basic Sciences, Faculty of Odonto-Stomatology, University of Medicine and Pharmacy at Ho Chi Minh City, Ho Chi Minh City, Vietnam

²Tissue Engineering and Regenerative Medicine Department, School of Biomedical Engineering, International University, Vietnam

³Vietnam National University, Ho Chi Minh City, Vietnam

Correspondence should be addressed to Hiep Thi Nguyen; nthiep@hcmiu.edu.vn
and Nam Cong-Nhat Huynh; namhuynh@ump.edu.vn

Received 12 March 2020; Revised 8 May 2020; Accepted 26 May 2020; Published 9 July 2020

Guest Editor: Anuj Kumar

Copyright © 2020 Mai Thi-Hoang Nguyen et al. This is an open access article distributed under the Creative Commons Attribution License, which permits unrestricted use, distribution, and reproduction in any medium, provided the original work is properly cited.

Objective. Currently, there is no study evaluating the effect of nano-curcumin on human oral cells in vitro. In this study, we developed gelatin encapsulated curcumin nanoparticles (GelCur) and cultured the primary human gingival fibroblasts (hGFs) to verify the effect of GelCur on the cellular events related to oral wound healing capacities, such as cell migration and proliferation of gingival fibroblasts. **Materials and Methods.** GelCur was produced by the sonoprecipitation method. Particle size, zeta potential, SEM morphological observation, entrapment efficiency, and drug loading were used to characterize new GelCur. Primary hGFs were cultured from the attached gingival tissue of healthy third molar teeth. The effect of different concentrations of GelCur on hGFs was investigated by cell toxicity assay (MTT), cell proliferation assay, and cell migration assays by scratch test and transwell migration assay. **Results.** The average particle size of GelCur was around 356 nm with a moderate zeta potential of 26.5 mV. The mean PDI value of GelCur was 0.2, while the entrapment efficiency and drug loading of curcumin in this study were around 57% and 2.4%, respectively. IC_{30} of GelCur on hGFs was 3.96 mg/ml, while IC_{50} was 12.37 mg/ml. More than 70% of cells were viable after 24 hours incubated with 1, 2, and 3 mg/ml GelCur. At the concentration of 2 mg/ml GelCur virtually limited cell proliferation and migration. **Conclusions.** GelCur remained physically stable and did not alter cell proliferation and migration. The concentration of GelCur <3.96 mg/ml did not cause hGF cytotoxicity. Our study showed that within appropriate doses, GelCur can be used safely for hGFs.

1. Introduction

With the current situation of drug resistance and abuse, natural medicines have been considered for patients. Turmeric (*Curcuma longa*), the major source of the curcumin (*diferuloylmethane*), has long been recognized for its beneficial pharmacological properties and is still being widely practiced as a noninvasive wound therapy in many cultures [1]. Traditionally, curcumin has been a popular remedy for the treatment of anti-inflammation, accelerate wound healing, and minimal scar formation. The wound healing potential of curcumin, which correlated to its biochemical effects such as

anti-inflammatory, anti-infectious, and antioxidant activities, has been investigated over recent years, leading to a remarkable increase of clinical trials and publications [1–3]. Furthermore, many curcumin-based wound dressings have been developed such as PVA/Chitosan/Curcumin, PVA-SA/TiO₂-CUR, or sodium alginate/PVA incorporated curcumin patch for its anti-inflammatory, antioxidant, and antibacterial properties that aid in the wound healing process [4–6]. Despite the medicinal biological significances, the applications of these findings into clinical treatments have so far been impeded due to several physicochemical inherent limitations of curcumin, especially its poor absorption,

hydrophobicity, instability, rapid metabolism, and elimination [1, 7]. To overcome these obstacles, various curcumin formulations, including emulsified micelles, nanofibers, nanocapsules, or hydrogel, have been developed.

A variety of curcumin-based systems have been produced to resolve those problems and enhance the applications of curcumin can be referred. For instance, Slika et al. have prepared curcumin-poly (allyl amine) hydrochloride-based nanocapsules to accelerate the encapsulation and release of curcumin to enhance its effectiveness against colon cancer [8]. Mouslmani and colleagues have developed a curcumin associated poly (allylamine hydrochloride)-phosphate self-assembled nanocapsules to control curcumin release and its antioxidant activity [9]. Venkatasubbu's group has incorporated curcumin into chitosan/TiO₂ nanoparticles to control its release for infectious wound management [10]. Especially, the development of nanobiotechnology allows for the encapsulation of curcumin in drug delivery systems such as gelatin nanoparticles has emerged as a remedial approach [11]. Gelatin nanoparticles have been recognized as potential candidates for medical applications by owning biodegradable, biocompatible, and nontoxicity properties. Moreover, the encapsulation of drug in gelatin nanoparticles enhance drug stability and control drug release effectively [12].

Oral fibroblast, including gingival fibroblast, plays important role in oral tissue homeostatic maintenance, wound healing, and tissue repair by synthesizing and secreting various extracellular matrix (ECM) proteins, containing collagen, fibronectin, and proteoglycans [13]. To investigate the natural remedies, which are safe, effective to accelerate oral wound healing and reduce the treatment costs is necessary. However, there is no study to investigate the effect of nano-curcumin in oral cells regarding cell toxicity, proliferation, and migration. Ngo and colleagues have previously developed and characterized gelatin encapsulated curcumin nanoparticles (GelCur) to implement in transdermal drug delivery study [11]. Following up on those insights, in this study, we synthesized GelCur based on established work and cultured the primary human gingival fibroblasts to verify the effect of GelCur on the cellular events related to oral wound healing capacities, such as cell migration and proliferation of gingival fibroblasts.

2. Materials and Methods

2.1. Fabrication of Gelatin Encapsulated Curcumin. Curcumin powders were supplied by Shanghai Zhanyun Chemical Co. Ltd. (China). Gelatin (bovine skin, type B) and poloxamer 407 (POX 407) were obtained from Sigma-Aldrich, Inc. (USA). The method of encapsulating curcumin using gelatin followed the sonoprecipitation method in the previous study [11]. Briefly, 20 mg curcumin and 250 mg poloxamer 407 (POX407) were dissolved in 5 ml methanol to form solvent phase suspension. 20 ml of gelatin solution 1 wt% was prepared by dissolving gelatin powder in distilled water and stirring at 400 rpm at 40°C for 1 hour. The prepared solvent phase suspension (Cur/POX407) was added dropwise into antisolvent phase (gelatin solution 1 wt%) while stirring at 750 rpm. The mixture was then sonicated

for 20 minutes using probe sonication (QSONICA, USA) with an amplitude of 30%. The mixture was kept in an ice-cold water bath to maintain the temperature below 30°C. After sonication, the mixture was left stirring at 30°C for 2 hours for methanol to evaporate. In the subsequent step, the mixture was centrifuged at 1000 rpm for 30 minutes to remove the pellets, then the supernatant was collected and lyophilized at -50°C for 48 hours using Labconco Freeze Dryer (USA) to obtain GelCur powders (Figure 1(a)).

2.2. Characterization of Gelatin Encapsulated Curcumin

2.2.1. Particle Size and Zeta Potential. The particle size and zeta potential (parameter correlates with the surface charge of nanosuspension) of GelCur were analyzed using Zetasizer Nano Series (Malvern Instrument Limited, UK). 10 μ l of GelCur suspension was diluted with 10 ml methanol as dispersing solution, followed by vortex shaking prior analysis. Measurements were performed in triplicate at 25°C.

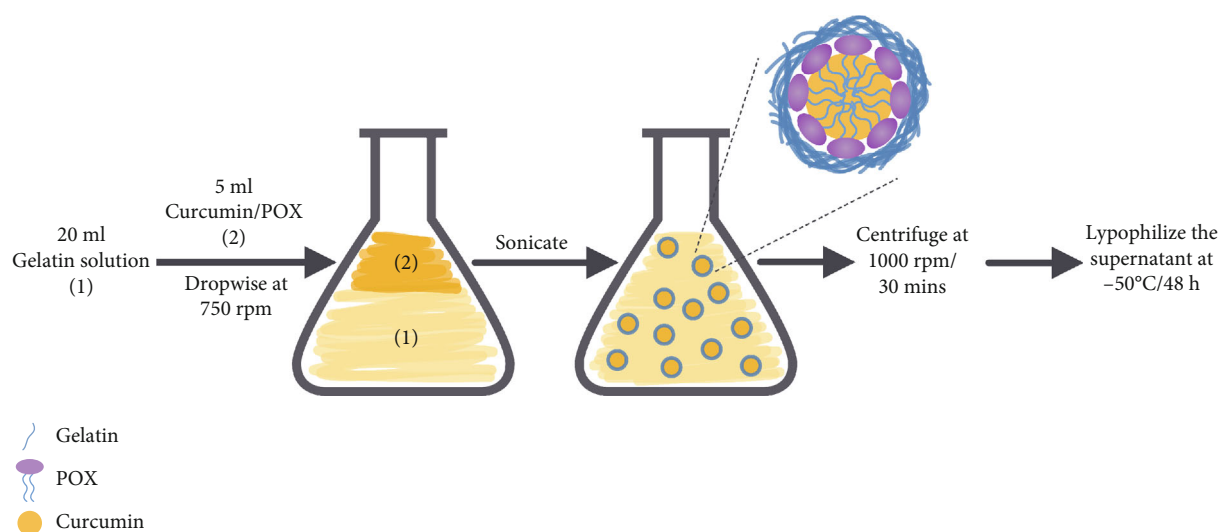
2.2.2. Entrapment Efficiency and Drug Loading. The quantity of curcumin was determined using Ultimate 3000 HPLC (Thermo Fisher Scientific Inc., USA) followed previous studies' settings [11]. 23.5 mg of GelCur powders (equivalent to 1 mg of curcumin corresponding to theoretical mass) was dispersed in 25 ml distilled water, followed by ultrasonication at 50°C for 30 minutes. Then, absolute ethanol was added into the cooled down mixture and adjusted accurately to obtain 50 ml of the total solution. 100 μ l of the solution was diluted with 900 μ l methanol for HPLC analysis. The measurement was performed three times for each sample; the entrapment efficiency (EE) and drug loading (DL) were calculated using the given equations:

$$EE = \frac{\text{the mass of drug in nanoparticles}}{\text{total mass of drug used in the preparation of nanoparticles}} \times 100\%$$

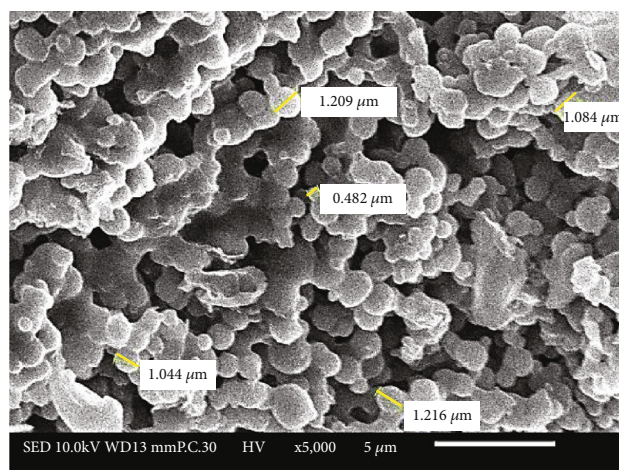
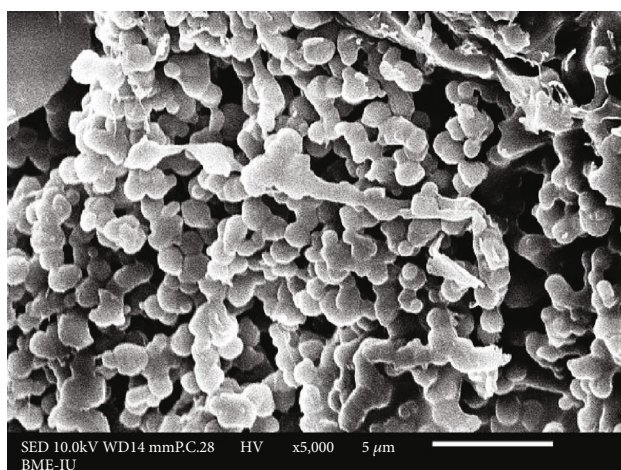
$$DL = \frac{\text{the mass of drug in nanoparticles}}{\text{the mass of nanoparticles}} \times 100\%$$

2.2.3. Morphological Observation. A scanning electron microscope (SEM, JSM-IT100, JEOL, Japan) was employed to observe the morphology of GelCur powders at 10 kV. Before SEM observation, the samples were coated with Au using the sputter-coater (Cressington Sputter Coater 108 auto).

2.3. Primary Human Gingival Fibroblast Culture. Ten third molars from seven 18 to 25-year-old healthy volunteers were extracted as recommended by their dentist. Tissues were obtained individually as previous studies [13, 14]. Immediately after extraction, the teeth were transferred to the lab in ice-cold storage medium Dulbecco's Modified Eagle's Medium/Ham's Nutrient Mixture F12 (DMEM/F12) supplemented with 10% FBS, 500 UI/ml penicillin, 500 μ g/ml streptomycin (Sigma, USA). The gingival tissues attached to the cervical area were carefully removed from the tooth and rinsed twice with PBS. The tissue was minced into 1 \times 2 mm pieces with a surgical blade and seeded in DMEM/F12 supplemented with 10% FBS, 1% antibiotics. The tissue samples were incubated separately at 37°C humidified atmosphere with 5% CO₂, the medium was replaced every 3 days until outgrowing cells reached confluence. The primary



(a)



(b)

FIGURE 1: (a) Schematic of gelatin encapsulated curcumin nanoparticles (GelCur) production. (b) SEM micrographs of GelCur (left) and the nanoparticle size measurements (right) at $\times 5000$ magnification.

hGFs at the 3rd–6th passage were used for the experiments. The patients provided written informed consent for the use of discarded tissues for research purposes. Tissue samples were de-identified and analyzed anonymously. The use of gingival tissues for research purposes was approved by the Ethics Committee of the University of Medicine and Pharmacy at Ho Chi Minh City (No. 277/DHYD-HDDD).

2.4. Cell Toxicity Assay. Cell toxicity assay was assessed by 3-(4,5-dimethylthiazol-2-yl)-2,5-diphenyl tetrazolium bromide assay (MTT, USB Corporation, USA) [15, 16]. The cells were plated at 10^4 cells/well in 96-well plates. Cells were incubated with 1, 2, 3, 4, and 5 mg/ml GelCur with the approximate concentration of curcumin being 66, 132, 198, 264, and $330 \mu\text{M}$, respectively (diluted in 10% FBS DMEM/F12 and serum-free DMEM/F12). DMSO 20% was used as the control based on the ability to induce cell death of DMSO from 20% as the previous studies [17, 18]. After 24 h, the medium was replaced with $100 \mu\text{l}$ MTT solution and incubated for 30 min at 37°C . The formazan product was

dissolved in solubilization/stop solution. Using a microplate reader (EZ Read 400, Biochrom, UK), the optical densities were measured at 570 nm. The relative growth rate (RGR) as ISO 10993-5 was calculated by: $\%RGR = (OD_{570e}/OD_{570b}) \times 100\%$, in which OD_{570e} is the optical density of GelCur treated group and OD_{570b} is the optical density of 10% FBS DMEM/F12 group. Cells were toxic when %RGR which is lower than 70% [19].

2.5. Cell Proliferation Assay. For proliferation assay, cells were plated at 10^3 cells/well in 96-well plate. From the result of toxicity assay, cells were treated with a proper dose of GelCur (diluted in 10% FBS DMEM/F12 and serum-free DMEM/F12) and control groups. After 1, 3, 5, 7, 9, 11 days, cell numbers were counted by trypan blue 0.4% as previously [16]. Briefly, $20 \mu\text{l}$ of cell suspension from each well was mixed with $20 \mu\text{l}$ trypan blue solution following by 3 minutes incubation at room temperature. The cells mixture was loaded into a hemocytometer and counted by a light microscope [16].

2.6. Scratch-Test Assay (“wound healing assay”). Firstly, 10^5 cells/well were seeded in 6-well-plate. After cell starving, a sterile $100\ \mu\text{l}$ pipette tip was used to make a straight scratch line on the monolayer of confluent cells at the bottom of the culture plate. The debris was washed away with PBS, and the cells were then cultured at 37°C , humidified 5% CO_2 . The cells were treated with GelCur at the concentration of 2 mg/ml by diluting in DMEM (with or without FBS). Culture medium contains 10% FBS was used as positive control, while the serum-free medium was used as the negative control. At time point 0 h and 24 h, the whole cell-free areas of each well were observed and recorded by an inverted microscope (CKX53, Olympus, Japan) and digital camera in the same position. The area of “wound healing” was analyzed using the Image-Analysis J 1.45S software as described previously [13].

2.7. Transwell Migration Assay. 3D cell migration assay was performed in 24-well size transwell inserts with $8.0\text{-}\mu\text{m}$ -pore polycarbonate membrane and $0.3\ \text{cm}^2$ effective growth area (BD Falcon™ Cell Culture Inserts, BD Biosciences, USA). 3×10^5 cells in a total of $200\ \mu\text{l}$ medium were seeded in each insert. To prevent cell proliferation, the migration assay was performed with serum-free medium in the presence or absence of GelCur for 16 hours. On the next day, nonmigrated cells from the upper surface of the membrane were carefully removed by a cotton swab. The cells that migrated to the other side of the membrane were fixed by formaldehyde 3,7% in PBS for 2 minutes following by 100% methanol. Then, cells were stained with Giemsa’s azur eosin methylene blue solution (Merck, Germany) and washed two times in PBS [20].

2.8. Data Analysis. All experiments were repeated with three different cell lines, each line was repeated three times. For statistical analysis, Kruskal-Wallis rank sum test and Dunn Kruskal-Wallis multiple comparisons posthoc test were used to compare between groups. We analyzed by package drc (dose-response curve), R version 3.6.1 with the level of significance being 0.05. p values were adjusted with Bonferroni correction for multiple testing.

3. Results

3.1. Characteristics of GelCur. Following the production of GelCur, the analysis showed that the average particle size of GelCur was around 356 nm with a moderate zeta potential of 26.5 mV (Table 1), which remained physically stable and considered to be acceptable in this study. The PdI reveals the particle size distribution of nanosuspension, where the smaller range of particle size, the smaller PdI values and the contrary. The mean PdI value of GelCur was as small as 0.2 indicating that this GelCur nanosuspension possessed a uniform size distribution for monodisperse standards.

The entrapment efficiency measures the amount of curcumin that can be loaded into nanoparticles. The entrapment efficiency and drug loading of curcumin in this study were around 57% and 2.4%, respectively. The entrapment efficiency is determined by the concentration of drug carriers

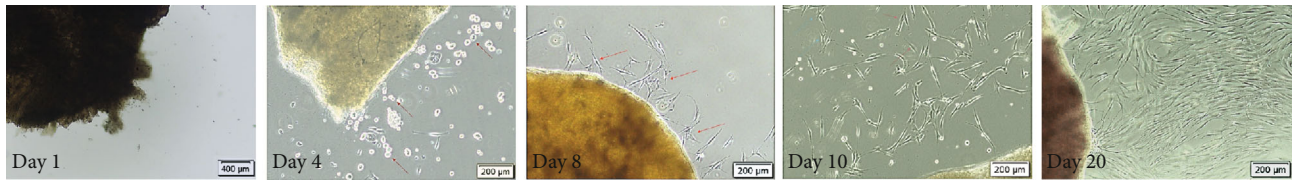
TABLE 1: Characteristics of GelCur including particle size, particle size distribution (PdI), zeta potential, entrapment efficiency, and drug loading. Each measurement was repeated at least in three independent experiments (SD: standard deviation).

Parameter	Value \pm SD
Particle size (nm)	356.8 ± 35.3
PdI	0.21 ± 0.07
Zeta potential (mV)	26.5 ± 2.1
Entrapment efficiency (%)	57.03 ± 5.5
Drug loading (%)	2.43 ± 0.23

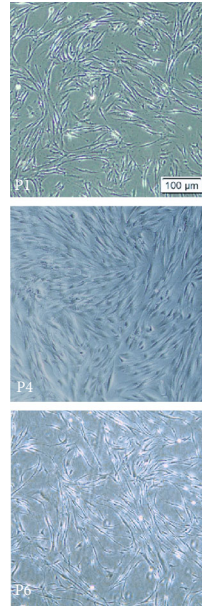
(gelatin), in which the higher the concentration of gelatin, the higher the viscosity of nanosuspension. The increase in viscosity could prevent diffusion between solution and anti-solvent, where the larger particles containing higher curcumin content were fabricated. SEM was also employed to confirm the morphology of GelCur powders (Figure 1(b)). Further characterizations of GelCur including Fourier-transform infrared spectroscopy, X-ray diffraction, and Cur release profile can be found in the previous study [11].

3.2. Primary Culture of hGFs. At day 4-8, cells appeared from gingiva tissues by outgrowth culture method (Figure 2(a)). These cells started with different shapes (star, round, elongated shapes) and then gradually exhibited uniformed typical fibroblast-like morphology with a large oval nucleus and many cytoplasmic tails on day 10 (Figures 2(a) and 2(c)). The cells were healthy growing and reached confluent at day 20, even at passage 6th (Figure 2(b)).

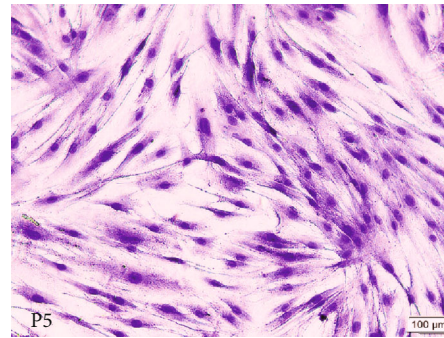
3.3. GelCur Induces Cytotoxicity of hGFs in a Dose-Dependent Manner. To assess the cell viability, hGFs were treated with different concentrations of GelCur (1–5 mg/ml) for 24 hours, and cytotoxicity was measured by MTT assays. Results indicated that GelCur induced cytotoxicity in a dose-dependent manner (Figure 2(e)). The alteration of the shape and morphology of hGFs upon their incubation with GelCur was observed by an optical microscope (Figure 2(d)). Different concentrations of GelCur diluted in culture medium produced different shade of yellow colors. hGFs with normal morphology (spindle shape) were observed at the concentration 1, 2, and 3 mg/ml of GelCur, which are homologous with the negative control group. Meanwhile, treated with higher concentrations of GelCur (4 and 5 mg/ml), some hGFs with abnormal morphologies (shrinkage) are detected. More particularly, hGFs viability was decreased to 88.8%, 78.7%, 72.5%, 69.9%, and 68.1% for the concentrations of 1, 2, 3, 4, and 5 mg/ml, respectively. However, there was no significant difference within serum medium and GelCur groups by adjusted p values. Only DMSO 20% gave to significant cytotoxicity on hGFs. From the % of cell viability, IC_{50} and IC_{30} of GelCur on hGF were calculated (12,37 mg/ml and 3,96 mg/ml, respectively). According to ISO 10993-5:2009 standard for in vitro cytotoxicity, a dose of GelCur $>3.96\ \text{mg/ml}$ which resulting in $<70\%$ viable cells after 24 hours will be cytotoxic to hGFs [19].



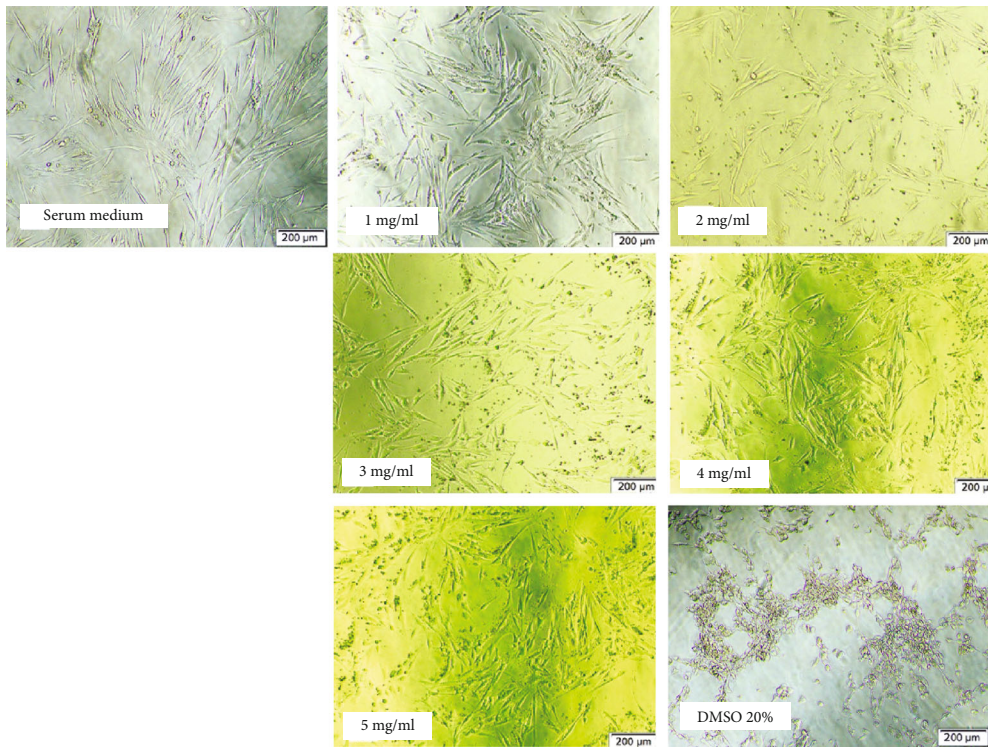
(a)



(b)



(c)



(d)

FIGURE 2: Continued.

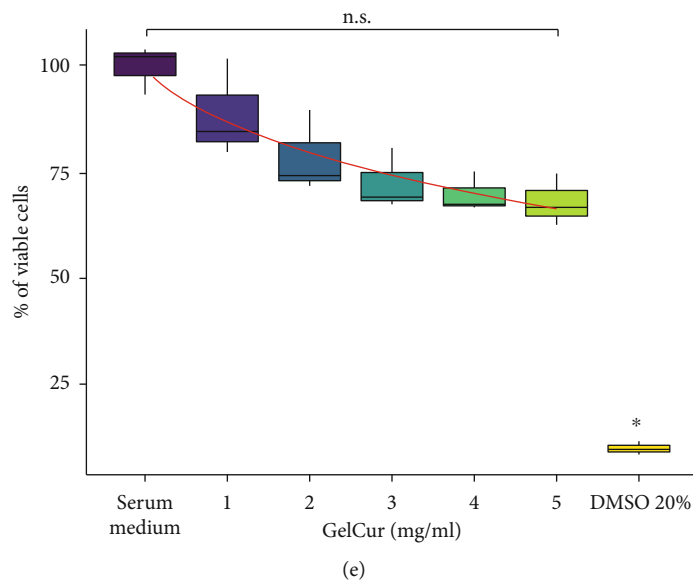


FIGURE 2: (a) Primary culture of hGFs from the gingival tissue at day 1-20. (b) hGFs at passage 1st, 4th, and 6th. (c) hGF morphology by H&E staining at passage 5th. (d) hGF culture under various conditions and concentrations of GelCur after 24 h. (e) % of hGF viability under different conditions (Dunn Kruskal-Wallis multiple comparisons, there was a significant difference between DMSO 20% vs. serum medium group with adjusted $*p < 0.05$, no significant difference was found in GelCur, serum medium groups).

3.4. GelCur Inhibits hGFs Proliferation. Base on the results of the cell toxicity assay, the concentration of 2 mg/ml was used to evaluate the effects of nano-curcumin on the proliferation of hGFs. hGFs allowed to proliferate through serum-free and serum-supplemented DMEM were used as negative and positive controls. GelCur inhibited hGFs proliferation in a time-dependent manner (Figure 3(a)). The cell number of the positive control group significantly increased and reached a peak at day 7, while a reverse trend was observed in other groups. Data indicated that from day 5 to 11, cell proliferation was significantly (adjusted $p < 0.05$) suppressed in both hGFs treated with GelCur in serum-free and serum medium in comparison with the positive control group. Additionally, on day 9, cell numbers in GelCur/serum medium groups were higher than GelCur/serum-free group. Generally, the proliferation of hGFs was substantially reduced after curcumin administration.

3.5. GelCur Do Not Influence the Migration of hGFs. To investigate the effect of nano-curcumin in hGFs migration during the oral wound-healing process, a scratch-test assay was conducted. After 24 hours, migrated cells toward the provisional gap were observed only in the serum medium group, which indicated the natural rate of cell migration (Figure 3(b)). The migrated hGFs were noted to be the lower in the presence of GelCur. However, the analysis showed no significant difference among groups (Figure 3(c)). Overall, although at the nontoxicity level, GelCur did not influence the migration of gingival fibroblasts.

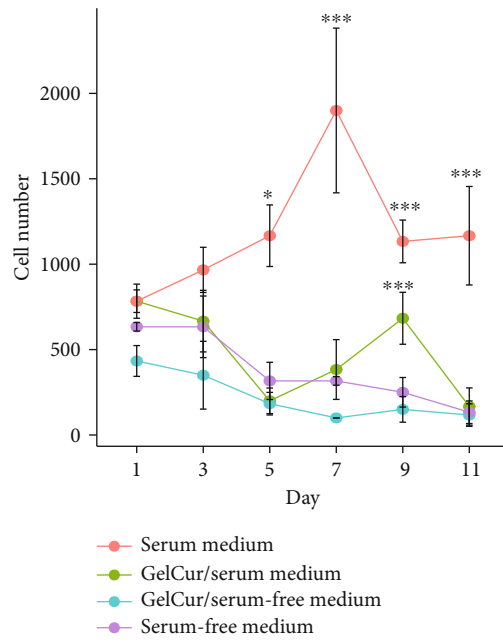
3.6. GelCur Is Not a Chemoattractant Factor Moderating hGFs Motility. To clarify whether nano-curcumin plays a role as a chemoattractant factor stimulating fibroblast migration, a transwell migration assay was performed. hGFs

were seeded in the upper chamber, while the bottom chamber contained 2 mg/ml GelCur diluted in serum-free DMEM or 10% FBS DMEM. hGFs were allowed to migrate through the membrane in the medium with or without FBS as positive and negative controls, respectively. GelCur treatments were found to reduce the number of migrated hGFs after 16 hours (Figure 3(d)). The significant reduction was noted in hGFs incubated with 2 mg/ml GelCur in both serum-free ($2, 29 \pm 1, 36$) and serum-supplemented DMEM ($3, 52 \pm 1, 77$) compared with positive control group ($25, 01 \pm 4, 01$) (Figure 3(e)).

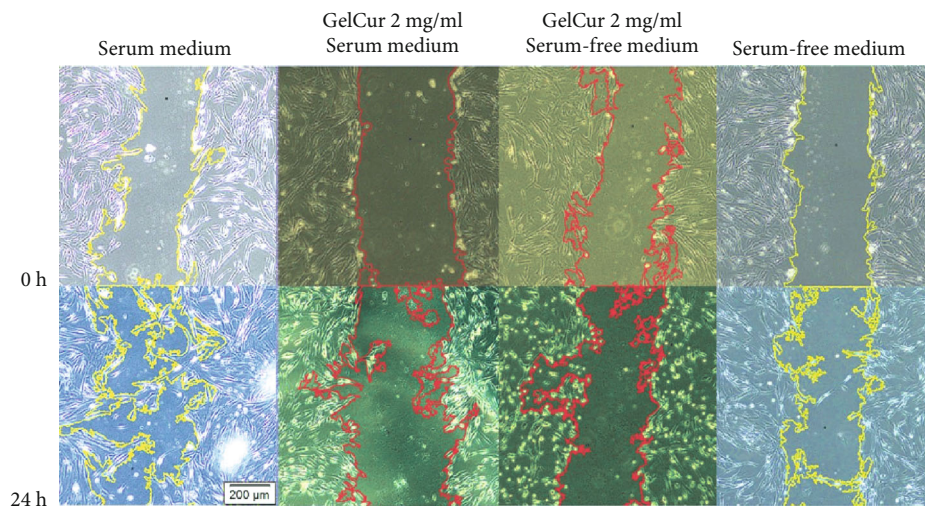
4. Discussion

The therapeutic applications of curcumin have been limited due to its low solubility, short half-life, and poor bioavailability. To overcome those problems, a variety of curcumin formulations have been developed including emulsified micelles, nanoformulations, or incorporating in hydrogels, microgels, and nanofibers [2, 10]. Among the possible approaches, we chose gelatin, a natural protein obtained from the hydrolysis of collagen, which has been well-known for its biodegradability, biocompatibility, and nontoxicity as curcumin carrier (emulsifier). The use of gelatin as a curcumin carrier can increase curcumin solubility, stability as well as control its release. Most importantly, gelatin has been commonly used as an effective drug carrier owing to its diverse functional groups within its backbone, which offers many benefits for chemical modification and drug attachment, giving the site-specificity for efficient drug delivery [21, 22].

Particle size and surface charge (represented as zeta potential) are among the two important characteristics of nanocomposite. They determine the drug loading, drug

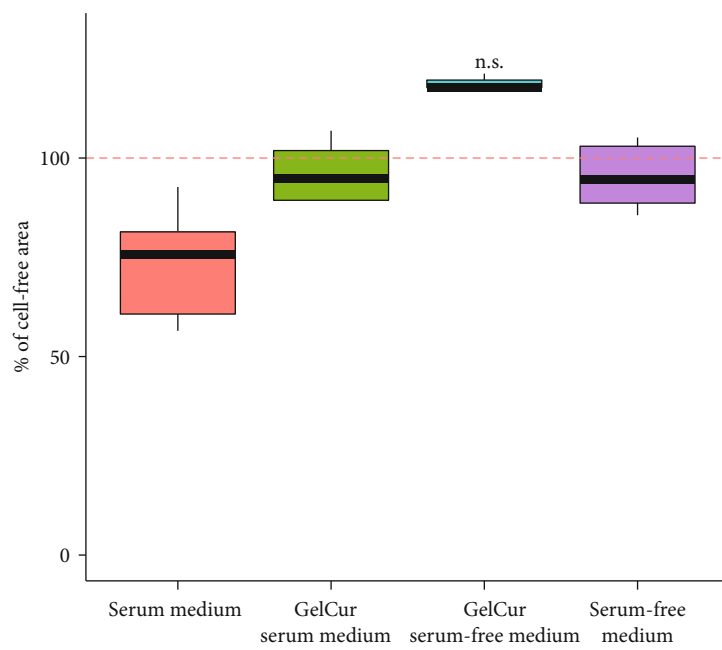


(a)

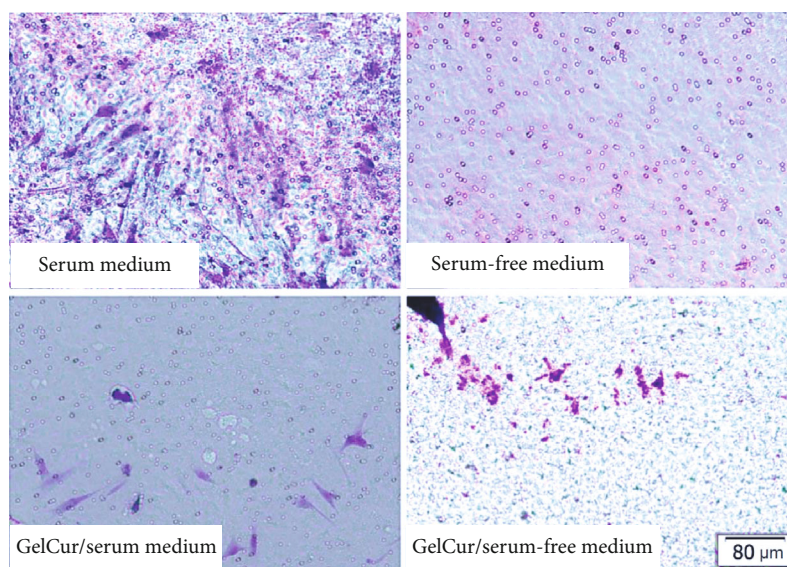


(b)

FIGURE 3: Continued.



(c)



(d)

FIGURE 3: Continued.

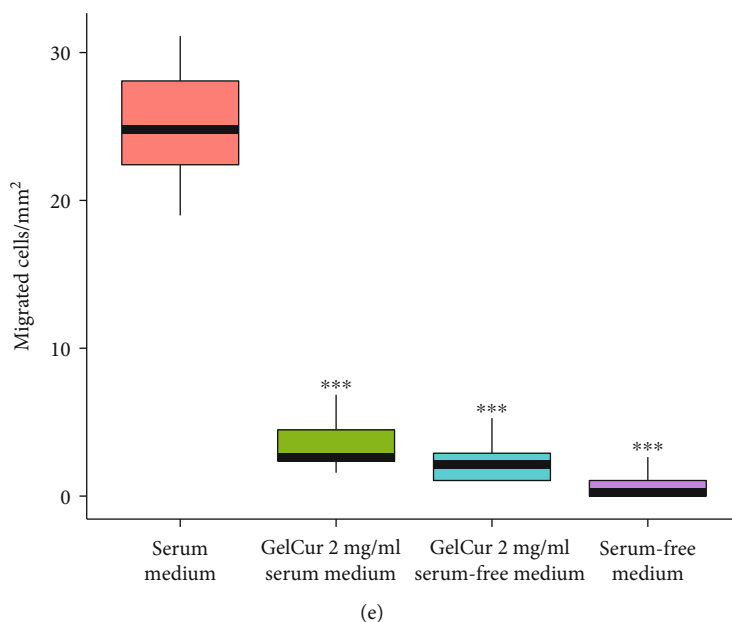


FIGURE 3: (a) Cell number of proliferation assay from day 1 to day 11 (Dunn Kruskal-Wallis multiple comparisons p-values adjusted with the Bonferroni method, there were significant differences between groups with $*p < 0.05$ or $***p < 0.001$ vs. other groups in the same day). (b) In vitro scratch test assay at 0 h and 24 h. (c) % of cell-free area after 24 hours (Kruskal-Wallis rank sum test, there was no significant difference between groups, n.s. non-significant). (d) Migrated hGFs by transwell migration assay after 16 hours. (e) Number of migrated cells in different conditions (Dunn Kruskal-Wallis multiple comparisons, there were significant differences between groups with adjusted $***p < 0.001$ vs. serum medium group).

release, stability, and bioactivity of nanocomposite as well as influence cell-drug interactions [23]. In particular, the surface charge of near ± 30 mV suggests that the GelCur nanocomposite is stable and has a low risk of particle aggregate. In terms of particle size, the size of submicroscale of GelCur particles can enhance their surface interaction while not enable direct penetration through the cell membrane. Once GelCur particles attach to the surface, Cur can slowly be released, thus, lower the unexpected toxicity caused by high concentrations of Cur as reported previously [24]. Due to the smaller particle size than curcumin and improved drug permeation and drug release (85% after 24 h) [11], GelCur could overcome the low oral bioavailability of curcumin and increase the level and effectiveness of curcumin. On the side note, our GelCur nanosuspension produced the lyophilized-spherical particles that were slightly larger than in reported particle size results. The increase in particle size could be due to the pressure and stress emerged during lyophilization, which altered the interactions between particles and caused particle aggregation. Therefore, the use of lyophilization protectants should be considered in further research to prevent possible alteration of nanocomposite properties [25, 26].

Toxicity of nanomaterials is a common concern during developing a new topical wound healing agent, which is essential for clinical translation. Previous clinical trials shown that receiving high oral doses of curcumin (8 g/day) does not lead to cytotoxic concentrations due to the low oral bioavailability of curcumin [27]. However, a relatively high number of reports demonstrated that curcumin, at concentrations exerts a beneficial effect, can induce DNA damage and chro-

mosomal alterations both in normal and malignant cells. Cao et al. reported 2.5-5 $\mu\text{g}/\text{ml}$ of curcumin-induced nuclear DNA damage and apoptosis in human hepatoma G2 cells [28, 29]. Curcumin nanoparticles were developed to increase the levels of curcumin in tissues by enhancing particle penetration [27]. Aimee et al. shown that keratinocytes treated with 5 mg/ml nano-curcumin exhibited 81.7% cell viability as compared to untreated cells [30, 31]. Our results from our cell toxicity assay demonstrated that the survival of hGFs gradually decreased with the subsequent increase of GelCur concentration. Notably, a dose of GelCur >3.96 mg/ml will be cytotoxic to hGFs. Previous in vitro studies used direct curcumin leading to lower safe doses than our nano-curcumin [28, 29, 31]. Additionally, human gingival fibroblasts express a specific phenotype in extracellular matrix remodeling as mentioned [13, 32, 33]. The application of nano-curcumin and human oral fibroblasts in our study may contribute to the optimal implementation of drug delivery by nanoparticles in the oral environment. As in vitro studies do not thoroughly simulate the physiologic environment, further *in vivo* studies and clinical trials should be conducted for providing a complete insight into the potential toxicity of GelCur.

hGFs not only enable the maintenance of the barrier function of normal oral mucosal but also play a critical role in normal wound healing [34]. Upon wounding, cells proliferate and migrate into the wound area for synthesizing and depositing newly formed matrix components. To investigate the effect of GelCur on the cellular events of hGFs related to oral wound healing capacity, including proliferation and migration, the nontoxicity concentration of GelCur (2 mg/ml) was used.

Our data showed that the proliferation of hGFs was substantially reduced after GelCur administration. The results may explain the ability of curcumin to control the wound healing process and prevent scar formation. Nanoformulated curcumin inhibited the growth and mobility of several types of cells both *in vivo* and *in vitro* in previous studies [35, 36]. Fibrotic progression, characterized by fibroblast proliferation and the deposition of collagens, has been effectively reduced when treated by curcumin [37]. Most of the recent studies demonstrated that the mechanism of inhibiting fibroblast proliferation by curcumin is related to blocking the TGF- β 1 signaling cascade and upregulation of cathepsin K/L expressions [38]. Furthermore, curcumin upregulated the expression and activity of p53 which associated with the inhibition of proliferation and increases apoptosis in a variety of different cell lines [39, 40]. Our data from proliferation assay correlated well with data obtained from previous studies that curcumin exhibit an antifibrotic effect by the significantly inhibited proliferation of human fibroblast [38]. We found no evidence that GelCur influences the hGF migration, in congruence with past investigations using dermal fibroblast [30]. The reason may be because gingival fibroblasts express specific molecules involved in the regulation of inflammation and extracellular matrix remodeling in comparison to other fibroblasts. It may explain the ability of gingival wounds to heal faster with less scar formation as compared to skin wounds [13, 32, 33]. From these results, our next study will focus on the anti-inflammatory and antioxidant properties of our nano-curcumin by *in vitro* inflammation model using LPS induced gingival fibroblasts. Additionally, more studies with shorter treatment durations of nano-curcumin on hGFs and other oral cell types need to be performed to have a comprehensive understanding of nano-curcumin.

5. Conclusion

In this study, gelatin encapsulated curcumin nanoparticles GelCur was developed which remained physically stable and did not cause hGF cytotoxicity at concentrations <3.96 mg/ml. Our study showed that within the nontoxicity dose, GelCur did not alter the proliferation and migration of hGFs. The results suggest that GelCur can be used safely in oral fibroblasts *in vitro*. Further studies can focus on the antibacterial and antioxidant properties of GelCur in the oral environment.

Data Availability

Requests for access to the data in this study should be made to the corresponding author.

Ethical Approval

The use of human gingival tissues for research purposes was approved by the Ethics Committee of the University of Medicine and Pharmacy at Ho Chi Minh City (No. 277/DHYD-HDDD).

Conflicts of Interest

The authors declare that they have no conflicts of interest.

Acknowledgments

We would like to thank Associate Professor Tran Le Bao Ha, Department of Physiology and Animal Biotechnology, Laboratory of Tissue Engineering and Biomedical Materials, Faculty of Biology—Biotechnology, University of Science, Vietnam National University, Ho Chi Minh City, Viet Nam for supporting this study. This work was granted in part by The University of Medicine and Pharmacy at Ho Chi Minh City as No. 175/2018/HD-NCKH.

References

- [1] S. Hewlings and D. Kalman, "Curcumin: a review of its' effects on human health," *Food*, vol. 6, no. 10, p. 92, 2017.
- [2] C. Mohanty and S. K. Sahoo, "Curcumin and its topical formulations for wound healing applications," *Drug Discovery Today*, vol. 22, no. 10, pp. 1582–1592, 2017.
- [3] G. D. Venkatasubbu and T. Anusuya, "Investigation on Curcumin nanocomposite for wound dressing," *International Journal of Biological Macromolecules*, vol. 98, pp. 366–378, 2017.
- [4] R. Niranjana, M. Kaushik, J. Prakash et al., "Enhanced wound healing by PVA/Chitosan/Curcumin patches: *In vitro* and *in vivo* study," *Colloids and Surfaces B: Biointerfaces*, vol. 182, article 110339, 2019.
- [5] R. Thamarai Selvi, A. P. S. Prasanna, R. Niranjana et al., "Metal Oxide Curcumin Incorporated polymer patches for Wound Healing," *Applied Surface Science*, vol. 449, pp. 603–609, 2018.
- [6] R. Niranjana, M. Kaushik, R. T. Selvi et al., "PVA/SA/TiO₂-CUR patch for enhanced wound healing application: *in vitro* and *in vivo* analysis," *International Journal of Biological Macromolecules*, vol. 138, pp. 704–717, 2019.
- [7] S. Bisht, G. Feldmann, S. Soni et al., "Polymeric nanoparticle-encapsulated curcumin ("nanocurcumin"): a novel strategy for human cancer therapy," *Journal of Nanobiotechnology*, vol. 5, no. 1, p. 3, 2007.
- [8] L. Slika, A. Moubarak, J. Borjac, E. Baydoun, and D. Patra, "Preparation of curcumin-poly (allyl amine) hydrochloride based nanocapsules: Piperine in nanocapsules accelerates encapsulation and release of curcumin and effectiveness against colon cancer cells," *Materials Science and Engineering: C*, vol. 109, p. 110550, 2020.
- [9] M. Mouslmani, J. M. Rosenholm, N. Prabhakar, M. Peurla, E. Baydoun, and D. Patra, "Curcumin associated poly (allylamine hydrochloride)-phosphate self-assembled hierarchically ordered nanocapsules: size dependent investigation on release and DPPH scavenging activity of curcumin," *RSC Advances*, vol. 5, no. 24, pp. 18740–18750, 2015.
- [10] G. D. Venkatasubbu, S. Nagamuthu, T. Anusuya et al., "TiO₂-nanocomposite for the controlled release of drugs against pathogens causing wound infections," *Materials Research Express*, vol. 5, no. 2, article 024003, 2018.
- [11] H. V. Ngo, P. H. L. Tran, B. J. Lee, and T. T. D. Tran, "Development of film-forming gel containing nanoparticles for transdermal drug delivery," *Nanotechnology*, vol. 30, no. 41, p. 415102, 2019.

- [12] N. Sahoo, R. K. Sahoo, N. Biswas, A. Guha, and K. Kuotsu, "Recent advancement of gelatin nanoparticles in drug and vaccine delivery," *International Journal of Biological Macromolecules*, vol. 81, pp. 317–331, 2015.
- [13] N. C.-N. Huynh, V. Everts, C. Leethanakul, P. Pavasant, and R. S. Ampornaramveth, "Rinsing with saline promotes human gingival fibroblast wound healing in vitro," *PLoS One*, vol. 11, no. 7, article e0159843, 2016.
- [14] M. T. N. Nguyen and H. L. B. Tran, "Effect of modified bovine pericardium on human gingival fibroblasts in vitro," *Cells, Tissues, Organs*, vol. 206, no. 6, pp. 296–307, 2019.
- [15] N. C.-N. Huynh, V. Everts, P. Pavasant, and R. S. Ampornaramveth, "Inhibition of histone deacetylases enhances the osteogenic differentiation of human periodontal ligament cells," *Journal of Cellular Biochemistry*, vol. 117, no. 6, pp. 1384–1395, 2016.
- [16] N. C.-N. Huynh, S. H. Le, V. N. Doan, L. T. Q. Ngo, and H. L. B. Tran, "Simplified conditions for storing and cryopreservation of dental pulp stem cells," *Archives of Oral Biology*, vol. 84, pp. 74–81, 2017.
- [17] H. Apdik, A. Dogan, S. Demirci, S. Aydin, and F. Sahin, "Dose-dependent effect of boric acid on myogenic differentiation of human adipose-derived stem cells (hADSCs)," *Biological Trace Element Research*, vol. 165, no. 2, pp. 123–130, 2015.
- [18] G. Da Violante, N. Zerrouk, I. Richard, G. Provot, J. C. Chau-meil, and P. Arnaud, "Evaluation of the cytotoxicity effect of dimethyl sulfoxide (DMSO) on Caco2/TC7 colon tumor cell cultures," *Biological & Pharmaceutical Bulletin*, vol. 25, no. 12, pp. 1600–1603, 2002.
- [19] International Organization for Standardization ISO 10993-5, 2009 *Biological evaluation of medical devices – Part 5: Tests for in vitro cytotoxicity*, International Organization for Standardization, Geneva, 2009.
- [20] T. Fukuda, T. Ezawa, K. Tanaka, and K. Ito, "Peripheral occluding effects of non-absorbable membranes on ingrowth of cultured gingival connective tissue cells," *Journal of Periodontology*, vol. 71, no. 11, pp. 1680–1686, 2000.
- [21] Z. Zhou, S. He, T. Huang et al., "Preparation of gelatin/hyaluronic acid microspheres with different morphologies for drug delivery," *Polymer Bulletin*, vol. 72, no. 4, pp. 713–723, 2015.
- [22] H. Yan, Z. Zhou, T. Huang et al., "Controlled release in vitro of icariin from gelatin/hyaluronic acid composite microspheres," *Polymer Bulletin*, vol. 73, no. 4, pp. 1055–1066, 2016.
- [23] S. M. A. Sadat, S. T. Jahan, and A. Haddadi, "Effects of Size and Surface Charge of Polymeric Nanoparticles on *in Vitro* and *in Vivo* Applications," *Journal of Biomaterials and Nanobiotechnology*, vol. 7, no. 2, pp. 91–108, 2016.
- [24] S. R. Damarla, R. Komma, U. Bhatnagar, N. Rajesh, and S. M. A. Mulla, "An evaluation of the genotoxicity and subchronic oral toxicity of synthetic curcumin," *Journal of Toxicology*, vol. 2018, Article ID 6872753, 27 pages, 2018.
- [25] W. Abdelwahed, G. Degobert, S. Stainmesse, and H. Fessi, "Freeze-drying of nanoparticles: formulation, process and storage considerations," *Advanced Drug Delivery Reviews*, vol. 58, no. 15, pp. 1688–1713, 2006.
- [26] L. L. Khanh, N. T. Truc, N. T. Dat et al., "Gelatin-stabilized composites of silver nanoparticles and curcumin: characterization, antibacterial and antioxidant study," *Science and Technology of Advanced Materials*, vol. 20, no. 1, pp. 276–290, 2019.
- [27] E. Burgos-Morón, J. M. Calderón-Montaño, J. Salvador, A. Robles, and M. López-Lázaro, "The dark side of curcumin," *International Journal of Cancer*, vol. 126, no. 7, pp. 1771–1775, 2010.
- [28] J. Cao, L. Jia, H.-M. Zhou, Y. Liu, and L.-F. Zhong, "Mitochondrial and nuclear DNA damage induced by curcumin in human hepatoma G2 cells," *Toxicological Sciences*, vol. 91, no. 2, pp. 476–483, 2006.
- [29] J. Cao, Y. Liu, L. Jia et al., "Curcumin induces apoptosis through mitochondrial hyperpolarization and mtDNA damage in human hepatoma G2 cells," *Free Radical Biology & Medicine*, vol. 43, no. 6, pp. 968–975, 2007.
- [30] A. E. Krausz, B. L. Adler, V. Cabral et al., "Curcumin-encapsulated nanoparticles as innovative antimicrobial and wound healing agent," *Nanomedicine*, vol. 11, no. 1, pp. 195–206, 2015.
- [31] C. Syng-Ai, A. L. Kumari, and A. Khar, "Effect of curcumin on normal and tumor cells: role of glutathione and bcl-2," *Molecular Cancer Therapeutics*, vol. 3, no. 9, pp. 1101–1108, 2004.
- [32] W. Mah, G. Jiang, D. Olver et al., "Human gingival fibroblasts display a non-fibrotic phenotype distinct from skin fibroblasts in three-dimensional cultures," *PLoS One*, vol. 9, no. 3, article e90715, 2014.
- [33] F. Guo, D. E. Carter, A. Mukhopadhyay, and A. Leask, "Gingival fibroblasts display reduced adhesion and spreading on extracellular matrix: a possible basis for scarless tissue repair?," *PLoS One*, vol. 6, no. 11, article e27097, 2011.
- [34] C. A. G. McCulloch and S. Bordin, "Role of fibroblast subpopulations in periodontal physiology and pathology," *Journal of Periodontal Research*, vol. 26, no. 3, pp. 144–154, 1991.
- [35] S. Hosseini, J. Chamani, M. R. Hadipanah et al., "Nano-curcumin's suppression of breast cancer cells (MCF7) through the inhibition of cyclinD1 expression," *Breast Cancer: Targets and Therapy*, vol. 11, pp. 137–142, 2019.
- [36] F. Milano, L. Mari, W. van de Luijtgarden, K. Parikh, S. Calpe, and K. K. Krishnadath, "Nano-curcumin inhibits proliferation of esophageal adenocarcinoma cells and enhances the T cell mediated immune response," *Frontiers in Oncology*, vol. 3, p. 137, 2013.
- [37] X. Zhou, J. Zhang, C. Xu, and W. Wang, "Curcumin ameliorates renal fibrosis by inhibiting local fibroblast proliferation and extracellular matrix deposition," *Journal of Pharmacological Sciences*, vol. 126, no. 4, pp. 344–350, 2014.
- [38] D. Zhang, C. Huang, C. Yang et al., "Antifibrotic effects of curcumin are associated with overexpression of cathepsins K and L in bleomycin treated mice and human fibroblasts," *Respiratory Research*, vol. 12, no. 1, p. 154, 2011.
- [39] E. Wawryk-Gawda, P. Chylinska-Wrzos, M. Lis-Sochocka et al., "P 53 protein in proliferation, repair and apoptosis of cells," *Protoplasma*, vol. 251, no. 3, pp. 525–533, 2014.
- [40] H. Fu, C. Wang, D. Yang et al., "Curcumin regulates proliferation, autophagy, and apoptosis in gastric cancer cells by affecting PI3K and P53 signaling," *Journal of Cellular Physiology*, vol. 233, no. 6, pp. 4634–4642, 2018.

Review Article

Recent Trends in Nanocarrier-Based Targeted Chemotherapy: Selective Delivery of Anticancer Drugs for Effective Lung, Colon, Cervical, and Breast Cancer Treatment

Ke-Tao Jin ¹, Ze-Bei Lu,^{2,3,4} Jin-Yang Chen,⁵ Yu-Yao Liu,¹ Huan-Rong Lan,⁶ Hai-Ying Dong,³ Fan Yang ², Yuan-Yuan Zhao,⁷ and Xiao-Yi Chen ^{3,4}

¹Department of Colorectal Surgery, Shaoxing People's Hospital (Shaoxing Hospital, Zhejiang University School of Medicine), Shaoxing, 312000 Zhejiang Province, China

²Department of Stomatology, Zhejiang Provincial People's Hospital (People's Hospital of Hangzhou Medical College), Hangzhou, 310014 Zhejiang Province, China

³Key Laboratory of Tumor Molecular Diagnosis and Individualized Medicine of Zhejiang Province, Zhejiang Provincial People's Hospital (People's Hospital of Hangzhou Medical College), Hangzhou 310014, China

⁴Clinical Research Institute, Zhejiang Provincial People's Hospital (People's Hospital of Hangzhou Medical College), Hangzhou 310014, China

⁵Research and Development Department, Zhejiang Health Future Institute for Cell-Based Applied Technology, Hangzhou, 310052 Zhejiang Province, China

⁶Department of Breast and Thyroid Surgery, Shaoxing People's Hospital (Shaoxing Hospital, Zhejiang University School of Medicine), Shaoxing, 312000 Zhejiang Province, China

⁷Department of Neurosurgery, Zhejiang Provincial People's Hospital (People's Hospital of Hangzhou Medical College), Hangzhou, 310014 Zhejiang Province, China

Correspondence should be addressed to Fan Yang; yangfan@hmc.edu.cn and Xiao-Yi Chen; chenxiaoyi@hmc.edu.cn

Received 18 March 2020; Revised 23 May 2020; Accepted 10 June 2020; Published 2 July 2020

Guest Editor: Anuj Kumar

Copyright © 2020 Ke-Tao Jin et al. This is an open access article distributed under the Creative Commons Attribution License, which permits unrestricted use, distribution, and reproduction in any medium, provided the original work is properly cited.

Chemotherapy drugs are cytotoxic to tumor cells, but their lack of specificity leads to a range of side effects. The off-target effects of such drugs can be improved through the use of nanoparticles (NPs). Administered NPs show enhanced accumulation in tumor tissue near the blood vessels, enhancing both anticancer drug permeability and tumor retention. Several nanocarriers are now approved for clinical use in a range of cancer therapies, and many novel formulations are in the later stages of clinical trials. Here, we describe the advances in this area through the review of novel NP drug formulations developed over the last year. We focus specifically on lung, colon, cervical, and breast cancers and discuss the future of NPs as potential treatment options in these areas.

1. Introduction

Cancer encompasses a variety of diseases that result from the deregulated growth and spread of malignant cells. According to recent World Health Organization (WHO) statistics, up to 10 million new cancer cases are estimated to occur each year and are projected to increase to 13 million cases in the next 20 years [1]. Despite the increased occurrence, cancer-related mortality has decreased due to improved diagnostics,

molecular knowledge of cancer cell biology, and treatments [2]. Cancer therapy typically involves surgery, chemotherapy, and radiation therapy alone or in combination, with sequencing technologies, permitting the era of precision therapy that tailors cancer treatments to the genetic basis of each individual cancer [3, 4]. Chemotherapy drugs primarily interfere with DNA synthesis, targeting rapidly dividing cancer cells. These agents, whilst effective, are nonspecific, leading to healthy tissue damage and subsequent side effects that

can contribute to the high mortality rates of cancer patients [5]. An additional issue with chemotherapy drugs is the increased incidence of drug resistance [6]. Hence, the ability to develop chemotherapeutics that actively target cancer cells is highly desirable.

In recent years, the improved understanding of tumor biology combined with the advancements in the development of versatile materials has led to improved drug delivery systems of chemotherapeutics to tumor sites. More specifically, nanotechnology has profoundly improved clinical cancer therapeutics in the last 20 years [7–12]. NP-based drug delivery systems or nanocarriers can improve drug efficacy and selectivity through enhanced permeability and retention (EPR) effects in tumor tissues [13–20]. Nanocarriers also display improved cellular uptake in comparison to standard chemotherapy drugs. Among the nanocarriers, liposomes, polymeric nanoparticles, and micelles have received the most attention [21]. To date, several nanoparticle-based chemotherapeutics are clinically approved whilst others are in the advanced stages of clinical development. However, nanocarriers are associated with certain drawbacks such as poor biodegradation, bioavailability, stability, tissue distribution, and toxicity, thus causing safety concerns, particularly for long-term cancer treatment. Herein, we will discuss drug delivery nanocarriers for cancer therapy to improve chemotherapeutics that have been developed recently. We will further discuss the future directions of NP-based cancer chemotherapy with a focus on lung, colon, and female cancers.

2. Nanocarriers

The physical and chemical properties of NPs greatly influence their efficacy. Nanoscale compounds from synthetic polymers, lipids, proteins, and inorganic particles have been developed [21–29]. They promote drug protection, solubility, and stability, enhancing drug delivery. NP functionalization with target specific ligands, such as folic acid, aptamers, peptides, and antibodies, permits the targeted delivery of drugs. The culmination of these benefits is numerous drug delivery vehicles with reduced toxic side effects and improved pharmacokinetics, which vary according to surface physicochemical properties and size [30–35].

Among organic nanocarriers, liposomes are spherical lipid vesicles composed of a self-forming phospholipid bilayer that surrounds an aqueous internal cavity [25, 36]. The commercially available lipids for liposome NPs include cholesterol, phosphatidylcholine, phosphatidylethanolamine, and phosphatidylserine. Liposomes are attractive as they lack toxicity and easily internalize into tumor cells, permitting drug transport across cellular membranes. However, their major disadvantages are expensive preparation methods, low drug-loading capacity and stability, and rapid disintegration in the human body before achieving the therapeutic effect. ThermoDox[®], a thermosensitive liposomal formulation (TSL) containing doxorubicin, is the only TSL in development. This formulation selectively unloads its payload in the tumor microenvironment due to its responsiveness to a temperature above 40°C, thus resulting in increased anticancer efficacy of its loaded drug [37]. The

use of lipid-based nanocarriers as opposed to liquid oils permits controlled drug release through reducing drug mobility [38]. Solid lipid NPs (SLNs) are frequently used as NPs for intravascular administration and consist of a hydrophobic lipid core into which drugs can be dissolved permitting high drug-loading efficiencies [39]. Polymeric micelles are another form of lipid based-NP < 100 nm in size and composed of phospholipids and polymers that spontaneously form in aqueous solution [40, 41]. They are suitable carriers for drugs with poor water solubility due to their amphiphilic characteristics, viz., hydrophobic core and hydrophilic shell. Reverse micelles (RMs) are frequently used due to their ease of solubility in oil phases [42–44]. However, a disadvantage of RMs is their lack of tissue specificity and inability to mediate targeted drug delivery [42]. Micellar nanocomplex (MNC) NPs are mainly composed of (–)-epigallocatechin-3-O-gallate (EGCG), an anti-inflammatory polyphenol [45]. MNCs can shield protein drugs from the action of proteolytic enzymes during transportation to the tumor tissues. Genexol-PM[®] is amphiphilic polymer-based micellar formulation loaded with paclitaxel and is used for the effective treatment of metastatic breast and small-lung-cell carcinoma. The formulation achieves enhanced anticancer activity of the drug to its long circulation as it gets avoidance body clearance [46].

Among nonlipid-based NPs, mesoporous materials hold promise due to their facile synthesis, highly ordered structures, biocompatibility, and large pore sizes, typically prepared from assemblies of inorganic components such as silica [30]. The pore size of mesoporous silica NPs (MSNs) influences their pharmacological potential in terms of drug adsorption, loading capacity, and drug release [30]. Pore diameters vary from 2 to 50 nm enabling the production of NPs that bind to small drug molecules or macromolecules. The stability of the pore also dictates controlled drug-release kinetics. So far, MSNs characterized by temperature, pH, irradiation, enzymes, magnetic field, ultrasound, and redox-based stimuli-responsive drug release have been developed [47].

Metal-organic frameworks (MOFs) constitute a class of porous NPs with differing hybrid structures that consist of a metal ion and an organic linker or spacer [48]. MOFs show promise for controlled drug release due to their large surface area and tunable pore size. However, MOFs must be scaled down to the nanoscale level for utility as *in vivo* anticancer drug carriers [49, 50]. Nano-MOFs have particular utility in pharmaceutical applications as they permit controlled drug release [49, 50]. Compared to conventional porous materials, nano-MOFs incorporate much higher amounts of drugs offering obvious advantages to cancer treatment. MOF-based stimuli-responsive systems responding to pH, redox-based, ATP, magnetic fields, temperature, pressure, irradiation, and humidity have been developed.

Recently, NPs based on biocompatible and biodegradable polymers such as polylactic acid (PLA) esters and their copolymers with glycolic acid (PLGA), poly(ϵ -caprolactone), polyglutamic acid, and poly(alkyl cyanoacrylate) have gained popularity for nanocarrier fabrication [51]. These polymers are broken down in the body to oligomers and monomers

which are further eliminated via metabolic pathways. To surmount the issue of phagocytosis upon intravenous administration, the NPs may be coated with a hydrophilic polymer such as polyethylene glycol (PEG), which hinders the identification of the NPs by the reticuloendothelial system. Dendrimers, inorganic NPs, nanoemulsions, carbon-based nanomaterials, etc. are some of the other popular nanocarriers (Figure 1).

The first nanobased therapeutic approved by the FDA was the liposomal NP doxorubicin Doxil®, a chemotherapeutic primarily employed for breast cancer (BCa), bladder cancer, and acute lymphocytic leukemia treatment. This liposomal formulation results in enhanced anticancer activity of the drug due to long circulating properties of the liposomes achieved through inclusion of polyethylene glycol in their composition [52–56]. The development of this NP system was followed by Abraxane® (nab-paclitaxel), a BCa chemotherapy drug. Abraxane® is based on albumin NPs; albumin NPs not only increase the drug solubility but also localize the drug into tumors due to its higher affinity for hydrophobic molecules [57–61]. Notable nanocarriers that have undergone FDA approval or are in clinical trials are presented in Table 1 [54, 62–67]. Even though most of the FDA-approved nanocarriers rely on passive targeting via EPR, a few next-generation nanocarriers in clinical trials utilize active targeting approaches due to the recent advances in protein engineering and polymer chemistry.

3. Recent Advances in Nanocarrier Delivery Systems for Cancer Treatment

3.1. Anticancer Drug Targeted Delivery through NPs. Improved chemotherapy requires the drugs to cross the biological barriers followed by their selective localization in the target tumor tissues, thus leading to enhanced anticancer activity with minimum off-target side effects. Passive and active NP drug targeting is a widely used approach [86, 87]. In passive targeting, nanocarriers localize their loaded anticancer drugs passively in tumor tissues exploiting the physiopathologic characteristics of tumors such as tumor vasculature. Tumor vessel architecture becomes highly defective along with poor lymphatic drainage, thus leading to enhanced permeation and retention (EPR) effect [88, 89]. Small size of nanocarriers and defective tumor vasculature are also exploited for anticancer drug passive targeting [90]. Blood vessels in the tumor tissue microenvironment have larger gaps (100 nm–2 μm) in the endothelium; thus, they differ from that of the normal. Therefore, nanocarriers in this size range can easily reach tumors, resulting in selective localization of the drugs in tumors [91, 92]. Furthermore, tumor tissues are associated with poor lymphatic system which results in higher interstitial pressure at their centers than peripheries. This in turn leads to nanocarrier access into the interstitial space; thus, nanocarriers remain in interstitia for longer time with ultimate enhanced anticancer activity in tumors [93]. Passive targeting strategies through nanocarriers are depicted in Figure 2. Anticancer drugs can also be passively targeted through making nanocarriers long circulating. Such

nanocarriers avoid clearance from the body and remain in biological systems for a longer time; thus, they pass through the tumor microenvironment repeatedly with ultimate increased anticancer activity of their loaded drugs. Similarly, cationic nanocarriers are also used to localize their loaded drugs in tumors due to their electrostatic interactions with angiogenic endothelial cells in tumor blood vessels [86, 87].

Active drug targeting uses nanocarrier surface modified with a targeting moiety. Targeting moiety attached to the surface of nanocarriers recognizes specific receptors or antigens associated with tumors as shown in Figure 3. This results in the selective localization of drugs in the site of action whilst preventing their uptake in healthy cells and tissues. Furthermore, some targeting ligands can trigger drug release from nanocarriers inside target cells via receptor-mediated endocytosis process [94]. Drug tumor internalization through receptor targeting is an effective approach for improved chemotherapy [95]. Cancer cells overexpress certain types of receptors; thus, targeting moieties recognize these receptors and highly selective drug localization in tumors is achieved [96, 97]. Similarly, nanocarriers are also made responsive to the changes in the tumor microenvironment; drugs get released from nanocarriers in the tumor vicinity as a result of their responsiveness to those stimuli such as pH, hyperthermia, redox potential, and certain enzymes in the tumor microenvironment [86, 87]. Thus, increased drug concentration is achieved in the tumor microenvironment with ultimate improved chemotherapy.

3.1.1. Targeting Lung Cancer. Lung cancer (LCa) is a leading global cause of cancer-related deaths [98]. A chemotherapy regimen, dependent on it being either adenocarcinoma or squamous cell carcinoma, is often administered, combining 2 or 3 chemotherapy agents including cisplatin, docetaxel, gemcitabine, Abraxane®, paclitaxel, pemetrexed, and vinorelbine [98, 99]. Many promising NP formulations for LCa therapy have been described recently.

Due to their ability to permeate blood vessels and tissues into tumors, metal-based NPs can be applied as drug carriers for reducing cytotoxicity to healthy cells. Using nonorganic-based approaches, Ramalingam and coworkers conjugated Dox onto gold NPs using polyvinylpyrrolidone [100]. The NPs inhibited the proliferation of A549 cells, increased cellular ROS production, and led to the induction of apoptosis. Similarly, Kalaiarasi and colleagues synthesized copper oxide NPs that could downregulate specific oncogenes including histone deacetylase in A549 cells, leading to apoptotic induction [101]. Although platinum-based antitumor agents have been widely used for LCa, their clinical outcomes are largely limited by severe side effects and multidrug resistance. Hence, platinum(II)-loaded drug nanocarriers have been developed to overcome these drawbacks. For instance, Tsai and coworkers synthesized diaminocyclohexane-platinum(II)- (DACHPt-) loaded NPs through self-assembly that could be efficiently internalized by platinum- (Pt-) resistant LCa cell lines, inducing high levels of tumor toxicity [6]. Therefore, these DACHPt-loaded NPs provide a novel potent nanocarrier platform for combating multidrug-resistant LCa.

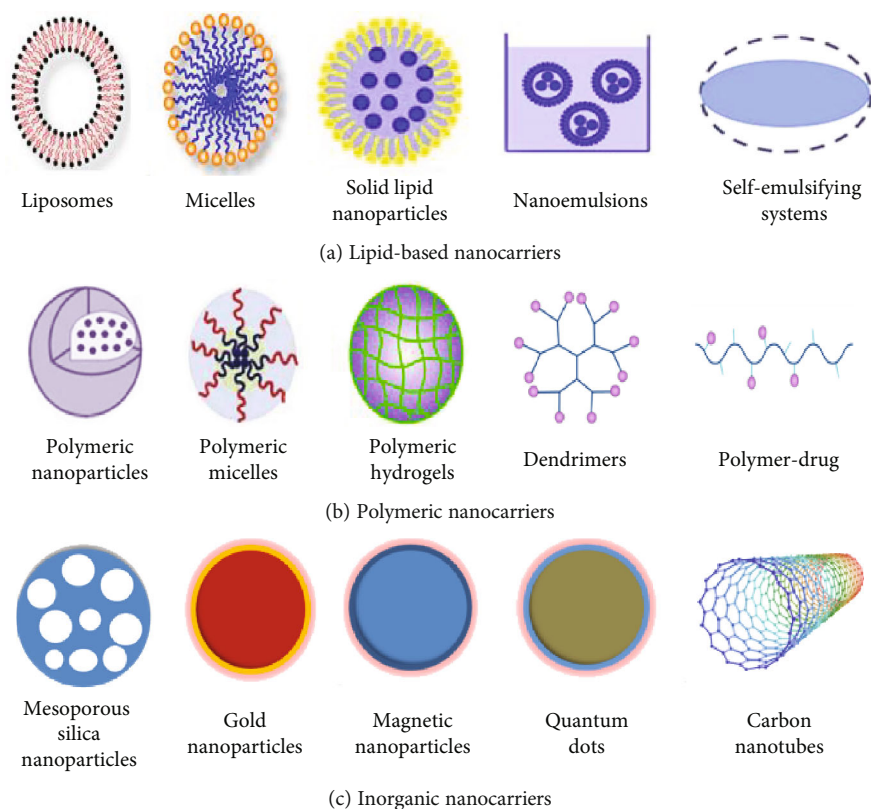


FIGURE 1: Different types of nanocarriers for drug delivery in cancer therapy.

Active targeting can be achieved by coupling drugs or nanocarriers with cell-specific targeting moieties such as ligands, peptides, antibodies, and aptamers, which can distinguish between normal and tumor cells. For instance, Song and colleagues designed epidermal growth factor- (EGF-) conjugated core-shell lipid-polymer hybrid NPs (LPNs) to actively deliver docetaxel (DTX) and resveratrol (RSV) to tumor cells [36]. The biodegradable EGF-DTX/RSV-NPs showed synergistic tumor inhibition with minimal off-target effects, highlighting their promise for LCa treatment. Nanocarriers based on vitamin E succinate display biocompatibility, hydrophobicity, ease of synthesis, and anticancer activity. On the other hand, hyaluronic acid (HA), a biocompatible and biodegradable anionic polysaccharide, permits active targeting of tumor cell CD44 receptors. To enhance tumor cell targeting and specific drug release, Song and coworkers synthesized redox-sensitive NPs from hyaluronic acid- (HA-) disulfide-vitamin E succinate conjugates that were loaded with paclitaxel (PTX) [12]. The PTX-loaded redox-sensitive NPs showed greater cytotoxicity in A549 cells and A549 mouse xenograft models compared to redox-insensitive NPs and PTX alone, indicating their potential for PTX-targeted delivery for LCa treatment.

The clinical application of naringenin (NAR), a flavonoid, is limited by its low aqueous solubility, bioavailability, and stability. These drawbacks could be overcome by designing polymeric nanoparticles based on biocompatible and biodegradable polymers. Parashar et al. [102] designed chitosan- and HA-decorated naringenin poly caprolactone

NPs (NAR-HA@CS-PCL-NPs) that were cytotoxic to A549 cells but had no effect on noncancer cell lines. *In vivo*, the chemopreventive effects of the NAR-HA@CH-PCL-NPs were shown in urethane-induced LCa rat models. AS1411 is a 26-base G-rich DNA oligonucleotide that functions as a nucleolin-binding aptamer overexpressed in a range of cancer cells [103]. Guo et al. [5] developed a multifunctional nanocarrier consisting of methotrexate-loaded fluorescent gold nanocluster-conjugated chitosan and AS1411 aptamers (MTX@AuNCs-CS-AS1411), which exhibited significant anticancer activity in A549 cells and inhibited tumor growth in BALB/c mice. The codelivery of functionally distinct anticancer drugs is an efficient strategy to overcome drug resistance during LCa treatment. To achieve this, Amreddy et al. [104] synthesized folic acid-conjugated polyamidoamine (PAMAM) dendrimers to codeliver human antigen R (HuR) siRNA and *cis*-diamine platinum to folate receptor- α overexpressing LCa cells. The dendrimers produced greater therapeutic effects than the individual therapies alone whilst being nontoxic towards normal lung fibroblasts, which was attributed to the elevated HuR in LCa cells.

miRNA-29b inhibits DNA methylation in LCa cells by targeting DNA methyltransferases, further resulting in inhibition of cell proliferation and apoptosis. Its limitations including off-target effects, degradation, and poor cellular uptake might be mitigated by a nanocarrier system. MUC1, a transmembrane protein overexpressed in LCa, aids the active targeting of drugs to the tumors. Perepelyuk and colleagues [105] synthesized mucin1-aptamer miRNA-29b-

TABLE 1: Nanocarriers for cancer either in the market or in clinical trials.

Commercial name (company)	Drug/agent	Delivery system	Indication	Status	Ref.
Doxil®/Caelyx™ (Schering-Plough; Ortho Biotech)	Doxorubicin	Liposome	Kaposi's sarcoma; ovarian cancer; multiple myeloma	Approved	[68]
Myocet® (Sopherion; Cephalon)	Doxorubicin	Liposome	Metastatic breast cancer	Approved	[68]
Lipodox® (Sun)	Doxorubicin	Liposome	Ovarian cancer	Approved	[69]
DaunoXome® (Galen)	Daunorubicin	Liposome	Kaposi's sarcoma	Approved	[70]
Marqibo® (Talon; Merrimack)	Vincristine	Liposome	Acute lymphoblastic leukemia	Approved	[68]
Onivyde® (Ipsen)	Irinotecan	Liposome	Pancreatic cancer	Approved	[71]
Oncaspar® (Enzon)	PEG-L-asparaginase	Polymeric nanoparticles	Acute lymphoblastic leukemia	Approved	[69]
Eligard® (Tolmar)	Leuprolide acetate	Polymer (poly(DL-lactide-co-glycolide))	Prostate cancer	Approved	[72]
NanoTherm® (MagForce)	Iron oxide	Iron nanoparticles	Brain tumors	Approved	[73]
Abraxane® (Abraxis; AstraZeneca)	Paclitaxel	Albumin-bound nanoparticles	Various cancers	Approved	[68]
Rexin-G® (Epeius)	Targeting protein marked phospholipid @ miRNA-122	Retrovector	Osteosarcoma, pancreatic cancer	Approved	[74]
Ontak® (Eisai)	Diphtheria toxin and interleukin 2 bound to liposomes	Protein nanoparticles	T-cell lymphoma	Approved	[75]
Vyxeos (Jazz)	Daunorubicin+cytarabine	Liposomes	Acute myeloid leukemia	Approved	[76]
Genexol-PM® (Samyang Biopharm)	Paclitaxel	Polymeric micelles	Ovarian cancer	Phase II	[68]
LEP-ETU (NeoPharma)	Paclitaxel	Liposomes	Ovarian, breast, lung cancers	Phase I/II	[77]
Paclical (Oasmia)	Paclitaxel	Micelles	Ovarian cancer	Phase III	[78]
OSI-211 (OSI)	Lurtotecan	Liposomes	Lung, ovarian cancer	Phase II	[79]
SGT-53 (SynerGene)	Wild-type p53 gene	Liposomes	Solid tumors; glioblastoma; pancreatic cancer	Phase II	[80]
Atragen (Aronex)	All-trans-retinoic acid	Liposomal	Acute promyelocytic leukemia	Phase II	[79]
Lipoplatin (Regulon)	Cisplatin	Liposomal	Various cancers	Phase III	[79]
Aurimmune (CytImmune Sciences)	TNF- α	Colloidal gold nanoparticles	Solid tumors	Phase II	[79]
NK012 (Nippon Kayaku)	7-Ethyl-10-hydroxycamptothecin	Polymeric micelle	Advanced solid tumor	Phase II	[79]
NK105 (Nippon Kayaku)	Paclitaxel	Micelles	Metastatic breast cancer	Phase III	[81]
PEP02 (Merrimack)	Irinotecan	Liposomes	Advanced solid tumor	Phase I	[82]
CriPec (Cristal)	Docetaxel	Polymeric micelles	Solid tumor	Phase I	[76]
CRLX101 (Cerulean)	Camptothecin	Cyclodextrin-based nanoparticles	Non-small-cell lung cancer	Phase II completed	[75]
ABI-009 (AADi)	Rapamycin	Albumin-bound nanoparticles	Bladder cancer	Phase I/II	[79]
ThermoDox (Celsion)	Doxorubicin	Thermal-sensitive liposomes	Hepatocellular carcinoma	Phase III	[83]
CPX-351 (Fred Hutchinson Research Center)	Cytarabine+daunorubicin	Liposomes	Acute myeloid leukemia	Phase I/II	[79]
LiPlaCis (Oncology Venture)	Cisplatin	Liposomes	Various cancers	Phase II	[71]
PLM60 (CSPC ZhongQi)	Mitoxantrone hydrochloride	Liposomes	Non-Hodgkin lymphoma; breast cancer	Phase I/II	[84]
MM-302 (Merrimack)	Trastuzumab	Liposomes	Breast cancer	Phase I	[78]
NBTXR3 (Nanobiotix)	Radiotherapy	Hafnium oxide nanoparticles	Liver cancer	Phase I/II	[76]

TABLE 1: Continued.

Commercial name (company)	Drug/agent	Delivery system	Indication	Status	Ref.
Onco-TCS (Inex)	Vincristine	Liposomes	Non-Hodgkin's lymphoma	Phase I/II	[79]
Aroplatin (Antigenics)	Cisplatin analog	Liposomes	Colorectal cancer	Phase I/II	[79]
EndoTAG-I (SynCore Biotechnology)	Paclitaxel	Liposomes	Breast, pancreatic cancers	Phase II	[79]
Nektar-102 (Nektar)	Irinotecan	PEGylated liposome	Breast, colorectal cancers	Phase III	[79]
NKTR-105 (Nektar)	Docetaxel	PEG-docetaxel	Solid tumor	Phase I	[85]

loaded NPs which exhibited enhanced stability and delivery of miRNA-29b to LCa tissue *in vivo*, resulting in inhibited tumor growth.

An emerging area in lung cancer treatment is the inhalation delivery of NPs to improve tumor targeting. Inhaled Dox NPs exhibit lower cardiac side effects compared to the same standard dose of Dox after intratracheal administration, and paclitaxel-polyglutamic acid conjugates have been shown to be well tolerated by mice following intratracheal administration [106]. Studies in this area also highlight how lipid-based NPs display higher tumor accumulation and remain resident in the lungs for longer time periods postinhalation delivery. These and other inhalation-based nanocarriers hold promise for the effective delivery of anticancer agents specifically to lung tumors in the future.

Recent advancements in pharmaceutical nanotechnology have enabled formulation scientists to design surface-engineered smart NP system for highly localized delivery of chemotherapeutic agents in cancerous tissues. A recent study reported PLGA-based dual-functionalized NP surface engineered with epidermal growth factor receptor (EGFR) aptamer for targeted delivery of homoharringtonine to lung cancer. The NPs were capable of delivering and releasing their loaded drug selectively to lung cancer cells due to their receptor recognition ability and responsiveness to glutathione present in the microenvironment of lung cancer [107].

3.1.2. Targeting Colon Cancer. Colon cancer is among the most common cancer types [108]. Patients with localized colon cancer typically receive surgery as the frontline treatment, and chemotherapy regimens are typically administered after surgery for ~6 months but their effectiveness remains limited. As the enhanced expression of CD98, a transmembrane glycoprotein, is a characteristic of the apical membranes of colon cancer cells, it is now established as a therapeutic target for drug delivery to colon tumors. To target this receptor, Xiao and colleagues [13] synthesized CD98-siRNA and camptothecin-loaded PEGylated Fab'-NPs embedded in a hydrogel for colon targeting. The efficacy of the dual system was highlighted in mouse models of orthotropic colon tumors in which the therapeutic efficacy was higher than NPs containing a single drug due to higher drug internalization into the tumor cells.

A number of miRNAs display anticancer activity *in vitro*, but their *in vivo* applications are limited by degradation in biofluids and limited cellular uptake. miR-204-5p is significantly downregulated in colorectal cancer tissues compared with normal tissues. Using a surface-

functionalizing technique, Zheng and colleagues [19] synthesized poly(D,L-lactide-co-glycolide)/poly(L-lactide)-block-poly(ethylene glycol)-folate polymer NPs that were loaded with miR-204-5p and demonstrated their anticancer effects on colon cancer cells and xenograft colon tumor models *in vivo*. This study highlighted the NP system as a novel option for miRNA delivery to colon cancer cells in an *in vivo* setting.

Galactins are galactoside-binding proteins overexpressed in colorectal cancer and are involved in regulating its development, progression, and metastasis. In addition, they display high affinity for sugars such as galactose and lactose. Liu and colleagues [30] developed 5-fluorouracil-loaded mesoporous silica NP-based galactosylated chitosans as galectin-recognition materials for colon cancer-specific drug delivery. The NPs displayed a high loading capacity, sustained release, and increased cytotoxicity to human colon cancer cells compared to free 5-fluorouracil *in vitro*, demonstrating the efficacy of the inorganic-organic nanocomposite. Similarly, Jiang and coworkers prepared HA-conjugated mesoporous silica NPs loaded with 5-fluorouracil and demonstrated their cytotoxicity to colon cancer cells [109]. HA on the surface of NPs targeted the CD44 receptors overexpressed in the cancer cells.

Biotin is capable of targeted binding to biotin receptors overexpressed on the surfaces of colon cancer cells. So, Lin et al. [110] developed poly(ethylene glycol) and biotin-modified Dox-loaded silica NPs. Dox release from the NPs was redox-sensitive, and its tumor accumulation was potentiated in both HCT116 cells and tumor-bearing mice, enhancing its anticancer efficacy. In another study, the effects of silymarin (SLM), previously limited as an anticancer agent due to its low bioavailability, were enhanced using nanostructured SLM encapsulated in micelles. These NPs inhibited colon cancer cell growth and enhanced their apoptotic and necrotic indexes, with no effects on healthy colon cells [33].

Curcumin has been extensively shown to have anticancer properties, but its use is restricted by poor absorption, degradation, and rapid metabolism. In an interesting study by Alkhader and colleagues [111], curcumin was encapsulated into a chitosan-pectinate NP system (CUR-CS-PEC-NPs) to enhance its colon targeting ability. The NPs significantly enhanced the oral bioavailability of curcumin due to its protection from gastric degradation by pectin. These findings highlight the potential of the CUR-CS-PEC-NPs for oral delivery during colon cancer treatment and pave the way for the development of similar carriers to improve the tumor

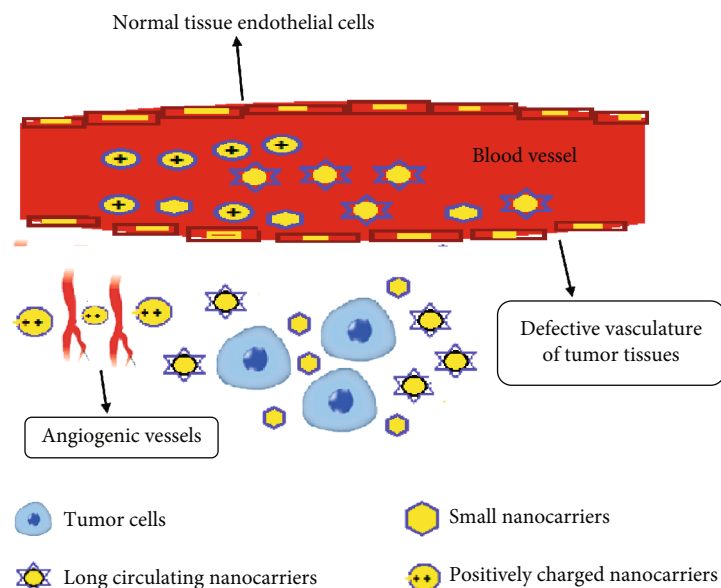


FIGURE 2: Schematic representation of passive anticancer drug targeting through nanocarriers.

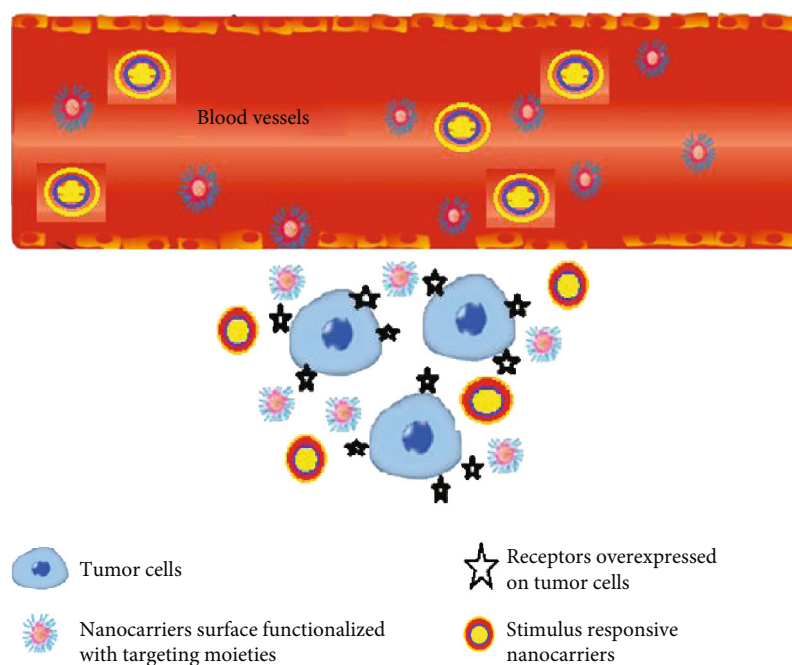


FIGURE 3: Schematic representation of active anticancer drug targeting through nanocarriers.

targeting of natural anticancer compounds. In another study, pH-responsive xylan-curcumin prodrug NPs were synthesized for improving curcumin anticancer efficacy against colon cancer. The synthesized NPs were capable of releasing their loaded drug at acidic pH owing to their pH-responsive nature and increased the drug efficacy against human colon cancer cells as compared to pure drug [112]. A recent study has reported novel xylan-SS-curcumin redox-sensitive prodrug NPs for codelivery of curcumin and 5-fluorouracil against human colorectal cancer cells. Novel NPs were capable of increasing anticancer activity of their loaded drugs, showing them promising drug delivery systems for improved

cancer therapy [113]. Another similar study reported xylan-5-fluorouracil-1-acetic acid conjugates for colon cancer targeted therapy. Results revealed polymeric conjugates improved the drug anticancer efficacy against human colon cancer [114]. The same research group also reported improved anticancer activity for 5-fluorouracil against human colon cancer cells upon delivery in amphiphilic xylan-stearic acid-based NPs [115].

Colchicine is a natural alkaloid prodrug and acts as anti-mitotic anticancer agent; however, its cytotoxicity is a challenge for its effective anticancer efficacy. A recent study reported mesoporous silica NP surface functionalized with

phosphonate groups and decorated with folic acid chitosan-glycine complex for colchicine effective delivery against colon cancer cells [116]. Enhanced anticancer activity of colchicine-laded NPs was proposed to be due to intrinsic apoptosis achieved via increased antimetabolic activity. Another recent study reported targeted delivery of 5-fluorouracil (5Fu) and perfluorocarbon for effective treatment of colon cancer through epidermal growth factor-(EGF-) functionalized PLGA NPs. The functionalized NPs were capable of selective localization of both the drugs into colon cancer cells and inhibited tumor growth through their ability of recognizing specific receptors present on colon cancer cells [117].

3.1.3. Targeting Cervical Cancer. Cervical cancer accounts for ~3% of new cancer cases and the fourth most frequent cancer in women [1]. Several studies highlighted how NPs improve the activity of known anticancer drugs and natural products and enhance their efficacy against cervical cancer cell lines *in vitro*. However, *in vivo* studies on the effectiveness of these NPs remain limited. Silver NPs display antimicrobial, anti-inflammatory, and anticancer activities. Al-Sheddi and coworkers [118] synthesized silver NPs using aqueous extracts of the plant *Nepeta deflersiana* and demonstrated their anticancer activity in HeLa cells through their ability to enhance ROS, lipid peroxidation, and subG1 cell cycle arrest. Yuan and colleagues investigated the synergistic effects of camptothecin, an inhibitor of topoisomerase with potent anticancer activity, and silver NPs on cultured human cervical cancer (HeLa cells) [15]. This combination was beneficial in the treatment of cervical cancer by altering the mitochondrial membrane permeability, increasing ROS formation, and activating caspases 9, 6, and 3. Hence, the combination of NPs and anticancer agents represents as a promising strategy in cancer research.

Regarding other nanomaterials, Luo and coworkers produced biotin-modified poly(lactic-co-glycolic acid) NPs and demonstrated their ability to improve the antiproliferative effects of 15,16-dihydroartemisinin I in HeLa cells by decreasing intracellular ROS generation [31]. Transferrin has been extensively employed as a cancer cell-targeting molecule since transferrin receptor is overexpressed on cancer cells relative to normal cells. Boondireke and colleagues [119] enhanced the cytotoxicity of monomyristin, a monoacylglycerol from saw palmetto palm, in HeLa cells through its encapsulation into dextran-covered polylactide NPs conjugated to transferrin. Encapsulation and transferrin receptor targeting synergistically improved the water solubility and anticancer efficacy of monomyristin.

Cisplatin (CDDP) is an effective anticancer drug, but its lack of selectivity to cervical cancer tissue has limited its use. Therefore, Cheng and colleagues incorporated CDDP into fluorescein PEG amine grafted-aldehyde HA (Cy5.5-PEG-g-A-HA) NPs to increase its selectivity for cervical cancer through tumoral acidic pH response [120]. Although HA is used as a targeting agent in nanocarriers, a major fraction might accumulate in the liver and might be cleared rapidly. The application of aldehyde HA (A-HA) in this study seems to have mitigated this issue. The experiments revealed

favourable CDDP biocompatibility and cervical tumor targeting, with the NPs able to internalize and induce tumor cell apoptosis. Fluorescent imaging *in vivo* revealed high levels of CDDP-Cy5.5-PEG-g-A-HA accumulation at the cervical tumor site, thus demonstrating improved CDDP targeting.

A recent study reported development of pH-sensitive lipid polymer conjugate NP surface decorated with folic acid for targeted delivery of paclitaxel and carboplatin to cervical cancer. The dual-functionalized NPs resulted in higher cellular uptake of the loaded drugs in cervical cancer cells and tumor inhibition via pH-responsive drug release and receptor recognition [121]. Similarly, another recent study reported multifunctional layer-by-layer controlled released mesoporous CaCO₃ NPs for doxorubicin delivery to cervical cancer cells. The intelligent NPs were constructed with chitosan and sodium alginate as alternative materials, folic acid as cancer cell targeting ligand, and layer-by-layer as pH-responsive approach. Cervical cancer cell-targeted delivery of doxorubicin was achieved in a controlled manner via pH responsiveness and receptor recognition [122]. Another recent study reported a novel bioinspired NP strategy for simultaneous delivery of paclitaxel and siRNA for effective treatment of cervical malignancies. Biomimetic dual-drug delivery system was designed through camouflaging HeLa cell membrane on PLGA NPs loaded with paclitaxel and siRNA. The innovative biomimetic dual-drug delivery system increased the drug selective tumor localization through immune escaping ability. As a result, almost 83% cervical tumor volume inhibition was achieved without side effects in major organs [123].

3.1.4. Targeting Breast Cancer. Breast cancer (BCa) is the second most frequent cancer and the leading cause of death in women globally [1]. Although photothermal therapy (PTT) is considered an attractive anticancer strategy, PTT-treated cancer cells may attain thermoresistance due to the upregulation of heat shock proteins (HSPs), mainly HSP70. Hence, inhibiting upregulated HSP70 may diminish the resistance of tumor cells to PTT. Quercetin, a dietary flavonoid, is not only a HSP70 inhibitor but also a protein kinase B and caspase 3 inhibitor. On the other hand, a cell membrane-camouflaged system bestows NPs with powerful advantages. In this context, Zhao and colleagues produced macrophage membrane- (M-) camouflaged quercetin- (QE-) loaded hollow bismuth selenide NPs (M@BS-QE NPs) as a novel BCa therapeutic [17]. The M@BS-QE NPs remained resident in the circulation for longer time periods and enhanced BCa tumor drug accumulation through their ability to evade the immune system. A combination of macrophage membranes, quercetin, and bismuth-based NPs promoted active targeting, sensitized the tumor cells to phototherapy, and inhibited tumor invasiveness and metastasis. Actin cytoskeletal remodelling is highly correlated with tumor metastasis. Qin and colleagues designed novel small-sized fullerene NPs that caused cytotoxicity in migratory BCa cells. The NPs could disturb actin cytoskeleton reorganization and dynamics in cancer cells and inhibited metastasis of aggressive BCa [124].

Dhanapal and Balaraman Ravindran synthesized chitosan- and PLA-coated nanocarriers for piceatannol, a

polyphenol with anticancer activity [24]. The degradation of chitosan was inhibited by combining it with the polymer PLA. These polymeric NPs provided a continuous release of the entrapped piceatannol, leading to higher cytotoxic efficacy for BCa and other cancer cell lines via mitochondria-dependent pathways.

Kong et al. developed docetaxel- (DTX-) loaded cholic acid-functionalized AS1411 aptamer-polydopamine-poly(ϵ -caprolactone-*ran*-lactide) (CA(PCL-*ran*-PLA)) NPs which displayed potent *in vitro* and *in vivo* cytotoxicity in combination with photothermal treatment for BCa therapy [125]. With excellent biocompatibility and reduced side effects, these NPs appear promising for the synergistic chemophotothermal strategy of BCa. Shafiei-Irannejad et al. established that metformin, a biguanide antidiabetic drug, enhances the sensitivity of Dox-resistant BCa cells to Dox via inhibition of P-gp activity [126]. They synthesized biodegradable poly(lactide-*co*-glycolide)-D- α -tocopheryl PEG 1000 succinate NPs encapsulating Dox and metformin, which displayed efficacy towards inactivation of resistant BCa cells [127]. Therefore, codelivery of Dox and metformin by polymeric NPs might be a promising approach to overcome MDR in BCa treatment.

Zeolitic imidazolate framework-8 (ZIF-8) is the most frequently employed MOF for pH-responsive drug release, due to its porosity, sensitivity, and superior drug-loading capacity. Tian et al. fabricated fluorescein-ZIF-8/graphene oxide nanocrystals with acidic pH-responsive release of fluorescein [128]. These nanocrystals inactivated breast cancer 4T1 cells with high efficacy due to photothermal effect under near-infrared light. Chen and colleagues developed ATP-responsive Dox-loaded aptamer-gated nano-MOFs, which induced 40% and 55% cell death, respectively, within 5 days in MDA-MB-231 BCa cells [129]. They also reported a Dox-loaded ATP/Mg²⁺-responsive Zr-MOF which displayed selective cytotoxicity against MDA-MB-231 cells [130]. Due to overexpression of ATP in cancer cells, the aptamer targets the nucleolin receptor sites, leading to enhanced cell permeation of nano-MOFs.

A recent study reported multiwalled carbon nanotubes decorated with glycopolymers conjugated with folic acid for targeted delivery of doxorubicin for effective breast cancer therapy. Doxorubicin was selectively delivered to breast cancer cells through dual targeting of glucose transporter protein and folic acid receptors in breast cancer cells [131]. Another recent study reported methotrexate-loaded silica-coated gold NP system surface functionalized with folic acid for combined chemo-phototherapy of breast cancer. The nano system increased the effects of combined chemo-phototherapy selectively in breast cancer cells due to its selective delivery via folic acid receptor recognition overexpressed on the surfaces of those cancer cells [132]. Furthermore, another recent study reported dual targeting polymeric NPs for selective delivery of paclitaxel for the treatment of bone metastatic breast cancer. The NPs were decorated with folic acid and alendronate-modified D- α -tocopheryl polyethylene glycol succinate for achieving dual drug targeting. The novel system showed binding affinity for hydroxyapatite followed by receptor-mediated internal-

ization, thus showing greater therapeutic effects for the drug against bone metastatic cancer through inhibition of tumor growth and increasing survival rate [133].

4. Conclusion and Future Perspectives

Chemotherapy is preferred for effective treatment of various types of cancer due to its noninvasive nature and killing of cancerous cells. However, optimum clinical efficacy of chemotherapeutics cannot be achieved due to their unique physicochemical properties and lack of target selectivity. As a result, minimum anticancer efficacy is achieved at the cost of massive contamination of the rest of the body, thus leading to severe off-target side effects. Furthermore, the tumor microenvironment also presents various obstacles due to its abnormal pathophysiology. Due to their small size and modulated physicochemical properties, nanocarriers are now established as materials that can be increasingly utilized in cancer therapeutics. In particular, stimuli-responsive and surface-engineered targeted nanocarriers that release their payloads at the tumor site are of particular interest to cancer therapy. Recent advances in the field of pharmaceutical nanotechnology have led formulation scientists to develop smart nanocarrier-based targeted delivery systems for effective treatment and management of lung, colon, cervical, and breast cancers. Published reports show that various types of nanocarriers including liposomes, lipid, metal and polymeric NPs and micelles, nano-MOFs, and carbon nanotubes have been effectively used for targeted delivery of chemotherapeutic agents for lung, colon, cervical, and breast cancer treatment. Various types of surface-functionalized nanocarriers such as high redox status, acidic pH, or hypoxia-responsive NPs have also been reported for overcoming the barriers of the tumor microenvironment and selective localization of anticancer drugs in lung, colon, cervical, and breast tumors. Recently, several nanodrugs have received FDA approval, and many more are in clinical trials. Most of the presently approved nanodrugs are based on approved conventional drugs and simple NPs.

However, the lack of standard protocols for nanocarrier and nanodrug characterization toxicity, physical, chemical, and biological instability, disease heterogeneity, and irregular *in vivo* behaviour of NPs frequently restrict the efforts of researchers, thus leading to NP failure in late-phase clinical trials. To prevent their failure in clinical trials, it is crucial to understand the cancer heterogeneity and inherent properties of NPs so they can be effectively modulated for increasing their stability and biocompatibility and uniform *in vivo* behaviour. Similarly, research in nanomedicine for lung, colon, cervical, and breast cancer treatment is mostly focused on material and formulation investigations which represent the preliminary stages. Data for their potential applications as therapeutics needs to be acquired only from animal studies, and multidisciplinary approaches should be adopted. With the global trend towards precision medicine, the future for a multicentered strategy of nanocarrier technology appears promising. Furthermore, regularity procedures also remain as major obstacles; thus, an easy and integrated approval procedure approach should be designed.

Nevertheless, nanodrug platforms are incorporating a broad range of NP types and becoming more complex. The research occurring in this arena predicts the availability of numerous new nanodrugs for clinical use in the future. Intelligent NP systems capable of simultaneous targeted chemotherapy, disease monitoring, and diagnosis can also be predicted from the current advancements being made in this area. Although many challenges complicate nanodrug development, it may only be a matter of time until these agents offer unique solutions for unmet clinical needs.

Conflicts of Interest

All the authors declare no conflict of interest.

Authors' Contributions

Ke-Tao Jin and Ze-Bei Lu contributed equally to this work.

Acknowledgments

This work was supported by the Zhejiang Provincial Science and Technology Projects (No. LGF18H160026 to YYZ, No. LGD19H160001 to JKT, and No. LGF20H140010 to FY), the National Natural Science Foundation of China (No. 81772537 to JKT and No. 81374014 to JKT), the Zhejiang Provincial Natural Science Foundation of China (No. LY17H180010 to XYC and No. LY15H160055 to HYD), and the Zhejiang Medical Technology Plan Project (No. 2015KYA023 to HYD).

References

- [1] M. M. Fidler, F. Bray, and I. Soerjomataram, "The global cancer burden and human development: a review," *Scandinavian Journal of Public Health*, vol. 46, no. 1, pp. 27–36, 2018.
- [2] J. L. Caswell-Jin, S. K. Plevritis, L. Tian et al., "Change in survival in metastatic breast cancer with treatment advances: meta-analysis and systematic review," *JNCI Cancer Spectrum*, vol. 2, no. 4, article pky062, 2018.
- [3] M. Fardi, S. Solali, and M. Farshdousti Hagh, "Epigenetic mechanisms as a new approach in cancer treatment: an updated review," *Genes & Diseases*, vol. 5, no. 4, pp. 304–311, 2018.
- [4] A. Guglielmo, N. Staropoli, M. Giancotti, and M. Mauro, "Personalized medicine in colorectal cancer diagnosis and treatment: a systematic review of health economic evaluations," *Cost Effectiveness and Resource Allocation*, vol. 16, no. 1, p. 2, 2018.
- [5] X. Guo, Q. Zhuang, T. Ji et al., "Multi-functionalized chitosan nanoparticles for enhanced chemotherapy in lung cancer," *Carbohydrate Polymers*, vol. 195, pp. 311–320, 2018.
- [6] H. I. Tsai, L. Jiang, X. Zeng et al., "DACHPT-loaded nanoparticles self-assembled from biodegradable dendritic copolymer polyglutamic acid-b-D- α -tocopheryl polyethylene glycol 1000 succinate for multidrug resistant lung cancer therapy," *Frontiers in Pharmacology*, vol. 9, p. 119, 2018.
- [7] S. Rangaraj and R. Venkatachalam, "In vitro and in vivo characteristics of biogenic high surface silica nanoparticles in A549 lung cancer cell lines and Danio rerio model systems for inorganic biomaterials development," *Artificial Cells, Nanomedicine, and Biotechnology*, vol. 46, no. 7, pp. 1415–1424, 2017.
- [8] P. Rychahou, Y. Bae, D. Reichel et al., "Colorectal cancer lung metastasis treatment with polymer-drug nanoparticles," *Journal of Controlled Release*, vol. 275, pp. 85–91, 2018.
- [9] H. Shali, M. Shabani, F. Pourgholi et al., "Co-delivery of insulin-like growth factor 1 receptor specific siRNA and doxorubicin using chitosan-based nanoparticles enhanced anticancer efficacy in A549 lung cancer cell line," *Artificial Cells, Nanomedicine, and Biotechnology*, vol. 46, no. 2, pp. 293–302, 2017.
- [10] A. Sharma, B. Gorey, and A. Casey, "In vitro comparative cytotoxicity study of aminated polystyrene, zinc oxide and silver nanoparticles on a cervical cancer cell line," *Drug and Chemical Toxicology*, vol. 42, no. 1, pp. 9–23, 2018.
- [11] Y. Shoja, A. Kermanpur, and F. Karimzadeh, "Diagnosis of EGFR exon21 L858R point mutation as lung cancer biomarker by electrochemical DNA biosensor based on reduced graphene oxide/functionalized ordered mesoporous carbon/Ni-oxytetracycline metallopolymer nanoparticles modified pencil graphite electrode," *Biosensors & Bioelectronics*, vol. 113, pp. 108–115, 2018.
- [12] Y. Song, H. Cai, T. Yin et al., "Paclitaxel-loaded redox-sensitive nanoparticles based on hyaluronic acid-vitamin E succinate conjugates for improved lung cancer treatment," *International Journal of Nanomedicine*, vol. Volume 13, pp. 1585–1600, 2018.
- [13] B. Xiao, E. Viennois, Q. Chen et al., "Silencing of intestinal glycoprotein CD98 by orally targeted nanoparticles enhances chemosensitization of colon cancer," *ACS Nano*, vol. 12, no. 6, pp. 5253–5265, 2018.
- [14] R. Yokchom, S. Laiwejpithaya, W. Maneepakorn, S. Tapaneeyakorn, J. Rabablert, and T. Dharakul, "Paper-based immunosensor with signal amplification by enzyme-labeled anti-p16INK4a multifunctionalized gold nanoparticles for cervical cancer screening," *Nanomedicine*, vol. 14, no. 3, pp. 1051–1058, 2018.
- [15] Y. G. Yuan, S. Zhang, J. Y. Hwang, and I. K. Kong, "Silver nanoparticles potentiates cytotoxicity and apoptotic potential of camptothecin in human cervical cancer cells," *Oxidative Medicine and Cellular Longevity*, vol. 2018, Article ID 6121328, 21 pages, 2018.
- [16] X. Zhang and C. Xiao, "Biofabrication of silver nanoparticles and their combined effect with low intensity ultrasound for treatment of lung cancer," *Journal of Photochemistry and Photobiology. B*, vol. 181, pp. 122–126, 2018.
- [17] H. Zhao, L. Li, J. Zhang et al., "C-C chemokine ligand 2 (CCL2) recruits macrophage-membrane-camouflaged hollow bismuth selenide nanoparticles to facilitate photothermal sensitivity and inhibit lung metastasis of breast cancer," *ACS Applied Materials & Interfaces*, vol. 10, no. 37, pp. 31124–31135, 2018.
- [18] Y. Zhao, Q. Sun, X. Zhang, J. Baeyens, and H. Su, "Self-assembled selenium nanoparticles and their application in the rapid diagnostic detection of small cell lung cancer biomarkers," *Soft Matter*, vol. 14, no. 4, pp. 481–489, 2018.
- [19] B. Zheng, L. Chen, C. C. Pan et al., "Targeted delivery of miRNA-204-5p by PEGylated polymer nanoparticles for colon cancer therapy," *Nanomedicine*, vol. 13, no. 7, pp. 769–785, 2018.
- [20] D. Zheng, J. Wang, S. Guo, Z. Zhao, and F. Wang, "Formulations, pharmacodynamic and clinical studies of nanoparticles

- for lung cancer therapy - an overview," *Current Drug Metabolism*, vol. 19, no. 9, pp. 759–767, 2018.
- [21] C. Conte, F. Mastrotto, V. Taresco et al., "Enhanced uptake in 2D- and 3D- lung cancer cell models of redox responsive PEGylated nanoparticles with sensitivity to reducing extra- and intracellular environments," *Journal of Controlled Release*, vol. 277, pp. 126–141, 2018.
- [22] W. Chengzheng, W. Jiazhi, C. Shuangjiang et al., "Biogenic synthesis, characterization and evaluation of silver nanoparticles from *Aspergillus niger* JX556221 against human colon cancer cell line HT-29," *Journal of Nanoscience and Nanotechnology*, vol. 18, no. 5, pp. 3673–3681, 2018.
- [23] N. Dasgupta, S. Ranjan, D. Mishra, and C. Ramalingam, "Thermal co-reduction engineered silver nanoparticles induce oxidative cell damage in human colon cancer cells through inhibition of reduced glutathione and induction of mitochondria-involved apoptosis," *Chemico-Biological Interactions*, vol. 295, pp. 109–118, 2018.
- [24] J. Dhanapal and M. Balaraman Ravindran, "Chitosan/poly (lactic acid)-coated piceatannol nanoparticles exert an in vitro apoptosis activity on liver, lung and breast cancer cell lines," *Artificial Cells, Nanomedicine, and Biotechnology*, vol. 46, supplement 1, pp. 274–282, 2018.
- [25] N. Dudhipala and G. Puchchakayala, "Capecitabine lipid nanoparticles for anti-colon cancer activity in 1,2-dimethylhydrazine-induced colon cancer: preparation, cytotoxic, pharmacokinetic, and pathological evaluation," *Drug Development and Industrial Pharmacy*, vol. 44, no. 10, pp. 1572–1582, 2018.
- [26] N. Gonzalez-Ballesteros, M. C. Rodriguez-Arguelles, S. Prado-Lopez et al., "Macroalgae to nanoparticles: study of *Ulva lactuca* L. role in biosynthesis of gold and silver nanoparticles and of their cytotoxicity on colon cancer cell lines," *Materials Science & Engineering. C, Materials for Biological Applications*, vol. 97, pp. 498–509, 2019.
- [27] S. Gurunathan, M. Qasim, C. Park, H. Yoo, J. H. Kim, and K. Hong, "Cytotoxic potential and molecular pathway analysis of silver nanoparticles in human colon cancer cells HCT116," *International Journal of Molecular Sciences*, vol. 19, no. 8, p. 2269, 2018.
- [28] S. Handali, E. Moghimipour, M. Rezaei, S. Saremy, and F. A. Dorkoosh, "Co-delivery of 5-fluorouracil and oxaliplatin in novel poly(3-hydroxybutyrate-co-3-hydroxyvalerate acid)/poly(lactic-co-glycolic acid) nanoparticles for colon cancer therapy," *International Journal of Biological Macromolecules*, vol. 124, pp. 1299–1311, 2019.
- [29] F. T. Hsu, H. S. Liu, A. A. Ali et al., "Assessing the selective therapeutic efficacy of superparamagnetic erlotinib nanoparticles in lung cancer by using quantitative magnetic resonance imaging and a nuclear factor kappa-B reporter gene system," *Nanomedicine*, vol. 14, no. 3, pp. 1019–1031, 2018.
- [30] W. Liu, Y. Zhu, F. Wang et al., "Galactosylated chitosan-functionalized mesoporous silica nanoparticles for efficient colon cancer cell-targeted drug delivery," *Royal Society Open Science*, vol. 5, no. 12, article 181027, 2018.
- [31] J. Luo, X. Meng, J. Su et al., "Biotin-modified polylactic-co-glycolic acid nanoparticles with improved antiproliferative activity of 15,16-dihydrotanshinone I in human cervical cancer cells," *Journal of Agricultural and Food Chemistry*, vol. 66, no. 35, pp. 9219–9230, 2018.
- [32] J. Marquez, I. Fernandez-Pineiro, M. J. Arauzo-Bravo et al., "Targeting liver sinusoidal endothelial cells with miR-20a-loaded nanoparticles reduces murine colon cancer metastasis to the liver," *International Journal of Cancer*, vol. 143, no. 3, pp. 709–719, 2018.
- [33] M. Mombeini, G. Saki, L. Khorsandi, and N. Bavarsad, "Effects of silymarin-loaded nanoparticles on HT-29 human colon cancer cells," *Medicina*, vol. 54, no. 1, p. 1, 2018.
- [34] M. Moskvina, M. Babic, S. Reis et al., "Biological evaluation of surface-modified magnetic nanoparticles as a platform for colon cancer cell theranostics," *Colloids and Surfaces. B, Biointerfaces*, vol. 161, pp. 35–41, 2018.
- [35] L. Pan, F. Ye, J. J. Liu, X. Q. Ba, and Q. S. Sheng, "A study of using carbon nanoparticles to improve lymph nodes staging for laparoscopic-assisted radical right hemicolectomy in colon cancer," *International Journal of Colorectal Disease*, vol. 33, no. 8, pp. 1131–1134, 2018.
- [36] Z. Song, Y. Shi, Q. Han, and G. Dai, "Endothelial growth factor receptor-targeted and reactive oxygen species-responsive lung cancer therapy by docetaxel and resveratrol encapsulated lipid-polymer hybrid nanoparticles," *Biomedicine & Pharmacotherapy*, vol. 105, pp. 18–26, 2018.
- [37] C. E. Swenson, D. Haemmerich, D. H. Maul, B. Knox, N. Ehrhart, and R. A. Reed, "Increased duration of heating boosts local drug deposition during radiofrequency ablation in combination with thermally sensitive liposomes (ThermoDox) in a porcine model," *PLoS one*, vol. 10, no. 10, article e0139752, 2015.
- [38] A. A. Attama, M. A. Momoh, and P. F. Builders, "Lipid nanoparticulate drug delivery systems: a revolution in dosage form design and development," *Recent advances in novel drug carrier systems*, vol. 5, pp. 107–140, 2012.
- [39] L. Genc, H. M. Kutlu, and G. Guney, "Vitamin B12-loaded solid lipid nanoparticles as a drug carrier in cancer therapy," *Pharmaceutical Development and Technology*, vol. 20, no. 3, pp. 337–344, 2013.
- [40] O. S. Muddineti, A. Shah, S. V. K. Rompicharla, B. Ghosh, and S. Biswas, "Cholesterol-grafted chitosan micelles as a nanocarrier system for drug-siRNA co-delivery to the lung cancer cells," *International Journal of Biological Macromolecules*, vol. 118, Part A, pp. 857–863, 2018.
- [41] Y. Shen, J. Zhang, W. Hao et al., "Copolymer micelles function as pH-responsive nanocarriers to enhance the cytotoxicity of a HER2 aptamer in HER2-positive breast cancer cells," *International Journal of Nanomedicine*, vol. Volume 13, pp. 537–553, 2018.
- [42] Y. Guo, W. He, S. Yang, D. Zhao, Z. Li, and Y. Luan, "Co-delivery of docetaxel and verapamil by reduction-sensitive PEG-PLGA-SS-DTX conjugate micelles to reverse the multi-drug resistance of breast cancer," *Colloids and Surfaces. B, Biointerfaces*, vol. 151, pp. 119–127, 2017.
- [43] Z. Li, H. Wang, Y. Chen et al., "pH- and NIR light-responsive polymeric prodrug micelles for hyperthermia-assisted site-specific chemotherapy to reverse drug resistance in cancer treatment," *Small*, vol. 12, no. 20, pp. 2731–2740, 2016.
- [44] L. Lv, K. Qiu, X. Yu et al., "Amphiphilic copolymeric micelles for doxorubicin and curcumin co-delivery to reverse multi-drug resistance in breast cancer," *Journal of Biomedical Nanotechnology*, vol. 12, no. 5, pp. 973–985, 2016.
- [45] K. Liang, J. E. Chung, S. J. Gao, N. Yongvongsoontorn, and M. Kurisawa, "Highly augmented drug loading and stability of micellar nanocomplexes composed of doxorubicin and poly(ethylene glycol)-green tea catechin conjugate for cancer

- therapy," *Advanced Materials*, vol. 30, no. 14, article e1706963, 2018.
- [46] S. Movassaghian, O. M. Merkel, and V. P. Torchilin, "Applications of polymer micelles for imaging and drug delivery," *Wiley Interdisciplinary Reviews: Nanomedicine and Nanobiotechnology*, vol. 7, no. 5, pp. 691–707, 2015.
- [47] T. Li, S. Shi, S. Goel et al., "Recent advancements in mesoporous silica nanoparticles towards therapeutic applications for cancer," *Acta Biomaterialia*, vol. 89, pp. 1–13, 2019.
- [48] D. Eom, J. Kim, K. Lee et al., "Fabrication of AlN nanostructures using polarity control by high temperature metalorganic chemical vapor deposition," *Journal of Nanoscience and Nanotechnology*, vol. 15, no. 7, pp. 5144–5147, 2015.
- [49] N. Bhardwaj, S. K. Pandey, J. Mehta, S. K. Bhardwaj, K. H. Kim, and A. Deep, "Bioactive nano-metal-organic frameworks as antimicrobials against Gram-positive and Gram-negative bacteria," *Toxicology Research*, vol. 7, no. 5, pp. 931–941, 2018.
- [50] B. Khezri and M. Pumera, "Metal-organic frameworks based nano/micro/millimeter-sized self-propelled autonomous machines," *Advanced Materials*, vol. 31, no. 14, article e1806530, 2019.
- [51] E. Calzoni, A. Cesaretti, A. Polchi, A. Di Michele, B. Tancini, and C. Emiliani, "Biocompatible polymer nanoparticles for drug delivery applications in cancer and neurodegenerative disorder therapies," *Journal of Functional Biomaterials*, vol. 10, no. 1, p. 4, 2019.
- [52] H. Choudhury, M. Pandey, P. X. Chin et al., "Transferrin receptors-targeting nanocarriers for efficient targeted delivery and transcytosis of drugs into the brain tumors: a review of recent advancements and emerging trends," *Drug Delivery and Translational Research*, vol. 8, no. 5, pp. 1545–1563, 2018.
- [53] B. Deng, P. Ma, and Y. Xie, "Reduction-sensitive polymeric nanocarriers in cancer therapy: a comprehensive review," *Nanoscale*, vol. 7, no. 30, pp. 12773–12795, 2015.
- [54] R. M. Farid, N. A. H. A. Youssef, and A. A. Kassem, "Platform for lipid based nanocarriers' formulation components and their potential effects: a literature review," *Current Pharmaceutical Design*, vol. 23, no. 43, pp. 6613–6629, 2018.
- [55] M. Fojtu, J. Gumulec, T. Stracina et al., "Reduction of doxorubicin-induced cardiotoxicity using nanocarriers: a review," *Current Drug Metabolism*, vol. 18, no. 3, pp. 237–263, 2017.
- [56] Y. C. Barenholz, "Doxil® — The first FDA-approved nano-drug: Lessons learned," *Journal of Controlled Release*, vol. 160, no. 2, pp. 117–134, 2012.
- [57] A. Cadete and M. J. Alonso, "Targeting cancer with hyaluronic acid-based nanocarriers: recent advances and translational perspectives," *Nanomedicine*, vol. 11, no. 17, pp. 2341–2357, 2016.
- [58] W. Q. Lim, S. Z. F. Phua, H. V. Xu, S. Sreejith, and Y. Zhao, "Recent advances in multifunctional silica-based hybrid nanocarriers for bioimaging and cancer therapy," *Nanoscale*, vol. 8, no. 25, pp. 12510–12519, 2016.
- [59] G. K. Rout, H.-S. Shin, S. Gouda et al., "Current advances in nanocarriers for biomedical research and their applications," *Artificial Cells, Nanomedicine, and Biotechnology*, vol. 46, supplement 2, pp. 1053–1062, 2018.
- [60] X. Yue and Z. Dai, "Recent advances in liposomal nanohybrid cerasomes as promising drug nanocarriers," *Advances in Colloid and Interface Science*, vol. 207, pp. 32–42, 2014.
- [61] N. Desai, "Nanoparticle albumin-bound paclitaxel (Abraxane®)," in *Albumin in Medicine*, pp. 101–119, Springer, 2016.
- [62] A. Garg, R. Sharma, V. Pandey, V. Patel, and A. K. Yadav, "Heparin-tailored biopolymeric nanocarriers in site-specific delivery: a systematic review," *Critical Reviews in Therapeutic Drug Carrier Systems*, vol. 34, no. 1, pp. 1–33, 2017.
- [63] M. Moreno-Sastre, M. Pastor, C. J. Salomon, A. Esquisabel, and J. L. Pedraz, "Pulmonary drug delivery: a review on nanocarriers for antibacterial chemotherapy," *The Journal of Antimicrobial Chemotherapy*, vol. 70, no. 11, pp. 2945–2955, 2015.
- [64] S. M. Mousavi, S. A. Hashemi, Y. Ghasemi, A. M. Amani, A. Babapoor, and O. Arjmand, "Applications of graphene oxide in case of nanomedicines and nanocarriers for biomolecules: review study," *Drug Metabolism Reviews*, vol. 51, no. 1, pp. 12–41, 2019.
- [65] J. V. Natarajan, C. Nugraha, X. W. Ng, and S. Venkatraman, "Sustained-release from nanocarriers: a review," *Journal of Controlled Release*, vol. 193, pp. 122–138, 2014.
- [66] N. Olov, S. Bagheri-Khoulenjani, and H. Mirzadeh, "Combination drug delivery using nanocarriers for breast cancer treatments: a review," *Journal of Biomedical Materials Research. Part A*, vol. 106, no. 8, pp. 2272–2283, 2018.
- [67] S. Pimentel-Moral, M. C. Teixeira, A. R. Fernandes et al., "Lipid nanocarriers for the loading of polyphenols - a comprehensive review," *Advances in Colloid and Interface Science*, vol. 260, pp. 85–94, 2018.
- [68] A. Smith, *Big Moment for Nanotech: Oncology Therapeutics Poised for a Leap*, 2013, *OnLive*.
- [69] R. Bawa, G. F. Audette, and I. Rubinstein, "Copaxone® in the era of biosimilars and nanosimilars," in *Handbook of Clinical Nanomedicine*, pp. 829–872, Jenny Stanford Publishing, 2016.
- [70] L. Chen, H. Shiah, T. Chao et al., "Phase I study of liposome irinotecan (PEP02) in combination with weekly infusion of 5-FU/LV in advanced solid tumors," *Journal of Clinical Oncology*, vol. 28, 15, pp. e13024–e13024, 2010.
- [71] S. Tran, P.-J. DeGiovanni, B. Piel, and P. Rai, "Cancer nanomedicine: a review of recent success in drug delivery," *Clinical and Translational Medicine*, vol. 6, no. 1, p. 44, 2017.
- [72] S. Rezvantalab, N. I. Drude, M. K. Moraveji et al., "PLGA-based nanoparticles in cancer treatment," *Frontiers in Pharmacology*, vol. 9, p. 1260, 2018.
- [73] G. Ledet and T. K. Mandal, "Nanomedicine: emerging therapeutics for the 21st century," *U.S. Pharmacist*, vol. 37, no. 3, pp. 7–11, 2012.
- [74] R. Wang, P. S. Billone, and W. M. Mullett, "Nanomedicine in action: an overview of cancer nanomedicine on the market and in clinical trials," *Journal of Nanomaterials*, vol. 2013, 12 pages, 2013.
- [75] D. Bobo, K. J. Robinson, J. Islam, K. J. Thurecht, and S. R. Corrie, "Nanoparticle-based medicines: a review of FDA-approved materials and clinical trials to date," *Pharmaceutical Research*, vol. 33, no. 10, pp. 2373–2387, 2016.
- [76] A. C. Anselmo and S. Mitragotri, "Nanoparticles in the clinic: an update," *Bioengineering & Translational Medicine*, vol. 4, no. 3, article e10143, 2019.

- [77] E. Beltrán-Gracia, A. López-Camacho, I. Higuera-Ciajara, J. B. Velázquez-Fernández, and A. A. Vallejo-Cardona, "Nanomedicine review: clinical developments in liposomal applications," *Cancer Nanotechnology*, vol. 10, no. 1, p. 11, 2019.
- [78] C. L. Ventola, "Progress in nanomedicine: approved and investigational nanodrugs," *Pharmacy and Therapeutics*, vol. 42, no. 12, p. 742, 2017.
- [79] I. Ali, M. Alsehli, L. Scotti et al., "Progress in polymeric nanomedicines for theranostic cancer treatment," *Polymers*, vol. 12, no. 3, p. 598, 2020.
- [80] N. Senzer, J. Nemunaitis, D. Nemunaitis et al., "Phase I study of a systemically delivered p53 nanoparticle in advanced solid tumors," *Molecular Therapy*, vol. 21, no. 5, pp. 1096–1103, 2013.
- [81] K. Kato, K. Chin, T. Yoshikawa et al., "Phase II study of NK105, a paclitaxel-incorporating micellar nanoparticle, for previously treated advanced or recurrent gastric cancer," *Investigational New Drugs*, vol. 30, no. 4, pp. 1621–1627, 2012.
- [82] N.-J. Chiang, T.-Y. Chao, R.-K. Hsieh et al., "A phase I dose-escalation study of PEP02 (irinotecan liposome injection) in combination with 5-fluorouracil and leucovorin in advanced solid tumors," *BMC Cancer*, vol. 16, no. 1, p. 907, 2016.
- [83] M. Z. El-Readi and M. A. Althubiti, "Cancer nanomedicine: a new era of successful targeted therapy," *Journal of Nanomaterials*, vol. 2019, article 4927312, 2019.
- [84] V. Thakur and R. V. Kutty, "Recent advances in nanotheranostics for triple negative breast cancer treatment," *Journal of Experimental & Clinical Cancer Research*, vol. 38, no. 1, p. 430, 2019.
- [85] S. Parveen, F. Arjmand, and S. Tabassum, "Clinical developments of antitumor polymer therapeutics," *RSC Advances*, vol. 9, no. 43, pp. 24699–24721, 2019.
- [86] X. Chi, K. Liu, X. Luo, Z. Yin, H. Lin, and J. Gao, "Recent advances of nanomedicines for liver cancer therapy," *Journal of Materials Chemistry B*, vol. 8, no. 17, pp. 3747–3771, 2020.
- [87] S. Khan, M. Imran, T. T. Butt et al., "Curcumin based nanomedicines as efficient nanoplatform for treatment of cancer: new developments in reversing cancer drug resistance, rapid internalization, and improved anticancer efficacy," *Trends in Food Science & Technology*, vol. 80, pp. 8–22, 2018.
- [88] G. W. Sledge and K. D. Miller, "Exploiting the hallmarks of cancer: the future conquest of breast cancer," *European Journal of Cancer*, vol. 39, no. 12, pp. 1668–1675, 2003.
- [89] B. A. Teicher, "Molecular targets and cancer therapeutics: discovery, development and clinical validation," *Drug Resistance Updates*, vol. 3, no. 2, pp. 67–73, 2000.
- [90] L. Basile, R. Pignatello, and C. Passirani, "Active targeting strategies for anticancer drug nanocarriers," *Current Drug Delivery*, vol. 9, no. 3, pp. 255–268, 2012.
- [91] S. K. Hobbs, W. L. Monsky, F. Yuan et al., "Regulation of transport pathways in tumor vessels: role of tumor type and microenvironment," *Proceedings of the National Academy of Sciences*, vol. 95, no. 8, pp. 4607–4612, 1998.
- [92] P. Rubin and G. Casarett, "Microcirculation of tumors part II: the supervascularized state of irradiated regressing tumors," *Clinical Radiology*, vol. 17, no. 4, pp. 346–355, 1966.
- [93] B. Haley and E. Frenkel, "Nanoparticles for drug delivery in cancer treatment," in *Urologic Oncology: Seminars and original investigations*, pp. 57–64, Elsevier, 2008.
- [94] D. C. Drummond, O. Meyer, K. Hong, D. B. Kirpotin, and D. Papahadjopoulos, "Optimizing liposomes for delivery of chemotherapeutic agents to solid tumors," *Pharmacological Reviews*, vol. 51, no. 4, pp. 691–743, 1999.
- [95] A. A. Gabizon, "Pegylated liposomal doxorubicin: metamorphosis of an old drug into a new form of chemotherapy," *Cancer Investigation*, vol. 19, no. 4, pp. 424–436, 2001.
- [96] G. P. Adams, R. Schier, A. M. McCall et al., "High affinity restricts the localization and tumor penetration of single-chain fv antibody molecules," *Cancer Research*, vol. 61, no. 12, pp. 4750–4755, 2001.
- [97] S. Gosk, T. Moos, C. Gottstein, and G. Bendas, "VCAM-1 directed immunoliposomes selectively target tumor vasculature in vivo," *Biochimica et Biophysica Acta (BBA)-Biomembranes*, vol. 1778, no. 4, pp. 854–863, 2008.
- [98] M. Radovic, R. Kaneshwaran, A. Rittmeyer et al., "Multidisciplinary treatment of lung cancer in older patients: a review," *Journal of Geriatric Oncology*, vol. 10, no. 3, pp. 405–410, 2019.
- [99] L. M. Hess, A. M. DeLozier, F. Natanegara et al., "First-line treatment of patients with advanced or metastatic squamous non-small cell lung cancer: systematic review and network meta-analysis," *Journal of Thoracic Disease*, vol. 10, no. 12, pp. 6677–6694, 2018.
- [100] V. Ramalingam, K. Varunkumar, V. Ravikumar, and R. Rajaram, "Target delivery of doxorubicin tethered with PVP stabilized gold nanoparticles for effective treatment of lung cancer," *Scientific Reports*, vol. 8, no. 1, p. 3815, 2018.
- [101] A. Kalaiarasi, R. Sankar, C. Anusha et al., "Copper oxide nanoparticles induce anticancer activity in A549 lung cancer cells by inhibition of histone deacetylase," *Biotechnology Letters*, vol. 40, no. 2, pp. 249–256, 2018.
- [102] P. Parashar, M. Rathor, M. Dwivedi, and S. Saraf, "Hyaluronic acid decorated naringenin nanoparticles: appraisal of chemopreventive and curative potential for lung cancer," *Pharmaceutics*, vol. 10, no. 1, p. 33, 2018.
- [103] S. Vandghanooni, M. Eskandani, J. Barar, and Y. Omid, "AS1411 aptamer-decorated cisplatin-loaded poly(lactic-co-glycolic acid) nanoparticles for targeted therapy of miR-21-inhibited ovarian cancer cells," *Nanomedicine*, vol. 13, no. 21, pp. 2729–2758, 2018.
- [104] N. Amreddy, A. Babu, J. Panneerselvam et al., "Chemo-biologic combinatorial drug delivery using folate receptor-targeted dendrimer nanoparticles for lung cancer treatment," *Nanomedicine*, vol. 14, no. 2, pp. 373–384, 2018.
- [105] M. Perepelyuk, K. Sacko, K. Thangavel, and S. A. Shoyele, "Evaluation of MUC1-aptamer functionalized hybrid nanoparticles for targeted delivery of miRNA-29b to nonsmall cell lung cancer," *Molecular Pharmaceutics*, vol. 15, no. 3, pp. 985–993, 2018.
- [106] H. M. Abdelaziz, M. Gaber, M. M. Abd-Elwakil et al., "Inhalable particulate drug delivery systems for lung cancer therapy: nanoparticles, microparticles, nanocomposites and nanoaggregates," *Journal of Controlled Release*, vol. 269, pp. 374–392, 2018.
- [107] Z. Zhang, W. Cheng, Y. Pan, and L. Jia, "An Anticancer agent-loaded PLGA nanomedicine with glutathione-response and targeted delivery for the treatment of lung cancer," *Journal of Materials Chemistry B*, vol. 8, no. 4, pp. 655–665, 2020.

- [108] F. Bénard, A. N. Barkun, M. Martel, and D. von Renteln, "Systematic review of colorectal cancer screening guidelines for average-risk adults: summarizing the current global recommendations," *World Journal of Gastroenterology*, vol. 24, no. 1, pp. 124–138, 2018.
- [109] H. Jiang, X. Shi, X. Yu, X. He, Y. An, and H. Lu, "Hyaluronidase enzyme-responsive targeted nanoparticles for effective delivery of 5-fluorouracil in colon cancer," *Pharmaceutical Research*, vol. 35, no. 4, p. 73, 2018.
- [110] Y. Q. Lin, J. Zhang, S. J. Liu, and H. Ye, "Doxorubicin loaded silica nanoparticles with dual modification as a tumor-targeted drug delivery system for colon cancer therapy," *Journal of Nanoscience and Nanotechnology*, vol. 18, no. 4, pp. 2330–2336, 2018.
- [111] E. Alkhader, C. J. Roberts, R. Rosli et al., "Pharmacokinetic and anti-colon cancer properties of curcumin-containing chitosan-pectinate composite nanoparticles," *Journal of Biomaterials Science. Polymer Edition*, vol. 29, no. 18, pp. 2281–2298, 2018.
- [112] Sauraj, S. U. Kumar, V. Kumar, R. Priyadarshi, P. Gopinath, and Y. S. Negi, "pH-responsive prodrug nanoparticles based on xylan-curcumin conjugate for the efficient delivery of curcumin in cancer therapy," *Carbohydrate Polymers*, vol. 188, pp. 252–259, 2018.
- [113] B. Kumar, R. Priyadarshi, F. Deeba et al., "Redox responsive xylan-SS-curcumin prodrug nanoparticles for dual drug delivery in cancer therapy," *Materials Science and Engineering: C*, vol. 107, p. 110356, 2020.
- [114] S. U. Kumar, P. Gopinath, and Y. S. Negi, "Synthesis and bio-evaluation of xylan-5-fluorouracil-1-acetic acid conjugates as prodrugs for colon cancer treatment," *Carbohydrate Polymers*, vol. 157, pp. 1442–1450, 2017.
- [115] V. Kumar, B. Kumar, F. Deeba et al., "Lipophilic 5-fluorouracil prodrug encapsulated xylan-stearic acid conjugates nanoparticles for colon cancer therapy," *International Journal of Biological Macromolecules*, vol. 128, pp. 204–213, 2019.
- [116] K. AbouAitah, H. A. Hassan, A. Swiderska-Sroda et al., "Targeted nano-drug delivery of colchicine against colon cancer cells by means of mesoporous silica nanoparticles," *Cancers*, vol. 12, no. 1, p. 144, 2020.
- [117] P. Wu, Q. Zhou, H. Zhu, Y. Zhuang, and J. Bao, "Enhanced antitumor efficacy in colon cancer using EGF functionalized PLGA nanoparticles loaded with 5-fluorouracil and perfluorocarbon," *BMC Cancer*, vol. 20, no. 1, p. 354, 2020.
- [118] E. S. Al-Sheddi, N. N. Farshori, M. M. Al-Oqail et al., "Anticancer potential of green synthesized silver nanoparticles using extract of *Nepeta deflersiana* against human cervical cancer cells (HeLa)," *Bioinorganic Chemistry and Applications*, vol. 2018, Article ID 9390784, 12 pages, 2018.
- [119] S. Boondireke, M. Léonard, A. Durand, and B. T. Wongsatayanon, "Encapsulation of monomyristin into polymeric nanoparticles improved its in vitro antiproliferative activity against cervical cancer cells," *Colloids and Surfaces. B, Biointerfaces*, vol. 176, pp. 9–17, 2019.
- [120] C. Cheng, Y. Meng, Z. Zhang, Y. Li, and Q. Zhang, "Tumoral acidic pH-responsive cis-diaminodichloroplatinum-incorporated Cy5.5-PEG-g-A-HA nanoparticles for targeting delivery of CDDP against cervical cancer," *ACS Applied Materials & Interfaces*, vol. 10, no. 32, pp. 26882–26892, 2018.
- [121] J. Wang, "Combination treatment of cervical cancer using folate-decorated, pH-sensitive, carboplatin and paclitaxel co-loaded lipid-polymer hybrid *Nanoparticles*," *Drug Design, Development and Therapy*, vol. Volume 14, pp. 823–832, 2020.
- [122] J. Xing, Y. Cai, Y. Wang, H. Zheng, and Y. Liu, "Synthesis of polymer assembled mesoporous CaCO₃ nanoparticles for molecular targeting and pH-responsive controlled drug release," *Advances in Polymer Technology*, vol. 2020, 8 pages, 2020.
- [123] C. Xu, W. Liu, Y. Hu, W. Li, and W. Di, "Bioinspired tumor-homing nanopatform for co-delivery of paclitaxel and siRNA-E7 to HPV-related cervical malignancies for synergistic therapy," *Theranostics*, vol. 10, no. 7, pp. 3325–3339, 2020.
- [124] Y. Qin, K. Chen, W. Gu et al., "Small size fullerene nanoparticles suppress lung metastasis of breast cancer cell by disrupting actin dynamics," *Journal of Nanobiotechnology*, vol. 16, no. 1, p. 54, 2018.
- [125] N. Kong, M. Deng, X.-N. Sun, Y.-D. Chen, and X.-B. Sui, "Polydopamine-functionalized CA-(PCL-ran-PLA) nanoparticles for target delivery of docetaxel and chemophotothermal therapy of breast cancer," *Frontiers in Pharmacology*, vol. 9, p. 125, 2018.
- [126] V. Shafiei-Irannejad, N. Samadi, B. Yousefi, R. Salehi, K. Velaei, and N. Zarghami, "Metformin enhances doxorubicin sensitivity via inhibition of doxorubicin efflux in P-gp-overexpressing MCF-7 cells," *Chemical Biology & Drug Design*, vol. 91, no. 1, pp. 269–276, 2018.
- [127] V. Shafiei-Irannejad, N. Samadi, R. Salehi et al., "Reversion of multidrug resistance by co-encapsulation of doxorubicin and metformin in Poly(lactide-co-glycolide)-d- α -tocopheryl polyethylene glycol 1000 succinate nanoparticles," *Pharmaceutical Research*, vol. 35, no. 6, p. 119, 2018.
- [128] Z. Tian, X. Yao, and Y. Zhu, "Simple synthesis of multifunctional zeolitic imidazolate frameworks-8/graphene oxide nanocrystals with controlled drug release and photothermal effect," *Microporous and Mesoporous Materials*, vol. 237, pp. 160–167, 2017.
- [129] W.-H. Chen, X. Yu, W.-C. Liao et al., "Drug delivery: ATP-responsive aptamer-based metal-organic framework nanoparticles (NMOFs) for the controlled release of loads and drugs (Adv. Funct. Mater. 37/2017)," *Advanced Functional Materials*, vol. 27, no. 37, 2017.
- [130] W.-H. Chen, X. Yu, A. Ceconello, Y. S. Sohn, R. Nechushtai, and I. Willner, "Stimuli-responsive nucleic acid-functionalized metal-organic framework nanoparticles using pH- and metal-ion-dependent DNazymes as locks," *Chemical Science*, vol. 8, no. 8, pp. 5769–5780, 2017.
- [131] P. S. O. Ozgen, S. Atasoy, B. Z. Kurt, Z. Durmus, G. Yigit, and A. Dag, "Glycopolymer decorated multiwalled carbon nanotubes for dual targeted breast cancer therapy," *Journal of Materials Chemistry B*, vol. 8, no. 15, pp. 3123–3137, 2020.
- [132] R. Agabeigi, S. H. Rasta, M. Rahmati-Yamchi, R. Salehi, and E. Alizadeh, "Novel chemo-photothermal therapy in breast cancer using methotrexate-loaded folic acid conjugated Au@SiO₂ Nanoparticles," *Nanoscale Research Letters*, vol. 15, p. 62, 2020.
- [133] S.-H. Chen, T.-I. Liu, C.-L. Chuang, H.-H. Chen, W.-H. Chiang, and H.-C. Chiu, "Alendronate/folic acid-decorated polymeric nanoparticles for hierarchically targetable chemotherapy against bone metastatic breast cancer," *Journal of Materials Chemistry B*, vol. 8, no. 17, pp. 3789–3800, 2020.

Research Article

A Combination Therapy of pHRE-Egr1-HSV-TK/Anti-CD133McAb-¹³¹I/MFH Mediated by FePt Nanoparticles for Liver Cancer Stem Cells

Mei Lin ¹, Yanhong Xiao ², Xingmao Jiang,³ Jun Zhang,⁴ Ting Guo ⁵ and Yujuan Shi²

¹Clinical Laboratory, Taizhou People's Hospital Affiliated to Nantong University, Taizhou, Jiangsu 225300, China

²Imaging Department, Taizhou People's Hospital Affiliated to Nantong University, Taizhou, Jiangsu 225300, China

³Hubei Key Lab of Novel Reactor & Green Chemical Technology, Key Laboratory for Green Chemical Process of Ministry of Education, School of Chemical Engineering and Pharmacy, Wuhan Institute of Technology, Wuhan 430205, China

⁴Isotopic Laboratory, Taizhou People's Hospital Affiliated to Nantong University, Taizhou, Jiangsu 225300, China

⁵Institute of Clinical Medicine, Taizhou People's Hospital Affiliated to Nantong University, Taizhou, Jiangsu 225300, China

Correspondence should be addressed to Mei Lin; l_mei@163.com

Received 3 February 2020; Revised 13 April 2020; Accepted 24 April 2020; Published 12 June 2020

Guest Editor: Anuj Kumar

Copyright © 2020 Mei Lin et al. This is an open access article distributed under the Creative Commons Attribution License, which permits unrestricted use, distribution, and reproduction in any medium, provided the original work is properly cited.

It has been evidenced that liver cancer stem cells (LCSCs) are to blame hepatocellular carcinoma (HCC) occurrence, development, metastasis, and recurrence. Using iron-platinum nanoparticles (FePt-NPs) as a carrier and CD133 antigen as a target, a new strategy to targetly kill LCSCs by integrating HSV-TK suicide gene, ¹³¹I nuclide irradiation, and magnetic fluid hyperthermia (MFH) together was designed and investigated in the present study. The results showed that FePt-NPs modified with PEI (PEI-FePt-NPs) could bind with DNA, and the best binding ratio was 1 : 40 (mass ratio). Moreover, DNA binding to PEI-FePt-NPs could refrain from Dnase1 enzyme digestion and could release under certain conditions. LCSCs (CD133⁺ Huh-7 cells) were transfected with pHRE-Egr1-HSV-TK by PEI-FePt-NPs, and the transfection efficiency was 53.65 ± 3.40%. These data showed a good potential of PEI-FePt-NPs as a gene transfer carrier. ¹³¹I was labeled with anti-CD133McAb in order to facilitate therapy targeting. The combined intervention of pHRE-Egr1-HSV-TK/anti-CD133McAb-¹³¹I/MFH mediated by PEI-FePt-NPs could greatly inhibit LCSCs' growth and induce cell apoptosis *in vitro*, significantly higher than any of the individual interventions ($p < 0.05$). This study offers a practicable idea for LCSC treatment, and PEI-FePt-NPs may act as novel nonviral gene vectors and a magnetic induction medium.

1. Introduction

As an extremely malignant tumor, hepatocellular cell carcinoma (HCC) severely endangers human health and life. There were about 800 thousand people that died of HCC all over the world in every past year [1, 2]. In the past decades, much progress has been made in hepatoma diagnosis and treatment, but the overall prognosis of HCC is still not satisfactory and the 5-year survival rate is only 10% or so. It is therefore pivotal to seek an effective strategy for HCC therapy.

In recent years, cancer stem cell (CSC) theory has drawn wide attention from scholars in the whole world [3]. Specifi-

cally, CSCs, accounting for merely 5% of tumor cells, are the root of tumor heterogeneity, with the ability for self-renewal, unlimited proliferation, and multidirectional differentiation potential. Normally, most of them exist in the G0 and hypoxic microenvironment, resistant to radiotherapy and chemotherapy in a way. Moreover, they are mostly to blame for the occurrence, progress, metastasis, and recurrence of tumor. CSCs have been discovered in blood malignant tumors and many solid tumors, such as breast cancer, colorectal cancer, HCC, lung cancer, pancreatic cancer, and multiple myeloma [4–10].

According to CSC theory, it is significant to eliminate liver cancer stem cells (LCSCs), which can be served as one

of the crucial indicators to monitor HCC progress and evaluate curative effect, for HCC treatment and prognosis improvement. Now, LCSCs are mainly isolated by flow cytometry and immune magnetic bead, the principles of which are both based on some specific markers to identify LCSCs. Many molecular markers of LCSCs have been discovered, including ALDH, CD133, CD13, CD90, CD44, CD24, OV6, and EpCAM. CD133, a five-transmembrane single-chain glycoprotein known as prominin-1, was first identified from human hematopoietic stem cells and mouse CD34⁺ neural stem cells in 1997. It has been proved that CD133⁺ HCC cells have the ability for proliferation, differentiation, and self-renewal. Suetsugu et al. [11] isolated CD133⁺ cells from the Huh-7 cell line, which have a stronger ability to proliferate than CD133⁻ Huh-7 cells *in vitro*. Hence, it has become a key research hotspot to integrate various means to specifically kill LCSCs in HCC therapy.

As a green therapy, tumor hyperthermia has shown ideal potential, and the techniques for thermotherapy have been continuously improved in recent years. Jordan et al. [12] developed magnetic fluid hyperthermia (MFH) for cancer treatment by integrating nanotechnology and magnetic induction hyperthermia together and achieved remarkable results. Specifically speaking, after delivery into the tumor area, magnetic fluid (contains magnetic nanoparticles) can warm up to the temperature capable of killing cancer cells by the rearrangement mechanism of the relaxation magnetic vector in an applied magnetic field (AMF). For the surrounding normal tissues, they are not adversely impacted without magnetic materials there, which makes the therapy highly targeted and specific. Furthermore, hyperthermia can not only directly kill tumor cells but also enhance the sensitivity of radiotherapy and chemotherapy.

Radiation-gene therapy is a strategy to combine a therapeutic gene with a radiation-inducible regulatory sequence to form recombinant plasmids. After transfection into tumor cells and administration of radiation, the therapeutic genes are induced to express themselves, resulting in a double kill of the tumor by radiation and the genes. In this regard, this method can relatively lower the equivalent irradiation dose and the damage to normal tissues, by which therapeutic genes can express locally by local irradiation as well. However, two key factors are involved in the desired therapeutic effect, with one being an applicable vector to transfer the therapeutic genes and the other gene expression regulation.

In view of the above background, exploiting CD133 antigen as a target, using PEI-FePt-NPs as a gene transferring carrier and magnetic thermotherapy medium, taking advantage of the solid tumor hypoxic microenvironment, we integrated anti-CD133McAb (anti-CD133 monoclonal antibody) labeled with ¹³¹I, pHRE-Egr1-HSV-TK (suicidal genes driven by hypoxia/radiation double sensitive promoters), and MFH together, complementing their advantages, to kill LCSCs in the present study and obtained encouraging results.

2. Methods

2.1. Main Materials. The main materials are as follows: Huh-7 cell line (human HCC cells) (Shanghai Institute of Cell

Research, Chinese Academy of Sciences), chloroplatinic acid (Chinese medicine), ferric nitrate (Chinese medicine), sodium chloride, (Chinese medicine), trimethylammonium bromide (CTAB) (Chinese medicine), polyethyleneimine (PEI) (Sigma, USA), dimethyl sulfoxide (Beijing Suo Laibao Technology Company), MTT (Sigma, USA), 0.25% trypsin-EDTA (Gibco, USA), DMEM (Gibco, USA), newborn bovine serum (Hangzhou Sijiqing Bioengineering Materials Research Institute), chloramine T (Sinopharm Chemical Reagent Co. Ltd.), Na¹³¹I (Gangwon Hospital), sodium sulfite (Sinopharm Chemical Reagent Co. Ltd.), BSA (Sinopharm Chemical Reagent Co. Ltd.), CD133 monoclonal antibody (ImmunoWay, USA), FcR Blocking Reagent (Miltenyi Biotec, Germany), epidermal growth factor (EGF) (PeproTech, USA), basic fibroblast growth factor (bFGF) (PeproTech Company, USA), insulin (PeproTech, USA), B27 (PeproTech, USA), DMEM/F12 medium (Gibco, USA), DNA marker (Shanghai Shenggong), PCR expansion additive kit (Shanghai Shenggong), Annexin V (Invitrogen), and propidium iodide (PI) (Invitrogen).

2.2. Sorting, Identification, and Culture of CD133⁺ Huh-7 Cells. CD133 expression of Huh-7 cells was detected by flow cytometry. CD133⁺ Huh-7 cells were sorted by flow cytometry and cultured in serum-free DMEM/F12 medium with 40 ng/ml EGF, 20 ng/ml bFGF, 1% B27, 0.4% bovine serum albumin, and 5 mg/ml insulin. The medium was replaced half every 3 days. The clone spheres were checked by a light microscope.

Soft agar cloning experiment process is as follows: (1) CD133⁺ Huh-7 cells were trypsinized into individual cells at 1×10^6 cells/l with DMEM of 20% FBS. (2) Two low-concentration agarose solutions of 1.2% and 0.7% were prepared with dH₂O and placed at 40°C of water bath after autoclaving. (3) 1.2% agarose and 2× DMEM (containing 20% fetal bovine serum and 2 times double antibody) were mixed at 1 : 1 in a dish. After cooling coagulation, the mixture was placed in a CO₂ incubator to be used as bottom agar. (4) 0.7% agarose and 2×DMEM were mixed at 1 : 1, and then, 0.2 ml cell suspension was added. After thoroughly mixing, the mixture was poured into the plate with a 1.2% agarose bottom layer; then, a double-layer agar medium was gradually formed. Placed in a biosafety cabinet after condensation, the cells were cultured in a 37°C, 5% CO₂ incubator for 12 days. (5) The cell clones in the plate were observed by an inverted microscope.

2.3. FePt-NP Synthesis, Modification, and Characterization. FePt-NPs were synthesized by reverse microemulsion method as follows. 0.087 g Fe(NO₃)₃·9H₂O, 0.1 g NaCl, and 5 ml H₂PtCl₆·6H₂O (0.02 g/ml) were dissolved in a conical flask, and 0.73 g CTAB and 90 ml benzene were added. Then, the mixture was mixed on a magnetic stirrer at 70°C for 6 h and then continued to be magnetically mixed at 90°C for 3 h. Subsequently, the water was removed, and the remainder mixture was dried and calcined in an air atmosphere for 5 h, then reduced in an H₂ atmosphere for 10 h. After washed with water to remove redundant NaCl and dried, FePt-NPs were obtained.

Some FePt-NPs were dissolved in deionized water to prepare 4% magnetic fluid, by ultrasonical dispersion. After

high-speed centrifugation, the supernatant was removed. The precipitate was resuspended in PBS and ultrasonically dispersed. Then, some PEI was slowly added to the mixture. The mass ratio of PEI to FePt-NPs is 1 : 5. After fully mixing and shaking for 24 h at room temperature, the nanoparticles were isolated by magnetic separation and washed repeatedly with distilled water and methanol, and then dried in vacuum to obtain FePt-NPs modified with PEI (PEI-FePt-NPs).

Some FePt-NPs were taken and dispersed in absolute ethanol for 15 min, respectively, then dropped to a copper mesh and observed under a transmission electron microscope (TEM, JEM-2100 (HR)). The morphology, size, and dispersion of FePt-NPs were checked and photographed, and then, a bar was marked in view of magnification in each picture. We counted 100 nanoparticles and calculated their size according to the bar, then figured out the mean and standard deviation (SD), applying mean \pm SD.

X-ray diffraction (XRD) of FePt-NPs was detected in the condition of Cu targeting $K\alpha$ ($\lambda = 0.154$ nm), 30 mA tube flow, and 40 kV tube pressure.

The magnetic fluids of FePt-NPs and PEI-FePt-NPs were prepared, respectively, and were placed at 4°C for one week to observe colloidal stability.

To detect magnetothermal effect, 0.25, 1.0, 1.5, and 2.0 g/l FePt-NP and PEI-FePt-NP magnetic fluids were prepared with 0.9% NaCl, respectively. Then, 5 ml of each magnetic fluid was put into a 25 cm² flat-bottomed test tube, respectively, and heated on the plate coil of high-frequency magnetic induction heating (SPG-10A-II) with 215 kHz frequency and 35 A output current at room temperature for 1 h. The test tube bottom was away about 0.5 cm from the heating coil center. The temperature was recorded every 5 min. Taking time as the abscissa and temperature as the ordinate, temperature rising curves of FePt-NP and PEI-FePt-NP magnetic fluids with different concentrations were drawn.

With 215 kHz and output currents 25 A, 30 A, 35 A, 40 A, 5 ml of 1.0 g/l FePt-NPs and PEI-FePt-NPs was heated for 1 h at room temperature as the above, respectively. Every five minutes, the temperature was recorded. Taking time as the abscissa and temperature as the ordinate, temperature rising curves of FePt-NP and PEI-FePt-NP magnetic fluids at different magnetic intensities were drawn.

2.4. Construction and Identification of Eukaryotic Expression Plasmids pHRE-Egr1-HSV-TK. Eukaryotic expression plasmids pCDNA3.1-pHRE-Egr1-HSV-TK (pHRE-Egr1-HSV-TK) were designed and constructed as References [13–17]. pHRE-Egr1-HSV-TK were digested by BglII+XhoI and then subjected to 1% agarose gel electrophoresis. The electrophoresis band was observed by a UV lamp. In addition, a 5HRE-Egr1 fragment in pCDNA3.1-5HRE-Egr1-HSV-TK was sequenced and then aligned with a 5HRE-Egr1 template sequence to further examine whether the plasmids were correctly constructed.

2.5. The Investigation of the Potential of PEI-FePt-NPs Used for Gene Transfer Carrier. Using pHRE-Egr1-EGFP constructed according to References [13–17] as a model, the potential of PEI-FePt-NPs used for gene transfer carrier was investigated.

2.5.1. Experiment of DNA Binding to PEI-FePt-NPs. PEI-FePt-NPs and pHRE-Egr1-EGFP were mixed at a mass ratio of 0 : 1, 5 : 1, 10 : 1, 20 : 1, 40 : 1, and 80 : 1, respectively, and the final concentration of plasmids was 20 ng/ μ l, then supplemented to 20 μ l of total volume with ultrapure water, and placed at room temperature for 30 min to form a complex. 5 μ l of each complex was taken for agarose gel electrophoresis (100 ng/lane) to detect the binding of DNA to a magnetic nanoparticle. And then, the most suitable ratio of pHRE-Egr1-EGFP binding to FePt-NPs was screened out.

2.5.2. The Experiment of Protection DNA from DNaseI Digestion by PEI-FePt-NPs. The complex of pHRE-Egr1-EGFP and PEI-FePt-NPs (1 : 40 of mass ratio) was mixed in Tango Buffer (Thermo) and DNaseI enzyme. After digestion for 1 min, 10 min, 30 min, 45 min, and 1 h at 37°C of water bath, the reaction was terminated by an equal volume of 0.5 mol/l EDTA solution, and DNaseI was further inactivated by a 55°C water bath. Then, pHRE-Egr1-EGFP binding to PEI-FePt-NPs was eluted with SDS, extracted with phenol and chloroform, precipitated with absolute ethanol, washed with 75% ethanol, and dissolved in equal double distilled water. Finally, agarose gel electrophoresis was performed to observe the ability of the complex to resist DNA enzymatic hydrolysis, and naked pHRE-Egr1-EGFP was used as a control.

2.5.3. The Examination of DNA Release from the Complex PEI-FePt-NPs/DNA. The total volume of the complex (mass ratio of pHRE-Egr1-EGFP and PEI-FePt-NPs was 1 : 40) was supplemented to 500 μ l with TE solution for 10 μ g plasmids, then shaken with 200 rpm at 37°C. An equal sample was taken out at hour 1, hour 4, hour 8, hour 12, day 1, day 2, day 3, and day 4, respectively, and subjected to agarose gel electrophoresis to observe DNA release from the complex.

2.5.4. The Detection of PEI-FePt-NP Gene Transfection Efficiency. pHRE-Egr1-EGFP was transferred into CD133⁺ Huh-7 cells by PEI-FePt-NPs, and the transfection efficiency was tested and compared with the lipofection method. In detail, PEI-FePt-NPs and pHRE-Egr1-EGFP were diluted with serum-free medium at a mass ratio of 40 : 1 (according to the results of Section 2.5.1), respectively. 5 min later, the two were mixed and incubated for 30 min to obtain the pHRE-Egr1-EGFP/PEI-FePt-NP complex. The logarithmic growth phase CD133⁺ Huh-7 cells were seeded in 6-well plates (5 \times 10⁵ cells/well) and cultured in 5% CO₂ at 37°C for about 18 h. Then, the original culture solution was discarded, and the cells were washed three times with sterile PBS and serum-free medium 2 times, respectively; then, serum-free medium containing pHRE-Egr1-EGFP/PEI-FePt-NPs complex (3 μ g pHRE-Egr1-EGFP per well) were added to the corresponding wells. 5 h incubation later, the whole medium was replaced with serum-free. After the cells were routinely cultivated for 2 days, the transfection efficiency was detected by flow cytometry. As the control, pHRE-Egr1-EGFP was transfected into CD133⁺ Huh-7 cells by liposome.

2.6. The Intervention of LCSCs by pHRE-Egr1-HSV-TK/Anti-CD133McAb-¹³¹I/MFH In Vitro. ¹³¹I-anti-CD133McAb were prepared, purified, and identified as Reference [16]. CD133⁺ Huh-7 cells were transfected with pHRE-Egr1-HSV-TK by PEI-FePt-NPs as the above, and then incubated in 5% CO₂ at 37°C. Two days later, the transfected cells were diluted into 3 × 10⁵/ml single cell suspension and seeded in 5 culture flasks (3 ml/flask). The grouping was as follows: (1) negative control group (untransfected), (2) ¹³¹I-antiCD133McAb group (untransfected, radioimmunotherapy group), (3) magnetic hyperthermia group (untransfected, MFH group), (4) pHRE-Egr1-HSV-TK/GCV/¹³¹I/anti-CD133McAb group (pHRE-Egr1-HSV-TK/¹³¹I-anti-CD133McAb group), and (5) pHRE-Egr1-HSV-TK/GCV/¹³¹I/anti-CD133McAb/MFH group (pHRE-Egr1-HSV-TK/¹³¹I-anti-CD133McAb/MFH group). DMEM, ¹³¹I-anti-CD133McAb (ultimate concentration: 50 μCi), and GCV (ultimate concentration: 5 μg/ml) were added to the corresponding group. After incubation for 24 h, PEI-FePt-NPs (ultimate concentration: 1 g/l) were added to the MFH group and pHRE-Egr1-HSV-TK/¹³¹I-anti-CD133McAb/MFH group. The groups involved in MFH were placed on a flat coil of high-frequency magnetic induction heater (SPG-10A-II) with 215 kHz, 2.4 kW, and output current of 35 A for 1 h. The pHRE-Egr1-HSV-TK/¹³¹I-anti-CD133McAb and pHRE-Egr1-HSV-TK/¹³¹I-anti-CD133McAb/MFH groups were cultured in a hypoxic environment at 37°C for 2 days, and the other groups were cultured in 5% CO₂ at 37°C for 2 days.

2.6.1. The Examination of the Cell Proliferation Inhibitory Rate of Each Group. Some cells of each group were taken out to prepare single cell suspension, respectively, and then seeded in 96-well plates (200 μl/well), and 5 replicate wells were set in each group. After incubation for 24 h, each well was added with 20 μl MTT, and then continued to incubate. 4 h later, the medium in each well was discarded, and then, DMSO was added (150 μl/well). After shaking for 10 min, OD values at 493 nm were examined by a microplate reader. Cell proliferation inhibitory rate = $(1 - (\text{OD of experimental group} - \text{OD of blank control group}) / (\text{OD of negative control group} - \text{OD of blank control group})) \times 100\%$.

2.6.2. The Detection of Cell Apoptosis of Each Group. The remaining cells of each group above were collected and washed with cold PBS 3 times. After centrifugation, the supernatant was discarded, and the cells were suspended in an annexin-binding buffer. Then, Annexin V and PI were added, respectively. After reaction at room temperature in dark for 15 min, the annexin-binding buffer was added, and the cell apoptosis rate of each group was analyzed by flow cytometry within 1 h.

2.7. The Analysis of VEGF and CD44 Protein Expression. After treatment for 24 h as Section 2.6, LCSCs were collected, and then, VEGF and CD44 protein of each group were detected by western blot, respectively.

2.8. Statistical Analysis. All data used in the experiments were expressed as mean ± SD. Statistical analysis was performed using SPSS 20.0 software. One-way analysis of variance was

used. ANOVA or *t* test was used for comparison. *p* < 0.05 was considered statistically significant.

3. Results

3.1. Sorting, Identification, and Culture of CD133⁺ Huh-7 Cells. Flow cytometry analysis showed that the CD133 expression rate of Huh-7 cells was 9.61% (Figure 1(a)), and then, CD133⁺ Huh-7 cells were sorted by flow cytometry and seeded in serum-free DMEM/F12 medium with cell growth factors. Six days later, a few small cell spheres appeared in the medium (Figure 1(b)). On the 13th day, many big cell spheres were suspended in the medium (Figures 1(c)–1(e)). Figure 1(d) is a cluster of CD133⁺ Huh-7 cells in an unstained bright field, and Figure 1(e) shows the clusters of CD133⁺ Huh-7 cells cloned with soft agar. These data indicate that the sorted liver cancer CD133⁺ Huh-7 cells have a strong clonality.

3.2. Characterization of FePt-NPs. Figure 2(a) is an XRD pattern of the prepared FePt-NPs, with sharp diffraction peaks. The interplanar spacing (*d* value) corresponding to each diffraction peak corresponded to the Powder Diffraction Standards Association Card (JCPDS: 43-1359), indicating FePt-NPs prepared were in crystalline state. TEM examination showed that FePt-NPs were about 3 ± 1 nm in size, with good dispersion (Figure 2(b)).

The magnetic fluid of FePt-NPs and PEI-FePt-NPs was placed at 4°C, respectively. 24 h later, the FePt-NP magnetic fluid showed a clear sedimentation layer with clear boundary. The upper layer was colorless and translucent, and the lower layer was black. By comparison, the PEI-FePt-NP magnetic fluid showed mild sedimentation after one week and homogeneously dispersed again after shaking. This indicates that PEI modification improved the suspension stability of FePt-NPs.

3.3. Magnetothermal Effect of FePt-NPs and PEI-FePt-NPs. Figure 3 shows the magnetothermal effects of FePt-NPs and PEI-FePt-NPs at different concentrations and different magnetic field intensities. When magnetic field intensity was constant, the temperature of four concentrated magnetic fluids increased with time. The larger the magnetic fluid concentration, the stronger the heating ability (Figures 3(a) and 3(b)). When the concentration of the magnetic fluid was constant, the temperature of the magnetic fluid increased under the four magnetic field strengths with time. The higher the magnetic field strength, the stronger the temperature rising ability (Figures 3(c) and 3(d)). Either the same concentration or the same magnetic field intensity, the magnetic fluid of FePt-NPs and PEI-FePt-NPs both warmed up fast within the first 20 minutes and then slowly remained at a certain temperature range. The results suggested that FePt-NPs and PEI-FePt-NPs had good heating performance in AMF and may be used for magnetic fluid hyperthermia.

3.4. Identification of Eukaryotic Expression Plasmids pHRE-Egr1-HSV-TK

3.4.1. Enzyme Digestion Identification. pEgr1-HSV-TK and pHRE-Egr1p-HSV-TK were identified by restriction enzyme

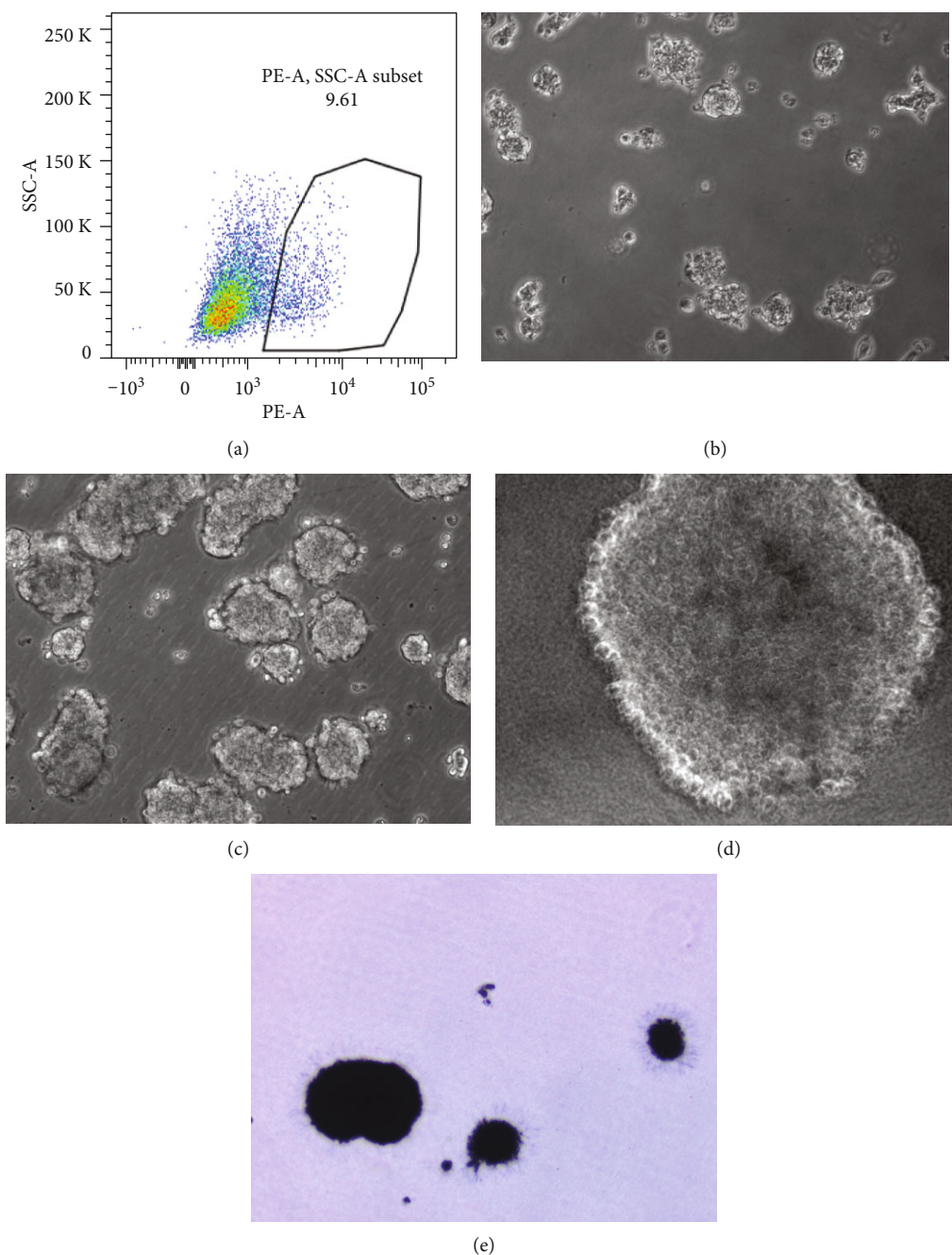


FIGURE 1: Identification and cloned spheres of CD133⁺ Huh-7 cells. (a) 9.61% CD133 expression rate of Huh-7 cells tested by flow cytometry. (b) Cloned spheres of CD133⁺ Huh-7 cells cultured for 6 days. (c) Cloned spheres of CD133⁺ Huh-7 cells cultured for 13 days. (d) CD133⁺ Huh-7 cell cluster photographed in an unstained bright field. (e) CD133⁺ Huh-7 cell clusters photographed after cloning with soft agar.

digestion, respectively. As shown in Figure 4(a), there was a small band of about 2500 bp and a large band of about 4500 bp after pEgr1-HSV-TK was digested. By comparison, there was a small band of about 400 bp between 250 bp and 500 bp bands after pHRE-Egr1-HSV-TK was digested (Figure 4(b)). It was indicated that the 5HRE fragment was successfully inserted into pEgr1-HSV-TK.

3.4.2. Sequencing Identification. Figure 4(c) is a sequencing map of pHRE-Egr1-HSV-TK. Compared with the canonical

sequence of 5HRE-Egr1p, the sequence examined of pHRE-Egr1-HSV-TK was completely correct, indicating that the 5HRE-Egr1p fragment was successfully inserted, and pHRE-Egr1-HSV-TK was successfully constructed.

3.5. Gene Transfection Using PEI-FePt-NPs Used as a Carrier *In Vitro*

3.5.1. Experiment of DNA Binding to PEI-FePt-NPs. Figure 5(a) is an agarose gel electrophoresis map of DNA

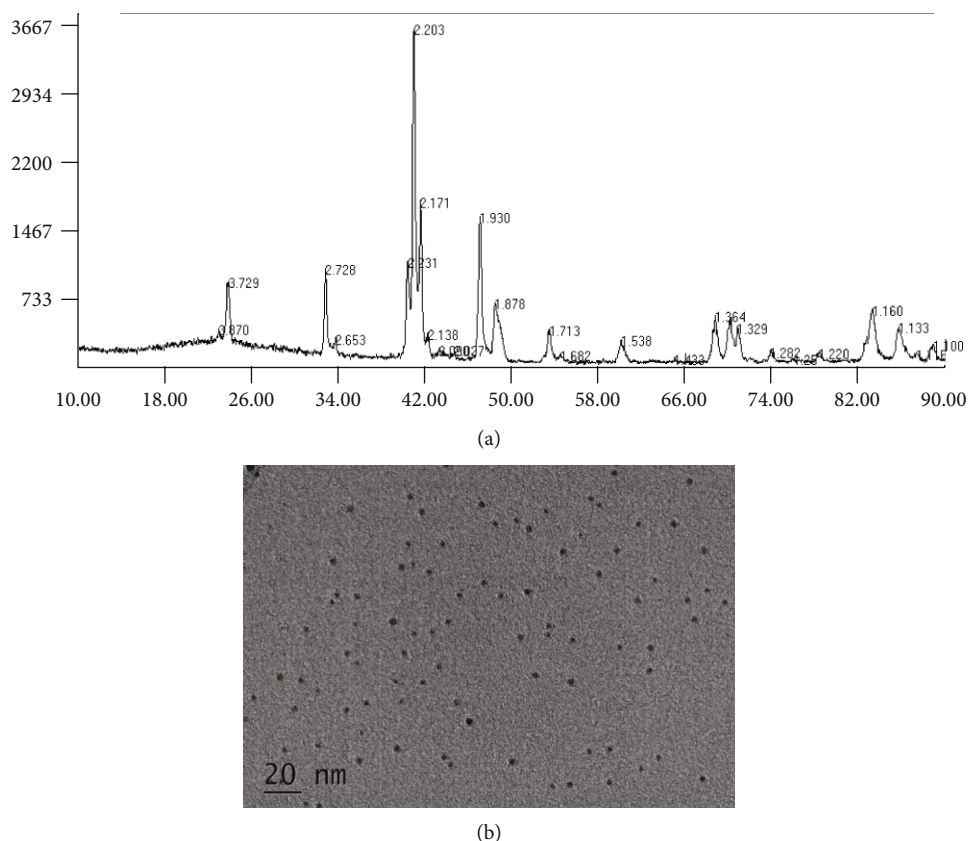


FIGURE 2: Characterization of iron-platinum nanoparticles. (a) XRD pattern of FePt-NPs. (b) TEM of FePt-NPs.

binding to PEI-FePt-NPs. It can be seen that when the mass ratio of pHRE-Egr1-HSV-TK and PEI-FePt-NPs was 1:40, all plasmids could bind to PEI-FePt-NPs. 1:40 (mass ratio) was thus considered the optimum ratio of DNA and PEI-FePt-NPs to bind.

3.5.2. DNA Protection from DNase1 Digestion by PEI-FePt-NPs. Figure 5(b) is an experimental electrophoresis of DNase1 digestion protection of PEI-FePt-NPs/DNA. It can be seen that PEI-FePt-NPs/pHRE-Egr1-HSV-TK remained stable after DNase1 digestion within 60 minutes, whereas the naked plasmids were almost completely digested at 1 min, with no bands observed, indicating that PEI-FePt-NPs could effectively protect the plasmids from DNase1 digestion.

3.5.3. DNA Release from PEI-FePt-NPs/DNA Complex. Figure 5(c) is an experimental gel electrophoresis of DNA release from the PEI-FePt-NPs/pHRE-Egr1-HSV-TK complex. Within 3 days, released DNA gradually increased, and there was almost no difference after the fourth day and the fifth day, indicating that DNA could effectively release from the complex (PEI-FePt-NPs/pHRE-Egr1-HSV-TK) in appropriate conditions.

3.5.4. PEI-FePt-NP Gene Transfection Efficiency. pHRE-Egr1-EGFP were transfected into CD133⁺ Huh-7 cells by PEI-FePt-NPs, and the transfection efficiency was $53.65 \pm 3.40\%$, signif-

icantly higher than $38.76 \pm 4.50\%$ transfection by lipofection, a common transfection reagent ($p < 0.05$), indicating that PEI-FePt-NPs can be served as vectors for gene transfer (Table 1).

3.6. Radioactivity Detection of ¹³¹I-Anti-CD133McAb. ¹³¹I was labeled to anti-CD133McAb, and the crude product of anti-CD133McAb labeled with ¹³¹I was purified by PD10 column to remove free ¹³¹I. Figure 6(a) is a TLC quality control chart of pure ¹³¹I-anti-CD133McAb, and Table 2 is quality control peak area % report form of pure ¹³¹I-CD133McAb TLC. The radiochemical purity of anti-CD133McAb labeled with ¹³¹I was 100%, and the labeling rate was 36%.

After being placed at room temperature for 6 h, the radiochemical purity of ¹³¹I-anti-CD133McAb was still 100% by TLC (Figure 6(b) and Table 3), indicating that ¹³¹I-anti-CD133McAb prepared had good radiation stability.

3.7. Liver Cancer Stem Cells Were Intervened by pHRE-Egr1-HSV-TK/¹³¹I-Anti-CD133McAb/MFH In Vitro

3.7.1. Cell Proliferation Inhibition and Apoptosis. Cell proliferation inhibition was tested by MTT, and cell apoptosis was examined by flow cytometry. As shown in Table 4 and Figure 7(a), PEI-FePt-NP-mediated radiation-gene therapy combined with magnetic fluid hyperthermia greatly inhibited LCSC proliferation and induced cell apoptosis. The cell

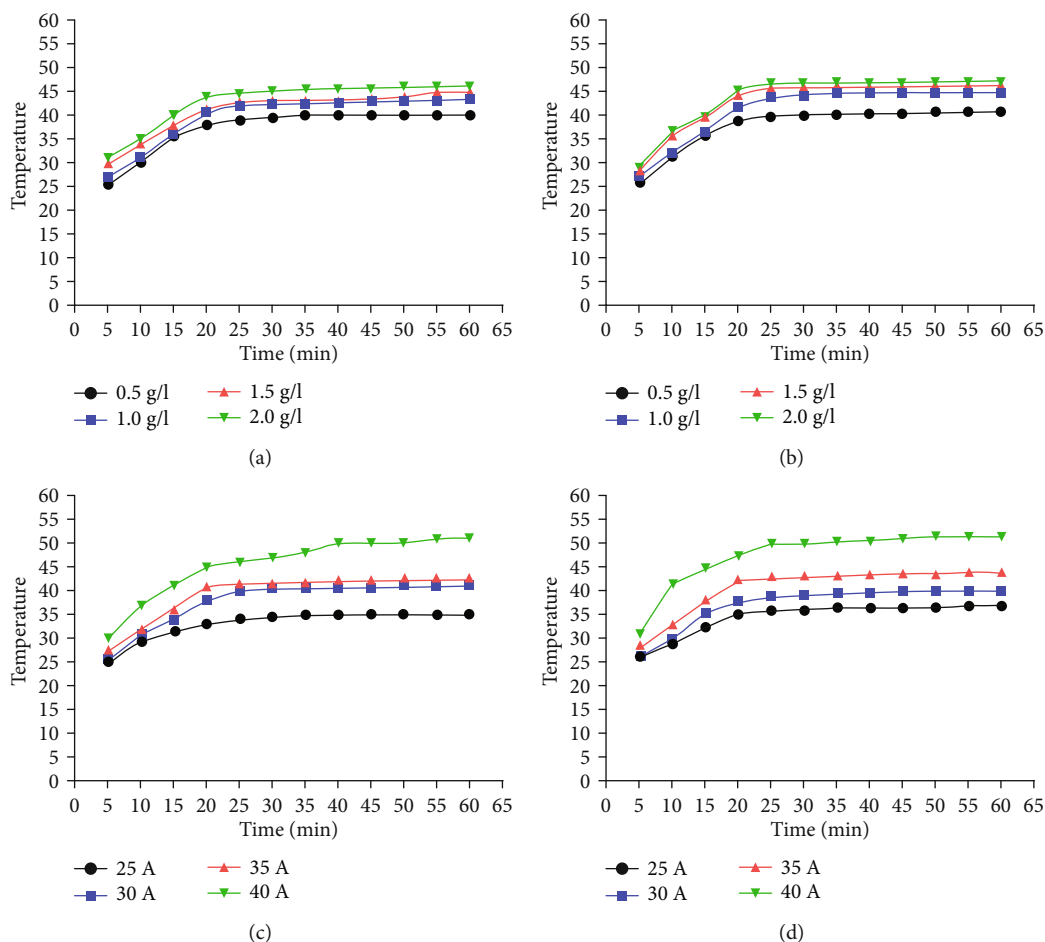


FIGURE 3: *In vitro* magnetic induction heating curves of FePt-NPs and PEI-FePt-NPs. (a) Magnetic induction heating curves of FePt-NPs with different concentrations. (b) Magnetic induction heating curves of PEI-FePt-NPs with different concentrations. (c) Magnetic induction heating curves of FePt-NPs under different magnetic field strengths. (d) Magnetic induction heating curves of PEI-FePt-NPs under different magnetic field strengths.

proliferation inhibition rate and apoptosis rate of the pHRE-Egr1-HSV-TK/ ^{131}I -anti-CD133McAb/MFH group was up to 63% and 49.22%, respectively, both significantly higher than those of any other groups ($p < 0.05$).

3.7.2. Expression of VEGF and CD44 Proteins. Figure 7(b) shows VEGF and CD44 protein expression in LCSCs by western blot. VEGF and CD44 proteins of the pHRE-Egr1-HSV-TK/ ^{131}I -anti-CD133McAb/MFH group both clearly decreased. Figure 7(c) displays the protein expression levels of VEGF and CD44 based on the β -actin gray value. Compared with the negative control group and all the other experimental groups, the expression levels of VEGF and CD44 proteins of the pHRE-Egr1-HSV-TK/ ^{131}I -anti-CD133McAb/MFH group were both reduced, and there was a statistically significant difference ($p < 0.001$). These data suggest that the combination of targeted radiation-gene therapy and magnetic fluid hyperthermia mediated by PEI-FePt-NPs significantly inhibited VEGF and CD44 protein expression in LCSCs.

4. Discussion

4.1. Preparation, Modification, and Characterization of FePt-NPs. Owing to the magnetic property at the nanometer scale, magnetic nanoparticles have been widely used in many fields, without the exception of the medical field, including magnetic resonance imaging systems, biological separation, immunoassays, and magnetic hyperthermia. They can be primarily classified into metals, metal oxides, and metal alloys. Among them, nanoiron oxides have been extensively exploited in tumor thermotherapy and imaging diagnosis because of their handy synthesis and good biocompatibility. As for metal alloy FePt-NPs, it has a strong magnetic property, excellent oxidation resistance [18], small superparamagnetic critical dimension, high magnetic energy level, high Curie temperature, and eximious biocompatibility [19–22], showing a promising application potential in the biomedicine field. Nowadays, chiefly prepared by mechanical condensation method [23], vacuum deposition method [24], magnetron sputtering method [25, 26], and some chemical methods, FePt-NPs were synthesized in this study by the

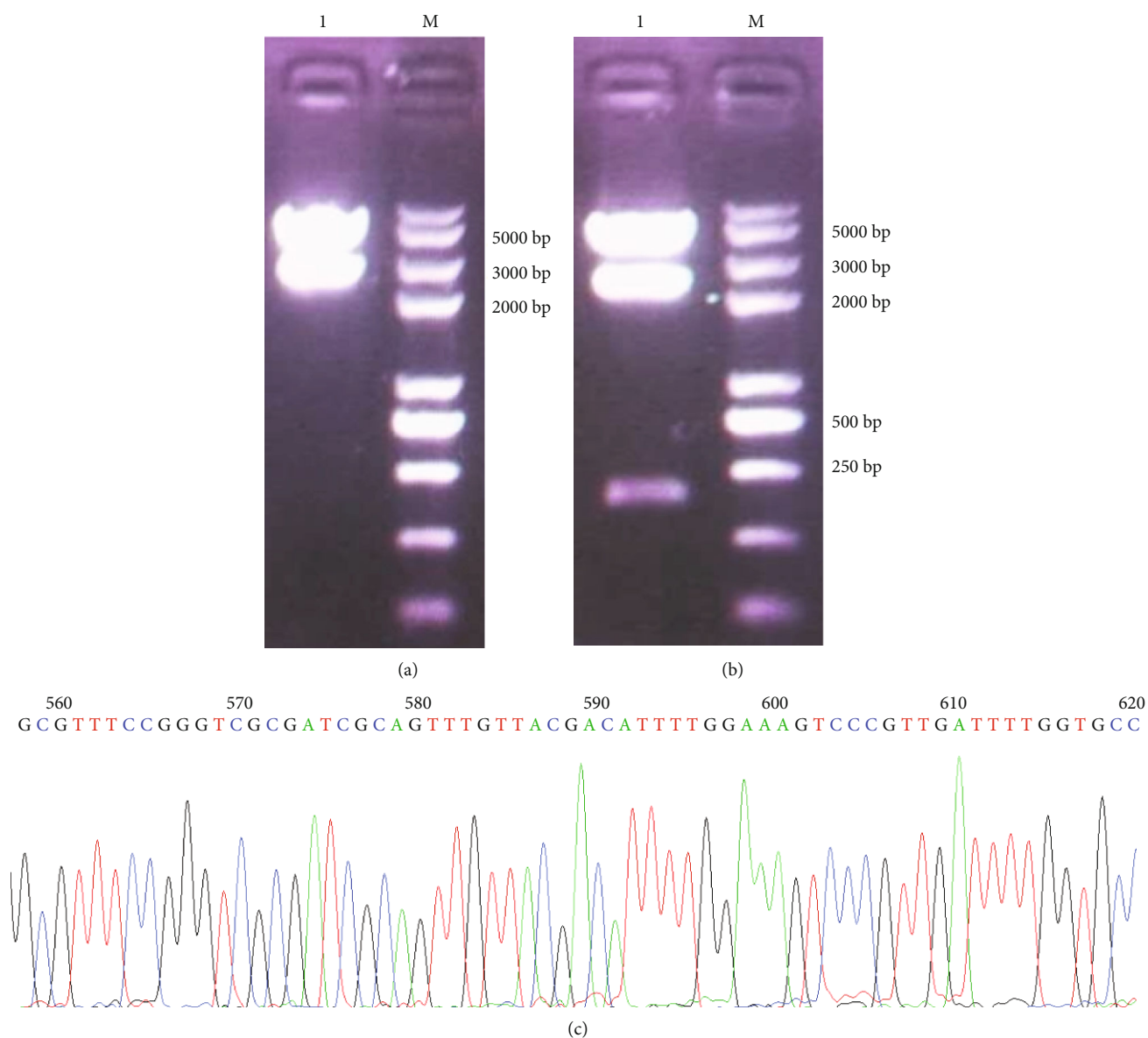


FIGURE 4: Identification of eukaryotic expression plasmids pHRE-Egr1-HSV-TK. (a) Enzyme identification map of pEgr1-HSV-TK (lane 1: pEgr1-HSV-TK digested with BglII+XhoI; lane M: marker). (b) Enzyme identification map of pHRE-Egr1-HSV-TK (lane 1: pHRE-Egr1-HSV-TK digested with BglII+XhoI; lane M: marker). (c) Sequencing map of pHRE-Egr1p-HSV-TK.

inverse microemulsion method in combination with the azeotropic distillation device (Organic benzene was used as the continuous phase. The iron precursor, the iron nitrate platinum precursor, chloroplatinic acid, and sodium chloride aqueous solution were exploited as the dispersed phase, and cetyltrimethylammonium bromide was added as the surfactant). After removing the redundant water by distillation, we removed the free surfactant at high temperature. Finally, hydrogen reduction was adopted to get FePt-NPs. TEM detected that the FePt-NPs were about 3.0 nm in diameter, uniform in size with good dispersion, meeting the requirements for particle size in the biomedical field. Meanwhile, the crystalline FePt-NPs were confirmed by X-ray diffraction analysis [27].

Polyethylenimine (PEI) is a commonly used cationic surfactant. Owing to the strong ability to bind DNA and adhere to cells, PEI can be used as the surface modifier for many substances to increase their biocompatibility, dispersibility, and chemical stability, which is thus applied to the biological science field [28]. The principle is that PEI can effectively diminish the surface potential energy of the nanoparticles by electrostatic repulsion, or establish a material barrier near the particles to prevent them from getting close to each other to stabilize the system, thereby improving the particles' dispersibility and biocompatibility [29–31]. In the current study, FePt-NPs were modified by PEI and the results showed good suspension stability of PEI-FePt-NPs.

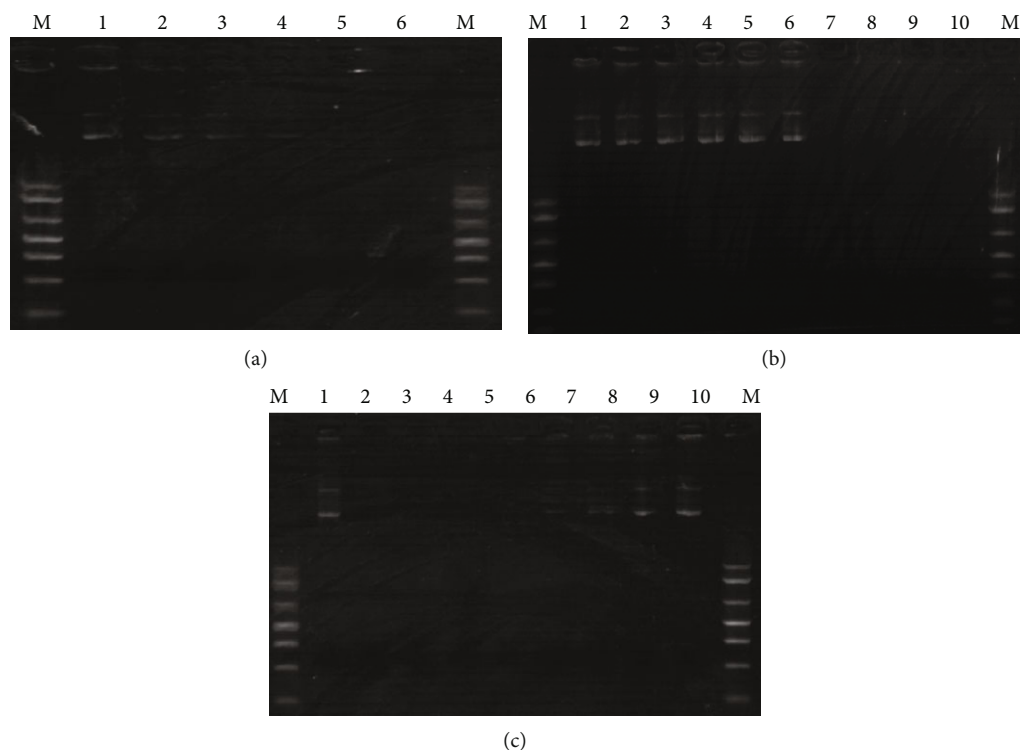


FIGURE 5: The potential investigation of PEI-FePt-NPs used as a carrier for gene transfection. (a) Electrophoresis of pHRE-Egr1-HSV-TK binding to PEI-FePt-NP (lane 1, 1 : 0 (100 ng plasmid DNA, no magnetic nanoparticles); lane 2, 1 : 5; lane 3, 1 : 10; lane 4, 1 : 20; lane 5, 1 : 40; lane 6, 1 : 80; and lane M: DNA marker (standard band from top to bottom is 2000 bp, 1500 bp, 1000 bp, 700 bp, 500 bp, 300 bp, and 100 bp)). (b) Electrophoresis map of DNaseI digestion protection of PEI-FePt-NPs/DNA (lane 1: 100 ng of nude pHRE-Egr1-HSV-TK; lane 2: complex digested for 1 min; lane 3: complex digested for 10 min; lane 4: complex digested for 30 min; lane 5: complex digested for 45 min; lane 6: complex digested for 1 h; lane 7: naked pHRE-Egr1-HSV-TK digested for 1 min; lane 8: naked pHRE-Egr1-HSV-TK digested for 10 min; lane 9: naked pHRE-Egr1-HSV-TK digested for 30 min; lane 10: naked pHRE-Egr1-HSV-TK digested for 45 min; and lane M: DNA marker (2000 bp, 1500 bp, 1000 bp, 700 bp, 500 bp, 300 bp, and 100 bp from top to bottom)). (c) Electrophoresis map of DNA release from PEI-FePt-NPs/pHRE-Egr1-HSV-TK (lane 1: 100 ng pHRE-Egr1-HSV-TK; lane 2: 1 h; lane 3: 4 h; lane 4: 8 h; lane 5: 12 h; lane 6: 1 d; lane 7: 2 d; lane 8: 3 d; lane 9: 4 d; lane 10: 5 d; and lane M: DNA marker (2000 bp, 1500 bp, 1000 bp, 700 bp, 500 bp, 300 bp, and 100 bp from top to bottom)).

TABLE 1: Transfection efficiency of CD133⁺ Huh-7 cells *in vitro*.

Group	Transfection efficiency (%)
PEI-FePt-NPs transfection	53.65 ± 3.40
Liposome transfection	38.76 ± 4.50

The PEI-FePt-NP group compared with liposome group, $p < 0.05$.

Under the action of AMF, ferromagnetic materials have thermogenesis because of postmagnetic effects, domain enthalpy resonance, hysteresis effect, and natural resonance. Magnetic fluid hyperthermia can control temperature within a desired range. In this study, FePt-NPs and PEI-FePt-NPs prepared by the reverse microemulsion method both had ideal magnetothermal effect in AMF. When the magnetic field strength was constant, the higher is the magnetic fluid concentration and the stronger is the heating ability. If the magnetic fluid concentration is invariable, the higher magnetic field strength indicates a stronger heating capacity. It is worth noting that the temperature rose fast in the first 20 minutes, and then slowly maintained at a certain level. In

terms of 1 g/l FePt-NP and 1 g/l PEI-FePt-NP magnetic fluids, the temperature was maintained at 43°C or so, which was a desired temperature for tumor thermotherapy. The reason lies in that tumor cells are subjected to be damaged when the temperature is maintained at 39-45°C, with few or no damage to the surrounding normal cells and tissues. This data suggest that PEI-FePt-NPs may be used for magnetic fluid hyperthermia.

4.2. Construction of pHRE-Egr1-HSV-TK Eukaryotic Expression Plasmids. As a remedy by transferring the exogenous gene into target cells and using the expression products of the exogenous gene to treat disease, gene therapy can treat cancer by inducing tumor cells' apoptosis, activating body immune system and inhibiting tumor angiogenesis. With the rapid progress of molecular biology and genetic engineering technology, gene therapy for HCC has undergone fast growth. The gene therapies for HCC principally encompass suicide gene therapy, antisense gene therapy, tumor suppressor gene therapy, immune gene therapy, antineovascularization therapy, combined gene therapy, resistant gene therapy, and RNA interference. HSV-TK, a widely used suicide gene,

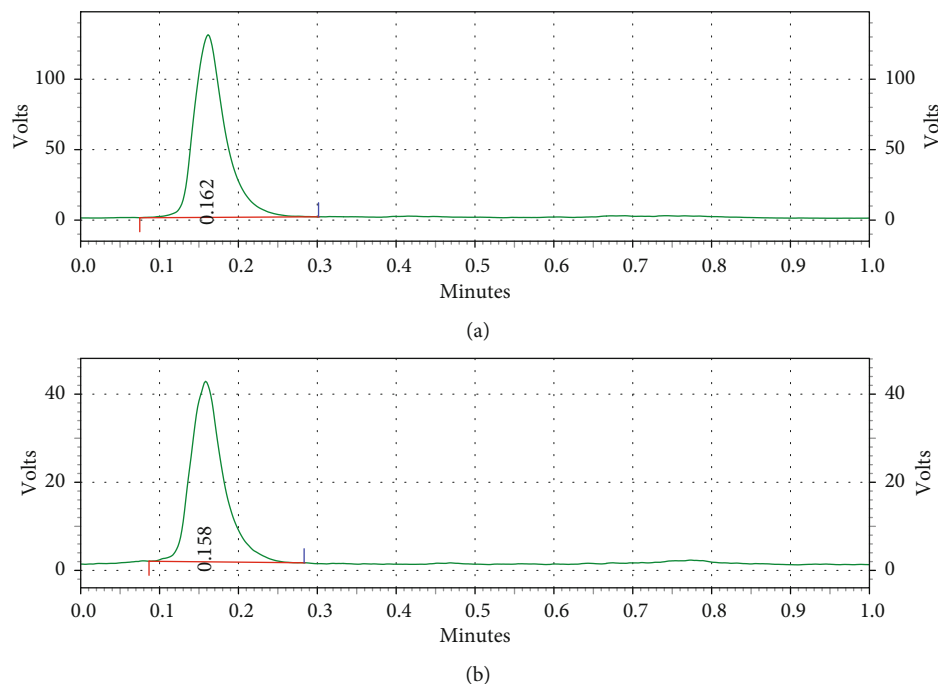


FIGURE 6: TLC quality control chart of ^{131}I labeled with anti-CD133McAb. (a). TLC quality control chart of ^{131}I -CD133McAb pure product. (b) TLC quality control chart after ^{131}I -anti-CD133McAb product was placed at room temperature for 6 h.

TABLE 2: ^{131}I -CD133 pure TLC quality control peak area % report form.

Retention time	Area	Area percentage (%)	Peak height	Percentage of height (%)
0.162	355656	100.000	129692	100.000
Total	355656	100.000	129692	100.000

TABLE 3: TCL control peak area % after ^{131}I -anti-CD133 placed at room temperature for 6 h.

Retention time	Area	Area percentage (%)	Peak height	Percentage of height (%)
0.158	117013	100.000	40969	100.000
Total	117013	100.000	40969	100.000

comes from herpes simplex virus and encodes thymidine kinase. The product HSV-TK expressed can concentrate in the tumor area to convert prodrug GCV into cytotoxic drug to selectively kill the tumor, thus reducing side effects [13]. But it is of extreme importance to select an appropriate regulatory sequence and activating mode to generate exact and efficient expression of the therapeutic gene. Egr-1 (early growth response gene 1, a radiation-inducing gene) promoter has some conserved domains that can feel physico-chemical stimulation inside and outside to induce the corresponding gene to express itself, which has a good application prospect in gene therapy [32, 33]. When Egr-1 promoter is ligated into the upstream of cDNA, it can regulate the related gene expression in time and space by radiation

[15]. As an anoxic sensitivity enhancer, HRE can mediate hypoxia and specifically bind up with the Egr-1 promoter to induce the downstream gene expression [14, 17]. We constructed pHRE-Egr1-HSV-TK, and the plasmids were confirmed correct by restriction enzyme digestion and sequencing in this study.

4.3. *PEI-FePt-NPs Were Used as a Vector for Gene Transfection.* The applicable gene delivery vector is another key to obtain the desired therapeutic effect. Although transfection efficiency of the viral vector system is high, its clinical application is strictly limited in consideration of security risks. While the nonviral vector system can avoid potential risks, its low transfection efficiency makes it difficult to obtain meaningful gene expression. Thus, how to break through the bottleneck of gene transfer has become a top priority in the gene therapy research field. With good potential in gene therapy, nanogene delivery is to encapsulate therapeutic genes, such as DNA and RNA, onto nanoparticles, which will then enter cells under the action of cell uptake to release the therapeutic molecules. If coupled with specific biomolecules, such as antibody, ligand, or aptamer, nanocarrier delivery is conducive to achieve targeted gene treatment for cancer and other diseases. Compared with traditional vectors, nanocarriers have many edges, including no immunogenicity, genotoxicity, and cytotoxicity, allowing genes to release slowly, improving transfection efficiency and bioavailability of transfection products, and obtaining long-term stable expression of transgenes [34–36]. It not only integrates the strength of viral vectors and conventional nonviral vectors but also averts the defects of both, thus having turned into a new carrier system with great application prospects. Currently, a variety of nanogene transfer vectors are being

TABLE 4: Results of MTT experiments after different methods of treatment.

Group	OD value	Proliferation inhibition rate (%)
Negative control group	1.322 ± 0.028	
¹³¹ I-anti-CD133McAb group	0.991 ± 0.019 ^{ab}	25
MFH group	0.945 ± 0.046 ^{ab}	29
pHRE-Egr1-HSV-TK/ ¹³¹ I-anti-CD133McAb group	0.795 ± 0.037 ^{ab}	40
pHRE-Egr1-HSV-TK/ ¹³¹ I-anti-CD133McAb/MFH group	0.488 ± 0.051 ^a	63

^a Compared with the control group, $p < 0.05$; ^b compared with the combination treatment group, $p < 0.05$.

developed. As a sort of inorganic nonviral carrier [37, 38], magnetic nanocarriers are handy to prepare and surface modify, with good biocompatibility and no tissue cytotoxicity. Besides the characteristics of general nanoparticles, it has superparamagnetism and can thus directionally migrate in AMF to realize gene-targeted therapy [39]. Furthermore, given that magnetic nanoparticles also can be induced to warm, they thus may be used for tumor thermotherapy in AMF [15].

In this study, PEI-FePt-NPs were combined with DNA (using pHRE-Egr1-EGFP as a model) to prepare composite nanoparticles. Biological characteristic detection experiments confirmed that the optimal ratio of DNA binding to PEI-FePt-NPs was 1:40 (the mass ratio); the plasmids in the composite nanoparticles could be protected from Dnase I enzyme digestion and could slowly release from the complex under certain conditions. The recombinant pHRE-Egr1-EGFP was transfected into CD133⁺ Huh-7 cells by PEI-FePt-NPs, the transfection efficiency of which was $53.65 \pm 3.40\%$ in line with flow cytometry analysis. These results indicate that PEI-FePt-NPs may be used as the vector for gene transfer.

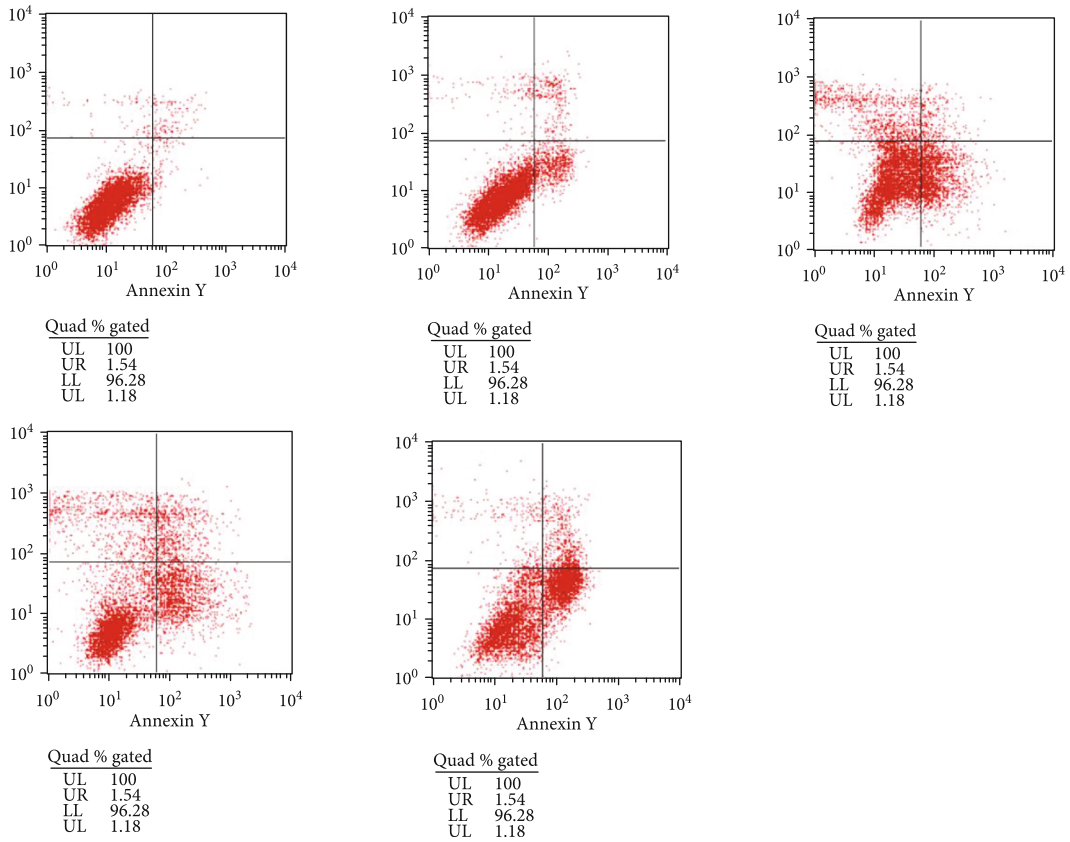
4.4. Preparation, Purification, and Identification of ¹³¹I-Anti-CD133McAb. Tumor radioimmunotherapy is a strategy to combine radionuclide with the tumor-specific monoclonal antibody to seek a targeted treatment for cancer, allowing target cells to be exposed with more radiation, while with less damage to the surrounding normal tissues and cells. In 1978, Golden et al. successfully applied radioimmunotherapy to tumor imaging and therapy study. The CD133 antigen, a specific molecule marker independently expressed on the surface of various tumor stem cells, is bound up with tumor self-renewal, differentiation potential, radiochemotherapy resistance, recurrence, and prognosis [9, 40–42]. The killing effect of paclitaxel nanoparticles labeled with anti-CD133McAb on breast cancer stem cells was remarkably better than that of free paclitaxel [43]. Anti-CD133McAb-directed toxins have also achieved good therapeutic effects on ovarian cancer stem cells [44]. In liver cancer tissues, the positive rate of CD133 antigen was 76.3%, and some researchers have utilized the CD133 antibody to separate liver cancer stem cells from liver cancer tissues and liver cancer cell lines [45, 46]. CD133 antigen is expected to be a new target for liver cancer stem cell treatment. ¹³¹I with 8.05-day physical half-life can emit both gamma and beta rays. The latter (β) can be used for tumor treatment, and the former (γ) for medical imaging. Numerous clinical practices have

shown that the human body has good tolerance to ¹³¹I, with few adverse effects. Anti-CD133McAb labeled with ¹³¹I can selectively concentrate in the tumor region, and it can improve the targeting of ¹³¹I and HSV-TK for LCSCs treatment. In this study, ¹³¹I-anti-CD133McAb prepared by the chloramine T method was purified by the PD10 column, with 100% of radiochemical purity and 36% of the labeling rate. After 6 h at room temperature, the radiochemical purity was still 100%, showing excellent radiological stability.

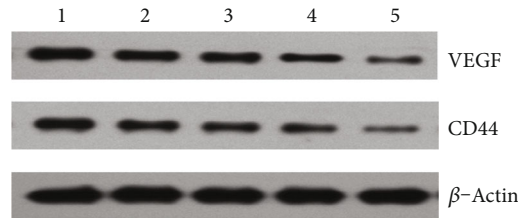
4.5. Targeted Intervention of pHRE-Egr1-HSV-TK/¹³¹I-Anti-CD133McAb/MFH for LCSCs In Vitro. LCSCs are to blame in the process of occurrence, progress, metastasis, and recurrence of HCC and responsible for the failure of HCC treatment. Therefore, a successful HCC treatment should aim for LCSCs, without an exception of nonstem cells differentiated from LCSCs. As the specific molecule marker independently expressed on the surface of various tumor stem cells, the CD133 antigen is closely involved in tumor self-renewal, differentiation potential, radiochemotherapy resistance, recurrence, and prognosis [47, 48], possibly becoming a new target for cancer stem cell treatment.

The expression rate of CD133 antigen in Huh-7 cell line was 9.61%, and CD133⁺ Huh-7 cells were sorted by flow cytometry in the present study. With serum-free culture, the screened CD133⁺ Huh-7 cells successfully formed into cloned spheres or clusters, indicating that LCSCs with cloning ability have been successfully sorted out. We combined anti-CD133McAb labeled with ¹³¹I, pHRE-Egr1-HSV-TK, and MFH together to intervene with LCSCs by using PEI-FePt-NPs as a linker. The results showed that radiation-gene therapy combined with MFH prominently inhibited LCSC proliferation and induced cell apoptosis, significantly better than any of the individual interventions.

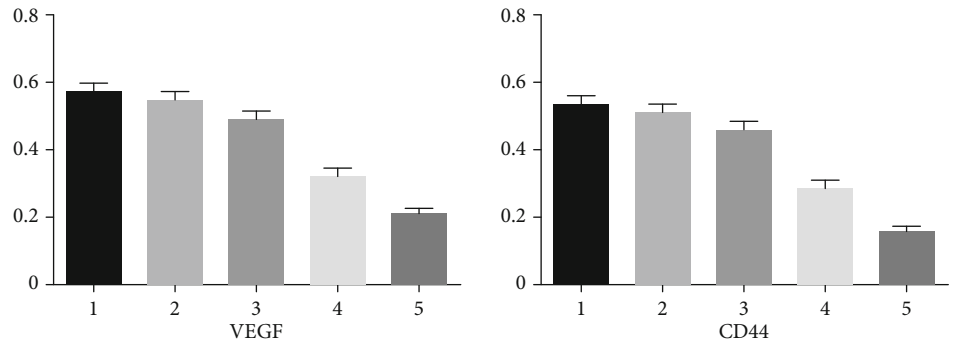
As one of the pivotal angiogenesis regulators, VEGF is overexpressed in HCC tissues, playing a vital role in the growth and metastasis of liver cancer [49]. CD44, the hyaluronic acid receptor that functions in tissue remodeling, cell matrix adhesion, and cell migration, has been recognized as one of critical biomarkers for multiple solid tumor stem cells [50]. Yang et al. [51] reported that CD44⁺ liver cancer cells exhibited more aggressiveness than CD44⁻ liver cancer cells did. In this study, western blot analysis showed that VEGF and CD44 proteins both dwindled at different levels in each experimental group. Notably, they decreased most significantly in the pHRE-Egr1-HSV-TK/¹³¹I-anti-CD133McAb/MFH group, indicating that radiation-gene therapy in combination with



(a)



(b)



(c)

FIGURE 7: Cell apoptosis and related proteins' protein expression of each group after treatment. (a) Cell apoptosis analyzed by flow cytometry. (1) Negative control group. (2) ¹³¹I-anti-CD133McAb group. (3) MFH group. (4) pHRE-Egr1-HSV-TK/¹³¹I-anti-CD133McAb group. (5) pHRE-Egr1-HSV-TK/¹³¹I-anti-CD133McAb/MFH group. (b) Expression of VEGF and CD44 proteins after treatment tested by western blot. (1) Negative control group. (2) ¹³¹I-anti-CD133McAb group. (3) MFH group. (4) pHRE-Egr1-HSV-TK/¹³¹I-anti-CD133McAb group. (5) pHRE-Egr1-HSV-TK/¹³¹I-anti-CD133McAb/MFH group. (c) Expression level of VEGF and CD44 proteins based on the β -actin gray value and analyzed by an image processing system. (1) Negative control group. (2) ¹³¹I-anti-CD133McAb group. (3) MFH group. (4) pHRE-Egr1-HSV-TK/¹³¹I-anti-CD133McAb group. (5) pHRE-Egr1-HSV-TK/¹³¹I-anti-CD133McAb/MFH group).

magnetic fluid hyperthermia may exert an antitumor effect by inhibiting angiogenesis, proliferation, and invasion through restraining the expression of VEGF and CD44 proteins.

In summary, LCSCs (CD133⁺) were separated from the Huh-7 cell line by flow cytometry and constructed recombinant plasmids pHRE-Egr1-HSV-TK in the present study. Using PEI-FePt-NPs as the vector, LCSCs were transfected with pHRE-Egr1-HSV-TK, with good transfection effect. Besides, ¹³¹I-anti-CD133McAb was successfully prepared, with 100% radiochemical purity, 36% labeling rate, and good radioactive stability. Targeted radiation-gene therapy combined with magnetic fluid hyperthermia mediated by PEI-FePt-NPs (pHRE-Egr1-HSV-TK/¹³¹I-anti-CD133McAb/MFH) could efficaciously inhibit LCSC proliferation and induce cell apoptosis. The mechanism may be related to the downregulation of VEGF and CD44 protein expression, thereby restraining tumor angiogenesis, tumor stem cell proliferation, and invasion. This study offers a theoretical and practicable approach for LCSC treatment but is simply limited to experiments *in vitro*. Animal experiments *in vivo* and the therapeutic mechanism are currently ongoing.

Data Availability

The graphics and quantitative data used to support the findings of this study are included within the article.

Conflicts of Interest

The authors declare that they have no conflicts of interest.

Authors' Contributions

Mei Lin conceived and designed the study, performed some experiments, analyzed the data, and wrote the manuscript. Yanhong Xiao conceived and performed some experiments, analyzed some data, and contributed to the manuscript writing. Xingmao Jiang and Jun Zhang gave some constructive guidance, performed some experiments and contributed to some data analysis. Ting Guo and Yujuan Shi performed some experiments and contributed to some data analysis. All authors reviewed the manuscript. Mei Lin and Yanhong Xiao contributed equally.

Acknowledgments

The work is financially supported by the National Natural Science Foundation of China (81571797), Natural Science Foundation of Jiangsu, China (BK20151352), and Taizhou People's Hospital Medical Innovation Team Foundation, China (CXTDA201901).

References

[1] K. J. Lafaro, A. N. Demirjian, and T. M. Pawlik, "Epidemiology of hepatocellular carcinoma," *Surgical Oncology Clinics of North America*, vol. 24, no. 1, pp. 1–17, 2015.

[2] J. Balogh, D. I. Victor, E. H. Asham et al., "Hepatocellular carcinoma: a review," *Journal of Hepatocellular Carcinoma*, vol. 3, pp. 41–53, 2016.

[3] M. Najafi, B. Farhood, and K. Mortezaee, "Cancer stem cells (CSCs) in cancer progression and therapy," *Journal of Cellular Physiology*, vol. 234, no. 6, pp. 8381–8395, 2019.

[4] F. Collina, M. di Bonito, V. Li Bergolis et al., "Prognostic value of cancer stem cells markers in triple-negative breast cancer," *BioMed Research International*, vol. 2015, Article ID 158682, 10 pages, 2015.

[5] F. de Sousa e Melo, A. V. Kurtova, J. M. Harnoss et al., "A distinct role for Lgr5⁺ stem cells in primary and metastatic colon cancer," *Nature*, vol. 543, no. 7647, pp. 676–680, 2017.

[6] T. Oikawa, "Cancer stem cells and their cellular origins in primary liver and biliary tract cancers," *Hepatology*, vol. 64, no. 2, pp. 645–651, 2016.

[7] G. Castelli, E. Pelosi, and U. Testa, "Liver Cancer: molecular characterization, clonal evolution and Cancer stem cells," *Cancers*, vol. 9, no. 12, p. 127, 2017.

[8] L. MacDonagh, S. G. Gray, E. Breen et al., "Lung cancer stem cells: the root of resistance," *Cancer Letters*, vol. 372, no. 2, pp. 147–156, 2016.

[9] A. Nomura, S. Banerjee, R. Chugh et al., "CD133 initiates tumors, induces epithelial-mesenchymal transition and increases metastasis in pancreatic cancer," *Oncotarget*, vol. 6, no. 10, pp. 8313–8322, 2015.

[10] M. Gao, Y. Kong, G. Yang, L. Gao, and J. Shi, "Multiple myeloma cancer stem cells," *Oncotarget*, vol. 7, no. 23, pp. 35466–35477, 2016.

[11] A. Suetsugu, M. Nagaki, H. Aoki, T. Motohashi, T. Kunisada, and H. Moriwaki, "Characterization of CD133⁺ hepatocellular carcinoma cells as cancer stem/progenitor cells," *Biochemical and Biophysical Research Communications*, vol. 351, no. 4, pp. 820–824, 2006.

[12] A. Jordan, P. Wust, R. Scholz et al., "Cellular uptake of magnetic fluid particles and their effects on human adenocarcinoma cells exposed to AC magnetic fields *in vitro*," *International Journal of Hyperthermia*, vol. 12, no. 6, pp. 705–722, 1996.

[13] Q. Tang, D. Chen, M. Lu, and P. Liu, "Combination of PEI-Mn_{0.5}Zn_{0.5}Fe₂O₄ nanoparticles and pHsp 70-HSV-TK/GCV with magnet-induced heating for treatment of hepatoma," *International Journal of Nanomedicine*, vol. 10, pp. 7129–7143, 2015.

[14] M. Lin, D. Zhang, J. Huang et al., "An evaluation on transfection efficiency of pHRE-Egr1-EGFP in hepatocellular carcinoma cells Bel-7402 mediated by PEI-MZF-NPs," *Journal of Nanomaterials*, vol. 2011, Article ID 136052, 10 pages, 2011.

[15] M. Lin, J. Huang, J. Zhang et al., "The therapeutic effect of PEI-Mn_{0.5}Zn_{0.5}Fe₂O₄ nanoparticles/pEgr1-HSV-TK/GCV associated with radiation and magnet-induced heating on hepatoma," *Nanoscale*, vol. 5, no. 3, pp. 991–1000, 2013.

[16] M. Lin, J. Huang, X. Jiang et al., "A combination hepatoma-targeted therapy based on nanotechnology: pHRE-Egr1-HSV-TK/¹³¹I-antiAFPMcAb-GCV/MFH," *Scientific Reports*, vol. 6, no. 1, 2016.

[17] J. Zhang, K. Guo, and S. Chai, "Cell-killing effect of MAR regulating HSV-tk/GCV suicide gene system on ECA109 cells," *International Journal of Clinical and Experimental Pathology*, vol. 10, pp. 817–822, 2017.

- [18] D. Ho, X. Sun, and S. Sun, "Monodisperse magnetic nanoparticles for theranostic applications," *Accounts of Chemical Research*, vol. 44, no. 10, pp. 875–882, 2011.
- [19] R.-J. Chung, K. L. Ou, S. P. Chen, and H. L. Liu, "Preparation of ICG-FePt nanoparticles promising for magnetic resonance imaging contrast agent and hyperthermia applications," *Advanced Powder Technology*, vol. 27, no. 3, pp. 994–999, 2016.
- [20] P. Srinoi, Y. T. Chen, V. Vittur, M. Marquez, and T. Lee, "Bimetallic nanoparticles: enhanced magnetic and optical properties for emerging biological applications," *Applied Sciences*, vol. 8, no. 7, article 1106, 2018.
- [21] S. Majidi, F. Zeinali Sehrig, M. Samiei et al., "Magnetic nanoparticles: applications in gene delivery and gene therapy," *Artificial Cells, Nanomedicine, and Biotechnology*, vol. 44, pp. 1–8, 2016.
- [22] C. Lin, W. Li, S. Huang, C. S. Yeh, and C. M. Yang, "Hollow mesoporous silica nanosphere-supported FePt nanoparticles for potential theranostic applications," *Journal of Materials Chemistry B*, vol. 5, no. 36, pp. 7598–7607, 2017.
- [23] N. H. Hai, N. M. Dempsey, M. Veron, M. Verdier, and D. Givord, "An original route for the preparation of hard FePt," *Journal of Magnetism and Magnetic Materials*, vol. 257, no. 2-3, pp. 139–145, 2003.
- [24] M. Yu, H. Ohguchi, A. Zambano et al., "Orientation and magnetic properties of FePt and CoPt films grown on MgO(1 1 0) single-crystal substrate by electron-beam coevaporation," *Materials Science and Engineering B*, vol. 142, no. 2-3, pp. 139–143, 2007.
- [25] N. Poudyal, K. H. Gandha, J. Liu, K. E. Elkins, H. Arami, and J. P. Liu, "Ferromagnetic FePt/Au core/shell nanoparticles prepared by solvothermal annealing," *IEEE Magnetics Letters*, vol. 7, pp. 1–5, 2016.
- [26] L. Wu, A. Mendoza-Garcia, Q. Li, and S. Sun, "Organic phase syntheses of magnetic nanoparticles and their applications," *Chemical Reviews*, vol. 116, no. 18, pp. 10473–10512, 2016.
- [27] S.-W. Chou, Y. H. Shau, P. C. Wu, Y. S. Yang, D. B. Shieh, and C. C. Chen, "In vitro and in vivo studies of fept nanoparticles for dual modal CT/MRI molecular imaging," *Journal of the American Chemical Society*, vol. 132, no. 38, pp. 13270–13278, 2010.
- [28] O. S. Muddineti, B. Ghosh, and S. Biswas, "Current trends in using polymer coated gold nanoparticles for cancer therapy," *International Journal of Pharmaceutics*, vol. 484, no. 1-2, pp. 252–267, 2015.
- [29] Y. Meng, S. Wang, C. Li et al., "Photothermal combined gene therapy achieved by polyethyleneimine-grafted oxidized mesoporous carbon nanospheres," *Biomaterials*, vol. 100, pp. 134–142, 2016.
- [30] C. Liu, Y. Yu, L. Miao, Y. Liu, and W. Sun, "A comparative study of transfection of rat mesenchymal stem cells using polyethyleneimine-coated magnetic ferro-ferric oxide nanoparticles and lipofectamine," *International Journal of Clinical and Experimental Medicine*, vol. 9, pp. 6062–6069, 2016.
- [31] M. Khoobi, S. F. Motevalizadeh, Z. Asadgol, H. Foroootanfar, A. Shafiee, and M. A. Faramarzi, "Polyethyleneimine-modified superparamagnetic Fe₃O₄ nanoparticles for lipase immobilization: characterization and application," *Materials Chemistry and Physics*, vol. 149–150, pp. 77–86, 2015.
- [32] W.-X. Peng, Y. Y. Wan, A. H. Gong et al., "Egr-1 regulates irradiation-induced autophagy through Atg4B to promote radioresistance in hepatocellular carcinoma cells," *Oncogenesis*, vol. 6, no. 1, article e292, 2017.
- [33] J. Tang, X. Wang, Y. Xu, Y. Shi, Z. Liu, and Y. Yang, "Sodium-iodine symporter gene expression controlled by the EGR-1 Promoter," *Technology in Cancer Research & Treatment*, vol. 14, no. 1, pp. 61–69, 2015.
- [34] H. Xu, Z. Li, and J. Si, "Nanocarriers in gene therapy: a review," *Journal of Biomedical Nanotechnology*, vol. 10, no. 12, pp. 3483–3507, 2014.
- [35] G. Liu, M. Swierczewska, S. Lee, and X. Chen, "Functional nanoparticles for molecular imaging guided gene delivery," *Nano Today*, vol. 5, no. 6, pp. 524–539, 2010.
- [36] K. Wang, F. M. Kievit, and M. Zhang, "Nanoparticles for cancer gene therapy: recent advances, challenges, and strategies," *Pharmacological Research*, vol. 114, pp. 56–66, 2016.
- [37] O. Madkhali, G. Mekhail, and S. D. Wettig, "Modified gelatin nanoparticles for gene delivery," *International Journal of Pharmaceutics*, vol. 554, pp. 224–234, 2019.
- [38] A. Amani, T. Kabiri, S. Shafiee, and A. Hamidi, "Preparation and characterization of PLA-PEG-PLA/PEI/DNA nanoparticles for improvement of transfection efficiency and controlled release of DNA in gene delivery systems," *Iranian Journal of Pharmaceutical Research*, vol. 18, no. 1, pp. 125–141, 2019.
- [39] M. Czugala, O. Mykhaylyk, P. Böhler et al., "Efficient and safe gene delivery to human corneal endothelium using magnetic nanoparticles," *Nanomedicine*, vol. 11, no. 14, pp. 1787–1800, 2016.
- [40] J. Jang, Y. Song, S. Kim, J. Kim, and H. R. Seo, "Potential mechanisms of CD133 in cancer stem cells," *Life Sciences*, vol. 184, pp. 25–29, 2017.
- [41] G.-Y. Liou, "CD133 as a regulator of cancer metastasis through the cancer stem cells," *The International Journal of Biochemistry & Cell Biology*, vol. 106, pp. 1–7, 2019.
- [42] C. Joseph, M. Arshad, S. Kurozomi et al., "Overexpression of the cancer stem cell marker CD133 confers a poor prognosis in invasive breast cancer," *Breast Cancer Research and Treatment*, vol. 174, no. 2, pp. 387–399, 2019.
- [43] S. K. Swaminathan, E. Roger, U. Toti, L. Niu, J. R. Ohlfest, and J. Panyam, "CD133-targeted paclitaxel delivery inhibits local tumor recurrence in a mouse model of breast cancer," *Journal of Controlled Release*, vol. 171, no. 3, pp. 280–287, 2013.
- [44] A. P. Skubitz, E. P. Taras, K. L. Boylan et al., "Targeting CD133 in an in vivo ovarian cancer model reduces ovarian cancer progression," *Gynecologic Oncology*, vol. 130, no. 3, pp. 579–587, 2013.
- [45] A. Rajanna, "Novel approach to target cancer stem cells for therapy," *Medical Hypotheses*, vol. 88, pp. 83–85, 2016.
- [46] Y. Wang, Y. Liu, J. Jiang, and H. B. Cui, "A new method for purification and identification of hepatocellular carcinoma stem cell of SMMC-7721," *Zhonghua Yi Xue Za Zhi*, vol. 92, no. 48, pp. 3434–3437, 2012.
- [47] S.-C. Dang, X. Qian, W. Jin, L. Cui, J. Chen, and M. Gu, "G-protein-signaling modulator 2 expression and role in a CD133⁺ pancreatic cancer stem cell subset," *Oncotargets and Therapy*, vol. 12, pp. 785–794, 2019.

- [48] E. K. Park, J. C. Lee, J. W. Park et al., "Transcriptional repression of cancer stem cell marker CD133 by tumor suppressor p53," *Cell Death & Disease*, vol. 6, no. 11, article e1964, 2015.
- [49] A. M. Mercurio, "VEGF/neuropilin signaling in cancer stem cells," *International Journal of Molecular Sciences*, vol. 20, no. 3, p. 490, 2019.
- [50] C. Chen, S. Zhao, A. Karnad, and J. W. Freeman, "The biology and role of CD44 in cancer progression: therapeutic implications," *Journal of Hematology & Oncology*, vol. 11, no. 1, p. 64, 2018.
- [51] Z. F. Yang, D. W. Ho, M. N. Ng et al., "Significance of CD90+ cancer stem cells in human liver cancer," *Cancer Cell*, vol. 13, no. 2, pp. 153–166, 2008.

Research Article

Galactosamine-Conjugating Zwitterionic Block Copolymer for Reduction-Responsive Release and Active Targeted Delivery of Doxorubicin to Hepatic Carcinoma Cells

Jingming Zhai,¹ Biyu Zhou,² Yanhui An,¹ Binzhong Lu,² Yonggang Fan ,¹ and Junbo Li ^{1,2}

¹The First Affiliated Hospital and College of Clinical Medicine, Henan University of Science and Technology, Luo Yang 471023, China

²School of Chemical Engineering & Pharmaceuticals, Henan University of Science & Technology, Luo Yang 471023, China

Correspondence should be addressed to Yonggang Fan; fanyonggang196809@163.com and Junbo Li; lijunbo@haust.edu.cn

Received 16 January 2020; Accepted 4 March 2020; Published 20 April 2020

Guest Editor: Anuj Kumar

Copyright © 2020 Jingming Zhai et al. This is an open access article distributed under the Creative Commons Attribution License, which permits unrestricted use, distribution, and reproduction in any medium, provided the original work is properly cited.

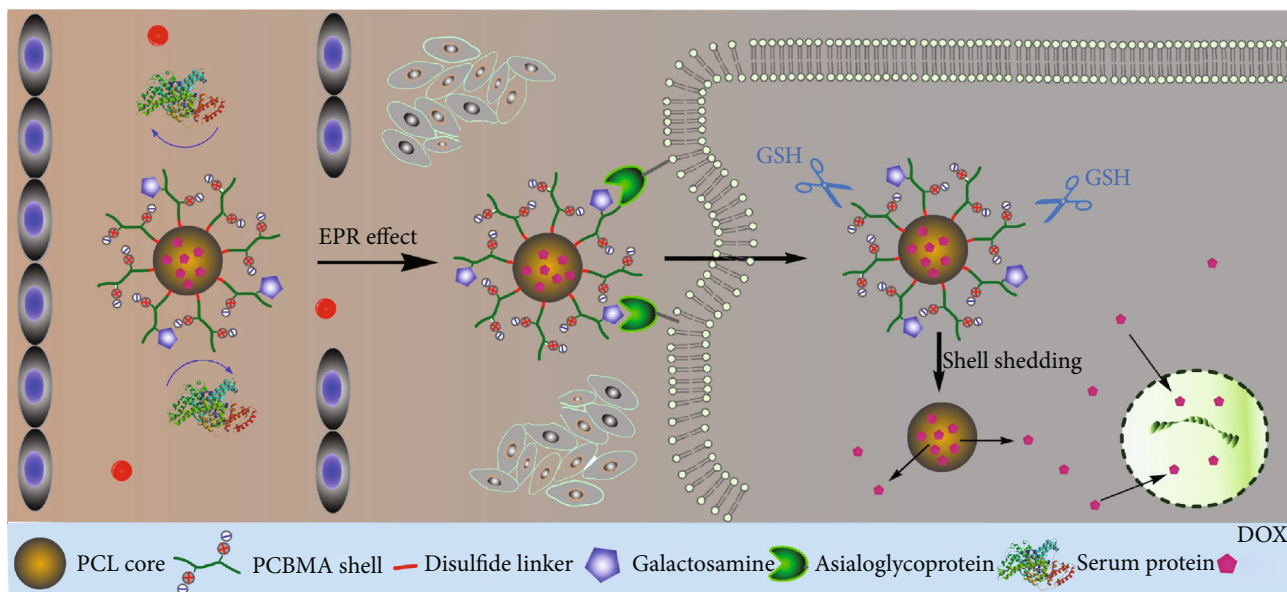
Nanocarriers with integrated advantage, such as excellent stealth property, active targeting function, and rapid intracellular drug release, are significant for cancer treatment. Herein, a biodegradable zwitterionic triblock copolymer containing disulfide-linked poly- ϵ -caprolactone and polycarboxybetaine methacrylate (PCB-SS-PCL-SS-PCB) was first synthesized and then partly modified with galactosamine (GAL) for constructing polymeric micelle drug carrier with multifunctionality. Polymeric micelles showed ultralow protein absorption in serum and obvious reduction-responsiveness in the presence of glutathione, provided by the zwitterionic polymer shell and the disulfide bond, respectively. Furthermore, active targeting of the carrier to hepatic carcinoma cells was achieved via GAL ligands on PCB shells due to their specific binding to asialoglycoprotein receptors on the cell surface. As expected, *in vivo* competition studies demonstrated that doxorubicin- (DOX-) loaded GAL-modified micelles have better anticancer effect in hepatic tumor-bearing mice than free DOX and nontargetable micelles. As a result, this novel multifunctional carrier provides a valuable strategy to design promising anticancer drug delivery systems for liver cancer treatment.

1. Introduction

Chemotherapeutics are still the main treatment strategy for human cancer [1]. To reduce side effects and enhance bioavailability of hydrophobic drugs, nanodrug delivery systems (NDDS) have been widely explored in cancer chemotherapeutics during past decades [2, 3]. Generally, therapeutic nanoparticles required a hydrophilic coating to ensure a stealthy and long circulation in the bloodstream [4]. To date, polyethylene glycol (PEG) is the most widely used biointerface materials to prevent nonspecific protein adhesion on nanoparticles [5, 6], resulting in a passive accumulation of cargo in the tumor site via a so-called enhanced permeability and retention (EPR) effect [7, 8]. However, recent reports revealed that anti-PEG immunoglobulin antibodies detected in PEGylated systems after repeated administration lead to an insufficient antitumor efficacy caused by an accelerated blood clearance (ABC) phenomenon [9, 10].

Zwitterionic polymers are also neutral and ultrahydrophilic since they bear an equimolar number opposite ionizable group in monomeric unit [1]. The unique structure enables a zwitterionic layer to tightly bind water molecules via ion interaction, giving rise in ultrahigh resistance to protein adsorption and excellent blood compatibility. Moreover, without detectable immune response and avoiding ABC phenomenon, zwitterionic polymers have been also identified as better biointerface material alternative PEG [11, 12]. Recently, a variety of zwitterionic therapeutic nanoparticles, such as polymer-drug conjugates [13], nanogels [14], and polymeric micelles [15] have been developed. However, overcoming their less efficient tumor cell uptake is still a challenge [16].

Among zwitterionic polymers, such as polyphosphobetaine and polysulfobetaine, polycarboxybetaine (PCB) has superior abilities because of its reactive carboxylate anion, which can readily conjugate with amine-containing biomolecules via simple carbodiimide chemistry [17]. Although the



SCHEME 1: Schematic representation of the structure of the multifunctional micelle carrier and its resistance protein adsorption in blood circulation, active targeting cell uptake to HepG2, and GSH-triggered intracellular drug release behavior.

modification has little influence on the antifouling property, it introduces novel functions [18–20]. For instance, to address the reduced cell uptake efficacy of zwitterionic nanoparticles, Lin et al. used c(RGDyK)-modified PCB to obtain micelle carriers with prolonged blood circulation time and active targeting property to improve therapeutic efficacy *in vivo* [21]. Furthermore, based on the specific recognition of asialoglycoprotein (ASGP) receptors to glycoproteins on hepatic carcinoma cells [22, 23], the immobilization of galactosamine on PCB substrates allows the adhesion-based selection of hepatocytes differing from other cell types [24]. Jiang's group also used fluorescein and galactose with the amine group to modify PLGA-PCB nanoparticles for selectively binding HepG2 cells [25]. The modification of galactose ligand on zwitterionic nanoparticles has exhibited an integrated ultrahigh antifouling and tumor-targeting properties to hepatic carcinoma cells. However, the *in vivo* antitumor effect of such NDDS needs further investigation.

In addition to long circulation and tumor-targeting properties, an optimal micellar carrier should precisely control drug release inside the cancer cell. However, therapeutic efficacy is always restricted by the gradual drug permeation for its hydrophobicity [26]. The development of stimuli-responsive carriers that quickly release encapsulated cargo triggered by intracellular environmental factor is an efficient strategy to improve drug bioavailability [27–29]. In our recent paper, we developed micelle platform with a PCB shell and disulfide linked to a biodegradable poly- ϵ -caprolactone (PCL) core. The carriers showed many advantages, such as ultralow protein absorption in serum and a fast intracellular drug release triggered by higher GSH intracellular concentration [30]. Herein, to enhance drug bioavailability *in vivo*, this micellar carrier was further optimized by introduction of a galactosamine ligand for integrating the multifunction, excellent stealth property, active targeting to

hepatic carcinoma, and reductively responsive intracellular release, as showing in Scheme 1.

2. Materials and Methods

2.1. Materials. PCL-diol ($M_n = 2000$, $PDI = 1.2$) was purchased from Sigma-Aldrich (Shanghai, China). Cystamine dihydrochloride (Cys.2HCl) (>96%) and 1, 1-carbonyldiimidazole (CDI) (>97.0%) were purchased from the National Pharmaceutical Group Chemical Reagent (Beijing, China) and used as received. 2, 2-Azobis(isobutyronitrile) (AIBN) (97%) was purchased from J&K Chemical (Beijing, China) and recrystallized before being used as an initiator. The monomers, carboxybetaine methacrylate (CBMA, 99%), RAFT reagent (4-cyanopentanoic acid)-4-dithiobenzoate (CPADB, 98%), doxorubicin hydrochloride (DOX-HCl, 99%), N-(3-dimethylaminopropyl)-N'-ethyl carbodiimide hydrochloride (EDC-HCl, 98%), and N-hydroxysuccinimide (NHS, 98%), were purchased from J&K Chemical (Beijing, China) and used as received. All other reagents and solvents were of analytical grade and used as received. Dulbecco's modified Eagle's medium (DMEM), penicillin-streptomycin, fetal bovine serum (FBS), and 3-[4, 5-dimethylthiazol-2-yl]-2, 5-diphenyltetrazolium bromide (MTT), were purchased from Thermo Fisher Scientific (Shanghai, China).

2.2. Synthesis of PCL Macro-RAFT Agent. For synthesis of the PCL macro-RAFT agent, two hydroxyl groups of PCL-diol were first activated by CDI and then conjugated with cystamine monomer to provide reductive disulfide bonds and reactive amino-end groups [29]. Next, the PCL macro-RAFT agent, CPADB-SS-PCL-SS-CPADB, was prepared by a condensation reaction between amino-end groups of PCL and the carboxylic group of CPADB through EDC/NHS chemistry. The detailed synthesis and characterization of

the PCL macro-RAFT agent were described in our previous paper [28].

2.3. Synthesis of PC-SS-PCL-SS-PCB. PCB-SS-PCL-SS-PCB was prepared by RAFT polymerization of CBMA by using CPADB-SS-PCL-SS-CPADB as the chain transfer agent. Typically, The CPADB-SS-PCL-SS-CPADB (0.4 g, 0.140 mmol) and AIBN (4.6 mg, 0.028 mmol) were dissolved in a sealed ampoule with 4 ml dry tetrahydrofuran (THF). Then, CBMA (0.6 g, 2.618 mmol) was dissolved in 4 ml saturated salt water and placed into an above reaction tube. After three freeze-evacuate-thaw cycles, the polymerization was conducted at 70°C for 48 h. The product was purified by dialysis (bag MWCO 3000) against deionized water to remove salt and unreacted CBMA. Finally, PCB-SS-PCL-SS-PCB was obtained by lyophilization as a light pink powder (0.574 g, 57.4%).

2.4. Modification of PCB-SS-PCL-SS-PCB with Galactosamine. Targeting molecule, GAL is used to conjugate on PCB-SS-PCL-SS-PCB by an amidation reaction between the amine of GAL and carboxylate group of PCB. To accomplish the purpose, 50 mg of PCB-SS-PCL-SS-PCB was first resolved in the 4 ml mixed solution of equivolumental dimethyl sulfoxide (DMSO) and pure water. Subsequently, the solution was incubated with 0.5 ml EDC-HCl (400 mM) and NHS (200 mM) in water for 30 min and then adjusted the pH value to 9 by adding in 10 mM sodium borate buffer. After that, 5 mg of GAL was added and reacted at room temperature (RT) for 4 h. The solution was transferred into a dialysis bag (MWCO 3500) against pure water for 48 h and then lyophilized to obtain GAL-modified PCB-SS-PCL-SS-PCB (GAL-m-polymer).

2.5. Preparation of GAL-M-Polymer Micelles. To prepare the GAL-m-polymer micelles (denoted as GAL-micelles), we used a similar procedure with that of PCB-SS-PCL-SS-PCB micelles (denoted as PCB micelles) reported in our previous paper [28]. The size and size distribution (PDI) of GAL-micelles were measured with a laser particle size analyzer (Nano ZS90, Malvern, UK). The morphology of GAL-micelles was characterized with a JEM2100 (JEOL, Japan) transmission electron microscopy (TEM) system at an operated voltage of 75 kV. For TEM observation, a drop of micelle solution was added onto the copper grid, and then, the resulting sample was air-dried and measured at RT.

2.6. DOX Loading and Release from GAL-Micelles. We used a coprecipitation method to prepare DOX-loaded GAL-micelles. Briefly, 2 mg DOX-HCl was first dissolved in DMSO and then treated by triethylamine solution (1 mg/ml) for 2 h. Subsequently, 10 mg GAL-m-polymer was added to the solution and stirred overnight. PB (50 mM, pH 7.4) was added at a rate of one drop every 6-7 s until the micellization of GAL-m-polymer. The solution was sealed using a dialysis bag (MWCO 3500) against PB at RT for 48 h, then filtered through a 0.45 μm filter for removal of the free DOX. To calculate drug loading content, lyophilized DOX-loaded GAL-micelles were dissolved in DMSO and analyzed at 485 nm with a UV-Vis spectrophotometer

(UV2550, Shimadzu, Japan). Drug loading content (DLC) and drug loading efficiency (DLE) were determined by the following equations:

$$\begin{aligned} \text{DLC} (\%) &= \frac{\text{weight of loaded drug}}{\text{weight of drug-loaded micelles}} \times 100\% \\ \text{DLE} (\%) &= \frac{\text{weight of loaded drug}}{\text{weight of drug in feed}} \times 100\% \end{aligned} \quad (1)$$

In vitro release profiles DOX from GAL-micelles were studied using a dialysis tube (MWCO 14000) at 37°C against PB (pH 5.0, 50 mM) and PB (pH 7.4, 50 mM) in the presence and absence of 10 mM DTT. At regular intervals, 3 ml of release media was collected and an equal volume of fresh media was added. The amount of released DOX was determined by UV-Vis spectroscopy. The release experiments were conducted in triplicate. The results showed the average value with standard deviations.

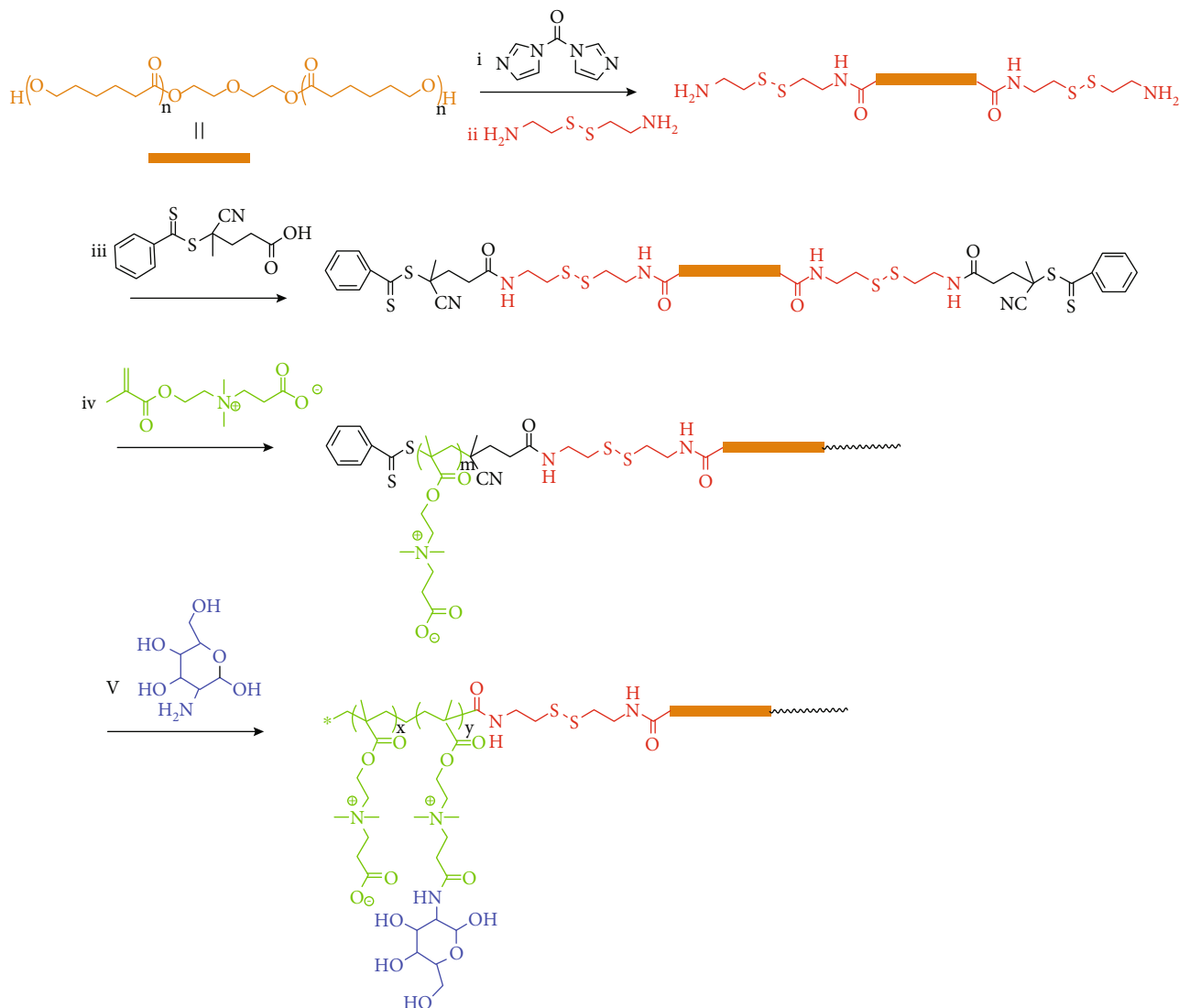
2.7. Cell Uptake Studies. The cellular uptake of DOX, DOX-loaded PCB micelles, and DOX-loaded GAL-micelles was observed by fluorescence microscopy. HepG2 and EC109 cells were seeded into 24-well plates with 5 · 10⁴ cells/well in 1 ml DMEM (10% FBS) and incubated at 37°C in 5% CO₂. After reaching about 80% confluence, the cells were incubated with free DOX, DOX-loaded PCB micelles, or DOX-loaded GAL-micelles, where the concentration of DOX was fixed at 5 μg/ml in each culture medium. After 4 h incubation, the cells were washed three times with PBS and then imaged by fluorescence microscopy (IX73, Olympus, Japan). After that, the cells were treated with 0.25% trypsin and resuspended in 500 μl PBS (pH 7.4) for flow cytometer (FC500, Beckman Coulter, US) measurement.

2.8. Cell Viability Assays. The cytotoxic effects of empty micelles or micelle-loading drug were determined using MTT assays. HepG2 and EC109 were seeded into 96-well plates at 5000 cells/well and cultured 24 h. The culture medium was replaced with PBS (pH 7.4) containing free DOX, DOX-loaded PCB micelles, or DOX-loaded GAL-micelles, and then, the cells were incubated for another 24 h. The medium was replaced with 200 μl of fresh medium, and 20 μl MTT (5 mg/ml in PBS) was then added to each well. After 4 h, unreacted dye was carefully removed and formazan crystals were dissolved in 200 μl/well DMSO. The plate was incubated in 37°C for 10 min before measuring absorbance at 570 nm with an ELISA microplate reader (Bio-Rad). Cell viability (%) was calculated as follows:

$$\text{Cell viability} (\%) = \frac{\text{OD}_{\text{sample}}}{\text{OD}_{\text{control}}} \times 100, \quad (2)$$

where OD_{sample} is the absorbance of the cells treated by polymers and OD_{control} is the absorbance of the untreated cells. Each experiment was done in triplicate.

2.9. In Vivo Antitumor Studies. The nude mice bearing HepG2 tumor model were injected via the tail vein with 200 μl PBS, DOX, DOX-loaded PCB micelles, or DOX-



SCHEME 2: Synthesis route of GAL-m-polymer. (i) CDI, anhydrous DCM, RT., 24 h; (ii) DMSO, pyridine, TEA, RT, 48 h; (iii) DCC, NHS, RT., 48 h; (iv) AIBN, THF, saturated salt water, 60°C, 48 h; (V) EDC-HCl, NHS, DMSO, water, RT.

loaded GAL-micelles at an equivalent DOX dose of 4 mg/kg every two days. The tumor size and the body weight of mice were measured before each injection. Tumor size was measured using vernier calipers and calculated using the following formula: $V = d^2 \times D/2$ (where d is width and D is length, respectively). The therapeutic efficacy of the treatment was evaluated by comparing the experimental groups with the control group.

3. Results and Discussion

3.1. Polymer Characterization. Scheme 2 represents the synthesis route of GAL-m-polymer. PCL-diol was first introduced the cystamine at the end groups [31]. Next, a PCL macro-RAFT agent was readily obtained by a conjugating reaction of amino-end groups of PCL and the carboxylic group of CPADB. PCB-SS-PCL-SS-PCB was prepared by RAFT polymerization of CBMA by using CPADB-SS-PCL-SS-CPADB as the chain transfer agent. Finally, GAL-m-

polymer was prepared by modified PCB-SS-PCL-SS-PCB with GAL via EDC/NHS chemistry.

The resulting PCB-SS-PCL-SS-PCB and GAL-modified PCB-SS-PCL-SS-PCB (GAL-m-polymer) were characterized with ^1H NMR and FT-IR spectrum. ^1H NMR spectrum of GAL-m-polymer (Figure 1(a)) presents new small characteristic peaks at 1, 2, 3, 4, and 5 (δ 5.2, 3.9, 3.8, 3.6, and 3.4 ppm, respectively) which are attributed to the protons of GAL [30], in addition to the characteristic protons of PCB-SS-PCL-SS-PCB [28]. FT-IR spectra were also used to determine the successful modification of PCB with GAL (Figure 1(b)). Compared with FT-IR spectrum of PCB-SS-PCL-SS-PCB, the absorption peak around 3400 cm^{-1} broadening in that of GAL-m-polymer indicates the increased hydroxyl after the modification. Besides, the newly emerging peaks around 1656 cm^{-1} belongs to vibration of C=O in the amide.

3.2. Characterization of GAL-m-Polymer Micelles. GAL-m-polymer was self-assembled into polymeric micelles in

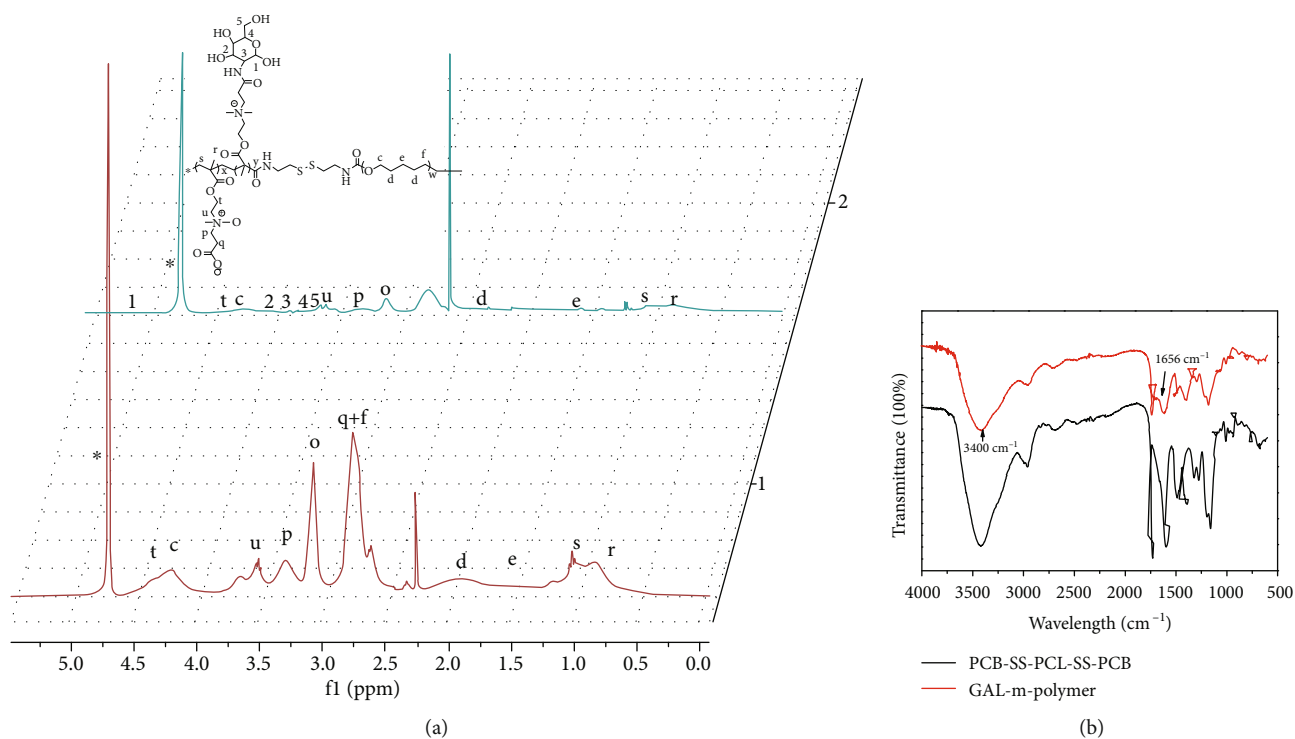


FIGURE 1: ¹H NMR spectra (a) and FT-IR spectra (b) of PCB-SS-PCL-SS-PCB and GAL-M-polymer.

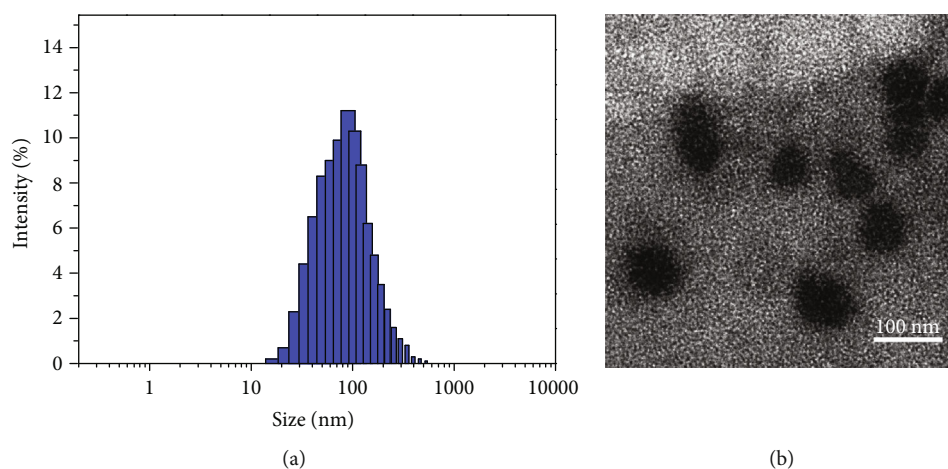


FIGURE 2: Hydrodynamic diameter distribution $f(D_h)$ (a) and TEM image (b) of GAL-m-polymer micelles.

aqueous solution with PCL as a core and modified PCB as a shell. The hydrodynamic diameter distribution (D_h) of micelle was measured by DLS (Figure 2(a)). The average diameter is approximately 91 ± 4 nm, showing a slight change compared to that of without modification [30]. The polydispersity index (PDI) is approximately 0.18. TEM imaging revealed that the micelles of GAL-m-polymer have a spherical morphology with a mean diameter of approximately 75 ± 3 nm (Figure 2(b)). The difference between DLS and TEM measurements of micellar size is likely due to the shape of micelle at different hydration states, from swelled at hydrated (DLS) to collapsed at dry (TEM).

The antifouling and redox-responsive properties of PCB micelles and GAL micelles were investigated by DLS analysis. After incubation with 50% FBS solution, both micelles show no significant changes in size even after incubation for 72 h (Figure 3(a)), indicating that the zwitterionic PCB shell effectively prevents protein adsorption from polymer micelles. High serum stability is helpful to prolong circulation in the bloodstream. Reductive response to GSH was further investigated by analyzing size change with DLS. Both micelles show an increased D_h and broadened PDI after addition of 10 mM GSH for 12 h. As disulfides are cleavable in the presence of GSH, the PCB shells are detached from the micellar surface, resulting in micelle aggregation.

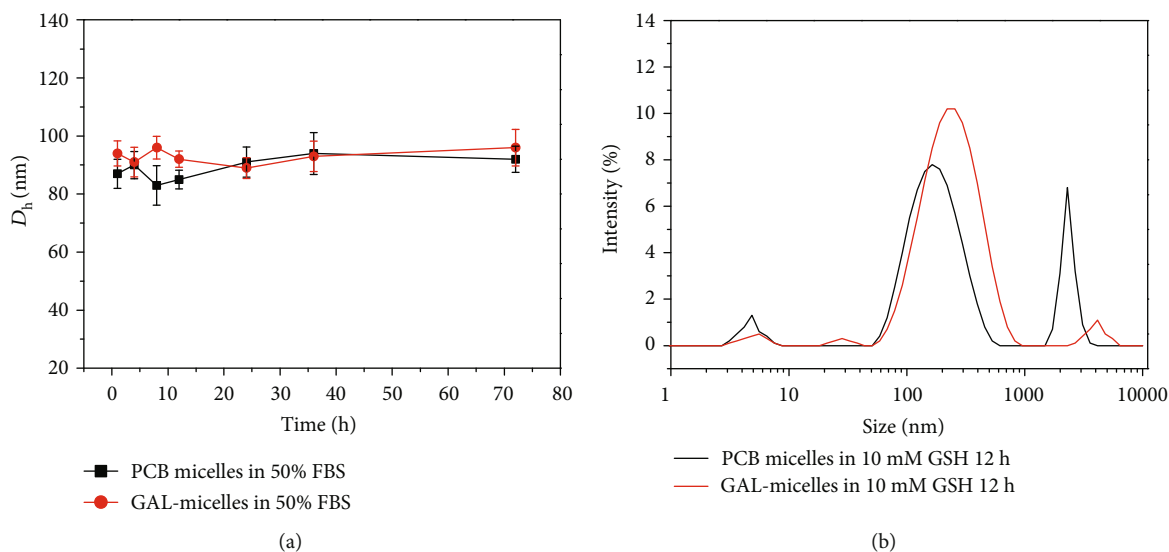


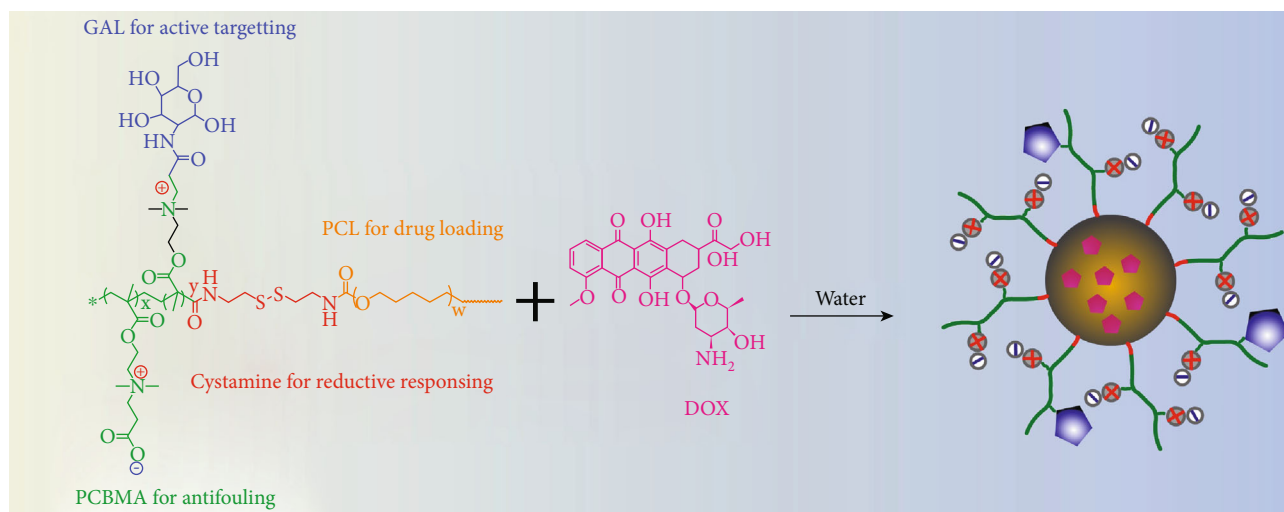
FIGURE 3: Hydrodynamic diameter distribution $f(D_h)$ of micelles and GAL-micelles in PB (50 mM, pH 7.4) containing 50% FBS (a) and in PB (50 mM, pH 7.4) containing 10 mM GSH (b). Data are presented as the average (standard deviation ($n = 3$)).

3.3. Preparation of DOX-Loaded GAL-Micelles. The multifunctional micellar carrier prepared by GAL-M-polymer is illustrated in Figure 4(a), where the PCB segment provided antifouling capability; the conjugated GAL ligand was expected an active targeting function; PCL was used for drug encapsulation and cystamine linkers offered a reductive response. Drug loading content was determined by UV-Vis spectrophotometry in DMSO. DLC and DLE were approximately 19.6% and 47.3%, respectively. The average diameter of DOX-loaded GAL-micelles increased to 143 ± 4 nm and also maintained a narrow size distribution (Figure 4(b)), when compared to GAL-micelles (Figure 2(b)). TEM image showed that DOX-loaded GAL-micelles have a spherical morphology with good dispersion and a diameter of approximately 167 ± 7 nm (Figure 4(c)). The results illustrate surface modification with GAL ligand show little influence on drug loading and carrier's properties [30] but may endow a novel function of active targeting to HepG2 cells. The stable structure and uniform small size facilitate intracellular uptake and EPR effect of carriers efficiently *in vivo* [32].

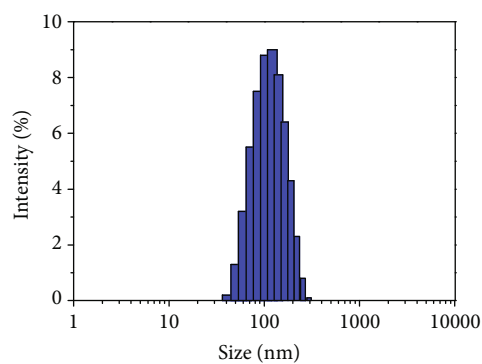
3.4. In Vitro Drug Release. *In vitro* drug release profile from DOX-loaded GAL-micelles was investigated at 37°C in PBS at pH 7.4 and 5.0 with or without 10 mM GSH and as shown in Figure 5, only approximately 24% of DOX was released from GAL-micelles within 48 h at pH 7.4 without treated by GSH. As the increase of acidity to pH 5.0, the DOX release reached to 48.2% within 24 h, which is likely to result from the protonation of DOX. In comparison, an accelerated release of DOX was activated in the presence of 10 mM GSH, in which over 60% and 80% of DOX was released from GAL-micelles at both pH 7.4 and 5.0, respectively. The reductive response triggered a rapid drug release which is due to the cleavage of disulfide bonds at the surface of the core [33], leading to shell shedding and micelle aggregating, followed by fast drug efflux during the reassembly of deprotected micelles [34].

3.5. In Vitro Cytotoxicity and Cell Uptake. *In vitro* cytocompatibility of PCB micelles and GAL-micelles was evaluated with MTT assays in HepG2 and EC109 cells. Cells without treatment were used as control and showed a viability of 100%. As shown in Figure 6(a), the viability of HepG2 and EC109 cell was over 90% incubation of both micelles, even at a concentration up to 200 mg/l. The micelles possess low cytotoxicity which was likely due to the biocompatible PCB, PCL, and GAL ligand. For the cytotoxicity assays, HepG2 and EC109 cells were incubated with free DOX, DOX-loaded PCB micelles, and DOX-loaded GAL-micelles (Figure 6(b)). The inhibitory concentrations to produce 50% of cell death (IC₅₀) in HepG2 cells were 0.26 mg/l, 1.44 mg/l, and 0.72 mg/l for free DOX, DOX-loaded PCB micelles, and DOX-loaded GAL-micelles, respectively (Figure 6(b)). The DOX-loaded PCB micelles showed significantly lower cytotoxicity than free DOX, which may be due to less efficient cell uptake caused by the stealth shielding shell of zwitterionic PCB [15, 16]. After the functionalization with GAL, DOX-loaded GAL-micelles exhibited increased inhibition of cellular proliferation when compared with DOX-loaded PCB micelles. However, DOX-loaded PCB micelles and DOX-loaded GAL-micelles showed similar anti-tumor activity in EC109 cells.

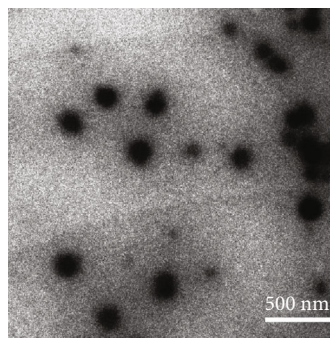
DOX is a popular chemotherapeutic drug and widely used in clinics for treating various hematological malignancies and solid tumors. Mechanistically, the insertion of DNA into tumor cells inhibits macromolecular biosynthesis, eventually leading to cell apoptosis [35, 36]. Intracellular drug accumulation depends on the efficacy of cell uptake and drug release from the loading carrier [37]. The increased therapeutic effect of DOX-loaded GAL-micelles in HepG2 cells can be attributed to improve cell uptake via active targeting, as demonstrated by fluorescence microscopy (Figure 6(c)). Indeed, empty micelles had no fluorescence signal, whereas the red fluorescence of DOX was easily detectable (Figure 6(c), B), showing that DOX is efficiently



(a)



(b)



(c)

FIGURE 4: Schematic diagram of the preparation process of DOX-loaded GAL-micelles (a); hydrodynamic diameter distribution $f(D_h)$ (b) and TEM image (c) of DOX-loaded GAL-micelles.

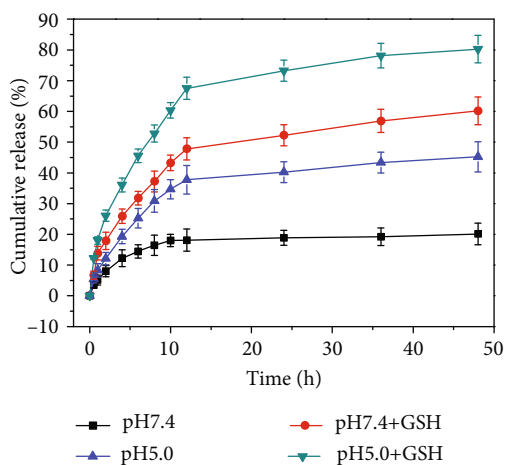


FIGURE 5: *In vitro* release profile of DOX-loaded GAL-micelles in PBS (0.1M) at pH 7.4 and pH 5.0 with or without GSH (10 mg/ml). Data are presented as the average (standard deviation ($n = 3$)).

released from DOX-loaded PCB micelles in response to intracellular GSH. Furthermore, DOX fluorescence in the cytoplasm and nucleus was brighter and more intense in DOX-loaded GAL-micelles (Figure 6(c), C), consistent with the increased cell uptake due to GAL binding to ASGP receptors on the surface of HepG2 cells [22]. However, DOX-loaded GAL-micelles showed a similar DOX fluorescence signal than DOX-loaded PCB micelles in EC109 cells, suggesting that active targeting of GAL is less effective in this cell type (Figure 6(d)). These results are consistent with the toxicity studies described above. Together, our data demonstrate that DOX-loaded GAL-micelles possess outside active targeting and inside redox-responsive release in HepG2 cells, suggesting they are promising nanocarriers for efficient treatment of liver cancer *in vivo*.

3.6. *In Vivo* Antitumor Efficacy. The antitumor efficacy of DOX-loaded micelles was investigated *in vivo* by using a nude mice bearing tumor model of human liver cancer. When the tumor size reached approximately 100 mm³, PBS, free DOX, DOX-loaded PCB micelles, or DOX-loaded micelles GAL were injected into the tumor-bearing mice

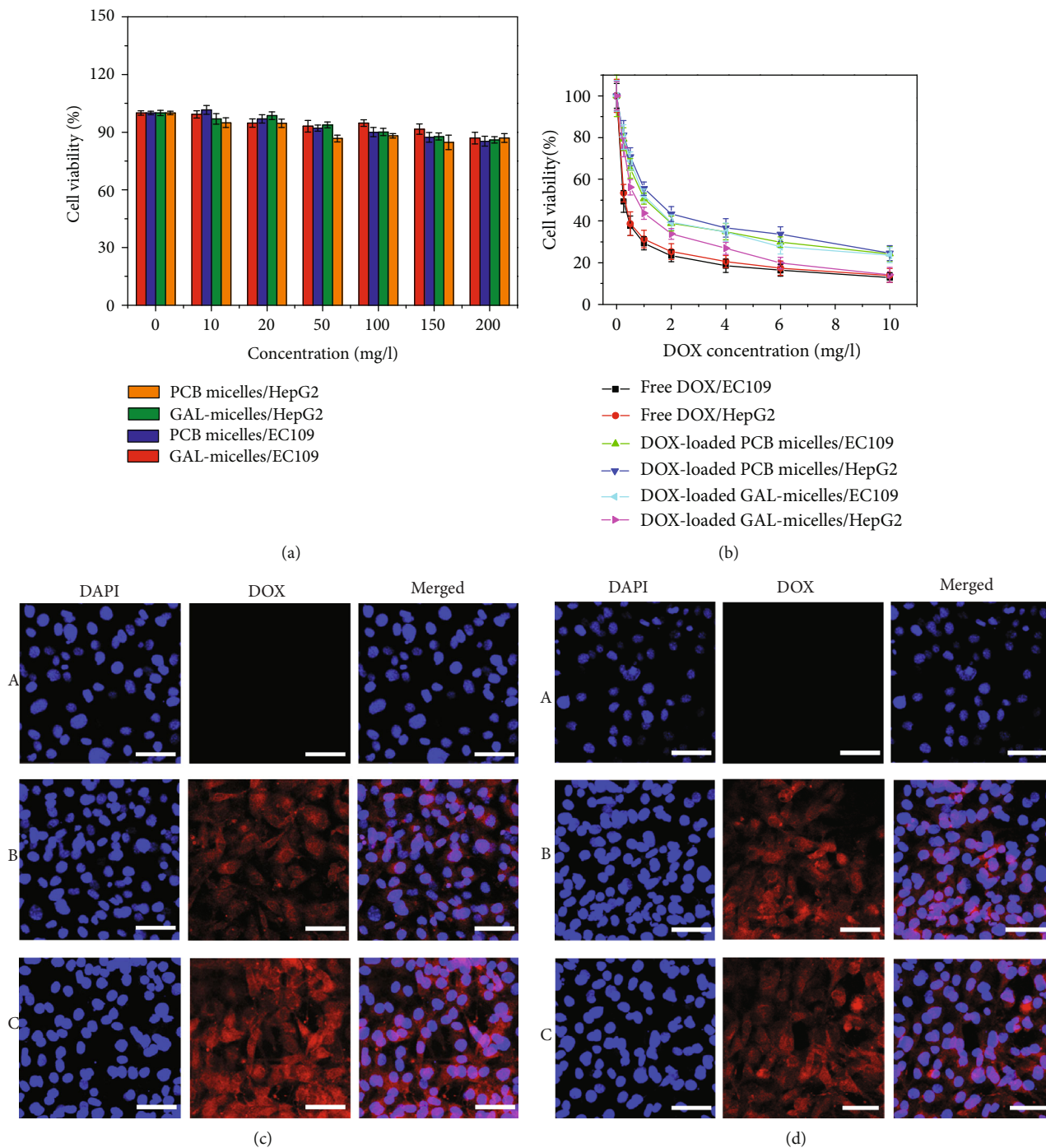


FIGURE 6: Toxicity of PCB micelles and GAL-micelles (a, b) and free DOX, DOX-loaded PCB-micelles, and DOX-loaded GAL micelles in HepG2 and EC109 cells incubated for 24 h. Data are presented as the average (standard deviation ($n = 3$)); fluorescence microscopy images of HepG2 (c) and EC109 cells (d) incubated with empty GAL-micelles (A), DOX-loaded PCB-micelles (B), and DOX-loaded GAL-micelles (C) for 4 h, where the concentration of DOX was fixed at $5 \mu\text{g/ml}$. The scale bars correspond to $50 \mu\text{m}$ in all the images.

through the tail vein. Tumor volume and body weight were measured and plotted as a function of time (Figure 7). As shown in Figure 7(a), the tumor volume in mice treated with PBS increased rapidly. In contrast, in the other groups, the tumors showed a slow growth, particularly, tumors in mice injected with DOX-loaded GAL-micelles. The body weight

of mice treated with free DOX showed a clear decrease in weight as a result of *in vivo* cytotoxicity [21] (Figure 7(b)), the mice in the other groups exhibited a slow increase in body weight. More importantly, mice treated with DOX-loaded GAL-micelles had the smallest increase in weight within 12 days, suggesting the most effective tumor inhibition.

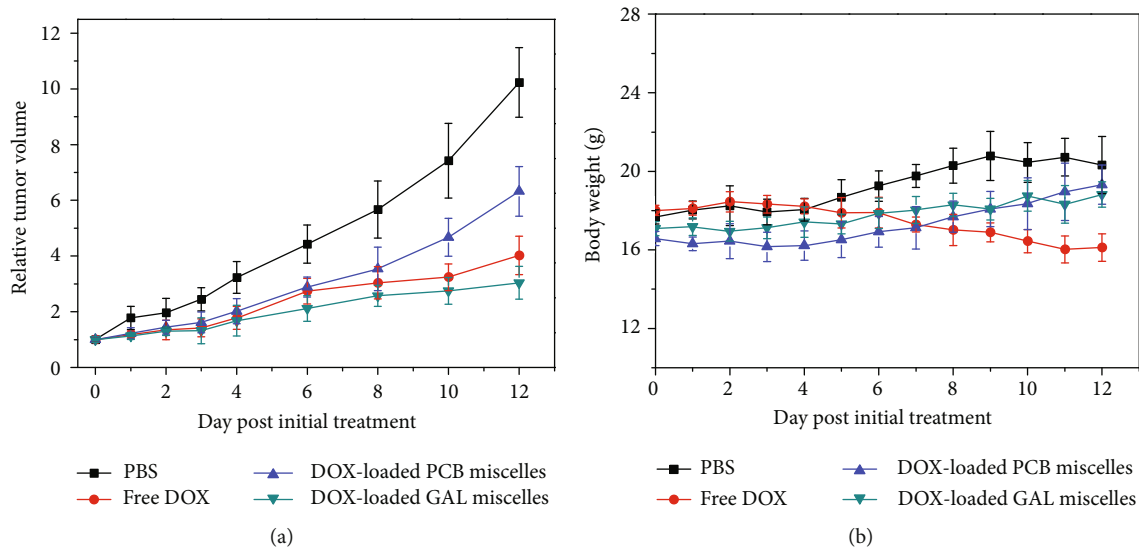


FIGURE 7: Tumor volume changes of the Bcap37 tumor-bearing nude mice after treatment with PBS or DOX at an equivalent dose of 4 mg/kg at each day (a). Changes in mice body weight during the treatment (b). Data are presented as the average (standard deviation, $n = 3$).

Excellent stealth property from zwitterionic shells provides drug-loaded micelles a prolonged circulation time [38, 39] and enhanced drug accumulation at tumor site via EPR effect. The active targeting of DOX-loaded GAL-micelles to HepG2 cells further improves cell uptake. Finally, DOX is rapidly released due to reductive cleavage of disulfide bonds inside HepG2 cells.

4. Conclusions

The multifunctionality of polymeric micelle carrier, including high antifouling ability, redox responsive property, and active targeting in hepatic carcinoma cells, was successfully achieved by the modification of a triblock copolymer with disulfide-linked zwitterionic and biodegradable polymer (PCB-SS-PCL-SS-PCB) with galactosamine. GAL-micelles loaded with DOX exhibit rapid drug release under reductive environment, enhanced drug levels, and antitumor activity in HepG2 cells. As expected, this carrier revealed better anticancer efficacy in hepatic tumor-bearing mice than free DOX or no-targetable micelles. Thus, multifunctional nanocarriers with a flexible design of zwitterionic polymeric micelles represent a valuable strategy for improving drug bioavailability in the treatment of liver cancer.

Data Availability

The authors confirm that the data supporting the findings of this study are available within the article.

Conflicts of Interest

The authors declare no conflict of interest.

Acknowledgments

The authors gratefully acknowledge the financial support from the National Natural Science Foundation of China (Project U1704150) and Scientific and Technological Projects of Henan province (182102410017).

References

- [1] S. Popat and M. O'Brien, "Chemotherapy strategies in the treatment of small cell lung cancer," *Anti-Cancer Drugs*, vol. 16, no. 4, pp. 361–372, 2005.
- [2] C. Yang, M. Zhang, and D. Merlin, "Advances in plant-derived edible nanoparticle-based lipid nano-drug delivery systems as therapeutic nanomedicines," *Journal of Materials Chemistry B*, vol. 6, no. 9, pp. 1312–1321, 2018.
- [3] K. Seidi, H. A. Neubauer, R. Moriggl, R. Jahanban-Esfahlan, and T. Javaheri, "Tumor target amplification: implications for nano drug delivery systems," *Journal of Controlled Release*, vol. 275, pp. 142–161, 2018.
- [4] V. Sauraj, V. Kumar, B. Kumar et al., "Lipophilic 5-fluorouracil prodrug encapsulated xylan-stearic acid conjugates nanoparticles for colon cancer therapy," *International Journal of Biological Macromolecules*, vol. 128, pp. 204–213, 2019.
- [5] F. Liu, Y. Sun, C. Kang, and H. Zhu, "Pegylated drug delivery systems: from design to biomedical applications," *Nano Life*, vol. 6, article 1642002, 2016.
- [6] J. Pei, H. Hall, and N. D. Spencer, "The role of plasma proteins in cell adhesion to PEG surface-density-gradient-modified titanium oxide," *Biomaterials*, vol. 32, no. 34, pp. 8968–8978, 2011.
- [7] C. Deng, Y. Jiang, R. Cheng, F. Meng, and Z. Zhong, "Biodegradable polymeric micelles for targeted and controlled anti-cancer drug delivery: promises, progress and prospects," *Nano Today*, vol. 7, no. 5, pp. 467–480, 2012.
- [8] J. Qi, C. Sun, A. Zebibula et al., "Real-time and high-resolution bioimaging with bright aggregation-induced emission dots in

- short-wave infrared region,” *Advanced Materials*, vol. 30, no. 12, article 1706856, 2018.
- [9] C. E. Henry, Y.-Y. Wang, Q. Yang et al., “Anti-PEG antibodies alter the mobility and biodistribution of densely PEGylated nanoparticles in mucus,” *Acta Biomaterialia*, vol. 43, pp. 61–70, 2016.
- [10] J. J. F. Verhoef and T. J. Anchordoquy, “Questioning the use of PEGylation for drug delivery,” *Drug Delivery and Translational Research*, vol. 3, no. 6, pp. 499–503, 2013.
- [11] C. Leng, H. Hung, S. Sun et al., “Probing the surface hydration of nonfouling zwitterionic and PEG materials in contact with proteins,” *ACS Applied Materials & Interfaces*, vol. 7, no. 30, pp. 16881–16888, 2015.
- [12] K. Seetho, S. Zhang, K. A. Pollack et al., “Facile synthesis of a phosphorylcholine-based zwitterionic amphiphilic copolymer for anti-biofouling coatings,” *ACS Macro Letters*, vol. 4, no. 5, pp. 505–510, 2015.
- [13] H. Sun, M. Y. Z. Chang, W.-I. Cheng et al., “Biodegradable zwitterionic sulfobetaine polymer and its conjugate with paclitaxel for sustained drug delivery,” *Acta Biomaterialia*, vol. 64, pp. 290–300, 2017.
- [14] Y. Men, S. Peng, P. Yang et al., “Biodegradable zwitterionic nanogels with long circulation for antitumor drug delivery,” *ACS Applied Materials & Interfaces*, vol. 10, no. 28, pp. 23509–23521, 2018.
- [15] H. Ou, T. Cheng, Y. Zhang et al., “Surface-adaptive zwitterionic nanoparticles for prolonged blood circulation time and enhanced cellular uptake in tumor cells,” *Acta Biomaterialia*, vol. 65, pp. 339–348, 2018.
- [16] E. Muro, T. Pons, N. Lequeux et al., “Small and stable sulfobetaine zwitterionic quantum dots for functional live-cell imaging,” *Journal of the American Chemical Society*, vol. 132, no. 13, pp. 4556–4557, 2010.
- [17] S. Jiang and Z. Cao, “Ultralow-fouling, functionalizable, and hydrolyzable zwitterionic materials and their derivatives for biological applications,” *Advanced Materials*, vol. 22, no. 9, pp. 920–932, 2010.
- [18] Z. Zhang, S. Chen, and S. Jiang, “Dual-functional biomimetic materials: nonfouling poly(carboxybetaine) with active functional groups for protein immobilization,” *Biomacromolecules*, vol. 7, no. 12, pp. 3311–3315, 2006.
- [19] H. Vaisocherová, W. Yang, Z. Zhang et al., “Ultralow fouling and functionalizable surface chemistry based on a zwitterionic polymer enabling sensitive and specific protein detection in undiluted blood plasma,” *Analytical Chemistry*, vol. 80, no. 20, pp. 7894–7901, 2008.
- [20] A. J. Keefe and S. Jiang, “Poly(zwitterionic)protein conjugates offer increased stability without sacrificing binding affinity or bioactivity,” *Nature Chemistry*, vol. 4, no. 1, pp. 59–63, 2012.
- [21] W. Lin, G. Ma, N. Kampf, Z. Yuan, and S. Chen, “Development of long-circulating zwitterionic cross-linked micelles for active-targeted drug delivery,” *Biomacromolecules*, vol. 17, no. 6, pp. 2010–2018, 2016.
- [22] D. Zhu, W. Tao, H. Zhang et al., “Docetaxel (DTX)-loaded polydopamine-modified TPGS-PLA nanoparticles as a targeted drug delivery system for the treatment of liver cancer,” *Acta Biomaterialia*, vol. 30, pp. 144–154, 2016.
- [23] H.-F. Liang, C.-T. Chen, S.-C. Chen et al., “Paclitaxel-loaded poly(γ -glutamic acid)-poly(lactide) nanoparticles as a targeted drug delivery system for the treatment of liver cancer,” *Biomaterials*, vol. 27, no. 9, pp. 2051–2059, 2006.
- [24] H.-W. Chien, P.-H. Cheng, S.-Y. Chen, J. Yu, and W.-B. Tsai, “Low-fouling and functional poly(carboxybetaine) coating via a photo-crosslinking process,” *Biomaterials Science*, vol. 5, no. 3, pp. 523–531, 2017.
- [25] Z. Cao, Q. Yu, H. Xue, G. Cheng, and S. Jiang, “Nanoparticles for drug delivery prepared from amphiphilic PLGA zwitterionic block copolymers with sharp contrast in polarity between two blocks,” *Angewandte Chemie International Edition*, vol. 49, no. 22, pp. 3771–3776, 2010.
- [26] Z. Cao, Y. Ma, C. Sun et al., “ROS-sensitive polymeric nanocarriers with red light-activated size shrinkage for remotely controlled drug release,” *Chemistry of Materials*, vol. 30, no. 2, pp. 517–525, 2018.
- [27] N. Rapoport, R. Gupta, Y. S. Kim, and B. E. O’Neill, “Polymeric micelles and nanoemulsions as tumor-targeted drug carriers: insight through intravital imaging,” *Journal of Controlled Release*, vol. 206, pp. 153–160, 2015.
- [28] Y.-w. Hu, Y.-z. Du, N. Liu et al., “Selective redox-responsive drug release in tumor cells mediated by chitosan based glycolipid-like nanocarrier,” *Journal of Controlled Release*, vol. 206, pp. 91–100, 2015.
- [29] Sauraj, S. U. Kumar, V. Kumar, R. Priyadarshi, P. Gopinath, and Y. S. Negi, “pH-responsive prodrug nanoparticles based on xylan-curcumin conjugate for the efficient delivery of curcumin in cancer therapy,” *Carbohydrate Polymers*, vol. 188, pp. 252–259, 2018.
- [30] J. Jiang, J. Li, B. Zhou et al., “Fabrication of polymer micelles with zwitterionic shell and biodegradable core for reductively responsive release of doxorubicin,” *Polymers*, vol. 11, no. 6, p. 1019, 2019.
- [31] P. Davoodi, M. P. Srinivasan, and C.-H. Wang, “Synthesis of intracellular reduction-sensitive amphiphilic polyethylenimine and poly(ϵ -caprolactone) graft copolymer for on-demand release of doxorubicin and p53 plasmid DNA,” *Acta Biomaterialia*, vol. 39, pp. 79–93, 2016.
- [32] Y. Chen, W. Zhang, Y. Huang, F. Gao, and X. Fang, “In vivo biodistribution and anti-tumor efficacy evaluation of doxorubicin and paclitaxel-loaded pluronic micelles decorated with c(RGDyK) peptide,” *PLoS One*, vol. 11, no. 3, article e0149952, 2016.
- [33] Sauraj, Vinay kumar, B. Kumar et al., “Redox responsive xylan-SS-curcumin prodrug nanoparticles for dual drug delivery in cancer therapy,” *Materials Science and Engineering: C*, vol. 107, article 110356, 2020.
- [34] H. Sun, B. Guo, X. Li et al., “Shell-sheddable micelles based on dextran-SS-poly(ϵ -caprolactone) diblock copolymer for efficient intracellular release of doxorubicin,” *Biomacromolecules*, vol. 11, no. 4, pp. 848–854, 2010.
- [35] X. Zhang, A. Poniewierski, K. Sozański, Y. Zhou, A. Brzozowska-Elliott, and R. Holyst, “Fluorescence correlation spectroscopy for multiple-site equilibrium binding: a case of doxorubicin–DNA interaction,” *Physical Chemistry Chemical Physics*, vol. 21, no. 3, pp. 1572–1577, 2019.
- [36] S. Wang, E. A. Konorev, S. Kotamraju, J. Joseph, S. Kalivendi, and B. Kalyanaraman, “Doxorubicin induces apoptosis in normal and tumor cells via distinctly different Mechanisms,” *Journal of Biological Chemistry*, vol. 279, no. 24, pp. 25535–25543, 2004.
- [37] H. Wei, R.-X. Zhuo, and X.-Z. Zhang, “Design and development of polymeric micelles with cleavable links for intracellular drug delivery,” *Progress in Polymer Science*, vol. 38, no. 3–4, pp. 503–535, 2013.

- [38] Z. Wang, G. Ma, J. Zhang et al., "Development of zwitterionic polymer-based doxorubicin conjugates: tuning the surface charge to prolong the circulation and reduce toxicity," *Langmuir*, vol. 30, no. 13, pp. 3764–3774, 2014.
- [39] W. Yang, S. Liu, T. Bai et al., "Poly(carboxybetaine) nanomaterials enable long circulation and prevent polymer-specific antibody production," *Nano Today*, vol. 9, no. 1, pp. 10–16, 2014.